p-ISSN 2521-4209
e-ISSN 2521-4217

جامعة التنمية البشرية
UNIVERSITY OF HUMAN DEVELOPMENT

UHD Journal of Science and Technology

A Scientific periodical issued by University of Human Developement

Vol.4 No.(2) December 2020

2020 2720

www.jst.uhd.edu.iq

Kurdistan Regional Government
University of Human Development

UHD Journal of Science and Technology

A periodic scientific journal issued by University of Human Development

Introduction

UHD Journal of Science and Technology (UHDJST) is a semi-annual journal published by the University of Human Development, Sulaymaniyah, Kurdistan Region, Iraq. UHDJST member of ROAD, e-ISSN: 2521-4217, p-ISSN: 2521-4209 and a member of Crossref, DOI: 10.21928/issn.2521-4217. UHDJST publishes original research in all areas of Science, Engineering, and Technology. UHDJST is a Peer-Reviewed Open Access journal with Creative Commons Attribution Non-Commercial No Derivatives License 4.0 (CC BY-NC-ND 4.0). UHDJST provides immediate, worldwide, barrier-free access to the full text of research articles without requiring a subscription to the journal, and has article processing charge (APC). UHDJST applies the highest standards to everything it does and adopts APA citation/referencing style. UHDJST Section Policy includes three types of publications: Articles, Review Articles, and Letters.

By publishing with us, your research will get the coverage and attention it deserves. Open access and continuous online publication mean your work will be published swiftly, ready to be accessed by anyone, anywhere, at any time. Article Level Metrics allow you to follow the conversations your work has started.

UHDJST publishes works from extensive fields including, but not limited to:

- Pure Science
- Applied Science
- Medicine
- Engineering
- Technology

Scope and Focus

UHD Journal of Science and Technology (UHDJST) publishes original research in all areas of Science and Engineering. UHDJST is a semi-annual journal published by the University of Human Development, Sulaymaniyah, Kurdistan Region, Iraq. We believe that if your research is scientifically valid and technically sound then it deserves to be published and made accessible to the research community. UHDJST aims to provide a service to the international scientific community enhancing swap space to share, promote and disseminate the academic scientific production from research applied to Science, Engineering, and Technology.

SEARCHING FOR PLAGIARISM

We use plagiarism detection: detection; According to Oxford online dictionary, Plagiarism means: *The practice of taking someone else's work or ideas and passing them off as one's own.*

Section Policies

No.	Title	Peer Reviewed	Indexed	Open Submission
1	Articles: This is the main type of publication that UHDJST will produce	☑	☑	☑
2	Review Articles: Critical, constructive analysis of the literature in a specific field through summary, classification, analysis, comparison.	☑	☑	☑
3	Letters: Short reports of original research focused on an outstanding finding whose importance means that it will be of interest to scientists in other fields.	☑	☑	☑

PEER REVIEW POLICIES

At UHDJST we are committed to prompt quality scientific work with local and global impacts. To maintain a high-quality publication, all submissions undergo a rigorous review process. Characteristics of the peer review process are as follows:

- The journal peer review process is a "double-blind peer review".
- Simultaneous submissions of the same manuscript to different journals will not be tolerated.
- Manuscripts with contents outside the scope will not be considered for review.
- Papers will be refereed by at least 2 experts as suggested by the editorial board.
- In addition, Editors will have the option of seeking additional reviews when needed. Authors will be informed when Editors decide further review is required.
- All publication decisions are made by the journal's Editors-in-Chief on the basis of the referees' reports. Authors of papers that are not accepted are notified promptly.
- All submitted manuscripts are treated as confidential documents. We expect our Board of Reviewing Editors, Associate Editors and reviewers to treat manuscripts as confidential material as well.
- Editors, Associate Editors, and reviewers involved in the review process should disclose conflicts of interest resulting from direct competitive, collaborative, or other relationships with any of the authors, and remove oneself from cases in which such conflicts preclude an objective evaluation. Privileged information or ideas that are obtained through peer review must not be used for competitive gain.
- Our peer review process is confidential and the identities of reviewers cannot be revealed.

Note: UHDJST is a member of CrossRef and CrossRef services, e.g., CrossCheck. All manuscripts submitted will be checked for plagiarism (copying text or results from other sources) and self-plagiarism (duplicating substantial parts of authors' own published work without giving the appropriate references) using the CrossCheck database. Plagiarism is not tolerated.

For more information about CrossCheck/iThenticate, please visit
http://www.crossref.org/crosscheck.html.

OPEN ACCESS POLICY

This journal provides immediate open access to its content on the principle that making research freely available to the public supports a greater global exchange of knowledge. Open Access (OA) stands for unrestricted access and unrestricted reuse which means making research publications freely available online. It access ensures that your work reaches the widest possible audience and that your fellow researchers can use and share it easily. The mission of the UHDJST is to improve the culture of scientific publications by supporting bright minds in science and public engagement.

UHDJST's open access articles are published under a Creative Commons Attribution CC-BY-NC-ND 4.0 license. This license lets you retain copyright and others may not use the material for commercial purposes. Commercial use is one primarily intended for commercial advantage or monetary compensation. If others remix, transform or build upon the material, they may not distribute the modified material. The main output of research, in general, is new ideas and knowledge, which the UHDJST peer-review policy allows publishing as high-quality, peer-reviewed research articles. The UHDJST believes that maximizing the distribution of these publications - by providing free, online access - is the most effective way of ensuring that the research we fund can be accessed, read and built upon. In turn, this will foster a richer research culture and cultivate good research ethics as well. The UHDJST, therefore, supports unrestricted access to the published materials on its main website as a fundamental part of its mission and a global academic community benefit to be encouraged wherever possible.

Specifically:

- The University of Human Development supports the principles and objectives of Open Access and Open Science
- UHDJST expects authors of research papers, and manuscripts to maximize the opportunities to make their results available for free access on its final peer-reviewed paper
- All manuscript will be made open access online soon after final stage peer-review finalized.
- This policy will be effective from 17th May 2017 and will be reviewed during the first year of operation.
- Open Access route is available at http://journals.uhd.edu.iq/index.php/uhdjst for publishing and archiving all accepted papers,
- Specific details of how authors of research articles are required to comply with this policy can be found in the Guide to Authors.

ARCHIVING

This journal utilizes the LOCKSS and CLOCKSS systems to create a distributed archiving system among participating libraries and permits those libraries to create permanent archives of the journal for purposes of preservation and restoration.

LOCKSS: Open Journal Systems supports the LOCKSS (Lots of Copies Keep Stuff Safe) system to ensure a secure and permanent archive for the journal. LOCKSS is open source software developed at Stanford University Library that enables libraries to preserve selected web journals by regularly polling registered journal websites for newly published content and archiving it. Each archive is continually validated against other library caches, and if the content is found to be corrupted or lost, the other caches or the journal is used to restore it.

CLOCKSS: Open Journal Systems also supports the CLOCKSS (Controlled Lots of Copies Keep Stuff Safe) system to ensure a secure and permanent archive for the journal. CLOCKSS is based upon the open-source LOCKSS software developed at Stanford University Library that enables libraries to preserve selected web journals by regularly polling registered journal websites for newly published content and archiving it. Each archive is continually validated against other library caches, and if the content is found to be corrupted or lost, the other caches or the journal is used to restore it.

PUBLICATION ETHICS

Publication Ethics and Publication Malpractice Statement

The publication of an article in the peer-reviewed journal UHDJST is to support the standard and respected knowledge transfer network. Our publication ethics and publication malpractice statement is mainly based on the Code of Conduct and Best-Practice Guidelines for Journal Editors (Committee on Publication Ethics, 2011) that includes;

- General duties and responsibilities of editors.
- Relations with readers.
- Relations with the authors.
- Relations with editors.
- Relations with editorial board members.
- Relations with journal owners and publishers.
- Editorial and peer review processes.
- Protecting individual data.
- Encouraging ethical research (e.g. research involving humans or animals).
- Dealing with possible misconduct.
- Ensuring the integrity of the academic record.
- Intellectual property.
- Encouraging debate.
- Complaints.
- Conflicts of interest.

ANIMAL RESEARCHES

- For research conducted on regulated animals (which includes all live vertebrates and/or higher invertebrates), appropriate approval must have been obtained according to either international or local laws and regulations. Before conducting the research, approval must have been obtained from the relevant body (in most cases an Institutional Review Board, or Ethics Committee). The authors must provide an ethics statement as part of their Methods section detailing full information as to their approval (including the name of the granting organization, and the approval reference numbers). If an approval reference number is not provided, written approval must be provided as a confidential supplemental information file. Research on non-human primates is subject to specific guidelines from the Weather all (2006) report (The Use of Non-Human Primates in Research).
- For research conducted on non-regulated animals, a statement should be made as to why ethical approval was not required.
- Experimental animals should have been handled according to the highest standards dictated by the author's institution.
- We strongly encourage all authors to comply with the '*Animal Research: Reporting In Vivo Experiments*' (ARRIVE) guidelines, developed by NC3Rs.
- Articles should be specific in descriptions of the organism(s) used in the study. The description should indicate strain names when known.

ARTICLE PROCESSING CHARGES

UHDJST is an Open Access Journal (OAJ) and has article processing charges (APCs). The published articles can be downloaded freely without a barrier of admission.

Address

University of Human Development, Sulaymaniyah-Kurdistan Region/Iraq
PO Box: Sulaymaniyah 6/0778

Contact

Principal Contact

Dr. Aso Darwesh

Editor-in-Chief

University of Human Development – Sulaymaniyah, Iraq

Phone: +964 770 148 5879

Email: jst@uhd.edu.iq

Support Contact

UHD Technical Support

Phone: +964 770 158 4888

Email: jst@uhd.edu.iq

Contents

ORIGINAL RESEARCH ARTICLE UHD JOURNAL OF SCIENCE AND TECHNOLOGY

Using Tobit Model for Studying Factors Affecting Blood Pressure in Patients with Renal Failure

Raz Muhammad H. Karim*, Samira Muhamad

Department of Statistics, College of administration and Economic, University of Sulaimani, Sulaymaniyah, Iraq

ABSTRACT

In this study, the Tobit Model as a statistical regression model was used to study factors affecting blood pressure (BP) in patients with renal failure. The data have been collected from (300) patients in Shar Hospital in Sulaimani city. Those records contain BP rates per person in patients with renal failure as a response variable (Y) which is measured in units of millimeters of mercury (mmHg), and explanatory variables (Age [year], blood urea measured in milligram per deciliter [mg/dl], body mass index [BMI] expressed in units of kg/m^2 [kilogram meter square], and Waist circumference measured by the Centimeter [cm]). The two levels of BP; high and low were taken from the patients. The mean arterial pressure (MAP) was used to find the average of both levels (high and low BP). The average BP rate of those patients equal to or >93.33 mmHg only remained in the dataset. The 93.33 mmHg is a normal range of MAP equal to 12/8 mmHg normal range of BP. The others have been censored as zero value, i.e., left censored. Furthermore, the same data were truncated from below. Then, in the truncated samples, only those cases under risk of BP (greater than or equal to BP 93.33mmHg) are recorded. The others were omitted from the dataset. Then, the Tobit Model applied on censored and truncated data using a statistical program (R program) version 3.6.1. The data censored and truncated from the left side at a point equal to zero. The result shows that factors age and blood urea have significant effects on BP, while BMI and Waist circumference factors have not to affect the dependent variable(y). Furthermore, a multiple regression model was found through ordinary least Square (OLS) analysis from the same data using the Stratigraphy program version 11. The result of (OLS) shows that multiple regression analysis is not a suitable model when we have censored and truncated data, whereas the Tobit model is a proficient technique to indicate the relationship between an explanatory variable, and truncated, or censored dependent variable.

Index Terms: Tobit Model, Censored Regression, Truncated Regression, Renal Failure, Blood Pressure

1. INTRODUCTION

In economic and social research, many types of regression models applied. Their use is dependent on the nature of the data. The Tobit model is regarded as the most appropriate statistical model for solving those cases that the dependent variable is censored or truncated [1]. Tobit regression has been the subject of great theoretical interests in numerous practical applications. It has been developed and used in many fields, such as econometrics, finance, and medicine [1], [2]. Furthermore, it is regarded as a linear regression model where only data on the response variable incompletely observed; the response variable is censored at zero. Kidney diseases are common diseases worldwide; it is a global public health problem affecting 750 million persons globally [3]. It plays an important role in preserving normal body functions. Most people are not aware of their impaired kidney functions. In

Access this article online

DOI: 10.21928/uhdjst.v4n2y2020.pp1-9

E-ISSN: 2521-4217
P-ISSN: 2521-4209

Corresponding author's e-mail: Raz Muhammad H. Karim Department of Statistics, College of administration and Economic, University of Sulaimani, Sulaymaniyah, Iraq. E-mail: razmauhammad@gmail.com

Received: 16-05-2020 Accepted: 26-07-2020 Published: 01-07-2020

fact, kidney failure is a "silent illness" that sometimes has no obvious early symptoms. Many people with kidney diseases are not conscious that they are at high risk of kidney failure, which could require dialysis or transplantation. Often the disease such as diabetes with high blood pressure (BP) may cause kidney damage. Hypertension (high BP) is both a cause and a consequence of renal diseases, which are difficult to distinguish its types clinically [4]. Hence, the importance of this research comes as studies the factors that affect BP in patients with renal disease and knowing the real causes of it. This is crucial for medical staff and specialists (doctors) to eliminate problems and limit the spread of kidney diseases because high BP is both a cause and a consequence of kidney diseases. In this study, we find an influence on each independent variable of the dependent variable (BP). It is known that the normal BP range is 12/8 mmHg [5]. This value change due to many factors, and any change in this range make many health problems. Therefore, controlling BP and finding factor, everybody should take care of it. In this study, the data collected from patients in a dialysis center at Shar hospital in Sulaimani city. The two levels of BP; high and low BP from the patients (as dependent variables) and some independent variables (Age, blood, urea, body mass index [BMI], and Waist circumference) were taken. Each patient has their own specific BP (high, low), then we could not take high and low BP separately for our study. That is why the mean arterial pressure (MAP) was performed. It is an average arterial pressure contains high and low BP [6]. A threshold point equal to 93.33 is determined and found by MAP equation [7], equal to 12/8 mmHg, which is a normal range of BP. We assumed any value lower that range is equal to zero. Therefore, the Tobit regression model is used because some variables are equal to zero for a number of observations. This is a phenomenon that can generally be termed censored or truncated data. After that multiple regression model performed for the same data based on ordinary least square (OLS) analysis, it is found that a multiple regression model is not suitable for analysis because there are a number of observations in the dependent variable equal to zero. The use of OLS models in the case of censored sample datasets and depending on the number of zeros makes OLS estimated bias [8].

2. AIM OF THE STUDY

The aim of this study is to detect the impact of the independent variables (Age, blood, urea, BMI, and waist circumference) on dependent variables (BP) in patients with renal failure putting these results in front of specialists to eliminate a problem using a statistical model (Tobit model). Knowing which factor in the independent variable more effect on the dependent variable also comparison between (OLS) and Tobit model estimation to knowing which of them are suitable models for estimation.

3. RELATED WORK

Odah *et al.* [9] displayed the most significant factors affecting loans provided by Iraqi banks and the best methods to estimate the data using a Tobit regression model and OLS method. Liquidity and loan repayment were found to affect loans from the Iraqi Banks, while the effects of interest rate and borrowers were not statistically significant. The outcome of Tobit and OLS estimations indicate that bias will result when estimating Iraqi bank loans using OLS if bank loans are limited.

Prahutama *et al.* [10] used a Tobit regression model to study factors that affect household expenditure on education in Semarang city. The dependent variable used in this study is household expenditure for education. The independent variables used include the Education of the Head of the Household, Occupation of the Head of the household, number of household members, Number of Working Household Members, the proportion of household members who attend school in Junior High School, Senior High School and College, and food expenditure in households and regions. Based on the Tobit regression analysis proportion of household members who are taking education in college is the most significant contribution to the high cost of household expenditure.

Ahmed [11] applied a Tobit (Truncated), (censored) data regression models and multiple regression with the least square method for persons whose levels exceed 120 g/dl under the risk of diabetes injure, in the sample data (n = 500) on the assumption that blood sugar (y), depends on the explanatory (Age: X1, Cholesterol: X2 gram/deciliter, and Triglycerides: X3 gram/deciliter). The results revealed that the censored regression model was more applicable than the other regression models (truncated, and multiple regression), the two factors (Age and triglycerides have highly significant effects on the blood sugar.

Ahmad *et al.* [12] used Tobit regression analysis and data envelopment analysis (DEA) to address some of the important working capital management policies and efficiency regarding the manufacturing sector of Pakistan. To achieve that data from 37 firms have been taken for the periods 2009–2014.

Tobit regression analysis concludes that the average period has significant negative impacts on efficiency and current ratio, gross working capital turnover ratio, and financial leverage ratio that have a positive significant impact on efficiency.

Samsudin *et al.* [13] applied the Tobit model and DEA to examine the efficiency of public hospitals in Malaysia and identify the factors affecting their performance. The study analysis was based on 25 public hospitals in the northern region of Malaysia. According to the result of this study found that the daily average number of admission, the number of outpatient per doctor, and hospital classification have significant influences on hospital inefficiencies.

Odah *et al.* [14] investigated the factors affect divorce decision, and determine the most important factors causing divorce in Iraq through using the Tobit regression model and probit regression model. The data were collected through the application of the questionnaire. According to Tobit regression analysis results, marital infidelity is the main reason for the increase in divorce cases, as well as the preoccupation of the couple with social networking sites. After using the probit model, it found that age, social media sites, and income have a significant impact on the decision to divorce.

Zorlutuna *et al.* [15] applied Tobit regression analysis for the measurement of lung cancer patients. Data taken from Sivas Cumhuriyet University Faculty of Medicine Research and Application Hospital Oncology Center consists of 535 patients who have lung cancer. Tobit regression results show that when the dependent variable phase of the patient's disease, the patient's gender, patient's condition, and the pathological consequences of the disease were found to be statistically significant variables. The sex of patient has positive effect on the stage of the disease, while pathological condition has negative influences.

Anastasopoulos *et al.* [16] provided a demonstration of Tobit regression as a methodological approach to gain new insights into the factors that significantly influence accident rates. Using 5 years of vehicle accident data from Indiana, the estimation results show that many factors relating to pavement condition, roadway geometrics, and traffic characteristics significantly affect vehicle accident rates.

4. TOBIT MODEL

The regression analysis is one of the statistical methods used to explain the relationship between explanatory variables and the dependent variable. Therefore, choosing an appropriate model for the available data is a necessity of this analysis. In many statistical analyses of individual data, the dependent variable is censored. If the dependent variable is censored, the use of a conventional regression model with this type of data will lead to a bias in the estimation of the parameters there for the best model for this type of data is the Tobit model [17]. The Tobit model family of statistical regression models defines the relationship between censored or truncated continuous dependent variables and some independent variables [18]. It has been used in many areas of applications, including dental health, medical research, and economics [2]. The Tobit model refers to a regression model where the range of dependent variables is limited in some ways [16]. A model invents by Tobin in which it is supposed that the dependent variable has a number of its values clustered at limited value, usually zero [19]. This model was first introduced statistical literature in the 1950s and was called "censored normal regression model." It has been used for health studies since the 1980s. The Tobit model is an efficient method for estimating the relationship from Probit between an explanatory variable and truncated or censored dependent variable. The origin of the Tobit model is from Probit analysis and multiple regressions. The benefit of this model, using all the information that either Probit models (or logit) or OLS, would allow separately [20].

4.1. The Structural Equation Model [21], [22]

The structural equation in the Tobit model is

$$y^{*}_{i=}X_i^{2} + e_i \tag{1}$$

Where $e_{i\sim} N(0,\sigma^2)$. y^* is a latent variable that is observed for values greater than τ and censored otherwise. The observed y is defined by the following measurement equation

$$y_i = \begin{cases} y^* \text{ if } |y^* > \tau \\ \tau_y \text{ if } |y^* \le \tau \end{cases} \tag{2}$$

In the typical Tobit model, we assume that τ=0, i.e., the data are censored at 0. T use we have

$$y_i = \begin{cases} y^* \text{ if } |y^* > 0 \\ 0 \text{ if } |y^* \le 0 \end{cases} \tag{3}$$

4.2. Estimations

As we have seen from earlier, the likelihood function for the censored normal distribution is

$$L = \prod_i^N [\frac{1}{\sigma} \varnothing \left(\frac{y-\mu}{\sigma} \right)]^{di} [1 - \varnothing(\frac{\mu-\tau}{\sigma})]^{1-di} \tag{4}$$

Where τ is the censoring point. In the traditional Tobit model, we set t=0 and parameterize μ as $X_i\beta$. This gives us the likelihood function for the Tobit model:

$$L = \prod_i^N [\frac{1}{\sigma} \varnothing\left(\frac{y_i - X_i\beta}{\sigma}\right)]^{di} [1 - \varnothing(\frac{X_i\beta}{\sigma})]^{1-di} \quad (5)$$

The log-likelihood function for the Tobit model is

$$\ln L = \sum_{i=1}^N \{d_i \left(-\ln\sigma + \ln\varnothing\left(\frac{y_i - X_i\beta}{\sigma}\right)\right) + (1-d_i)\ln\left(1 - \varnothing\left(\frac{X_i\beta}{\sigma}\right)\right)\} \quad (6)$$

The overall log-likelihood is made up of two parts. The first part corresponds to the classical regression for the uncensored observations, while the second part corresponds to the relevant probabilities that observation is censored.

5. TRUNCATION, CENSORING, (TRUNCATED AND CENSORED) DISTRIBUTION, AND MARGINAL EFFECT

The leading causes of incompletely observed data are truncation and censoring.

5.1. Truncation

The effect of truncation occurs when the observed data in the sample only drawn from a subset of a larger population [23]. On the other hand, a dependent variable in a model is truncated, if observations cannot be seen when taking value with a certain range. This means, both the independent and the dependent variables are not observed when the dependent variable is in that range [24]. There are two types of Truncation: from below and from above (Truncation from left and Truncation from right). Figs. 1 and 2 explain the probability distribution of Truncated from below [11].

5.2. Censoring

The idea of "censoring" is that some data above or below the threshold is misreported at the threshold. Hence, the observed data are generated by a mixed distribution with both a continuous and a discrete component. The censoring process may be explicit in the data collection process, or it may be a by-product of economic constraints involved in constructing the data set [24]. When the dependent variable is censored, values in a certain range are all transformed to (or reported as) a single value [25]. Fig. 3 Explain the probability distributions of Censored from below [11].

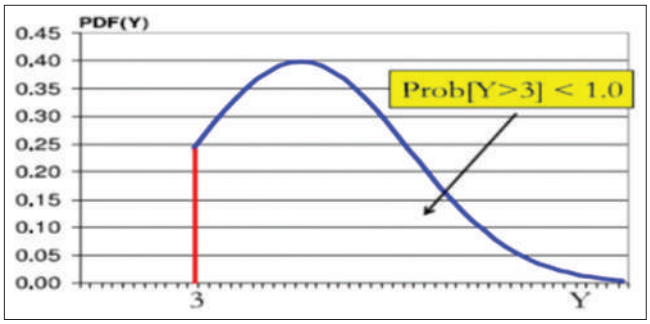

Fig. 1. Truncated from below with the probability distribution explaining (threshold = 3) [11].

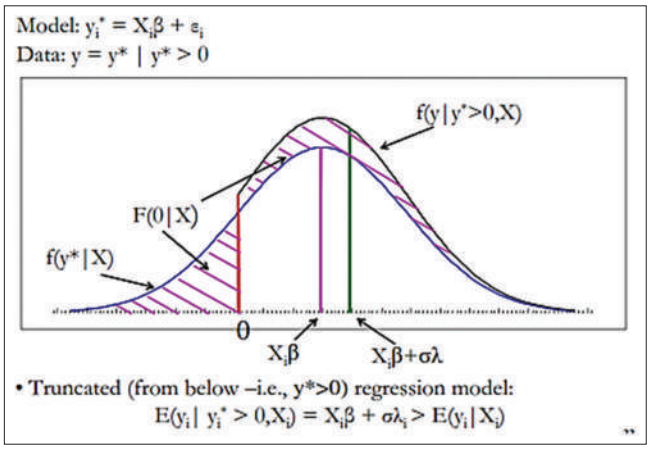

Fig. 2. Truncated normal distribution [11].

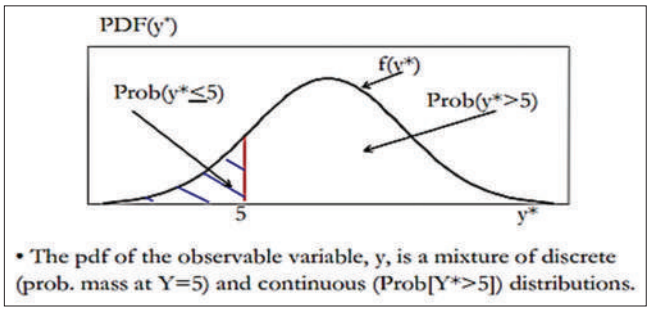

Fig. 3. Censored from below with the probability distributions explaining (threshold = 5) [11].

5.3. (Truncated and Censored) Distribution [21]

After formally considering the Tobit model, we need some results about truncated and censored normal distribution. These distributions are at the foundation of most models for truncation and censoring. The results are given for censoring and truncation on the left, which translate into censoring from below in the Tobit model. Corresponding formulas are given for censoring and truncation on the right, and both on the left and on the right.

5.3.1. Truncated normal distribution [21]

Let y denote the observed value of the dependent variable. Unlike the normal regression, y is the incompletely observed value of a latent depended variable y^*. Recall that with truncation, our sample data are drawn from a subset of a large population. In effects with truncation from below, we only observe $y=y^*$ if y^* is larger than truncation point τ. In effect, we lose the observation on y^* that are smaller or equal to τ when this is the case, we typically assume that the variable $y/y>\tau$ follows a truncated normal distribution. Thus, if a continuous random variable y has pdf f(y) and τ is constant. Then we have:

$$f\left(y / y>\tau\right)=\frac{f(y)}{P(y>\tau)} \tag{7}$$

We know that

$$P\left(y>\tau\right)=1-\Phi\left(\frac{\tau-\mu}{\sigma}\right)=1-\Phi\left(\alpha\right) \tag{8}$$

Where $\alpha=\frac{\tau-\mu}{\sigma}$ and $\Phi(.)$ is the standard normal cdf. The density of the truncated normal distribution is

$$f\left(y / y>\tau\right)=\frac{f(y)}{1-\Phi(\alpha)}=\frac{\frac{1}{\sigma}\phi(\frac{y-\mu}{\sigma})}{1-\Phi(\frac{\tau-\mu}{\sigma})}=\frac{\frac{1}{\sigma}\phi(\frac{y-\mu}{\sigma})}{1-\Phi(\alpha)} \tag{9}$$

Where $\Phi(.)$ is the standard normal pdf.

The likelihood function for the truncated normal distribution is

$$L=\prod_{i-1}^{N}\frac{f(y)}{1-\Phi(\alpha)} \tag{10}$$

Or

$$\ln L=\prod_{-1}^{N}(\ln\left[f(y)\right]-\ln\left[1-\Phi\left(\alpha\right)\right])$$

5.3.2. Censored normal distribution [21]

When a distribution is censored on the left, observations with values at or below τ are set to τ_y

$$y=\begin{cases} y^* \text{ if } y^*>\tau \\ \tau_y \text{ if } y^*\le\tau \end{cases} \tag{11}$$

The use of τ and τ_y is just a generalization of having τ and τ_y set as 0. If a continues variable y has a pdf f(y) and τ is constant, then we have

$$f\left(y\right)=\left[f(y^*)\right]^{d_i}\left[F(\tau)\right]^{1-d_i} \tag{12}$$

In other words, the density of y is the same as that for y^* for $y>\tau$ and is equal to the probability of observation of $y^*<\tau$ if $y=\tau$. d is an indicator variable that equals 1 if $y>\tau$. The observation is uncensored and is equal to 0 if $y=\tau$ the observation is censored.

$$\mathrm{P}\left(\text{censored}\right)=\mathrm{P}\left(y^*\le\tau\right)=\Phi\left(\frac{\tau-\mu}{\sigma}\right)=1-\Phi(\frac{\mu-\tau}{\sigma}) \tag{13}$$

And

$$\mathrm{P}\left(\text{uncensored}\right)=1-\Phi\left(\frac{\tau-\mu}{\sigma}\right)=\Phi(\frac{\mu-\tau}{\sigma}) \tag{14}$$

Thus, the likelihood function can be written as

$$L=\prod_{i}^{N}\left[\frac{1}{\sigma}\phi(\frac{y-\mu}{\sigma})\right]^{d_i}\left[1-\Phi(\frac{\mu-\tau}{\sigma})\right]^{1-d_i} \tag{15}$$

5.4. The Marginal Effect [11]

The estimated (β_k) vector shows the effect of (x_k) on (y). Thus, coefficients and the marginal effect of a variable is the effect of a unit change of this variable on the probability P(Y = 1 | X = x), given that all other variables are constant, The slope parameter of the linear regression model measures directly the marginal effect of the variable on the other variable. There are three possible Marginal Effect

1. Marginal effect on the latent dependent variable, y^*:

$$\frac{\partial E[y^*]}{\partial x_k}=\beta_k \tag{16}$$

Thus, the reported Tobit coefficients indicate how a one-unit change in an independent variable alters the latent dependent variable.

2. Marginal effect on the expected value for y for uncensored observations:

$$\frac{\partial E[y\mid y>0]}{\partial x_k}\beta_k\left\{1-\lambda(\alpha)\left[\frac{X_i\ \beta}{\rho}+\lambda(\infty)\right]\right\} \tag{17}$$

3. Marginal effect on the expected value for y (censored and uncensored):

$$\frac{\partial E[y]}{\partial x_k}=\Phi(\frac{X_i\,\beta}{\rho})\beta_k \tag{18}$$

TABLE 1: Samples are taken from (300) patients

ID	y: Blood pressure rate above 93.33 mmHg	X1: Age	X2: Blood urea	X3: BMI	X4: Waist circumference
1	96.67	28	132	17.82	110
2	105	31	140	21.8	65
3	86.54 (0)	35	50	35.16	32
4	104.67	55	70	28.72	102
5	45.66 (0)	32	35	28.96	101
6	90.41(0)	40	38	20.81	48
7	126.67	51	260.6	42.97	120
8	123.33	20	80	22.23	90
9	45.15(0)	25	36	32.53	115
.	.	.	.	.	.
.	.	.	.	.	.
.	.	.	.	.	.
98	96.67	32	148	21.91	60
99	77.88 (0)	33	47	24.56	60
100	123.33	77	113	25	97
.	.	.	.	.	.
.	.	.	.	.	.
197	100	40	172.4	16.89	100
198	96.67	35	147.8	37.5	60
199	93.33	73	195.4	20.9	60
200	88.99 (0)	34	67	21.12	55
.	.				
.	.				
299	93.33	65	129.7	20.68	37
300	146.67	50	120	25.71	112

TABLE 2: Descriptive statistics of dependent and independent variables in the study

Blood pressure (Y)	Min	Max	Mean	Median
	46.15	**146.67**	**82.25**	**100.00**
Age (X1)	18.00	87.00	51.39	49.00
Blood urea (X2)	17.40	404.00	118.86	117.00
BMI (X3)	13.84	42.97	25.46	23.44
Waist circumference (X4)	30.0	150.0	68.4	60.0

TABLE 3: Results of censored regression model: censored (formula=Y~X, left=0, right=Infinity, data=my data)

Coefficients	Estimate	Std. error	t value	Pr(>t)
Intercept	-5.85378	15.93610	-0.367	0.713
Age	0.80211	0.17584	4.562	5.08e-06 ***
Blood urea	0.48305	0.04437	10.886	2e-16 ***
BMI	-0.44822	0.45381	-0.988	0.323
Waist circumference	-0.06718	0.09777	-0.687	0.492

Total (*n*=300 observations, Left-censored=66 observations, Uncensored=234 observations, left censored (Y<93.33 then Y*=0: observation)

6. RESULTS

In this part, results will be presented to the applied side of the study using statically package (R program) version 3.6.1 and Stratigraphy program version 11.

TABLE 4: Results of the truncated regression model

Coefficients	Estimate	Std. error	*t* value	Pr(>t)
Intercept	3.669531	14.627314	0.2509	0.8019
Age	0.754674	0.160378	4.7056	2.531e-06 ***
Blood urea	0.432102	0.039962	10.8128	2.2e-16 ***
BMI	-0.429849	0.417015	-1.0308	0.3026
Waist circumference	-0.061769	0.089385	-0.6910	0.4895

Table 1 shows that a sample is taken from (300) patients with kidney diseases in dialyzes center in Shar Hospitals. The two levels of BP; high and low BP from the patients (as dependent variables) and some independent variables (age, blood, urea, BMI, and Waist circumference) were taken. We found the average of BP by MAP equation that is contain each (high and low) BP, we could not take high and low BP separately because we determined threshold point equal to 93.33 founded by MAP equation, equal to 12/8 mmHg which is a normal range of BP.

6.1. Descriptive Statistics of Dependent and Independent Variables

Table 2 shows all measures of descriptive statistics. The descriptive statistics give an overview of working with the minimum, maximum, mean, and median of (Age, blood urea, BMI, Waist Circumference), and the results are 18,

TABLE 5: Fitting multiple regression model (OLS) using Stratigraphy program

Model	Unstandardized confections		Standardized confections	*t*	Sig.	Collinearly statistic	
	B	Std. error	Beta			Tolerance	VIF
(Constant)	14.236	12.512		1.138	0.256		
Age	0.647	0.140	0.217	4.630	0.000	0.923	1.083
Blood urea	0.388	0.034	0.535	11.325	0.000	0.913	1.095
BMI	-0.315	0.358	-0.040	-0.881	0.379	0.982	1.019
Waist circumference	-0.048	0.077	-0.029	-0.627	0.531	0.976	1.024

TABLE 6: Model summery

Model	R	R square	Adjusted R square	Std. error of the estimate	Change statistics				
					R Square change	F change	df1	df2	Sig. F change
1	0.632a	0.399	0.391	34.85585	0.399	49.015	4	295	0.000

a. Predictors: (Constant), Waist Circumference, BMI, Blood Urea, Age

17.40, 13.84, and 30 respectively. The max numbers of those variables are 87, 404, 42.97, and 150 respectively. The mean and median of all independent variables are 51.39, 118.86, 25.46, 68.4, 49.00, 117.00, 23.44, and 60.0 respectively.

6.2. Fitting Tobit Model (Censored and Truncated): Regression Model Using Statically Package (R Program)

Table 3 shows that *P*-value: 2.22e-16 and Log-likelihood: -1278.455on 6 Df, wald- statistics 173.8 on 4 Df, Akaike information criterion (AIC)=2566.91, AIC={-2(log-likelihood)+2K}, where K is the number of model parameter plus the intercept. Log-likelihood is a measure of model fit the higher the number the better the fit, and the minimum AIC is the score for the best model. Mean square error (MSE)=0.9305

Table 4 shows that Log-likelihood= -1476.9 on 6 Df, and the AIC=2963.8. MSE=0.993.

From the output of Tables 5-7 shows that the results of fitting a multiple linear regression model to describe the relationship between BP and 4 independent variables. Since the *P*-value in the ANOVA table is <0.05, there is a statistically significant relationship between the variables at the 95.0% confidence level. Table 6 represent the R-Squared statistic indicates that the model as fitted explains 39.9258% of the variability in BP. The adjusted R-squared statistic, which is more suitable for comparing models with different numbers of independent variables, is 39.1112%. The standard error of the estimate shows the standard deviation of the residuals to be 34.8559. Table 7 shows the analysis Variance of dependent and independent variables.

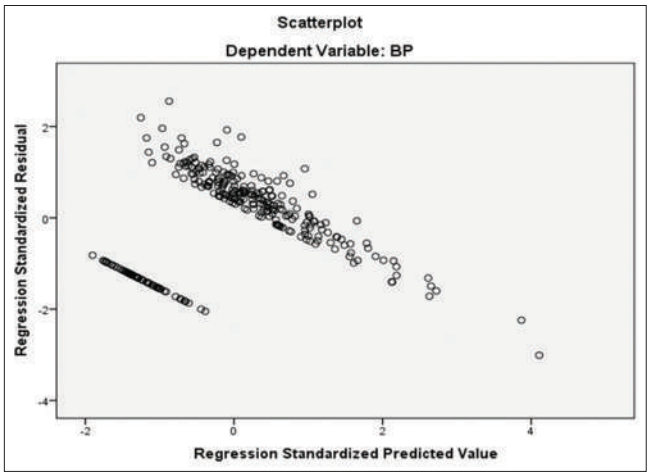

Fig. 4. Standardized residual for multiple regression model using (ordinary least square).

Fig. 4 is a standardized residual for multiple regression models using (OLS). It is clear that the (OLS) method not a suitable method when data censored.

7. DISCUSSION

Analyzing medical data with a Tobit model when it has a threshold point; it help experts (doctors and medical staffs) to identify factors affecting blood pressure in patients with kidney failure. In this study, the Tobit model (censored and truncated) regression model, and a multiple regression model with the least square method (OLS) applied to the data size (n=300) for the cases their rates are greater than or equal to (93.33). By taking the hypothesis that the (BP y) depends on the expletory variables (age, blood urea, BMI, and Waist

TABLE 7: Analysis of variance

Source	Sum of squares	Df	Mean Square	F-Ratio	P-Value
Model	238198.378	4	59549.595	49.015	0.000[b]
Residual	358404.477	295	1214.930		
Total (Corr.)	596602.856	299			

b. Dependent Variable: Blood Pressure

TABLE 8: Results of marginal effects

Coefficients	Marg. eff.	Std. error	*t* value	Pr(>t)
Age	0.772056	0.168918	4.5706	7.17e-06 ***
Blood urea	0.464948	0.042204	11.0168	2.2e-16 ***
BMI	-0.431430	0.436737	-0.9878	0.3240
Waist circumference	-0.064662	0.094095	-0.6872	0.4925

circumference) and comparing their results, the following important points are concluded below.

The result in Table 2 shows all measures of descriptive statistics. The descriptive statistics give an overview of working with the minimum, maximum, mean, and median of (age, blood urea, BMI, and Waist Circumference), and the results are 18, 17.40, 13.84, and 30, respectively. The maximum numbers of those variables are 87, 404, 42.97, and 150, respectively. The mean and median of all independent variables are 51.39, 118.86, 25.46, 68.4, 49.00, 117.00, 23.44, and 60.0, respectively.

The results of analysis censored regression model in Table 3 show the final result with all significant variables for the phenomenon study, the results of parameter estimation and t value analysis, the significant factors affecting BP. *P* = 2.22e-16 and Log-likelihood= -1278.455 on 6 Df, Wald statistic= 173.8 on 4 Df, AIC=2566.91. The Log-likelihood is a measure of the model fit the higher number of it is a better fit. The minimum AIC is the score for the best model. The MSE is equal to 0.9305. We know that the (β) is the relationship between the response variable and covariates, if (+β) it means a positive relationship and if (-β) means a negative relationship. Through the result in Table 3 appear the relationship between the variables (age and blood urea) is positive because the variables have a positive relationship with the dependent variables (BP) and those variables (Age and blood urea) have highly significant effects on BP. Furthermore, the relationship between (BMI) and BP is negative. If there is an increase in (BMI) by one unit the (BP) decreases by (-0.44822). The factors (BMI and Waist circumference) appeared to have no significant effects on BP.

From Tables 3-8 show that the censored regression model for the samples is a more suitable model than other regression models (Truncated, Marginal, and Multiple). This result found by comparing their AIC, log-like values, and MSE.

The censored with the marginal effects from Table 8 shows that the two variables (age and blood urea) have highly significant effects. The changes in years make BP significantly increasing by 0.77%. This means that the effect of age for any case in the sample with Std. error is by 0.16%. Furthermore, one unit of blood urea for each point increases by 0.46% with stander error (0.04).

In the result of multiple regression models, using (OLS) method, we detected that since the p-value in the ANOVA table is <0.05, there is a statistically significant relationship between the variables at the %95 confidence interval the R-square statistic indicates that the model as fitted explains 0.39 of the variability BP. And theoretically, as defined, the OLS (unconditional estimates) are bias.

8. CONCLUSION

In this study, both Tobit regression analysis and OLS analysis were used for studying factors affecting the BP. In this work, the data collected from 300 patients in a dialysis center at Shar hospital in Sulaimani city. The two levels of BP; high and low from the patients (as dependent variables) and some independent variables (age, blood, urea, BMI, and Waist circumference) were taken. Each patient has own specific BP (high and low). Then, we could not take high and low BP separately for our study. That is why the MAP was performed. It is an average arterial pressure contains high and low BP. When studying BP as a dependent variable, we find that variable data are censored at zero. In this case, the Tobit model is most suitable model to use. It was found that the two factors (age and blood urea) have highly significant effects on BP. However, the two variables (BMI and Waist circumference) appeared to have no effects on the dependent variable. The comparison of the result from Tobit and OLS estimations shows that biased can result when estimation BP using OLS if BP restricted at the threshold point

REFERENCES

[1] T. Amemiya. "Tobit models: A survey". *Search Results Journal of Economics*, vol. 24, no. 1-2, pp. 3-61, 1984.

[2] W. Wang and M. E. Griswold. "Natural interpretations in Tobit regression models using marginal estimation methods". *Statistical Methods in Medical Research*, vol. 26, no. 6, pp. 2622-2632, 2017.

[3] D. C. Crews, A. K. Bello and G. Saadi. “2019 World kidney day editorial-burden, access, and disparities in kidney disease”. *Brazilian Journal of Nephrology*, vol. 41, pp. 1-9, 2019.

[4] R. A. Preston, I. Singer, and M. Epstein. “Renal parenchymal hypertension: Current concepts of pathogenesis and management”. *Archives of Internal Medicine*, vol. 156, no. 6, pp. 602-611, 1996.

[5] J. A. Staessen, Y. Li, A. Hara, K. Asayama, E. Dolan and E. O’Brien. “Blood pressure measurement anno 2016”. *American Journal of Hypertension*, vol. 30, no. 5, pp. 453-463, 2017.

[6] R. N. Kundu, S. Biswas and M. Das. “Mean arterial pressure classification: A better tool for statistical interpretation of blood pressure related risk covariates”. *Cardiology and Angiology: An International Journal*, vol. 6, no. 1, pp. 1-7, 2017.

[7] D. Yu, Z. Zhao and D. Simmons. “Interaction between mean arterial pressure and HbA1c in prediction of cardiovascular disease hospitalisation: A population-based case-control study”. *Journal of Diabetes Research*, vol. 2016, p. 8714745, 2016.

[8] C. Wilson and C. A. Tisdell.“OLS and Tobit estimates: When is substitution defensible operationally?” In: *Economic Theory, Applications and Issues Working Papers*, University of Queensland, School of Economics, Queensland , 2002.

[9] M. H. Odah, A. S. M. Bager and B. K. Mohammed. “Tobit regression analysis applied on Iraqi bank loans”. *American Journal of Applied Mathematics and Statistics*, vol. 7, no. 4, p. 179, 2017.

[10] A. Prahutama, A. Rusgiyono, M. A. Mukid and T. Widiharih. “Analysis of Household Expenditures on Education in Semarang City, Indonesia Using Tobit Regression Model”. In: *E3S Web of Conferences*, vol. 125, p. 9016, 2019.

[11] N. M. Ahmed. “Limited Dependent Variable Modelling (Truncated and censored Regression models) with Application”. Vol. 7377. Cambridge University Press, New York, pp. 82-96, 2018.

[12] M. F. Ahmad, M. Ishtiaq, K. Hamid, M. U. Khurram and A. Nawaz. “Data envelopment analysis and Tobit analysis for firm efficiency in perspective of working capital management in manufacturing sector of Pakistan”. *International Journal of Economics and Financial Issues*, vol. 7, no. 2, pp. 706-713, 2017.

[13] S. Samsudin, A. S. Jaafar, S. D. Applanaidu, J. Ali and R. Majid. “Are public hospitals in Malaysia efficient? An application of DEA and Tobit analysis”. *Southeast Asian Journal of Economics*, vol. 4, no. 2, pp. 1-20, 2016.

[14] M. H. Odah, A. S. M. Bager and B. K. Mohammed. “Studying the determinants of divortiality in Iraq. A two-stage estimation model with tobit regression”. *International Journal of Applied Mathematics and Statistics*, vol. 7, no. 2, pp. 45-54, 2018.

[15] P. Zorlutuna, N. A. Erilli and B. Yücel. “Lung cancer study with tobit regression analysis: Sivas case”. *Eurasian Econonometrics, Statistics and Emprical Economics Journal*, vol. 3, no. 3, pp. 13-22, 2016.

[16] P. C. Anastasopoulos, A. P. Tarko and F. L. Mannering. “Tobit analysis of vehicle accident rates on interstate highways”. *Accident Analysis and Prevention*, vol. 40, no. 2, pp. 768-775, 2008.

[17] A. Henningsen. “Estimating censored regression models in R using the censReg Package”. *R Packag Vignettes*, Vol. 5. University of Copenhagen, Copenhagen, p. 12, 2010.

[18] A. C. Michalos. *Encyclopedia of Quality of Life and Well-Being*, Springer, Berlin, 2014.

[19] M. H. Odah. “Asymptotic least squares estimation of tobit regression model. An application in remittances of Iraqi immigrants in Romania”. *International Journal of Applied Mathematics and Statistics*, vol. 8, no. 2, pp. 65-71, 2018.

[20] C. Ekstrand and T. E. Carpenter. “Using a tobit regression model to analyse risk factors for foot-pad dermatitis in commercially grown broilers”. *Preventive Veterinary Medicine*, vol. 37, no. 1-4, pp. 219-228, 1998.

[21] J. S. Long. *Regression Models for Categorical and Limited Dependent Variables*. Vol. 7. Sage Publications, Thousand Oaks, 1997.

[22] A. Flaih, J. Guardiola, H. Elsalloukh and C. Akmyradov. “Statistical inference on the ESEP tobit regression model”. *J. Stat. Appl. Probab. Lett.*, vol. 6, pp. 1-9, 2019.

[23] B. R. Humphreys. “Dealing with zeros in economic data”. *University of Alberta, Department of Economics*, vol. 1, pp. 1-27, 2013.

[24] K. A. M. Gajardo. “*An Extension of the Normal Censored Regression*”. Pontificia Universidad Catolica De Chile, Santiago, Chile, 2009.

[25] W. H. Greene. *Limited Dependent Variables Truncation, Censoring and Sample Selection*. Sage, Thousand Oaks, CA, 2003.

ORIGINAL RESEARCH ARTICLE UHD JOURNAL OF SCIENCE AND TECHNOLOGY

Monthly Maximum load Demand Forecasting for Sulaimani Governorate Using Different Weather Conditions Based on Artificial Neural Network Model

Najat Hassan Abdulkareem

MoEI (Ministry of Electricity-KRG), Electricity control center, Sulaimani/Iraq

ABSTRACT

Medium-term forecasting is an important category of electric load forecasting that covers a time span of up to 1 year ahead. It suits outage and maintenance planning, as well as load switching operation. There is an on-going attention toward putting new approaches to the task. Recently, artificial neural network has played a successful role in various applications. This paper is presents a monthly peak load demand forecasting for Sulaimani (located in North Iraq) using the most widely used traditional method based on an artificial natural network, the performance of the model is tested on the actual historical monthly demand of the governorate for the years 2014–2018. The standard mean absolute percentage error (MAPE) method is used to evaluate the accuracy of forecasting models, the results obtained show a very good estimation of the load. The MAPE is 0.056.

Index Terms: Actual Load, Artificial Neural Network, Midterm Monthly Load Forecast, Multilayer Perceptron, Predicted Load. Yearly Ahead

1. INTRODUCTION

Power system planning starts with the forecast of load requirements. With the fast growth of power systems networks and increase in their complexity, many factors have become influential in electric power generation, demand, or load management. The forecasting of electricity demand has been one of the major research fields in electrical engineering. Massive investment decisions for network reinforcement and expansions are made based on the load forecast. Hence, it is necessary to have accurate load forecast to carry out proper planning [1], [2]. Although, load forecasting is one of the major factors for economic operation of power systems. Future load forecasting is also important for network planning, infrastructure development, and so on.

Power system load forecasting can be classified into three categories, namely, short-term, medium-term, and long-term load forecasting. The periods for these categories are not defined clearly in literature [2].

Thus, different authors use different time periods to define these categories. However, roughly, short-term load forecasting (STLF) covers hourly to weekly forecast. These forecasts are often needed for day-to-day economic operation of power generating units [3].

Midterm load forecasting has period time in 3 months–3 years, maintenance of plants and networks is often roofed in these types of forecast.

Access this article online

DOI: 10.21928/uhdjst.v4n2y2020.pp10-17

E-ISSN: 2521-4217
P-ISSN: 2521-4209

Corresponding author's e-mail: Najat Hassan Abdulkareem, MoEI (Ministry of Electricity-KRG), Electricity control center, Sulaimani/Iraq. E-mail: Qaradakhi@gmail.com

Received: 03-05-2020 Accepted: 07-01-2020 Published: 07-05-2020

Long-term forecasting, on the other hand, deals with forecast from few months to 1 year. It is primarily intended for capacity expansion plans, capital investments, and corporate budgeting. These types of forecasts are often complex in nature due to future uncertainties such as planning and extension of existing power system networks for both the utility and consumers required long-term forecasts [3].

The system load is a random non-stationary process composed of thousands of individual components. The system load behavior is influenced by a number of factors, which can be classified as economic factors, time, weather, and random effects. The economic environment in which the utility operates has a clear effect on the electric demand consumption patterns, such as the service area demographics, level of industrial activity, and changes in farming sector [4].

For the present, there are many algorithms for load forecasting in the computation intelligence such as fuzzy logic (Fs) [5], neural network, and genetic [6]. Many research purposed the article for load forecasting in the power system field: STLF using autoregressive integrated moving average (ARIMA) and artificial neural network (ANN) method based on non-linear load, a novel method approach to load forecasting using regressive model and ANN the combination of ANN, genetic algorithm, and Fs method is proposed for adjusting STLF of electric system. Genetic algorithm is used for selecting better rules and backpropagation algorithm is also for this network, papers show that more accuracy results and faster processor than other forecasting methods [7].

The aim of this paper is to provide a monthly peak demand forecast for Sulaimani Governorate (located in North Iraq). This forecast is of special importance to this region because of the present shortage of generating capacity and the need for extensive load shedding. It is thus important to estimate what the near-term demand will be, especially in the peak demand months, as a key input in determining the availability of enough generating capacity to meet the demand [8].

Sulaimani is one of the four Northern Governorates of Iraq (Iraqi Kurdistan Region). It is bounded by Iran; Erbil Governorate and Kirkuk Governorate. The land area of the governorate is about 18,240 Sq.Km. The city of Sulaimani is located in 335 km northeast to Baghdad.

This study is tried to find out the way to forecast the electrical power load in Sulaimani Governorate power distribution network using ANN with the help of MATLAB software. The input is involved three feature; precipitation, temperature, and humidity. These three parameters effect on power consumption directly. Mean square error is used as performance measure.

The method of learning in ANN which is used in this paper is feed forward backpropagation. Finally, by comparing different cases is tried to find best solution to estimate the load demand.

This dataset consists of 5 years of average monthly load collected from the Electricity Control Center (ECC) of Kurdistan Region in Iraq. The data are accumulated daily and involve the maximum electrical demand load in Mega Watt (MW) from January 1, 2014, to October 31, 2018. The dataset is also accompanied by temperature, humidity, and precipitation collected, which can be used to forecast the demand.

2. THE LOAD PROFILE OF SULAIMANI GOVERNORATE

There is a severe shortage of electricity supply in Sulaimani Governorate. Main sources of electricity supply are Dokan hydropower station (5×80 MW), Derdandikhan hydropower station (3×83 MW), Sulaimani combined cycle gas power plant which is consists of 10 units (8 simple cycle 125 MW per unit and 2 combined cycle 250 MW per unit), Tasluja Heavy Fuel Power Plant (51 MW), and Bazyan Gas Power Plant (4×125 MW), which is also supply Erbil and Dhuk Governorates. (For explain this: All of this power stations cannot work in its full capacity. And the generate power also go to Erbil and Duhok, therefore, the Sulaimani Governorate demand every time is bigger than the power generation and that is the problem).

However, the available supply from the above sources dose not meets the power requirements in the governorate. Consumers are provided for a very short duration, sometimes 10 h per day depending on the generation capacity. Monthly energy consumption demand (unit in MWh) data is recorded form (ECC) Kurdistan Region from 2014 to 2018. Fig. 1 shows the relationship between energy consumption demand and time (corrected divide each year into 12 months).

We consider the period from 2014 to 2018 to establish the parameters in forecast model. The original signal (behavior) of energy consumption demand is shown in Fig. 1. It grew the higher demand every year. The maximum demand is occurred on months 11, 12, 1, 2, 6, 7, and 8 and minimum demand is occurred in months 3, 4, 5, 9, and 10. Kurdistan regions climate is characterized by cool winters and hot summers. This extreme temperature swing affects the demand and

producing a typical summer and winter peak demand periods each year. The monthly peak temperature profile for the years 2014–2018 is shown in Fig. 2.

2.1. Forecasting Methods

In terms of lead time, load forecasting is divided into four categories:

- Long-term forecasting with the lead time of more than 1 year
- Midterm forecasting with the lead time of 1 week–1 year
- STLF with the lead time of 1 day–1 week
- Very STLF with the lead time shorter than 1 day.

The research approaches of load forecasting can be mainly divided into two categories:

Statistical methods and artificial intelligence methods. In statistical methods, equations can be obtained showing the relationship between load and its relative factors after training the historical data, while artificial intelligence methods try to imitate human beings way of thinking and reasoning to get knowledge from the past experience and forecast the future load. Some main STLF methods are introduced as follows. Regression methods regression is one of most widely used statistical techniques. For load forecasting, regression methods are usually employed to model the relationship of load consumption and other factors such as weather, day type, and customer class. Time series methods are based on the assumption that the data have an internal structure, such as autocorrelation, trend, or seasonal variation. The methods detect and explore such a structure. Time series have been used for decades in such fields as economics, digital signal processing, as well as electric load forecasting. In particular, ARMA (autoregressive moving average), ARIMA, and ARIMAX (ARIMA with exogenous variables) are the most often used classical time series methods. ARMA models are usually used for stationary processes while ARIMA is an extension of ARMA to non-stationary processes. ARMA and ARIMA use the time and load as the only input parameters. Since load generally depends on the weather and time of the day, ARIMAX is the most natural tool for load forecasting among the classical time series models. Similar day approach, this approach is based on searching historical data for days within 1, 2, or 3 years with similar characteristics to the forecast day. Similar characteristics include weather, day of the week, and the date. The load of a similar day is considered as a forecast. Instead of a single similar day load, the forecast can be a linear combination or regression procedure that can include several similar days. The trend coefficients can be used for similar days in the previous years. Expert systems are heuristic models, which are usually able to take both quantitative and qualitative factors into account. A typical approach is to try to imitate the reasoning of a human operator. The idea is then to reduce the analogical thinking behind the intuitive forecasting to formal steps of logic. A possible method for a human expert to create the forecast is to search in history database for a day that corresponds to the target day with regard to the day type, social factors, and weather factors. Then, the load values of this similar day are taken as the basis for the forecast.

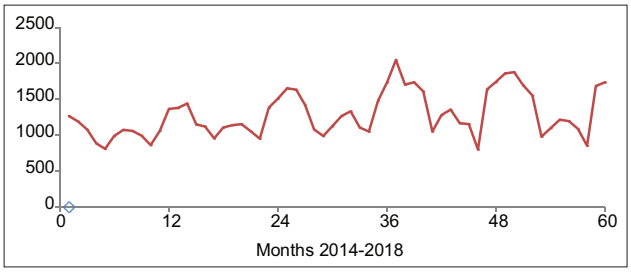

Fig. 1. Monthly energy consumption demand of Sulaimani city from January 2014 to December 2018 (DCC).

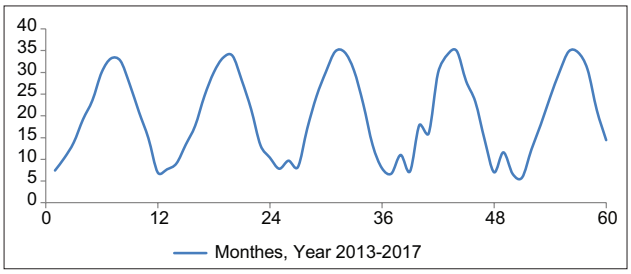

Fig. 2. Average temperature of Sulaimani Governorate from 2013 to 2017.

Fs is a generalization of the usual Boolean logic used for digital circuit design. An input under Boolean logic takes on a value of "True" or "False." Under Fs an input is associated with certain qualitative ranges. For instance, the temperature of a day may be "low," "medium," or "high." Fs allows one to logically deduce outputs from fuzzy inputs. In this sense, Fs is one of a number of techniques for mapping inputs to outputs. Among the advantages of the use of Fs are the absence of a need for a mathematical model mapping inputs to outputs and the absence of a need for precise inputs. With such generic conditioning rules, properly designed Fs systems can be very robust when used for forecasting. Integration of different algorithms are many presented methods for (STLF), it is natural to combine the results of several methods. One simple way is to get the average value of them, which can lower the risk of individual unsatisfactory prediction. A more complicated and reasonable

References:

1. http://www.motac.gov.krd/news.aspx?id=1226.
2. The (Sulaimani Directory of Meteorological and Seismology Data) Page on Facebook: shorturl.at/gmyY9.

way is to get the weight coefficient of every forecasting method by reviewing the historical prediction results. The comprehensive result is deduced by weighted average method.

2.2. Forecasting Requirements

This subsection lists and describes the requirements to develop a user friendly and a good load forecasting tool. A good load forecasting tool should fulfill the requirement of accuracy, fast speed, friendly interface, and automatic data access. Accuracy the most important requirement of designing a load forecasting tool is its prediction accuracy. As mentioned before, good accuracy is the basis of economic dispatch, system reliability, and electricity markets. The main goal of this paper is to make the forecasting result as accurate as possible. Fast speed employment of the latest historical data helps to increase the accuracy. When the deadline of the forecasted result is fixed, the longer the runtime of the forecasting program is, the earlier historical data can be employed by the program. Therefore, the speed of the forecasting is a basic requirement of the forecasting program. Programs with too long training time should be abandoned and new techniques shortening the training time should be employed.

Friendly interface the graphical user interface of the load forecasting tool should be easy, convenient, and practical. The users can easily define what they want to forecast, whether through graphics or tables. The output should also be with the graphical and numerical format, in order that the users can access it easily.

Automatic data access the historical data is stored in the database. The load forecasting tool should be able to access it automatically and get the needed data.

2.3. Advantages and Disadvantages of Load Forecasting

2.3.1. Advantages

1. It enables the utility company to plan well since they have an understanding of the future consumption or load demand
2. Useful to determine the required resources such as fuels required to operate the generating plants as well as other resources that are required to ensure uninterrupted and yet economical generation and distribution of the power to the consumers. This is important for all short-, medium-, and long-term planning
3. Planning the future in terms of the size, location, and type of the future generating plant is the factors which are determined by the help of load forecasting
4. Provides maximum utilization of power generating plants. The forecasting avoids under generation or over generation

2.3.2. Disadvantages

1. It is not possible to forecast the future with accuracy. The qualitative nature of forecasting, a business can come up with different scenarios depending on the interpretation of the data
2. Organizations should never rely 100% on any forecasting method
   However, an organization can effectively use forecasting with other tools of analysis to give the organization the best possible information about the future.
3. Making a decision based on a bad forecast can result in financial ruin for the organization, so the decisions of an organization should never base solely on a forecast

3. LOAD FORECASTING USING ANN

A large variety of artificial intelligence and statistical techniques has been developed for load forecasting. Some of the methods such as similar day approach, regression methods, time series, neural network, expert systems, and Fs are used nowadays, among them, ANN is one of a good choice to apply for the load demand forecasting problem because this technique is not requiring explicit models to represent the complex relationship between the load demand and factors. ANN methods are particularly attractive, as they have the ability to handle the non-linear relationships between load and the factors affecting it directly from historical data. ANNs use a dense interconnection of computing nodes to approximate non-linear functions each node constitutes a neuron and performs the multiplication of the input signals by constant weight, sums up the results, and maps the sum to a nonlinear activation function, the result is then transferred to its input [9].

3.1. Basic Theory – Feed Forward Backpropagation

In this paper, we use backpropagation feed forward neural network to model the problem. Fig. 1 shows an example of ANN structure; each neural network has at least three layers, input layer, a hidden layer, and output layer. In a typical multilayer network, the input units which are denoted by Xi are connected to all hidden layer units which are defined by Yj and the hidden layer units are connected to all output layer units which are denoted by Zk. The elements Wij or Vij of the weight matrix associate the weight of each connection between the input to hidden and hidden to output layer units. The hidden and output layer units also receive signals from weighted connections (bias) from units whose values are always 1.

In each output and hidden units, the incoming signals from the previous layer sum together and apply an activation function to form the response of the net for a given input pattern.

$$x_i: input\ i=1,2,\ldots n \quad (1)$$

$$(Y\,j) = f\ bj + \sum X\,i\,W\,ij \quad (2)$$

$$(Z\,k) = f\ b\,k + \sum Y\,j\,V\,jk \quad (3)$$

To determine the error, each output will be compare its output (Zk) with the actual output value which is identified by dk. Then, according to the calculated error, δk will be determined. δk is a factor which is used to distribute the error at Zk back to all units in the previous layer.

$$\delta\,k = f'(Z\,k)(d\,k - Z\,k) \quad (4)$$

Zk: Calculated output for each layer
Dk: Actual output
δk: the factor for calculation the errors.

Factor δj will be computes for each hidden unit. This factor is a weighted sum of all the back propagated delta terms from units in the previous layer multiplied by the derivative of the activation function for that unit.

$$\delta\,j = f\ '(Y\,j)\sum \delta\,k\ V\,jk \quad (5)$$

In the next step, the new value of bias and each element of weight matrix will be calculated where η is a learning rate coefficient that is given a value between 0 and 1 at the start of training.

$$b\,j\,(\text{new}) = b\,j\,(\text{old}) + \eta\delta\,j \quad (6)$$

$$W\,ij\,(\text{new}) = W\,ij\,(\text{old}) + \eta\delta j\,\text{Xi} \quad (7)$$

In each irritation, it will be checked if the stop condition is occurred or not. The stop condition can be reaching error threshold, defined irritation, etc. [10], [11].

3.2. Problem Formulation and Methodology

The following steps have been followed by the investigator to formulate the above said problem:

i. First of all historical weather and load data is scrutinized. All monthly and daily predictions have been read
ii. Then, database has been created by the investigator for developing load forecasting model
iii. Accordingly, temperature and humidity have been differentiated as average value
iv. Furthermore, the rainy season and predicted rainfall have been considered for making the algorithm for midterm load forecasting
v. After this classification some ANN technique has been used to train these input variables for getting the expected outcome. System has been simulated with the help of MATLAB/SIMULINK
vi. Then, percentage error (PE) has been calculated for the given forecasting model.

3.3. Accuracy of Forecasted

To evaluate forecasting accuracy of the whole procedure, the following indices have been calculated in Equations (8 and 9), mean square error (MSE) for each month of forecasting:

$$MSE = \sum_{i=1}^{M} \frac{\left(Actiual_i - Forecast_i\right)^2}{M} \quad (8)$$

Mean absolute percentage error (MAPE) given by:

$$MAPE = \frac{1}{M}\sum_{i=1}^{M} \frac{\left(Actiual_i - Forecast_i\right)^2}{Actiual_i} \times 100 \quad (9)$$

Where, *Actual* is the real value of monthly load demand at the each year, *Forecasted* is the forecasted value in the same year, and *M* is month [12], [13].

After forecasting the load patterns for each test month, these forecasts were compared with the real load data, and the average error percentages were calculated. In comparing different models, the average percentage forecasting error is used as a measure of the performance. The reason for using the average percentage error is the fact that its meaning can be easily understood. It is also the most often used error measure in the load forecasting literature used as reference of this work and therefore allows for some comparative considerations (although the results are not directly comparable in different situations).

However, when both measures calculated on some test models with relatively small errors, the orders of preference were in practice the same with both measures. Therefore, the average forecasting error will be used throughout this work. In case of the monthly forecast, the training algorithms of gradient backpropagation and Levenberg–Marquardt were compared, whereas in case of the monthly forecast, the simulation was done. Although Levenberg–Marquardt is a very fast training algorithm, it often has given fairly inaccurate results due to the large approximations it makes while calculating the Hessian matrix [14], [15].

From years 2014 to 2018 were chosen in different seasons.

of the year. The load of each month of the dataset was forecast without using the actual load data of that month.

Thereby, the monthly forecasting model was applied for each test of monthly peak demand recursively for all months in the year. After forecasting the load patterns for each test month, these forecasts were compared with the real load data, and the average error percentages were calculated.

4. CASE STUDY AND TEST RESULTS

The present study develops midterm electric load forecasting using neural network; based on historical series of power demand, the neural network chosen for this network is feed forward network, case study and test results will be present in this section by following:

4.1. Case Study

This study used the historical information or data for proposing ANN model to load forecasting as following:

Monthly energy consumption demand *(MWh)*, the humidity *(H)*, precipitation (P), and temperature (T). All of data information are recorded from 2014 to 2018.

Table 1 shows the block model for 2 years ahead demand forecasting which have four inputs: The historical load demands from −12 months to −48 months, maximum temperature from 1 months to −48 months, humidity from 1 months to −84 months, and precipitation 1 months to −48 months. These are feature inputs to ANN. The output of this model is the load demand of Sulaimani Governorate that is +24 months ahead or 2 years ahead. Note that: The historical load Demands: year 2018 (0), 2017 (−12), 2016 (−24), 2015 (−36), and 2014 (−48).

Various network models based on multilayer backpropagation feed forward architecture are tested with different designs and different configurations of hyperparameters (one and two) hidden layer with neurons of 10, 12, 15, and different transfer functions. After several trials, the near-optimal values have been taken. The information about different cases (for 1 month January 2014, for example) is described in Table 1. A backpropagation network with momentary and with adaptive learning rate was trained and the neural network can forecast future load 1 day peak load per month ahead given in various inputs to the network. A sigmoid transfer function was used in the hidden layer while a linear transfer function was used in. It has been observed that using 12 neurons and transfer function of logsig gave less percentage error for nearly all months. And depending on this result, the forecasted values (using model in Table 1) can be observed. Fig. 3 represents the results of 2 years forecasting.

TABLE 1: The model for 2 years ahead forecasting

−48	−36	−24	−12	0	12	+24
2014	2015	2016	2017	2018	2019	2020
Train						
test						
forecasted value						

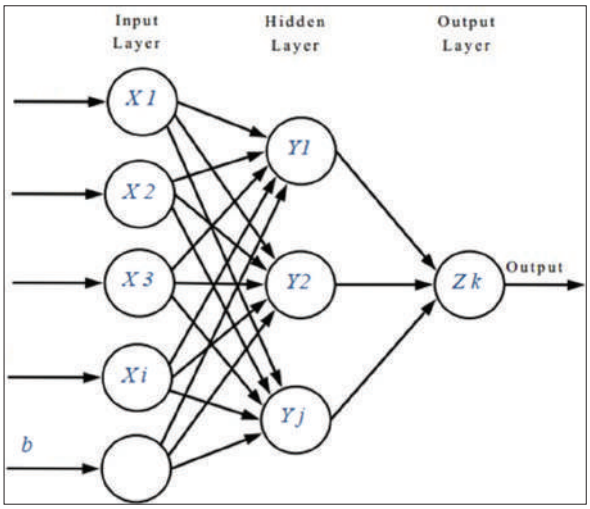

Fig. 3. Artificial neural network structure used in midterm load forecasting.

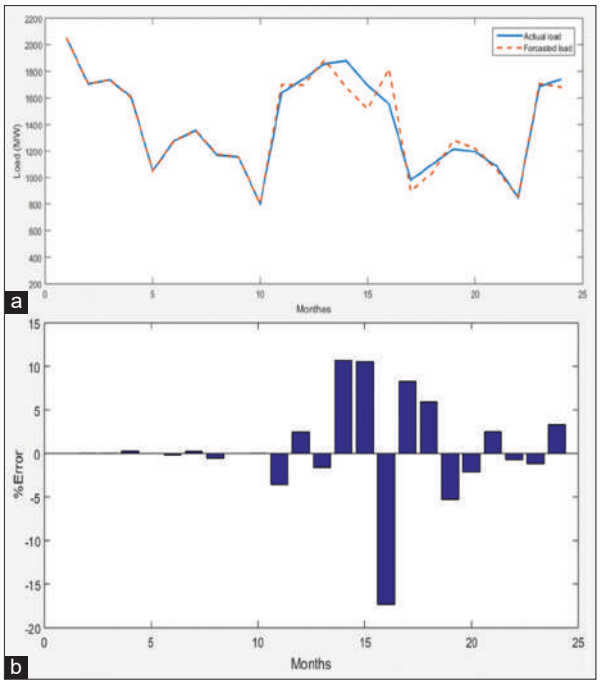

Fig. 4. (a) Actual and forecasted load demand for 24 months (b) percentage error for 24 months.

Fig. 4(a) and (b) shows the value of actual load demand in 2016–2017 on dash line. Solid line shows the forecasted values. The mean absolute percentage error is 5.6%.

Using the model developed, load, error, and % error of all the months have been calculated. Then, error and % error are found out using the below given formula.

$$\text{Error} = \text{Output by NN} - \text{Actual output}$$

$$\%\ \text{Error} = (\text{Error}/\text{actual output}) \times 100$$

Actual output, output by NN, error, and % Error in 2016 and 2017 are given in Tables 2 and 3.

TABLE 2: Percentage error of different cases for January 2013

No. of hidden layer	Neurons	Transfer function	PE
1	10	LOGSIG	−53.5031
	12		−25.4602
	15		−25.4602
1	10	TANSIG	0
	12		−119.092
	15		0
2	10	LOGSIG	−0.33203
	12		−40.0727
	15		−56.5244

TABLE 3: Actual, forecasted load demand, and percentage error

Month	Actual demand	Forecasted demand	%error
1	2050	2050	0
2	2176	2175.797	0.011883
3	2179	2178.866	0.00774
4	1839	1835.985	0.249687
5	1199	1199	0
6	1393	1395.096	−0.16384
7	1524	1520.822	0.234717
8	1468	1474.335	−0.54235
9	1324	1324	0
10	1421	1420.9246	0.009407
11	1640	1699	−3.59756
12	1740	1696.65	2.491406
13	2119	2149.73	−1.60011
14	2119	1918.241	10.67865
15	2086	1907.967	10.5034
16	1908	2179.83	−17.3104
17	1440	1358.92	8.273469
18	1102	1037	5.914468
19	1268	1332.29	−5.29136
20	1194	1219.61	−2.14489
21	1390	1362.76	2.508287
22	1391	1397.36	−0.74736
23	1191	1211	−1.18554
24	1285	1228.05	3.274871

(The error is different because of the different in actual output and the output in the NN).

5. CONCLUSIONS

ANN models provide a very useful tool for midterm load forecasting. Radically different from statistical methods, these models have shown promising results in load forecasting. The aim of this paper is to develop a practical model for the peak load demand of Sulaimani Governorate which gives a best expectation values with minimum errors so that directorate of central control planners can estimate what the near-term demand will be. The monthly peak demand estimation is a key input in determining if there is enough generating capacity available to meet the demand.

The result of this research shows the high efficiency of the neural network in estimating the electrical power load and this is because ANN can define the nonlinear relation between the weather data and the load with high accuracy.

Midterm monthly load forecasting using ANN can lead to very good results if the ANN structure is well designed and training data selection is appropriate.

As it can be seen on the table above, the electricity demand is increasing to the peak in January, February, and December every year. From this point, Sulaimani city needs extra investment on electricity energy load to satisfy the demand of consumption. In 2015 and 2016 years, electricity demand is above 2000 MW in January.

In this work, Sulaimani maximum electrical energy demand has been forecasted by considering different ANN models with high accuracy, to model the effects of weather, proper ANN models have been implemented. Because any prediction model does not give the best results, nine different ANN models for prediction were performed with the same period data and the superior ANN model was detected for forecasting electricity demand.

Forecasts model can be varied number of neuron in hidden layer 10, 12, and 15 neurons. The results show 2 years ahead midterm load forecasting model of 12 neurons in hidden layer can be reduced error. MAPE in this model is 5.6%.

This research and generally every research about load forecasting can be helpful for scheduling on requirement on

developing electrical distribution network, switching, selling energy, maintenance, and repairmen.

To have even better results, we may need to have more sophisticated topology for the neural network which can discriminate start-up months from other months. Here, we utilized only temperature, humidity, and precipitation among other weather information. Nevertheless, ANN may enable us to model such weather information for midterm procedure. The use of additional weather variables such as cloud coverage and wind speed should yield even better result.

6. ACKNOWLEDGMENT

The author would like to thank the staff Directory of Sulaimani Dispatch Control Center, especially operation department, and Sulaimani Directory of Metrological and Seismology data for the contribution of this work and providing.

REFERENCES

[1] H. S. Hippert, C. E. Pedreira and R. C. Souza. "Neural Networks for Short-term Load Forecasting: A Review and Evaluation". Vol. 16. In: *IEEE Transactions on Power Systems*, Piscataway, New Jersey, 2001.

[2] United Nations Development Programme. "*Electricity Network Development Plan Sulaimani Governorate, UNDP-ENRP, Distribution Sector Revision 1 February*". United Nations Development Programme, New York. 2002.

[3] A. Mohan. "Mid term electrical load forecasting for state of Himachal Pradesh using different weather conditions via ANN model". *International Journal of Research in Management, Science and Technology*, vol. 1, no. 2, 80, 2013.

[4] M. R. G. Al-Shakarchi and M. M. Ghulaim. "Short-term load forecasting for baghdad electricity region. *Electric Machines and Power Systems*, vol. 28, pp. 355-371, 2000.

[5] S. H. Ling, F. H. F. Leung, H. K. Lam and P. K. S. Tam. "Short-term Electric Load Forecasting Based on a Neural on a Neural Fuzzy Network". Vol. 50. In: *IEEE Transactions on Industrial Electronics*, 2003.

[6] G. C. Liao and T. P. Tsao. "Integrated genetic algorithm/Tabu search and neural fuzzy networks for short-term load forecasting". *Power Engineering Society General Meeting*, vol. 1, pp. 1082-1087, 2004.

[7] P. K. Dash, S. Mishra, S. Dash, A. C. Liew. "Genetic Optimization of a Self-organizing Fuzzy-Neural Network for Load Forecasting". In: *IEEE Power Engineering Society Winter Meeting, Conference Proceedings*, 2000.

[8] United States Agency for International Development. *Electricity Sector Master Plan for Iraq*. United States Agency for International Development, Washington, DC, United States, 2004.

[9] B. Islam. "Comparison of conventional and modern load forecasting techniques based on artificial intelligence and expert systems". *IJCSI International Journal of Computer Science Issues*, vol. 8, no. 3, pp. 504-513, 2011.

[10] G. B. Huang, Q. Y. Zhu, K. Mao, C. K. Siew, P. Saratchandran and N. Sundararajan. "Can threshold networks be trained directly". Vol. 53. In: *IEE Transactions on Circuits and Systems Part 2: Express Briefs*, pp. 187-191, 2006.

[11] A. Nahari, H. Rostami, R. Dashti. "Electrical load forecasting in power distribution network by using artificial neural network". *International Journal of Electronics Communication and Computer Engineering*, vol. 4, no. 6, 2013.

[12] Y. Y. Hsu and C. C. Yang. "Design of Artificial Neural Networks for Short-term Load Forecasting. Part I: Self-organizing Feature Maps for Day Type Selection". Vol. 138. In: *IEEE Proceedings-C*, pp. 407-413, 1991.

[13] M. Djukanovic, B. Babic, D. J. Sobajic and Y. H. Pao. "Unsupervised/ Supervised Learning Concept for 24-Hour Load Forecasting". Vol. 140. In: *IEE Proceedings-C*, pp. 311-318, 1993.

[14] Y. Wang and D. Gu. "Back Propagation Neural Network for Short-term Electricity Load Forecasting with Weather Features". In: *International Conference on Computational Intelligence and Natural Computing*, 2009.

[15] M. Buhari and S. Adamu. "Short Term Load Forecasting Using Artificial Neural Naetwork". Vol. 1. In: *Proceeding of the International Multi Conference of Engineering and Computer Scientists*, pp. 221-226, 2012.

ORIGINAL RESEARCH ARTICLE UHD JOURNAL OF SCIENCE AND TECHNOLOGY

Comparison between the Effect of Local Katira Gum and Xanthan Gum on the Rheological Properties of Water-based Drilling Fluids

Bayan Qadir Sofy Hussein[1]*, Khalid Mahmood Ismael Sharbazheri[1], Nabil Adiel Tayeb Ubaid[2]

[1]Department of Engineering, Kurdistan Institution for Strategic Study and Scientific Research, Sulaimani Polytechnic University, Sulaimani, Iraq, [2]Department of Petroleum and Energy Engineering, Faculty of Engineering, Sulaimani Polytechnic University, Sulaimani, Iraq

ABSTRACT

The rheological properties of drilling fluids have an important role in providing a stable wellbore and eliminating the borehole problems. Several materials including polymers (xanthan gum) can be used to improve these properties. In this study, the effect of the local Katira, as a new polymer, on the rheological properties of the drilling fluids prepared as the bentonite-water-based mud has been investigated in comparison with the conventional xanthan gum. Experimental work was done to study of rheological properties of several gums such as, local katira gum, and xanthan gum bentonite drilling mud. Different samples of drilling fluids are prepared adding the xanthan gum and local katira to the base drilling fluid at different concentrations using Hamilton Beach mixer. The prepared samples are passed through rheological property tests including the apparent viscosity, plastic viscosity, and yield point (YP) under different temperature conditions. The obtained results show that the viscosity is increased from 5 to 8.5 cp and YP is increased from 18.5 to 30.5 lb/100 ft^2, with increasing the concentration of the xanthan gum from 0.1 to 0.4. However, the effect of the local katira in increasing the viscosity and YP is lower compared with the xanthan gum, which are ranged between 5–6 cp and 18.5–20.5 cp.

Index Terms: Drilling mud, Polymer, Rheological properties, Xanthan gum, and Katira gum

1. INTRODUCTION

Drilling fluid which is simply called mud is one of the most important systems of drilling the borehole to extract hydrocarbon [1], [2]. This kind of fluid is used for providing several functions including bottom hole cleaning, providing a balance between borehole pressures, and controlling the wellbore stability [3]. To achieve these applications, the drilling fluids must be prepared with practicable properties that have a significant role, such as rheological and filtration properties [4]. For this purpose, many chemical additives are used including clays, solvents, and polymers. Polymers in different types are widely used with the water-based muds to improve the rheological properties of the mud, and the mud is sometime called polymer mud [5]-[7]. At present, researchers and companies are more focusing on the application of biopolymers which are definitely not poisonous and cheaper while having significantly less influence on formation damage [8], [9].

Natural gum polymers are widely used in the industry and studied by many researchers at the modern drilling process due to its low cost and high performance. Gums are

Access this article online

DOI: 10.21928/uhdjst.v4n2y2020.pp18-27

E-ISSN: 2521-4217
P-ISSN: 2521-4209

Corresponding author's e-mail: Bayan Qadir Sofy Hussein, Department of Engineering, Kurdistan Institution for Strategic Study and Scientific Research, Sulaimani Polytechnic University, Sulaimani, Iraq. E-mail: bayan.sofy@kissr.edu.krd

Received: 18-04-2020 Accepted: 14-07-2020 Published: 19-07-2020

generally used to provide a good influence on the rheological characteristics of several water-based drilling fluids that prepared from the mixture of water and bentonite [10], [11]. Several types of gum polymers that are used in drilling fluid application are suggested in the literature by researchers, such as tragacanth gum [8], xanthan gum [12], [13], tamarind tree gum [14], carboxymethyl cellulose [15], [16], and modified natural gum including diutan gum [17]. Among the gum polymers, guar and xanthan gums are most commonly used to modify the rheological and filtration properties of the water-based drilling fluids [11]. However, the identification and investigation of new types of the natural gums are necessary.

In 2018, Weikey *et al*. [9] investigated the effect of different gums including Babul, Dhawda, Katira, and Semal gums of the performance of the water-based mud. Their results showed that Babul, Semal, and Katira improved the rheological properties of the mud, however, Dhawda gum showed the highest performance. The comparison between the influences of the tamarind gum and polyanionic cellulose on the bentonite-water suspensions is investigated experimentally by Mahto and Sharma [14]; consequently, the tamarind gum produced more favorable rheological properties, optimal fluid loss, and lower formation damage at very low concentrations compared with the polyanionic cellulose. In addition, Benyounes *et al*. [15] investigated the effect of carboxymethyl cellulose and xanthan gum on rheological properties of the water-based mud. Their laboratory results revealed that the viscosity and yield point (YP) of bentonite suspension are increased and the flow index is decreased with increasing the xanthan concentration. However, carboxymethyl cellulose caused to increase viscosity along with decreasing the YP. On the other hand, Benmounah *et al*. [16] confirmed that the presence of carboxymethyl cellulose in the bentonite suspension helps to remove the yield stress and increase the viscosity of the mixture, and the xanthan gum induces an increase in the yield stress and in viscosity of the drilling muds. Dewangan and Sinha [18] developed water-bentonite suspension from the Babul tree gum and carboxymethyl cellulose and studied using marsh funnel. The results revealed that better rheological properties of mud can be achieved with using carboxymethyl cellulose compared with the Babul tree gum. However, they claimed that the Babul gum can be used to improve the rheological properties of mud to a favorite level. More recently in 2019, Ali *et al*. [19] enabled to greatly improve the rheological and filtration properties of the water-based mud by combining the xanthan gum with a nanocomposite of SiO_2/ZnO. In their work, the viscosity and gel strength are increased from 9 cP and 20 lb/100ft^2 to 22 cP and 49 lb/100ft^2, respectively. While, the fluid loss and filter cake are reduced by 54% and 92.5%, respectively.

The ultimate goal of this work is to investigate the effect of two polymers (xanthan and natural Katira gum) on the rheological behaviors of bentonite-water-based drilling fluid. For this purpose, different samples of drilling fluids are prepared at different concentrations of polymer gums. The rheological viscometer is used to study the viscosity and YP of the prepared drilling fluids under the effect of types of gum, concentration of gum, and test temperature.

2. MATERIALS AND METHODOLOGY

2.1. Materials

The drilling mud mixture utilized in this research are freshwater, bentonite, natural katira gum, and xanthan gum. The freshwater is used as the base fluid and for fluid conditioning, the bentonite along with other additives utilized in the drilling fluid formulations. The purpose of adding biopolymers, natural katira gum, and xanthan gum is used to increase viscosity and fluid loss control. The bentonite which is composed mostly of montmorillonite obtained from one of the Kurdistan's drilling companies. The additives utilized are natural katira gum that is purchased from the local market and xanthan gum is supplied from petroleum engineering department of Sulaimani Polytechnic University.

2.2. Xanthan Gum

Xanthan gum is the polysaccharide anionic item within a commercial level gained from the aerobic agitation of *Xanthomonas campestris* bacteria. Xanthan gum has a strong stability to the different conditions of heat, salinity, and pH [20]. One of the most attractive characteristics of xanthan is its ability to increase the viscosity for the drilling fluid with very low concentration [21]. Xanthan gum has a simple chemical structure as shown in Fig. 1 that comes with a typical molecular weight of 3×10^5-7.5×10^6 g/mole [22].

2.3. Local Katira Gum

Katira gum is mainly exist in rocky locations of Kurdistan Mountain. High-quality gum was harvested and dried during the spring season from April to June. It has mostly acetylated complex polysaccharide and includes about 80% acetyl groups as well as about 37% uronic acid remains with acidic quantity varying from 17.4 to 22.7. According to Weikey *et al*. [9], the molecular weight of Katira is about 9.5×10^6 g/mol. At low concentrations, Katira are capable to create a high gluey gum with a good swelling behavior due to the existence of the acetyl groups [9].

Katira gum is the sap of the thorny plant which mainly presents in Middle Eastern and West Asian countries. This particular gum is odor free, flavorless, and water-soluble mixing extracted from their drain for the plant. The gum through the plant will be gained obviously through the root and through cuts produced in their stem then dehydrated to be able to creates small pieces (Fig. 2).

2.4. Preparation of Drilling Fluids

The drilling fluids are prepared using 3-speed Type HMD200 Hamilton Beach mixer. The base drilling fluid is prepared from mixing 22.5 g bentonite within 350 mL distilled water within the mixing cup. Afterward, to identify the effect of the xanthan and Katira polymer gums on the rheological properties of the drilling mud, both polymers are separately added into the prepared base drilling fluids at different concentrations. For preparing the xanthan-based drilling mud, four samples of muds are prepared at different concentrations of 0.1, 0.2, 0.3, and 0.4 g, and four Katira drilling fluids are prepared at 20, 40, 60, and 80 mg concentrations (Table 1).

2.5. Rheological Measurements

For the prepared drilling fluids shown in Table 1, the six-speed rotary viscometer model ZNN-D6 is used to measure the rheological properties including apparent viscosity, YP, plastic viscosity (PV), and YP/PV proportion dependent on the shear

TABLE 1: Formulation of the prepared drilling fluids

Mud sample	Polymer gum	Concentration	Additives, g
S0	----	----	Bentonite, 22.5
XS1	Xanthan	0.1 g	
XS2		0.2 g	
XS3		0.3 g	
XS4		0.4 g	
KS1	Katira	20 mg	
KS2		40 mg	
KS3		60 mg	
KS4		80 mg	

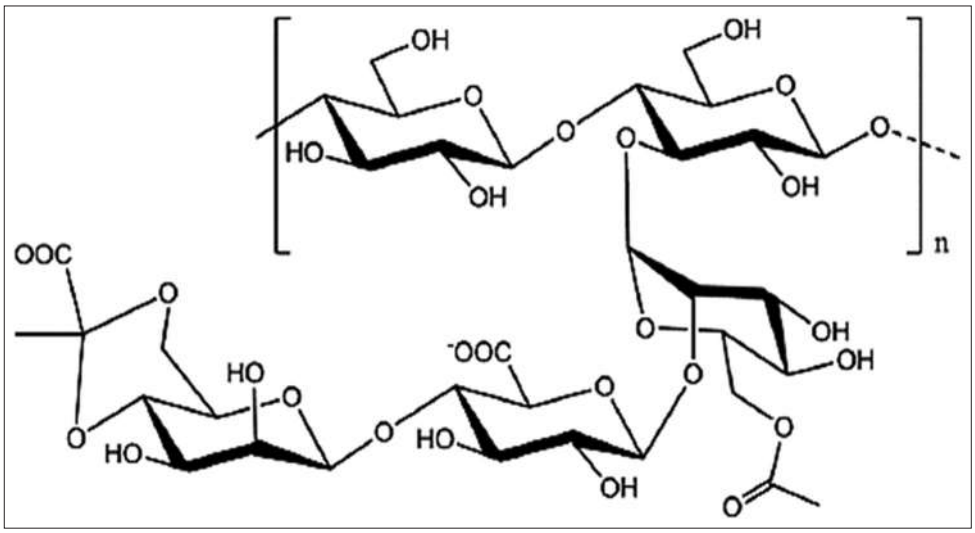

Fig. 1. Xanthan gum chemical structure [13].

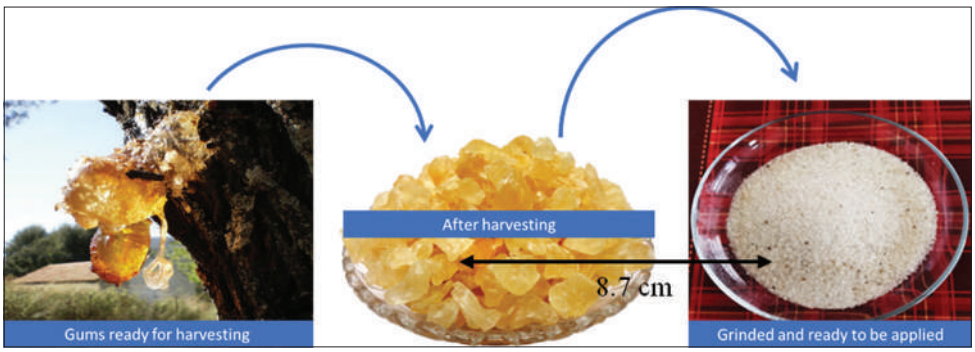

Fig. 2. The natural Katira gum on the tree, after harvesting and as a powder.

stress and shear rate. These measurements are performed at different temperature conditions of 25, 45, and 75°C. In general, the following procedural steps in accordance with [23] application programming interface specification 13A are applied:

- The mud mixture prepared using 22.5±0.01 g of bentonite added into 350 cm^3 of fresh water while stirring in the mixer putting the gums added at various concentrations.
- Immediately after mixing 5±0.5 min, the container taken from mixer and cleaned using spatula to remove bentonite on container walls, making sure bentonite adhering into the spatula is actually included in the mixture.
- Replacing the container in the blender following an additional 5 min as the edges scraped to free any clay adhering to container and blending again for 10 min, complete mixing duration will equate to 20±1 min.
- Put the mixture into viscometer cup supplied with the direct-indicating viscometer. The dial readings at 600 r/min as well as 300 r/min rotor speed settings of the viscometer will be recorded whenever a constant value for every r/min is achieved. The test temperature was 25±1°C.
- The PV, YP, and YP/PV ratio are generally calculated using the following equations:

$$Pv=R600-R300 \quad (1)$$

$$YP=R300-PV \quad (2)$$

$$C=\frac{YP}{PV} \quad (3)$$

$$AV=\frac{R600}{2} \quad (4)$$

where:
PV: Plastic viscosity in cp, centipoises.
YP: Yield point in Ib/100 ft^2.
C: YP/PV ratio.
R600: The viscometer dial reading at 600 rpm/min.
R300: The viscometer dial reading at 300 rpm/min.

3. RESULTS AND DISCUSSION

3.1. Effect of Xanthan Gum on Rheological Properties

By adding different concentrations of xanthan gum into the base drilling fluid, four samples (XS1, XS2, XS3, and XS4) are prepared. Fig. 3 shows the values of the reordered viscometer readings at different speeds starting from the low shear stresses 3 and 6 rpms to moderate 100 and 200 rpms and high shear stresses of 300 and 600 rpms. With increase the shear stress and the rotation speed per minute, the recorded value of shear rate is increasing. The same effect can be seen with increasing the concentration of the xanthan gum. The measured results of the rheological properties including the apparent viscosity, PV, YP, and PV to YP ratio under the influence of the xanthan gum are shown in Table 2. The measurements are carried out under different temperature conditions of 25, 45, and 75°C.

Fig. 4 illustrates the values of the apparent viscosity measured for the prepared drilling fluids containing the xanthan gum at different concentrations of 0.1, 0.2, 0.3, and 0.4 g. As can be seen, the apparent viscosity of the base mud is increased from 14.25 to 21.25 cP with adding 0.1 g of the xanthan gum and continued to increase to 28.25 cP with increasing the concentration of xanthan to 0.4 g. While, the apparent viscosity with all concentrations of xanthan gum is decreased with increasing the temperature of the experiment from 25 to 45 and 75°C. In general, the apparent viscosity of XS1, XS2, and XS3 samples is reduced by about 9% with increasing temperature from 25 to 75°C.

The PV behavior of the mud samples developed from different concentrations of xanthan gum is shown in Fig. 5. As can be seen, the PV of the base fluid is increased by 40% from 5 to 8.5 cP by adding 0.4 g of xanthan gum under 25°C. However, the impact of the xanthan in improving the PV is lower when the temperature of the experiment is increased. This is true with Benyounes *et al.* [15], where they demonstrate that the rheological behavior of the polymer solution predominates compared to their clay suspension system. In this situation, the macroscopic behavior for the bentonite-xanthan mixtures is influenced by xanthan.

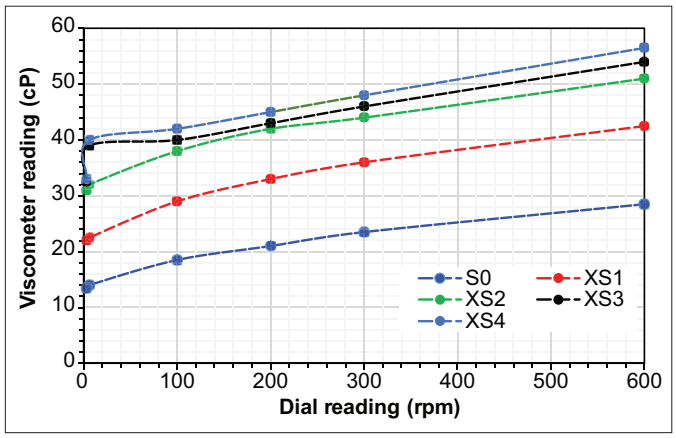

Fig. 3. Shear rate versus shear stress at various concentrations of xanthan gum and room temperature.

TABLE 2: Measured rheological properties of drilling fluids under the influences of xanthan gum at 25, 45, and 75°C

Mud sample	AV (cP)			PV (cP)			YP (lb/100 ft²)			YP/PV		
	25°C	45°C	75°C	25°C	45°C	75°C	25°C	45°C	75°C	25°C	45°C	75°C
S0	14.2	14.2	14.2	5.0	5.0	5.0	18.5	18.5	18.5	3.7	3.7	3.7
XS1	21.2	20.5	18.5	6.5	5.0	4.0	29.5	31.0	29.0	4.5	6.2	7.3
XS2	25.5	24.5	23.0	7.0	5.5	5.0	37.0	38.0	36.0	5.3	6.9	7.2
XS3	27.0	26.0	24.5	8.0	6.5	6.0	38.0	39.0	37.0	4.8	6.0	6.2
XS4	28.2	26.5	25.7	8.5	7.0	6.5	39.5	39.0	38.5	4.6	5.6	5.9

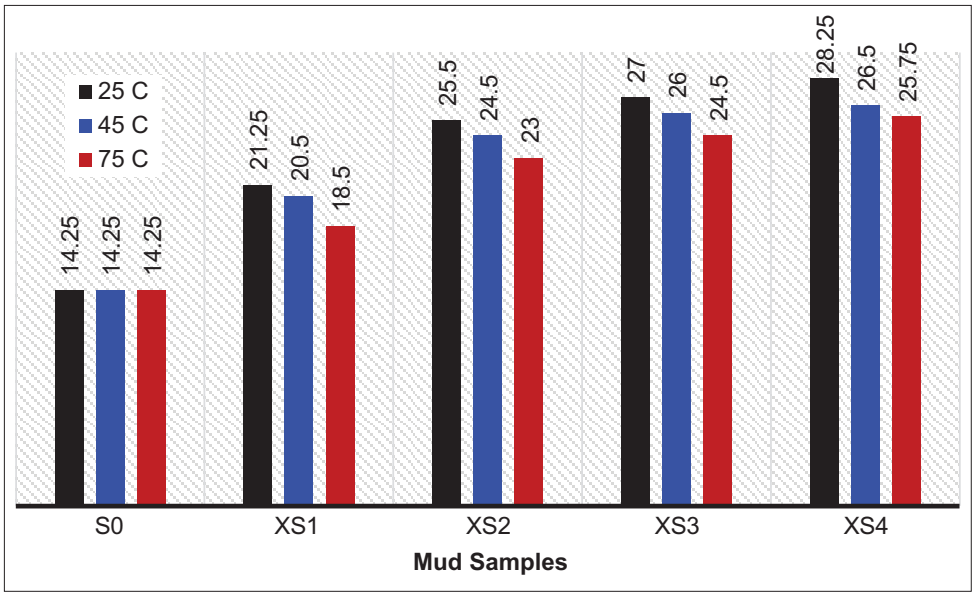

Fig. 4. Apparent viscosity measured at different concentrations of xanthan gum at 25, 45, and 75°C.

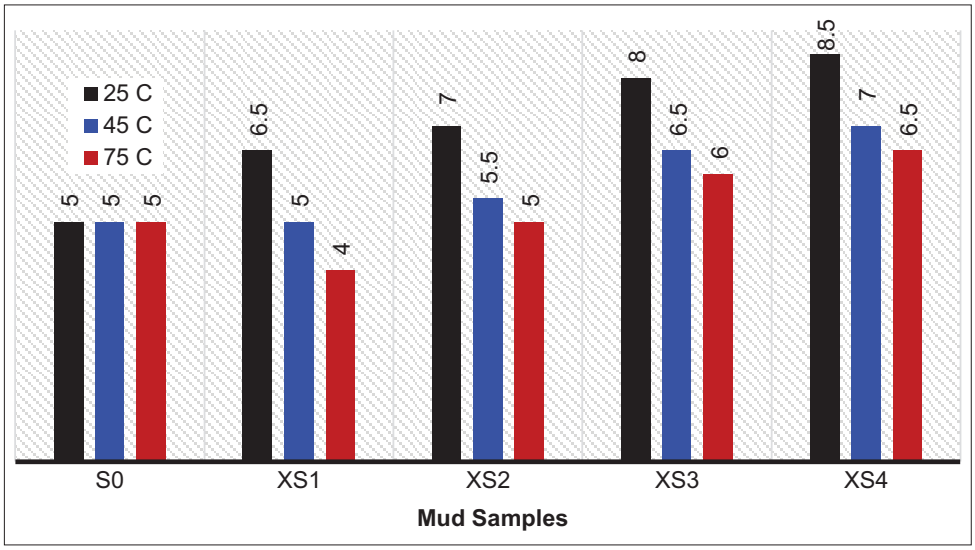

Fig. 5. Plastic viscosity measured at different concentrations of xanthan gum at 25, 45, and 75°C.

In addition, the values of the measured YPs for four prepared mud samples of xanthan gum are shown in Fig. 6. The used xanthan gum left the highest impact on the YP compared with other properties of the drilling fluids which is about 53%. The value of the YP is increased from 18.5 to 29.5 lb/100 ft^2 with adding 0.1 g xanthan, continued to increase to 39.5 lb/100 ft^2. Furthermore, the ratio of the YP to PV calculated from the measured properties of the drilling fluid samples under the influence of the xanthan gum and different temperature is shown in Fig. 7. As is obvious, the ratio between two considered parameters is varied dependents on the concentration of the xanthan gum and temperature. The high ratios between two parameters with XS1 and XS2 samples are obtained, especially at high temperatures.

3.2. Effect of Natural Katira Gum on Rheological Properties

To identify the impact of the Katira gum on the rheological properties of the drilling mud, the prepared Katira in powder is added into the base drilling mud at different concentrations. For the concentrations of 20 mg, 40 mg, 60 mg, and 80 mg, four samples of Katira gum (KS1, KS2, KS3, and KS4) are prepared.

Fig. 8 shows the values of the reordered viscometer readings at different speeds starting from the low shear stresses 3 and 6 rpms to moderate 100 and 200 rpms and high shear stresses of 300 and 600 rpms. With increase the shear stress and the rotation speed per minute, the recorded value of shear rate is increasing. The same effect can be seen with increasing the

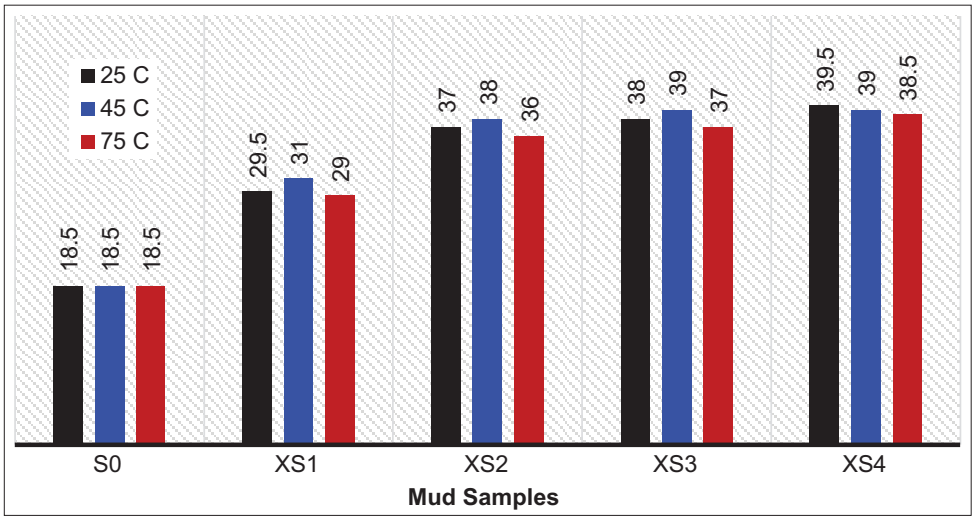

Fig. 6. Yield point measured at different concentrations of xanthan gum at 25, 45, and 75°C.

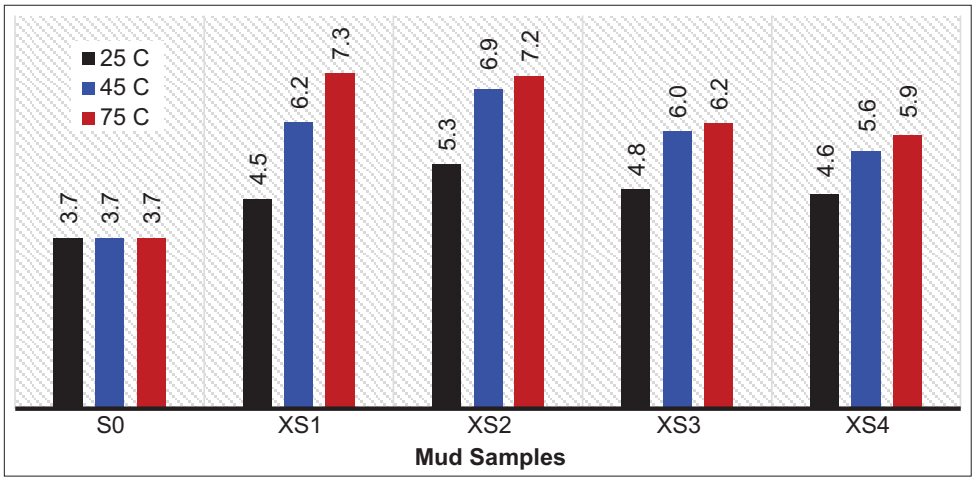

Fig. 7. Ratio of the yield point to plastic viscosity at different concentrations of xanthan gum at 25, 45, and 75°C.

concentration of the Katira gum. The measured results of the rheological properties including the apparent viscosity, PV, YP, and PV to YP ratio under the influence of the Katira gum are shown in Table 3. The measurements are carried out under different temperature conditions of 25, 45, and 75°C.

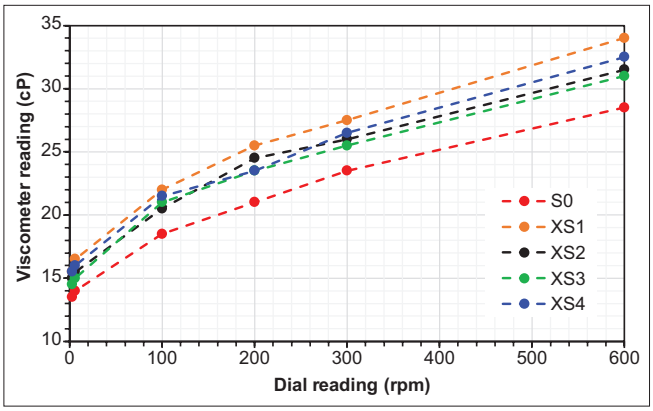

Fig. 8. Shear rate versus shear stress at different concentrations of natural Katira gum at 25°C.

Fig. 9 illustrates the values of the apparent viscosity measured for the prepared drilling fluids containing the Katira gum at different concentrations of 20 mg, 40 mg, 60 mg, and 80 mg. As can be seen, the apparent viscosity of the base mud is increased from 14.25 to 17 cP with adding 20 mg of the Katira gum and continued to increase to 17.75 cP with increasing the concentration of Katira to 40 mg. While, the apparent viscosity with all concentrations of xanthan gum is decreased with increasing the temperature of the experiment from 25 to 45 and 75°C. In general, the impact of the Katira gum on the apparent viscosity under all concentrations and temperature conditions is low. Only small variation in the value of the apparent viscosity is noticed by changing the experiment conditions.

The PV behavior of the mud samples developed from different concentrations of Katira gum is shown in Fig. 10. As can be seen, the PV of the base fluid is increased by 23% from 5 to 6.5 cP by adding 20 mg Katira gum under 25°C. However, the impact of the Katira in improving

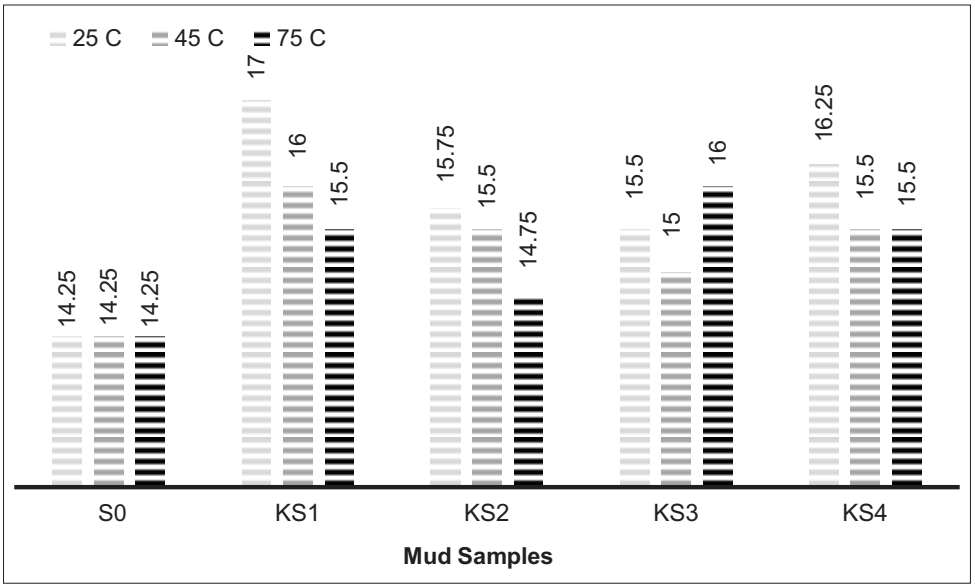

Fig. 9. Apparent viscosity measured at different concentrations of katira gum at 25, 45, and 75°C.

TABLE 3: Measured rheological properties of drilling fluids under the influences of katira gum at 25, 45, and 75°C

Mud sample	AV (cP)			PV (cP)			YP (lb/100 ft²)			YP/PV		
	25°C	45°C	75°C	25°C	45°C	75°C	25°C	45°C	75°C	25°C	45°C	75°C
S0	14.2	14.2	14.2	5.0	5.0	5.0	18.5	18.5	18.5	3.7	3.7	3.7
KS1	17.0	16.0	15.5	6.5	3.0	2.0	21.0	26.0	27.0	3.2	8.7	13.5
KS2	15.7	15.5	14.7	5.5	4.5	3.5	20.5	22.0	22.5	3.7	4.9	6.4
KS3	15.5	15.0	16.0	5.5	2.0	2.0	20.0	26.0	28.0	3.6	13.0	14.0
KS4	16.2	15.5	15.5	6.0	1.0	1.5	20.5	29.0	28.0	3.4	29.0	18.7

the PV is lower when the temperature of the experiment and gum concentration are increased. This is true with Benyounes *et al.* [15], where they demonstrate that the rheological behavior of the polymer solution predominates compared to their clay suspension system. In this situation, the macroscopic behavior for the bentonite-Katira mixtures is influenced by the gum.

In addition, the values of the measured YPs for four prepared mud samples of Katira gum are shown in Fig. 11. The used Katira gum left the highest impact on the YP compared with other properties of the drilling fluids which is about 36%. The value of the YP is increased from 18.5 to 27 lb/100 ft^2 with adding 20 mg Katira, continued to increase to 29 lb/100 ft^2. Furthermore, the ratio of the YP to PV calculated from the measured properties of the drilling fluid samples under the influence of the Katira gum and different temperature is shown in Fig. 12. As is obvious, the ratio between two considered parameters is varied dependents on the concentration of the Katira gum and temperature.

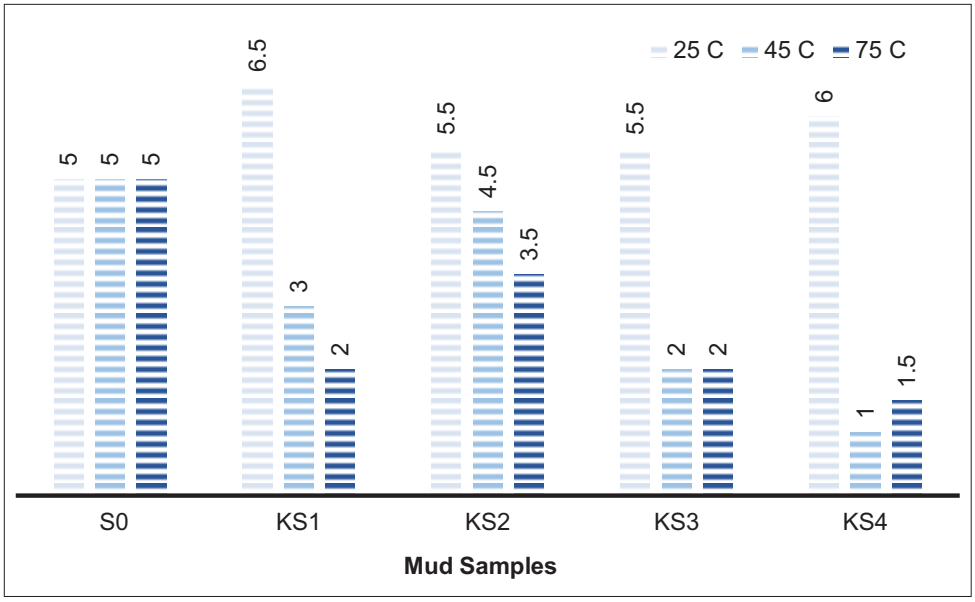

Fig. 10. Plastic viscosity measured at different concentrations of katira gum at 25, 45, and 75°C.

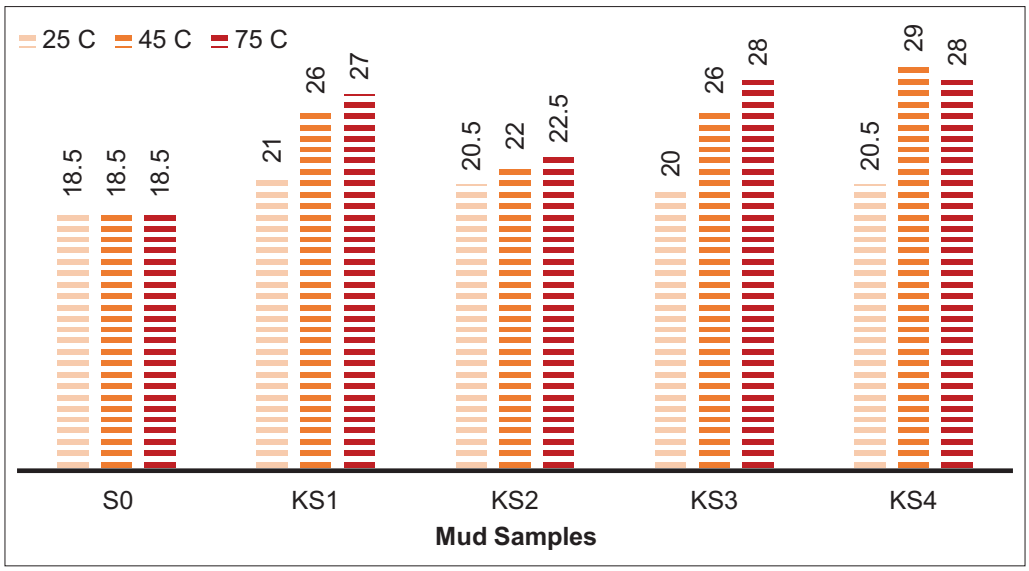

Fig. 11. Yield point measured at different concentrations of katira gum at 25, 45, and 75°C.

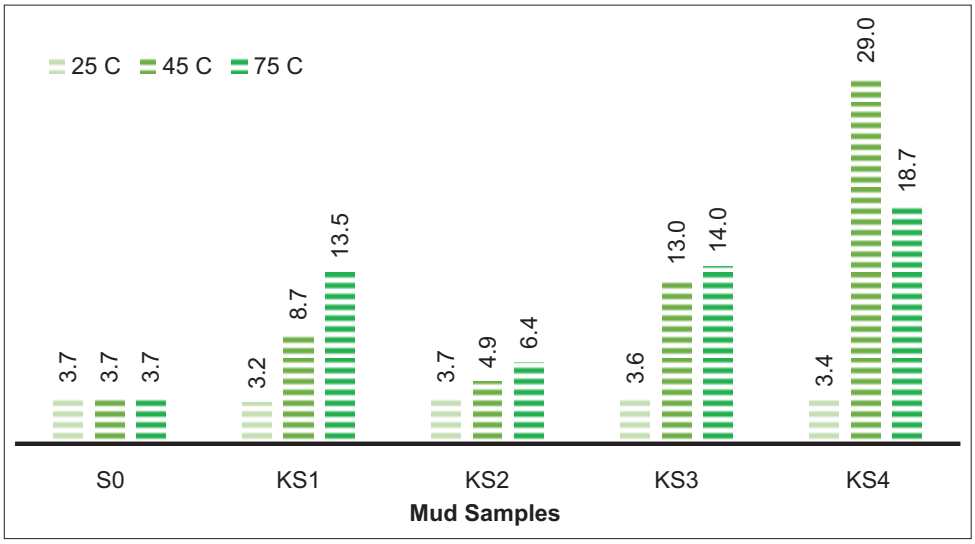

Fig. 12. Ratio of the yield point to plastic viscosity at different concentrations of katira gum at 25, 45, and 75°C.

The high ratio between two parameters with KS4 samples are obtained, especially at high temperatures.

4. CONCLUSION

In this study, the rheological properties of the drilling mud under the influences of two polymer gums including xanthan and local Katira gums are investigated. In general, both types of gums are used at low concentrations and they left an important impact on the rheological behaviors of the drilling mud. However, xanthan gum presented a better performance in improving all studied rheological properties of the mud; apparent viscosity is increased from 14.25 to 28.35 cP, PV increased from 5 to 8.5 cP, and YP (18.5 to 39.5 lb/100 ft^2). While, the effect of the Katira gum is lower on apparent viscosity, PV, and YP under all different concentrations and temperatures.

REFERENCES

[1] K. L. Goyal. "A review of: Drilling and Drilling Fluids, by G. V. Chilingarian and P. Vorabutr; published in 1981 by Elsevier Scientific Publishing Co., P.O. Box 211, 1000 AE Amsterdam, The Netherlands; distributed by El-sevier/North-Holland, Inc., 52 Vanderbilt Avenue, New York, N. Y. 10017; 767 pp., photos, illustrations, appendices, glossary; $136.50, U.S.: 1228.50, Rs". *Energy Sources*, vol. 7, no. 2, pp. 178-179, 1983.

[2] I. Imuentinyan and E. S. Adewole. "Feasibility study of the use of local clay as mud material in oil well drilling in Nigeria". In: *Africa's Energy Corridor Oppor. Oil Gas Value Maximization Through Integration and Global Approach*, Victoria Island, Lagos, vol. 2, pp. 1476-1491, 2014.

[3] A. W. A. Al-Ajeelt and S. N. Mahdi. "Sodium activation of Iraqi high grade montmorillonite clay stone by dry method". *Iraqi Bulletin of Geology and Mining*, vol. 9, no. 1, pp. 65-73, 2013.

[4] E. S. Al-Homadhi. "Improving local bentonite performance for drilling fluids applications". *Journal of King Saud University Engineering Sciences*, vol. 21, no. 1, pp. 45-52, 2007.

[5] K. A. Galindo, W. Zha, H. Zhou and J. P. Deville. "Clay-free high performance water-based drilling fluid for extreme high temperature wells". *SPE/IADC Drilling Conference and Exhibition*, 17-19 March, London, England, UK, pp. 179-188, 2015.

[6] S. D. Strickland. "Polymer Drilling Fluids". *Journal of Petroleum Technology*, vol. 46, no. 8, pp. 691-714, 1994.

[7] M. A. Tehrani, A. Popplestone, A. Guarneri and S. Carminati. "Water-based drilling fluid for HP/HT applications". *International Symposium on Oilfield Chemistry*, 28 February-2 March, Houston, Texas, USA, pp. 83-92, 2007.

[8] V. Mahto and V. P. Sharma. "Tragacanth gum: An effective oil well drilling fluid additive". *Energy Sources*, vol. 27, no. 3, pp. 299-308, 2005.

[9] Y. Weikey, S. L. Sinha, and S. K. Dewangan. "Effect of different gums on rheological properties of slurry". *IOP Conference Series Materials Science and Engineering*, vol. 310, no. 1, p. 012068, 2018.

[10] C. Vipulanandan and A. S. Mohammed. "Hyperbolic rheological model with shear stress limit for acrylamide polymer modified bentonite drilling muds". *Journal of Petroleum Science and Engineering.*, vol. 122, pp. 38-47, 2014.

[11] E. C. M. Vermolen, M. J. T. Van Haasterecht, S. K. Masalmeh, M. J. Faber, D. M. Boersma and M. Gruenenfelder. "Pushing the envelope for polymer flooding towards high-temperature and high-salinity reservoirs with polyacrylamide based ter-polymers". *SPE Middle East Oil and Gas Show and Conference*, 25-28 September, Manama, Bahrain., vol. 2, pp. 1001-1009, 2011.

[12] F. García-Ochoa, V. E. Santos, J. A. Casas and E. Gómez. "Xanthan gum: Production, recovery, and properties". *Biotechnology Advances*, vol. 18, no. 7, pp. 549–579, 2000.

[13] G. F. Sancet, M. Goldman, J. M. Buciak, O. Varela, N. D'Accorso, M. Fascio, V. Manzano, M. Luong. "Molecular

Structure Characterization and Interaction of a Polymer Blend of Xanthan Gum-polyacrylamide to Improve Mobility-control on a Mature Polymer Flood. *SPE EOR Conference at Oil and Gas West Asia*, 26-28 March, Muscat, Oman, 2018.

[14] V. Mahto and V. P. Sharma. "Rheological study of a water based oil well drilling fluid". *Journal of Petroleum Science and Engineering*, vol. 45, no. 1-2, pp. 123-128, 2004.

[15] K. Benyounes, A. Mellak and A. Benchabane. "The effect of carboxymethylcellulose and xanthan on the rheology of bentonite suspensions". *Energy Sources, Part A: Recovery, Utilization, and Environmental Effects*, vol. 32, no. 17, pp. 1634-1643, 2010.

[16] A. Benmounah, K. Benyounes, K. Chalah and D. Eddine. "Effect of Xanthan Gum and Sodium Carboxymethylcellulose on the Rheological Properties and Zeta Potential of Bentonite Suspensions. *23rd Congrès Français de Mécanique*, 2017.

[17] E. U. Akpan, G. C. Enyi and G. G. Nasr. "Enhancing the performance of xanthan gum in water-based mud systems using an environmentally friendly biopolymer". *Journal of Petroleum Exploration and Production Technology*, vol. 10, pp. 1933-1948, 2020.

[18] S. K. Dewangan and S. L. Sinha. "Effect of additives on the rheological properties of drilling fluid suspension formulated by bentonite with water". *International Journal of Fluid Mechanics Research*, vol. 44, no. 3, pp. 195-214, 2017.

[19] J. A. Ali, K. Kolo, S. M. Sajadi, K. H. Hamad, R. Salman, M. Wanli and S. M. Hama. "Modification of rheological and filtration characteristics of water-based mud for drilling oil and gas wells using green SiO2@ZnO@Xanthan nanocomposite". *IET Nano Biotechnology*, vol. 13, no.7, pp. 748-755, 2019.

[20] W. Xie and J. Lecourtier. "Xanthan behaviour in water-based drilling fluids". *Polym. Degrad. Stab.*, vol. 38, no. 2, pp. 155-164, 1992.

[21] Z. Rončević *et al.*, 'Effect of carbon sources on xanthan production by Xanthomonas spp. isolated from pepper leaves". *Food and Feed Research*, vol. 46, no. 1, pp. 11-21, 2019.

[22] P. F. D. Cano-Barrita and F. M. León-Martínez. "Biopolymers with viscosity-enhancing properties for concrete". In: *Biopolymers and Biotech Admixtures for Eco-Efficient Construction Materials*. Elsevier. Amsterdam, Netherlands, 2016.

[23] American Petroleum Institute. "*13A Specification for Drilling Fluid Materials*". 15th ed. American Petroleum Institute, Washington, DC, United States, 1993.

ORIGINAL RESEARCH ARTICLE UHD JOURNAL OF SCIENCE AND TECHNOLOGY

Fingerprint Authentication using Shark Smell Optimization Algorithm

Bakhan Tofiq Ahmed[1], Omar Younis Abdulhameed[2]

[1]Department of Information Technology, Technical College of Informatics, Sulaimani Polytechnic University, Sulaimani, Kurdistan Region, Iraq, [2]Department of Computer Science, College of Science, University of Garmian, Kalar, Garmian, Kurdistan Region, Iraq

ABSTRACT

Recognition of people relying on biometric characteristics is a common phenomenon in our society. It has increased in recent years in most areas of life such as government, department, companies, and banks. Fingerprint identification is one of the most common and credible personal biometric identification methods. Extracting features are one of the most important steps in the fingerprint identification; the strength of any system depends mainly on this step, where whenever the features obtained are accurate whenever the identification process is more accurate. Therefore, an effective and efficient method must be used to extract the features. This paper solved two main problems that were (1) improving security by designing and implementing an accurate, efficient, and fast authentication system for the identification and verification process using an intelligent algorithm to extract the best features from the fingerprint image and (2) evaluating the strength of the Shark Smell Optimization (SSO) in the search space with a chosen set of metrics. This paper aims to extract the best features of the fingerprint image using an algorithm that depends on nature for its movement and work; therefore, the SSO was used. In this paper, the SSO algorithm is used to extract the features. SSO is a new meta-heuristic algorithm that uses smart methods and random movements to get its prey. These methods and movements were used to extract features from the fingerprint image which will be used later for identification and verification process. The proposed method is implemented through four phases, namely, create a database to store and organize data, image pre-processing using median filter, feature extraction using SSO algorithm, and matching process using euclidean distance. The results demonstrated the strength, accurate, credible, and effectiveness of the algorithm used by applying it on (150) real fingerprint samples taken from university students, where the results of false acceptation rate, false rejection rate, and correct verification rate were 0.00, 0.00666, and 99.334%, respectively.

Index Terms: Fingerprint Authentication, Feature Extraction, Swarm Intelligent, Shark Smell Optimization, ZKT eco device

1. INTRODUCTION

The rapid enhancement of technology and electronically life raised the need for an extra level of security. Security is an increasing necessity throughout the globe because a lack of security can result in great damage. Security is well-defined as the degree of resistance to, or defense from harm. Physical security, personal security, and information security are the main forms of security. In the security field, authentication term means to verify an individual to access system based on their identity [1].

Many decades ago user's identity had been verified through a traditional method called knowledge-based authentication (e.g., password, smart-card, or personal identity number)

Access this article online

DOI: 10.21928/uhdjst.v4n2y2020.pp28-39

E-ISSN: 2521-4217
P-ISSN: 2521-4209

Corresponding author's e-mail: Bakhan Tofiq Ahmed, Department of Information Technology, Technical College of Informatics, Sulaimani Polytechnic University, Sulaimani, Kurdistan Region, Iraq. E-mail: Bakhan.tofiq.a@spu.edu.iq

Received: 05-06-2020 Accepted: 16-07-2020 Published: 20-07-2020

which might be easily forgotten or stolen. However, a fast upgrading in technology has replaced the traditional method to a new one called biometric-based authentication because is more convenient in which there is no need to memorize secret codes like password, and more secure which is harder to be stolen because it based on the unique human biometric features unlike knowledge-based authentication [2].

Biometric derived from the two Greek words the first one is Bios which means "life" and the second is Metric which means "measure." A biometric is a recognizing pattern system that identifies an individual relied on a feature extracted from an exact physiological or behavioral representative that the individual owns, for instance, Face, Hands, Eyes, Ears, or Voice to distinguish each other. This technology provides more reliability than the traditional approaches because of body characteristics cannot be easily stolen, copied, or forging by an intruder [3].

Fingerprint authentication is the most widely and commonly used biometric authentication mechanism because of its distinctiveness, ease of use, and long-term stability. The fingerprint is a gifted feature for biometric identification and verification. A fingerprint is the pattern of ridges and valleys on the fingertip surface. In fact, each individual has distinct fingerprints and leftovers almost the same entire life. The fingerprint is the most prominent and widely utilized human's trait for implementing a personal authentication system due to its uniqueness [4], [5].

2. LITERATURE REVIEW

In this section, some of the up-to-date researches in this field are reviewed which is from 2014 to 2019. These reviewed works are enlisted below:

Mela *et al.* [6], this research proposed an efficient fingerprint authentication model using the Haar Wavelet Transform (HWT) and Local Ridge Attribute. In this investigation, Gabor Filter is used to eliminating noise from the fingerprint image. Then, local ridge features are extracted from the enhanced image by 1-level HWT and 2-Level HWT. Afterward, the invariant moment is used to select only the critical features (i.e., 19 features) from 98 extracted features. Finally, the matching phase has been done by absolute difference. The experiments are done using Fingerprint Verification Competition (FVC 2004) DB1 and DB2 datasets. Each database contains 80 low-quality fingerprint images. The experimental results indicated that the proposed model was able to signify low-quality fingerprint images and gave a high recognition accuracy of 94.37% when 1-level HWT is used, while recognition accuracy of 96.87% is achieved when 2-level HWT is used using two decomposition levels of wavelet.

Abidin *et al.* [7], in this study, Gabor Wavelet Transform (GWT) and K-Nearest Neighbor (K-NN) are used to constructing a fingerprint authentication model. The main aim of using GWT was to extract local features from the gray-scale fingerprint image. Then, K-NN classifier is utilized for the recognition task. The Hong Kong Polytechnic University High Resolution Fingerprint (PolyU HRF) database has been used to test the proposed model. The outcome of this research has shown that the constructed model was credible because it gained the accuracy of 94.5%.

Umma *et al.* [8], this paper developed a fingerprint authentication system by utilizing the speeded-up robust feature (SURF) algorithm and Nearest Neighbor Matching Approach (NNMA). In this investigation, SURF algorithm is used to extract local features from the fingerprint image. Later, NNMA is used to compare the features of the test fingerprint image against two or more exiting template image features in the database. For simulating the model, 128 fingerprint images are collected from the web. The recognition accuracy of the system was 88.3%.

Mouad *et al.* [9], in this study, a fingerprint authentication proposed using Minutiae Extractor Algorithm (MEA) to perform the identification and verification process. The work is done in a sequence that began from the pre-processing stage that comprised of (enhancement, binarization, and thinning). First, image enhancement is done using the Fast Fourier Transform to eliminate undesirable data to increase the clarity of the fingerprint image. Second, the MEA is utilized to extract the fingerprint features. Finally, the Minutiae Matching Algorithm with Euclidean Distance (ED) is performed in the matching stage. The model is tested on two various public fingerprint databases which are FVC2000 and FVC2002. The experimental result obtained from the FVC2000 database was 0.2049 false acceptation rate (FAR), 0.1944 false rejection rate (FRR), and 60.07% correct verification rate (CVR), while 0.0154 FAR, 0.0137 FRR, and 97.09% CVR from FVC2002.

Hong *et al.* [10], in this paper, a Convolutional Neural Network (CNN) is used to propose fingerprint recognition. CNN is a renowned feature learning and classification algorithm which is utilized to detect relevant feature on fingerprint images. An Affine Fourier Moment Matching is suggested in this

research as a method of matching. The algorithm evaluation is done using a public database, namely, Hong Kong PolyU HRF which consisted of 30 images. The constructed model has achieved a satisfactory accuracy of 88.6%.

Zainab *et al.* [11], this study proposed a fingerprint authentication that used local energy distribution with three different levels of HWT, namely, 1-D, 2-D, and 3-D (Dimension) HWT. The proposed system included the primary stages such as pre-processing, feature extraction, and matching features. Pre-processing consisted of Color Conversion, Segmentation, Binarization Thresholding. Before extracting significant feature, the image is decomposed into four sub-bands using 1-D, 2-D, and 3-D (HWT) separately. After that feature vector is extracted by computing Energy Local Distribution. Finally, feature matching is carried out by utilizing the Mean Square Difference and Mean Absolute Difference. The FVC2004 databases used to test the proposed system. FVC 2004 databases consist of four various datasets; each dataset has 80 fingerprint image samples. The proposed system achieved good accuracy which was 94%, 91%, and 94% when 1-D, 2-D, and 3-D HWT are used, respectively.

Israa *et al.* [12], in this investigation, the design of a fingerprint authentication system is suggested that relied on Filter Bank Based (FBB) algorithm. Fingerprint images were enhanced using the Fourier Domain Analysis Filtering and Segmentation as a Pre-processing stage. FBB algorithm is used in the feature extraction stage. Using K-NN technique and 70% threshold value, the matching stage has been done. K-NN classifier and 70% threshold value provide an appropriate matching result. A collection of 90 fingerprint images are used to evaluate the proposed model. The CVR, FAR, and FRR achieved from this work were 93.9683%, 0.012698, and 0.047619, respectively.

Aung *et al.* [13], a Neural Network (NN) Classifier is used to propose a fingerprint authentication system in this research. First, the input fingerprint image is acquired by the Digital Persona 4500 fingerprint scanner. Second, the images are enhanced using Contrast Stretching and 2 Morphological techniques such as Dilation and Erosion. Third, Minutiae Based Approach used to extract features from the region of interest of a fingerprint image. Afterward, features were fed into the NN for user recognition. According to the experimental consequences, the proposed fingerprint recognition system reached 96.5% accuracy.

Harinder *et al.* [14], in this paper, an enhancement fingerprint authentication is proposed which is based on Non-Subsampled Contourlet Transform (N-SCT) and Zernike Moments (ZMs). Four various stages were conducted in this work. First, the fingerprint image decomposition stage is done through NSCT to decompose the fingerprint images into NSCT sub-samples. Second, the fingerprint image features were evaluated through ZMs. Third; potential features were selected using the determination coefficient. Finally, a Weighted Support Vector Machine is used to train and test the selected features for the matching stage. Extensive experimental results depicted that the proposed system gave significant improvement in terms of accuracy which was nearly 95%.

Nature-inspired optimization algorithms, especially swarm-based algorithms, solve many scientific and engineering problems due to their flexibility and simplicity. These algorithms are applicable for optimization problems without structural modifications. This work presents a novel nature-inspired metaheuristic optimization algorithm called SSO to extract the best features from the user's fingerprint image. The results proved that the swarm intelligence (SI) algorithm gave better results than other algorithms.

3. SI

SI stands for Swarm-Intelligence is an artificial intelligent (AI) method relied on group behavior that originated in nature. The SI term was utilized by Beni in Cellular-Robotic-System for the 1st time where modest agents arranged themselves through neighborhood collaborations. SI is enumerated as the most critical optimization scheme. SI is the characteristic of a system when the cooperative agent behaviors locally cooperate with their environment such as Ant-Colony's searching, Bird's flocking, Bacteria's evolving, and Fishes schooling. SI compromises of several algorithms such as Ant-Colony Optimization, Particle-Swarm Optimization (PSO), Artificial-Bee-Colony (ABC), Bacterial-Foraging Optimization, Fire-Fly Algorithm (FA), and Artificial-Fish-Swarm Optimization, and Shark Smell Optimization (SSO) [15]. Some of the critical SI algorithms are shown in Fig. 1.

3.1. SSO Algorithm

SSO is counted as the modern SI algorithm which was founded in 2014 by Oveis Abedinia, Nima Amjady, and Ali Ghasemi, which can be considered one of the best optimization tools. The development of this algorithm has relied on the ability of the shark because it has superiority in catching prey using a strong smell sense in a short time. In fact, the shark is one of the most renowned and superior hunters in nature. The reason for this superiority is the shark's ability to find the prey in a short time based on its

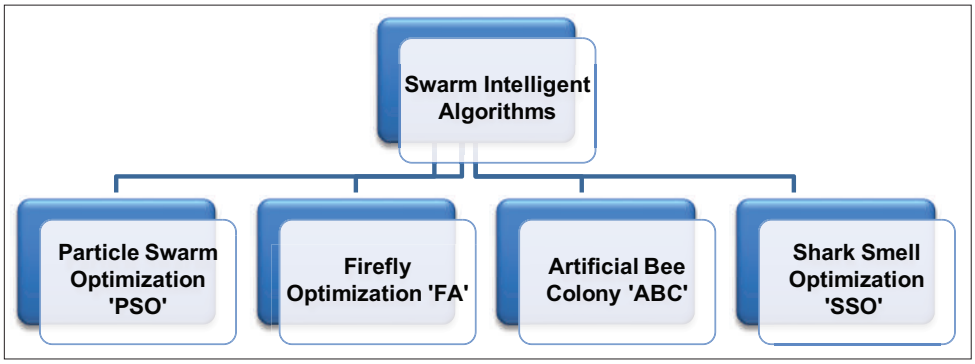

Fig. 1. Some algorithms of swarm intelligence [15].

strong smell sense in a large search space [16]. When prey is injured and blood is injected into the water, shark smells the odor of blood, and move toward the prey. The movement of shark toward prey is based mainly on the concentration and gradient of blood odor in the water particles.

The key factor that guides the shark toward its prey is concentration. Moreover, if the concentration is strong, the shark's movement will be increased [17], [18]. The pseudo code of the SSO Algorithm is described in the algorithm (1) below.

Algorithm (1): SSO description [16]

Begin

Step 1. Initialization

Set parameters NP, k_{max}, η_k, α_k, and (k=1, 2,…, k_{max})

Generate initial population with all individuals

Generate each decision randomly within the allowable range

Initialize the stage counter k = 1

For k= 1: k_{max}

Step 2. Forward Movement

Calculate each component of the velocity vector, $V_{i,j}$ (i=1,… NP, j=1,.. ND)

Obtain new position of shark based on forward movement, Y_i^{k+1} (i=1,…,NP)

Step 3. Rotational movement

Obtain the position of shark based on rotational movement, $Z_i^{k+1,m}$ (m = 1,…, M)

Select the next position of shark based on the two movements, X_i^{k+1} (i=1,…, NP)

End for k

Set k = k+1

Select the best position of shark in the last stage which has the highest OF value

End

3.2. The Steps of SSO Algorithm

SSO algorithm consists of four basic steps such as (initialization, forward movement, rotational movement, and position update), which can be listed as follows:

3.2.1. Initialization of SSO

To model the SSO algorithm, the population of the initial solution must be generated randomly within the search space.

Each of these solutions represents a particle of odor which shows a possible position of the shark at the beginning of the search process. The initial solution vector is shown in (1) and (2), respectively:

$$X^1 = \left[X_1^1, X_2^1, \ldots\ldots, X_{NP}^1 \right] \quad (1)$$

Where X_i^1 = ith initial position of the population vector and NP = population size. The related optimization problem can be expressed as:

$$X_i^1 = \left[X_{i,1}^1, X_{i,2}^1, X_{i,3}^1, .., X_{i,ND}^1 \right] \quad (2)$$

Where $X_{i,j}^1$ = jth dimension of the shark's ith position and ND = number of decision variables [19].

3.2.2. Forward movement of the SSO toward the target

When the blood is released in the water, the Shark in each position moves toward stronger odor particles with a velocity "V," to become closer to the prey (target). As a result, corresponding to the initial position vector, the velocity vector can be expressed by (3).

$$V^1 = \left[V_1^1, V_2^1, V_3^1, \ldots., V_{NP}^1 \right] \quad (3)$$

Each velocity vector has a dimensional component element as given in (4):

$$Vi^1 = \left[V_{i,1}^1, V_{i,2}^1, V_{i,3}^1, \ldots. V_{i,ND}^1 \right] \quad (4)$$

Hence, the velocity in each dimension is calculated by (5):

$$V_{i,j}^k = \eta k.\mathrm{R1}.\left.\frac{\partial(OF)}{\partial xj}\right|_{x_{i,j}^k} \quad (5)$$

Whereby: k= 1, 2,…., k_{max}, $\left.\frac{\partial(OF)}{\partial xj}\right|_{x_{i,j}^k}$ is a derivative of the objective function (OF) at the position $x_{i,j}^k$.

k_{max} = maximum number of stages for forwarding movement of the shark, k = number of stages, = a value in the interval (0, 1), and R1 = a random number in the interval (0, 1) [20].

The increase in shark's velocity is determined by the increase in the odor intensity. In each stage of $V_{i,j}^k$, the velocity limiter is employed by modifying (5) as shown in (6):

$$\mathrm{V}_{\mathrm{i,j}}^{\mathrm{k}} = \eta_{\mathrm{k}}.\mathrm{R1}.\left.\frac{\partial(\mathrm{OF})}{\partial \mathrm{xj}}\right|_{\mathrm{x}_{\mathrm{i,j}}^{\mathrm{k}}} + \alpha_{\mathrm{k}}.\mathrm{R2}.\mathrm{V}_{\mathrm{i,j}}^{\mathrm{k-1}} \quad (6)$$

Where $\beta\kappa$ is a velocity limiter ratio for stage k, αk is the inertia coefficient in (0, 1), and R2 like R1 is a random number in the interval (0, 1).

Due to forward movement of the shark, its new position is Y_i^{k+1} determined based on its previous position (X_i^k) and velocity (V_i^k), the new position of the shark is depicted by (7):

$$Y_i^{k+1} = X_i^k + V_i^k.\Delta \mathrm{t_k} \quad (7)$$

Where Δtk = is a time interval which is assumed to be 1 for simplicity [21]. The forward movement of the shark toward the prey is represented in Fig. 2.

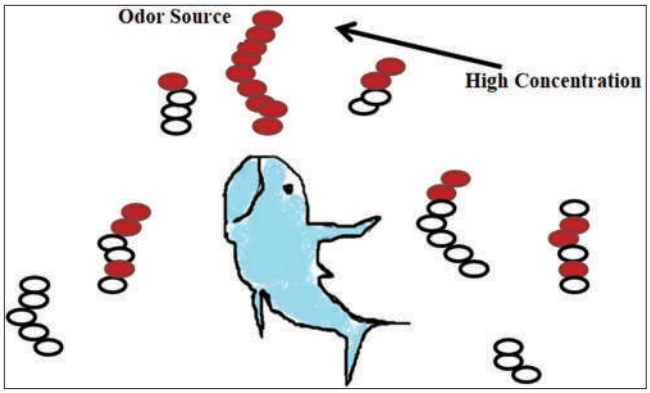

Fig. 2. Shark's forward movement [21].

3.2.3. Rotational movement of the SSO toward the target

The shark is also has a rotational movement which is used to find the stronger odor particles. This process is called the local search of the SSO algorithm modeled by (8).

$$Z_i^{k+1,m} = Y_i^{k+1} + \mathrm{R3}.Y_i^{k+1} \quad (8)$$

m = 1, 2,…, M, and R3 is a random number that can be considered in the interval (−1, 1). To model the rotational movement of the shark, the number of points M in the local search is connected to form closed contour lines, as shown in Fig. 3 [22].

3.2.4. Updating the particle position (Location)

The shark's search path will continue with the rotational movement as it moves closer to the point with a stronger

odor sense as revealed in Fig. 3. This specific feature in the SSO algorithm can be expressed as in (9).

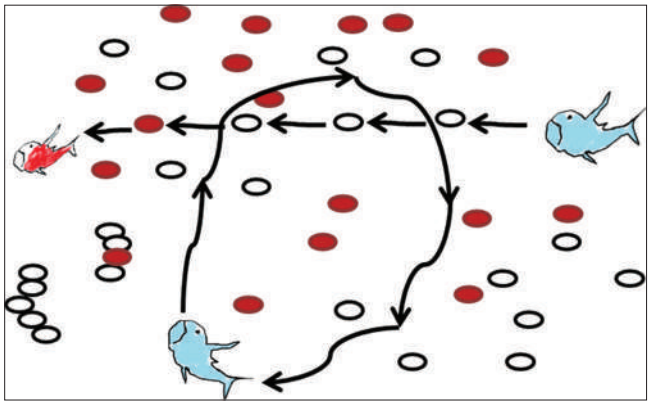

Fig. 3. Shark's rotational movement [23].

$$X_i^{k+1} = \arg\max\{OF(Y_i^{k+1}), OF\left(Z_i^{k+1,i}\right), .., OF(Z_i^{k+1,M})\} \quad (9)$$

Where: X_i^{k+1} represents the shark's next position with the highest value of the objective function (OF). The process will continue until k reaches the maximum value (best individual) in the given population in a search space chosen for an optimization problem [23].

4. THE PROPOSED METHOD

This section presents the critical stages of the proposed method, where the SSO algorithm is used to extract the best features from the user's fingerprint image.

All the stages of the proposed method have been implemented, designed, and written by java programming language because it is easy to write, compile, debug, and compatible with most of the platforms. For this, purpose Netbeans integrated development environment version 8.2 has been installed from oracle official website with Java Development Kit version 8u192. Microsoft Access 2010 is used to create a small database to store the user's features and biographic information. The graphs created by the proposed method. ZKTeco: ZK4500 fingerprint reader is used to acquire samples because it is an up-to-date and high-quality device. Furthermore, the proposed system was implemented using Windows 10 operating system 64-bit and computer with Intel® Core™ i7-7500U CPU running at a frequency of 2.90 GHz and (8) GB of RAM. The proposed method consists of four stages, namely, create a database to store and organize data, image pre-processing, feature extraction, and matching process. The detail of each stage has been illustrated

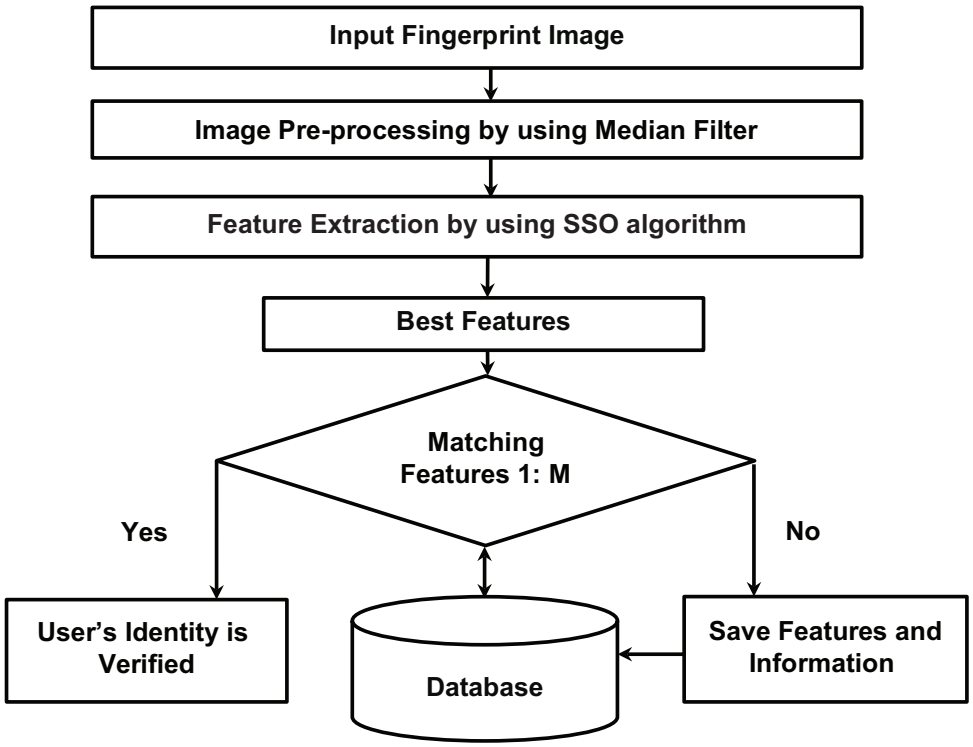

Fig. 4. Block diagram of the proposed method.

Fig. 5. Fingerprint image samples and ZKTeco device.

in the following subsections. Fig. 4 shows the block diagram of the proposed method.

4.1. Create a Database to Store and Organize Data

This is the first stage for handling this study, in which data acquisition is done using a newest and high-quality fingerprint device reader called (ZKT eco: ZK4500) which is the main requirement tool. Our dataset consists of merely (150) fingerprint images that were collected and acquired from various volunteer students of age ranging from 18 to 22 years at Technical College of Informatics (TCI) and Institute of Computer Science (ICS) at Sulaymaniyah city by the ZKTeco device. The taken real samples were resized to 128*128 and the format was also changed to Joint Photographic Experts Group. Furthermore, any image sizes with extensions bitmap, portable network graphics, and graphics interchange format can be handled by the proposed method. Fig. 5 demonstrates the ZKTeco device and some samples of fingerprint images. The database is created to store the information of the users and their seven features to be used later for the matching process.

4.2. Image Pre-processing Using Median Filter

This is the second stage of the proposed method. During live fingerprint scanning, a major issue that may be introduced is noise on the fingerprint image so that for removing and eliminating the noise from the fingerprint image and improve the performance and efficiency of the proposed system an efficient filter is required. In this stage, a (3*3) median filter is used as an efficient non-linear filter to remove noise from the user's fingerprint image. Therefore, an optimal image quality achieved after enhanced by utilizing the median filter

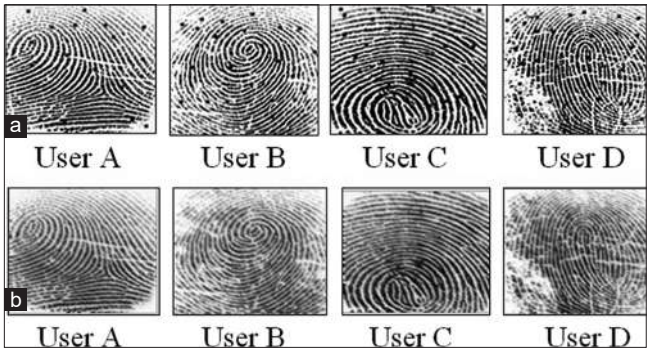

Fig. 6. (a) Original image and (b) fingerprint images before and after applying the median filter with mask (3*3).

which was ready for the feature extraction stage, as depicted in Fig. 6b.

4.3. Feature Extraction Using SSO Algorithm

In this stage, the SSO algorithm used to extract the best features from the user's fingerprint image. First, the SSO algorithm has applied to the fingerprint image. Second, the fitness or goodness has found for each location around the shark using fitness function (F). In this study, seven iterations have been applied by the SSO algorithm to extract seven best features from each user's fingerprint image where in each iteration only one feature extracted that has the highest fitness value. During the iteration of the algorithm, the shark's location has been updated to either forward according to seven or rotational according to eight. The determination of the shark's direction toward forwarding or rotational has relied on the fitness value of that location. The location that is visited by the SSO algorithm cannot be visited again. The applied SSO algorithm to find the best features is described in the algorithm (2) and the flowchart in Fig. 7.

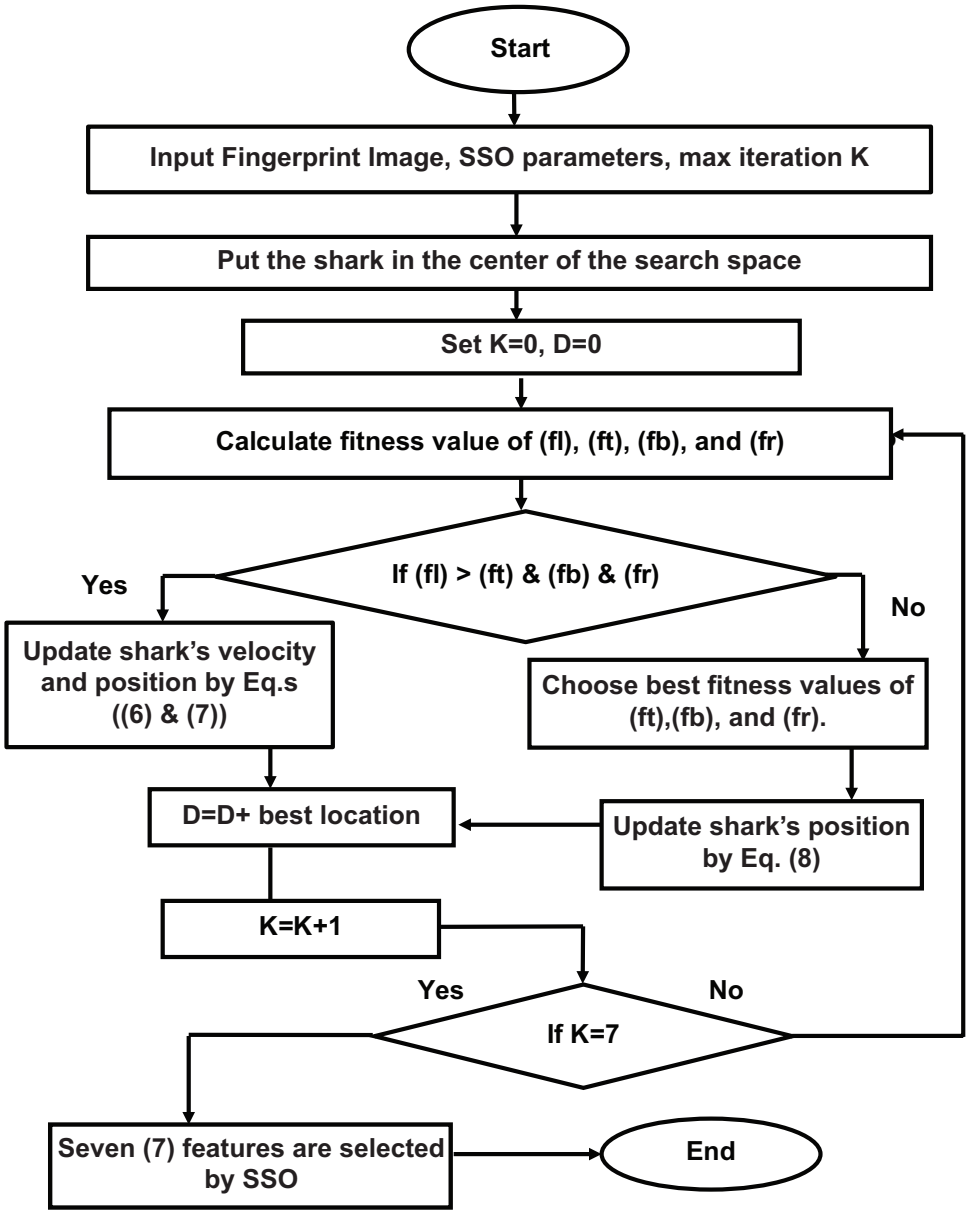

Fig. 7. Flowchart of the applied shark smell optimization algorithm.

4.4. Matching (Similarity) Process

This is the final stage and most significant stage of the proposed system because the reliability of any fingerprint authentication has relied on the matching process. The match (similar) operation is implemented using the ED calculated by (10) [24]. Similarity (matching) is carried out twice, the first is when entering the authorized user's data, where the fitness value of the user to be entered matches (similar) with all the fitness values of the database, this process called identification (1:M). The second takes place between the fitness value of the user claiming to be authorized and the fitness value of the authorized user that actually stored in the database, this process called verification (1:1).

$$\mathrm{ED}\left(\mathrm{p},\mathrm{q}\right) = \sqrt{\left(px - qx\right)^2 + \left(py - qy\right)^2} \qquad (10)$$

Where ED is the distance between point p and q at (x, y) coordinates.

Algorithm (2): Applied SSO algorithm for feature extraction

Input: User's Fingerprint Image, max iteration (k_{max}) = 7

Output: Selected 7 best features

Begin

Step 1: Set the SSO parameters (NP= 128, ND= 128, ηk=1, αk=1, Δt_k=1 and R1=R2=R3=1)

Step2: Put the shark in the center of the fingerprint image.

Step3: Calculate the fitness value of each location (ft, fb, fl and fr) around the shark by using fitness function (F).

Step4: If fitness (fl) > (fr) and (ft) and (fb) then

-Update Shark's velocity according to Eq. (6)

-Update Shark's position to forward movement according to Eq. (7)

Else

-Choose highest fitness value among (fr), (ft), (fb).

-Updating a shark's position to rotational movement according to Eq. (8)

Step5: new shark's position is identified

Step 6: If k is not equal to k_{max} then go to Step2

Step7: Seven (7) features are selected

End

End

5. RESULTS ANALYSIS AND DISCUSSION

In this section, the outcomes obtained from the proposed method have been explained in detail. The experimental results are tested with 150 fingerprint images and Fig. 8 shows only the first four samples. These samples are taken from students at both the TCI and the ICS at Sulaimani city using the ZKTeco device.

After loading the user's fingerprint image, it is pre-processed using a median filter with a mask (3*3) to remove the noise from the image without blurring the edges and other sharp details of the image. Both the original image and the filtered image for four various users are depicted in Fig. 6.

The proposed method used the SSO algorithm to extract seven best features from each user's fingerprint image and stored in the database for the matching process. Fig. 9 decomposes into four subfigures; each subfigure shows seven locations (best features) that are extracted by SSO for four users.

According to the results that are shown in the graphical representation of Fig. 9, it is confirmed that the SSO algorithm extracted seven best features depending on the fitness value of that location in a smart and random way.

Fig. 10 indicates the locations that are visited and chosen as features by the SSO algorithm after seven iterations for four fingerprint images. Since the unique features of each fingerprint

are located in the around of the center and those features are extracted indicated the efficiency of the algorithm used.

Table 1 displays the execution time elapsed in different iterations by the SSO algorithm to extract the best features. As a consequence, the SSO algorithm was highly efficient and required minimum time for extracting seven best features for each user's fingerprint image.

The elapsed execution time required for each stage of the proposed method for four users is tabulated in Table 2. According to the time execution results, the algorithm was highly efficient and fast. Based on the comparative results, the minimum and same time spent in both users (A) and (C) for features extraction when compared with the other users, followed by the user (B); however, the maximum time spent in user (D) for features extraction.

Moreover, the performance of the proposed method is evaluated and obtained from three renowned metrics, namely, FAR, FRR, and CVR. FAR, FRR, and CVR are calculated by (11), (12), and (13), respectively [25].

FAR= number of FAR/total number of the test sample (11)

FRR= number of false rejection/total number of the test sample (12)

CVR= (1-FAR-FRR) *100% (13)

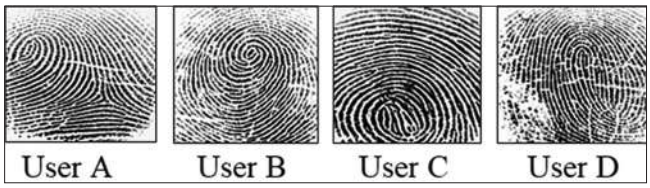

Fig. 8. Test fingerprint image samples for four users.

TABLE 1: Execution time and different iterations for SSO algorithm

Iteration no.	Time (s)
1	1
3	3.2
5	5.4
7	8

s=Second

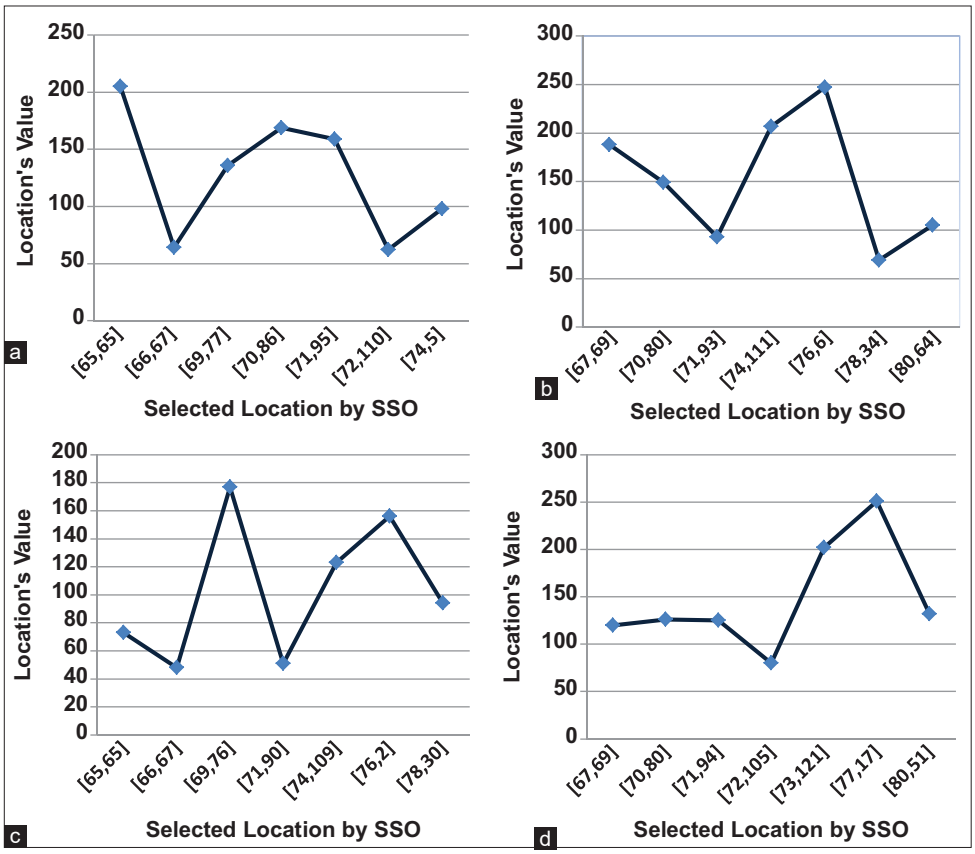

Fig. 9. (a-d) Relationship between the locations and their values for four users.

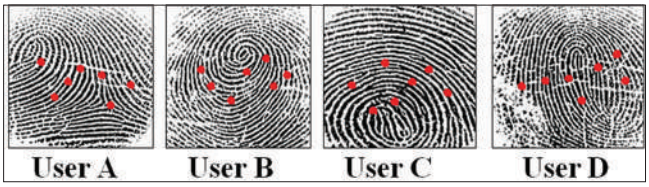

Fig. 10. Best locations that are visited by shark smell optimization algorithm.

TABLE 2: Execution time for each stage of the proposed method

No.	User	Pre-processing (s)	Features extraction (s)	Features matching (s)
1	A	11	7	8
2	B	12	8	9
3	C	11	7	8
4	D	11	9	10

For evaluating the performance of the proposed method, we tested our system using (15), (50), (100), and (150) user's fingerprint image, respectively. As a consequence, the system was extremely accurate according to FAR, FRR, and CVR which were 0.00, 0.00, and 100%, respectively, when (15) and (50) users used for the test. However, when we tested our system by incrementing the number of users to (100) and (150), solely (1) user was falsely rejected as an unauthorized user out of (100) and (150) users, as presented in Table 3.

TABLE 3: Performance of the proposed method

Fingerprint Image No.	Error rate metrics		
	FAR	FRR	CVR %
15	0.00	0.00	100
50	0.00	0.00	100
100	0.00	0.01	99
150	0.00	0.00666	99.334

FAR: False acceptation rate, FRR: False rejection rate, CVR: Correct verification rate

Ultimately, Table 4 displays the comparison that has been done in terms of error rate metrics between the performance of the proposed method and previous methods that are proposed by other researchers that are reviewed in the literature review. The performance of the proposed method was higher than the other methods when tested using the datasets of Mahale *et al.* [9] and Dakhil and Ibrahim [12] due to using an intelligence algorithm for feature extraction, as shown in Table 4.

TABLE 4: A comparison between the performance of the proposed method and previous methods

Ref.	Algorithm used	FAR	FRR	CVR%
[9]	Minutiae extractor algorithm (MEA)	0.0154	0.0137	97.09
[12]	Filter bank based (FBB) algorithm and K-nearest neighbor (K-NN)	0.012698	0.047619	93.9683
Proposed method	SSO algorithm	0.00	0.0125	98.75

FAR: False acceptation rate, FRR: False rejection rate, CVR: Correct verification rate

Moreover, the results that are shown in Table 4 proved that using a SI algorithm for proposing a fingerprint authentication system achieved higher CVR than the other algorithms used in the previous methods.

6. CONCLUSION AND FUTURE WORK

In this paper, a credible fingerprint authentication was proposed using a new SI algorithm named SSO. Conclusions that can be inferred from this study are listed as the following:

- Fig. 6 showed that the median filter was a good filter for noise elimination and image enhancement.
- Fig. 9 indicated that the 7 locations (best features) that are extracted by the SSO algorithm had high fitness value and were chosen in a smart and random way.
- Table 2 presented that the proposed method was fast and each stage elapsed minimum execution time.
- Table 3 presented that the proposed method was an excellent fingerprint authentication that based on intelligent algorithm because it gave higher CVR which was 99.334% and lower FAR and FRR which were 0.00 and 0.00666, respectively.
- According to Table 4, the performance of the proposed method was higher than the previous methods which proved that using an intelligence algorithm to propose fingerprint authentication gives a higher CVR rate than the traditional algorithms.

For future study, we intend to examine, practice, and mix more than one SI algorithms for instance: ABC, FA, PSO, and SSO variations such as chaotic binary SSO (CBSSO) algorithm to propose more complex unimodal fingerprint biometric authentication to achieve a better rate of FAR, FRR, and CVR.

7. AKNOWLEGMENT

The authors would like to thank the volunteer students at TCI and ICS at Sulaymaniyah city for their unconditional participation to give their fingerprint images during data collection.

REFERENCES

[1] O. J. Ayangbekun and A. P. Ajigboteso. "Simulation of an authorization system using access cards with chips and fingerprint". *IJRIT International Journal of Research in Information Technology*, vol. 2, no. 10, pp. 601-610, 2014. Available from: https://www.researchgate.net/publication/329538683_Simulation_of_an_Authorization_System_Using_access_cards_with_chips_and_fingerprint. [Last accessed on 2019 Oct 28].

[2] C. Wang, Y. Wang, Y. Chen, H. Liu and J. Liu. "User authentication on mobile devices: Approaches, threats and trends". *Computer Networks*, vol. 170, pp. 107-118, 2020.

[3] C. Rathgeb and A. Uhl. "A survey on biometric cryptosystems and cancelable biometrics". *EURASIP Journal on Information Security*, vol 1, p. 3, 2011.

[4] E. Chandra and K. Kanagalakshmi. "Noise elimination in fingerprint image using median filter". *The International Journal of Advanced Networking and Applications*, vol. 2, no. 6, pp. 950-955, 2011. Available from: http://www.citeseerx.ist.psu.edu/viewdoc/download?doi=10.1.1.419.1632&rep=rep1&type=pdf. [Last accessed on 2019 Nov 01].

[5] S. K. Sahoo, T. Choubisa and S. M. Prasanna. "Multimodal biometric person authentication: A review". *IETE Technical Review*, vol. 29, no. 1, pp. 54-75, 2012.

[6] M. G. Abdul-Haleem, L. E. George and H. M. Al-Bayti. "Fingerprint recognition using haar wavelet transform and local ridge attributes only". *International Journal of Advanced Research in Computer Science Software Engineering*, vol. 4, no. 1, 2014. Available from: https://www.researchgate.net/publication/335025795_Fingerprint_Recognition_Using_Haar_Wavelet_transform_and_local_ridge_attributes_only. [Last accessed on 2019 Sep 17].

[7] A. Çalışkan and Ö. F. Ertuğrul. "Wavelet Transform Based Fingerprint Recognition". In *2015 23nd Signal Processing and Communications Applications Conference*, pp. 1481-1484, 2015.

[8] U. H. L. Akter. "Speeded-up Robust Feature Extraction and Matching for Fingerprint Recognition". *2nd International Conference on Electrical Engineering and Information and Communication Technology*, 2015.

[9] V. H. Mahale, M. M. Ali, P. L. Yannawar and A. T. Gaikwad. "Fingerprint Recognition for Personal Identification and Verification Based on Minutiae Matching". In: *IEEE 6th International Conference on Advanced Computing*, pp. 332-339, 2016.

[10] H. R. Su, K. Y. Chen, W. J. Wong and S. H. Lai. "A Deep Learning Approach Towards Pore Extraction for High-Resolution Fingerprint Recognition". In: *2017 IEEE International Conference on Acoustics, Speech and Signal Processing*, pp. 2057-2061, 2017.

[11] Z. J. Ahmed and L. E. George. "Fingerprints recognition using the local energy distribution over haar wavelet subbands". *International Journal of Science Research*, vol. 6, no. 9, pp. 979-986, 2017.

[12] I. G. Dakhil and A. A. Ibrahim. "Design and implementation of fingerprint identification system based on KNN neural network". *Journal of Computer Communications*, vol. 6, no. 3, pp. 1-18, 2018.

[13] A. Kyaw and Z. L. Aung. "A robust fingerprint recognition technique applying minutiae extractors and neural network". *International Journal of Engineering Research and Advanced Technology*, vol. 5, no. 3, pp. 78-87, 2019.

[14] H. Kaur and H. S. Pannu. "Zernike moments-based fingerprint recognition using weighted-support vector machine". *Modern Physics Letters B*, vol. 33, no. 21, pp. 1950245.

[15] M. Mavrovouniotis, C. Li and S. Yang. "A survey of swarm intelligence for dynamic optimization: Algorithms and applications". *Journal of Swarm and Evolutionary Computation*, vol. 33, pp. 1-22, 2017.

[16] S. Mohammad-Azari, O. Bozorg-Haddad and X. Chu. "Shark smell optimization (SSO) algorithm". In: *Advanced Optimization by Nature-Inspired Algorithms*, Springer, Berlin, pp. 93-103, 2018.

[17] M. Ehteram, H. Karami, S. F. Mousavi, A. El-Shafie and Z. Amini. "Optimizing dam and reservoirs operation based model utilizing shark algorithm approach". *Journal Knowledge-Based Systems*, vol. 122, pp. 26-38, 2017.

[18] O. W. Salami, I. J. Umoh, E. A. Adedokun, M. B. Mu'azu and L. A. Ajao. "Efficient Method for Discriminating Flash Event from DoS Attack during Internet Protocol Traceback using Shark Smell Optimization Algorithm. In: *2019 2nd International Conference of the IEEE Nigeria Computer Chapter*, pp. 1-10, 2019.

[19] H. Hosseinzadeh and M. Sedaghat. "Brain image clustering by wavelet energy and CBSSO optimization algorithm". *Journal of Mind and Medical Sciences*, vol. 6, no. 1, pp. 110-120, 2019.

[20] N. Gnanasekaran, S. Chandramohan, P. S. Kumar and A. M. Imran. "Optimal placement of capacitors in radial distribution system using shark smell optimization algorithm". *Ain Shams Engineering Journal*, vol. 7, no. 2, pp. 907-916, 2016.

[21] O. Abedinia, N. Amjady and A. Ghasemi. "A new metaheuristic algorithm based on shark smell optimization". *Complexity*, vol. 21, no. 5, pp. 97-116, 2016.

[22] H. Hosseinzadeh. "Automated skin lesion division utilizing Gabor filters based on shark smell optimizing method". *Evolving Systems*, 43, pp. 1-10, 2018.

[23] S. A. Juma. "*Optimal Radial Distribution Network Reconfiguration Using Modified Shark Smell Optimization*". MSc. Thesis, Jkuat-Pausti. Available from: http://www.ir.jkuat.ac.ke/bitstream/handle/123456789/4854/Shaibu_Ali_Juma_EE300-0012%20%2017_Thesis%20Report.pdf?sequence=1&isAllowed=y.

[24] K. M. Sagayam, D. N. Ponraj, J. Winston, E. Jeba and A. Clara. "Authentication of biometric system using fingerprint recognition with euclidean distance and neural network classifier". *International Journal of Innovative Technology Exploring Engineering*, vol. 8, no. 4, pp. 766-771, 2019.

[25] T. W. A. Khairi. "Secure mobile learning system using voice authentication". *Journal of Engineering Applied Sciences*, vol. 14, no. 22, pp. 8180-8186, 2019.

ORIGINAL RESEARCH ARTICLE UHD JOURNAL OF SCIENCE AND TECHNOLOGY

Text Detection on Images using Region-based Convolutional Neural Network

Hamsa D. Majeed

Department of Information Technology, University of Human Development, Sulaymaniyah, Iraq

ABSTRACT

In this paper, a new text detection algorithm that accurately locates picture text with complex backgrounds in natural images is applied. The approach is based primarily on the region-based convolutional neural network anchor system, which takes into account the unique features of the text area, compares it to other object detection tasks, and turns the text area detection task into an object sensing task. Thus, the proposed text to be observed directly in the neural network's convolutional characteristic map, and it can simultaneously predict the text/non-text score of the proposal and the coordinates of each proposal in the image. Then, we proposed an algorithm for the construction of the text line, to increase the text detection model accuracy and consistency. We found that our text detection operates accurately, even in multiple language detection functions. We also discovered that it meets the 2012 and 2014 International Conference on Document Analysis and Recognition thresholds of 0.86 F-measure and 0.78 F-measure, which clearly shows the consistency of our model. Our approach has been programmed and implemented using Python programming language 3.8.3 for Windows.

Index Terms: Text Detection, Region-based Convolutional Neural Network, Text Images

1. INTRODUCTION

In recent years, enabling computers to read the text in natural images [1]-[3], [4] have been gaining increased attention. It can be used in optical character detection (optical character recognition), photography, and robot navigation. In this research, the two primary activities that concerned us were reading text and understanding text. Our research is based primarily on text identification in natural images, which is far more complex than text detection on a well-maintained text file.

In the previous text, detection works the majority of the works employs bottom-up pipelines, which often include the following steps: Grouping or filtering of characteristics and the configuration of the line text. Some common issues exist in all these processes. First, the effects of character detection using sliding window methods or related component-based approaches largely depend on their efficiency. Mainly low-level characteristics (e.g., based on stroke width transform [5], maximally stable extremal regions [6], or histogram of oriented gradients [7]) are studied in these approaches.

Without background knowledge, it is difficult to define each stroke or character separately. At the same time, it is easy to result in a low recall where ambiguous characters are easily discarded, causing more difficulties for handling them in the following steps. Second, there are several incremental phases with a bottom-up strategy, which makes the method very complex. These difficulties, therefore, reduce the power and efficiency of the program.

Deep learning technology has greatly increased the efficiency of target detection [1], [2], leading to advances

Access this article online

DOI: 10.21928/uhdjst.v4n2y2020.pp40-45

E-ISSN: 2521-4217
P-ISSN: 2521-4209

Corresponding author's e-mail: Hamsa D. Majeed, Department of Information Technology, University of Human Development, Sulaymaniyah, Iraq. E-mail: hamsa.al-rubaie@uhd.edu.iq

Received: 02-05-2020 Accepted: 27-07-2020 Published: 02-08-2020

in text detection. A variety of recent approaches has been used to create pixel predictions of text or non-text in fully convolutional networks (FCNs). In addition, segmentation of text semantic can lead to greater skill in exploiting rich field context data to identify ambiguous content, which leads to less erroneous detections. Two fully coevolutionary networks fell behind the paradigm to make the findings more robust. The second FCN produces word-level or character-level predictions on text region detected by the first FCN. All these steps just lead to a much more complex method. Many techniques are being used to forecast the limits of text in natural images through sliding windows by coevolutionary features, such as the state-of-the-art region-based convolutional neural network (R-CNN) technique where A Region Proposal Network (RPN) is proposed to generate high-quality object proposals directly from convolutional feature maps. And then, these region proposals are fed into a Faster R-CNN model for further classification. In object detection, each object has a well-defined closed boundary, while it is difficult to find one in-text, which makes it more challenging to predict the text line accurately.

The Region Proposal Network presented in [8] is extending in this paper to localize the text lines accurately. We have put into target detection the issue of text line detection. In the meantime, we use the benefits of profound convolution and computer networking systems. In Fig. 1, the results are shown on our network architecture and text proposal identification.

First, we break the function of text identification into a series of fine text proposals. To forecast the proposal position and text and non-text data together, we refine Faster R-CNNs anchor regression method. This can lead to better localization accuracy.

Second, the text line construction algorithm has been proposed to integrate with the fine-scale proposal into a text line area. The proposed method is to join and single process the multiscale and multilingual text.

Third, with using International Conference on Document Analysis and Recognition (ICDAR) 2012 and ICDAR 2014, our model showed reliable and accurate results with text detection.

2. RELATED WORK

The past text on image detections is primarily utilized bottom-up methods [9]-[11] or sliding window methods [12]-[15] to detect characters or screen components. The methods used for sliding windows detect text propositions by glancing through an image in a multiscale window and cascading behind the device a classifier to locate text proposals using manually built software or recent CNN features [13], [16], [17]. The methods are based on the related components primarily implement a fast filter to differentiate text from non-text using low-level properties, such as gradient, stroke distance, and color [18].These bottom-up methods do not perform well in character detection and the following steps have produced cumulative false answers. In addition, the bottom-up method is complex and computationally expensive; particularly the sliding windows approach that needs a ranking on several sliding windows).

Fig. 1. The output of our model.

The efficiency of text detection [1], [2], [4], [5], mostly sliding window system, has recently been advanced by deep learning technologies. They are all have enhanced, primarily using very deep CNN and sharing a coevolutionary mechanism [3], also used to minimize computational costs, to benefit from high-level deep characteristics. Many FCN-based methods were, therefore, provided and findings in text detection tasks were promising. Ren [10] recently introduced a Faster R-CNN object detection method that achieved state-of-the-art object detection tests. They proposed an area proposal network (RPN) that produces highly credible entity proposals directly from the coevolutionary functional maps, fast enough to exchange coevolutionary details. These works are inspiring for our model.

3. METHODOLOGY

There are two modules in our text detection system. In particular, the first module uses a very large, convolutional neural network to create fine-scale proposal regions. The second module is a text line construction that can complete text lines through the text proposal regions given in the

previous module. In the natural picture, the machine will correctly predict the text line. Section A provides us with the concept of faster area CNN and how it fits well in the role of text detection. We propose our text line algorithm in Section B. Fig. 2 shows the block diagram of the proposed method.

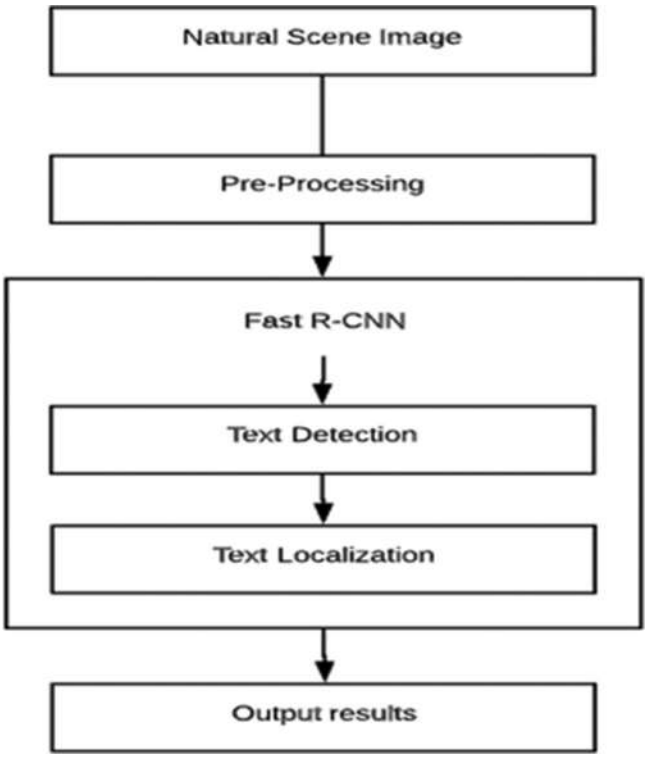

Fig. 2. Method block diagram.

3.1. Fine-scale Proposal Network

Concerning object detection, due to the many cutting-edge tests on object detection benchmark, Faster R-CNN has proved an effective and reliable object detection platform. Its central segment is the area proposal network, which slides a small window in the coevolutionary software, which takes arbitrary formats as input and generates a series of rectangular proposals. Faster R-CNN considers that both the network predicting proposals and classifier networks share a common set of convolutional. RCNN architecture is shown in Fig. 3.

In comparison to general sliding window techniques, (RPN) Fig. 4. applies an effective anchor regression system to identify multiscale items with a single sliding window. This, in turn, reduces to a certain degree the estimated costs for the whole network. The reason that a single-window will forecast mixed objects is primarily that a window maps the multiscaled objects in the original image into multiple anchors with different aspects ratios. We also apply this anchor function in our model in this paper for text detection. The task of text detection is not quite the same as the process of detection of objects. There could be no visible closed boundary in the text field in the picture as can also be used in object detection tasks. It consists of multilevel elements, such as character, text line, stroke, and text area that are not easy to discern.

In all respects, we optimize the anchor function to anticipate components in the text detection process in various stages. We note that a text line can be seen as a series of fine-scale

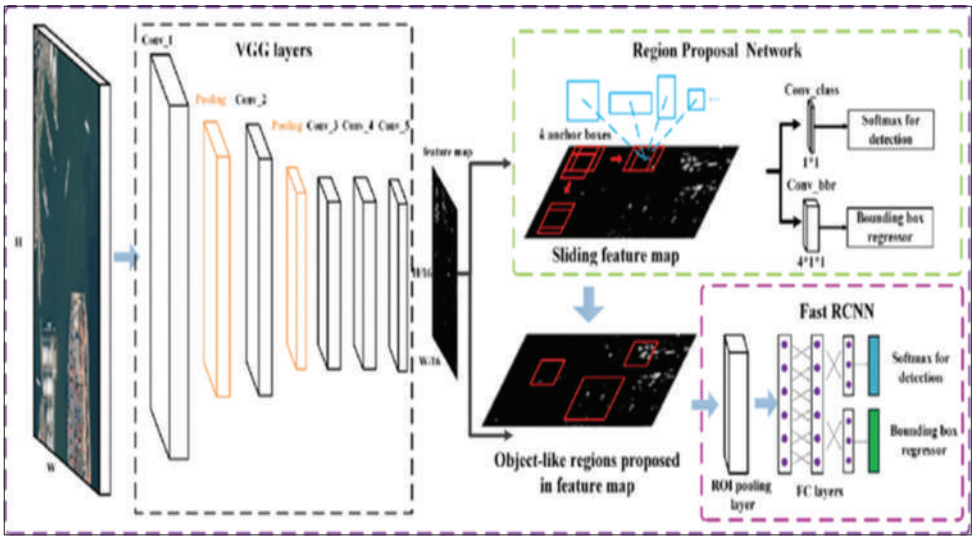

Fig. 3. The architecture of the region-based convolutional neural network.

$$L_{\text{loc}}(t^u, v) = \sum_{i \in \{x,y,w,h\}} \text{smooth}_{L_1}(t_i^u - v_i), \quad (2)$$

in which

$$\text{smooth}_{L_1}(x) = \begin{cases} 0.5x^2 & \text{if } |x| < 1 \\ |x| - 0.5 & \text{otherwise,} \end{cases} \quad (3)$$

Fig. 4. Loss function of the regressor.

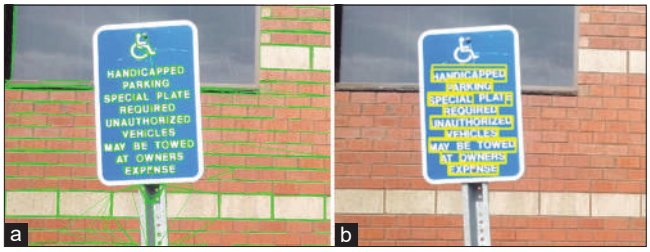

Fig. 5. (a). Results with no non-maximum. (b). Results with non-maximum.

text recommendations that can be used to some degree as an object detection function. We assume that a series of text recommendations from a text line will operate with small scale text detection and different aspect ratios. The anchor function was strengthened as follows: Each text proposal is designated as a 16-pixel fixed-width equivalent to the detector through the conv5 maps, the VGG 16's lasts coevolutionary map that can extract deeper input image features. Moreover, K anchors are established to predict the height of the proposals. (In our experiment, we use K = 10). They are all 16 pixels in width and not the same height to correspond to different scale text regions. Input an image of some size to the VGG 16 model and a Wh HhC functional maps on the conv5 convolution layer (which is the room structure, C is several channels). The transmission detection is as follows: And our model then rolls a 3h3 window through the conv5 function maps, making every window predictable. Moreover, each forecast shall contain K proposals with input picture coordinates and values. All the proposals are compiled and screened, and they do not exceed 0.7 in the next phases.

3.2. Construct the Text Line

Following the development of the text detection network from the Faster R-CNN encoding, a series of fine text proposals is introduced, as shown in Fig. 5a. Our primary goal is to break all these implicit text proposals into various sections of the text field and exclude proposals that do not belong to any text field. It is possible, for some non-text objects with identical composition to text patterns to generate false detection. The non-maximum suppression (NMS) algorithm that was recently widely used in computer vision activities was proposed by Alexander Neubeck and Luc Van Gool. NMS algorithm deletes non-maximum objects that can be called a local maximal search. This is generally used to determine the top scoring range, which normally indicates the tremendous potential for object detection to be the target object. Based on this work, we find the NMS algorithm to be used to eliminate proposals with low scores and create a specific text field for our text detection model. The findings from the results also supported our conjecture. The picture processed after NMS, as shown in Fig. 5b. There are a variety of simple text areas that are composed of a series of adjacent fine text recommendations after each of the above steps are completed. To recreate text lines in input imagery using adjacent text proposals, we suggest an algorithm for text line construction.

The following words are laid down for lines of text:

1. The text line is defined to appear as a quadrilateral in the original image;
2. As the vertical texture region written at the top-to-bottom is not protected in our paper, it is laid down in the text lines that the aspect ratio should not be <2.1;

The next task is to decide where the text region is located. The left and right sides of the quadrilateral text region should be calculated first.

Text line field consists of a series of fine-scale text proposals which are all small, vertical rectangular boxes, the left boundary of the build text line is a left-most boundary of the rectangular text line, and the right border is the right-most rectangular border of all the rectangular boxes that make up the text line. We used the linear regression with the other two parameters to evaluate the commonly used linear regression is often used to predict a sequence of discrete points to evaluate a regression curve that can represent as precisely as possible discrete points.

We use the least squares approach to evaluate a regression line as the top and bottom limits of the text field based on our statement above. Linear regression is used as a tool in the mathematical field specifically to perform curve modification at several discrete points. This allows an understanding of understanding how discrete points are represented as errors as possible.

The text area is completed after the above measure. Moreover, from all text areas built as the true text line blocks

of the original image, we then pick all text areas with a score of at least 0.9.

3.3. Implementation Details

The normal backpropagation and stochastic gradient descent are a qualified method for final text detection. Our samples were obtained from the ICDAR 2014 multilingual text detection competition training results and ICDAR 2012 language localization process competition. We are not larger than 1200 on all training pictures and shorter than 600 on the short side, until the training of the pattern. We have not used the fully ICDAR 2014 training data. We initialize the new fully convolutional layer utilizing the Gaussian distribution of the random 0 means and 0.01 standard variance with the VGG 16 model prepared on ImageNet results. We use 0.9 impulses and weight loss of 0.0005. The analysis limit in 50 K iterations is set to 0.00001. Moreover, our model was implemented in the TensorFlow framework.

4. RESULTS

In the results section, we test our model in both ICDAR 2012 and 2014, with a comparison with the previous researches results in both ICDAR 2012 and 2014 our model had a better result like the following:

4.1. ICDAR 2012 Experiments

The ICDAR 2012 dataset consists of 230 training and 252 sample images in their original. Predominantly, these images are deduced from born-digital images and real-scene photographs. In this article, we check our 2014 version dataset models that were revised in 2014 to optimize the initial version margin. Furthermore, in this case, our model reaches an F-measurement of 0.86, which is a higher than expected result. Our approach has major advantages over the other as Table 1 reveals. Our model supports a more reliable text line identification that enhances efficiency under the ICDAR 2012 and 2014.

The results showed that our proposed method and model had a better recall and precision rate better than previous models.

4.2. ICDAR 2014 Experiments

The ICDAR 2014 dataset has 242 training pictures, and 251 evaluation pictures, mainly of real scene photographs, close to the ICDAR 2012. In Table 2, we equate the performance of our model with other comparative outcomes. The ICDAR 2014 has to be developed for the near-horizontal identification of text, but cannot completely cover the actual text in slanted text images. In this case, our model will perform well, leading to improved results in inclined text detection tasks.

TABLE 1: Experiments results of the ICDAR 2012

Method	Recall	Precision
Yao	0.75	0.73
TextFlow	0.76	0.78
Ching	0.71	0.83
Huang	0.66	0.84
Lai	0.68	0.81
The proposed Method	0.89	0.86

International conference on document analysis and recognition

TABLE 2: Experiments results of the ICDAR 2014

Method	Recall	Precision
Yon	0.61	0.81
FAText	0.73	0.80
SDD	0.66	0.84
Neumen	0.70	0.82
The proposed method	0.79	0.88

International Conference on Document Analysis and Recognition

5. CONCLUSION

In the original picture, we have provided an effective and reliable model for text detection that predicts bounding line boxes. Using the Quicker Region-CNN with our anchor function, we predict a series of fine text proposals. In our experiment, we use an extremely deep network to quantify the image to obtain the deep characteristics of the image to boost the prediction performance. Instead, with the fine-scale texting proposals, we suggested a new structure algorithm for the text rows with the aid of a linear regression method. Such main strategies give the identification of the text line a valuable skill for the identification of text. Both ICDAR 2012 and ICDAR 2014 produced excellent results.

REFERENCES

[1] W. Tao, D. J. Wu, A. Coates and A. Y. Ng. "*End-to-end Text Detection with Convolutional Neural Networks*". Pattern Detection (ICPR), 2012 21st International Conference on IEEE, 2012.

[2] J. Max, A. Vedaldi and A. Zisserman. "Deep features for text spotting". In: *European Conference on Computer Vision*. Springer, Cham, 2014.

[3] N. Lukáš and J. Matas. "*Efficient Scene Text Localization and Detection with Local Character Refinement*". Document Analysis and Detection (ICDAR), 2015 13th International Conference on IEEE, 2015.

[4] M. Rodrigo, N, Thome, M. Cord, J. Fabrizio and B. Marcotegui. "*Snoopertext: A Multiresolution System for Text Detection in*

Complex Visual Scenes". Image Processing (ICIP), 2010 17th IEEE International Conference on IEEE, 2010.

[5] K. Dimosthenis, F. Shafait, S. Uchida, M. Iwamura, L. G. Bigorda, S. R. Mestre, J. Mas, D. F. Mota, J. A. Almazan and L. P. de las Heras. "*ICDAR 2013 Robust Reading Competition*". Document Analysis and Detection (ICDAR), 2013 12th International Conference on IEEE, 2013.

[6] H. Weilin, Z. Lin, J. Yang and J. Wang. "*Text Localization in Natural Images Using Stroke Feature Transform and Text Covariance Descriptors*". Computer Vision (ICCV), 2013 IEEE International Conference on IEEE, Sydney, NSW, Australia, 2013.

[7] W. Huang, Y. Qiao, and X. Tang. "*Robust Scene Text Detection with Convolutional Neural Networks Induced MSER Trees*". Vol. 1. European Conference on Computer Vision (ECCV), 2014.

[8] Y. Xu-Cheng, X. Yin, K. Huang and H. W. Hao. "Robust Text Detection in Natural Scene Images". *IEEE Transactions on Pattern Analysis and Machine Intelligence*, vol. 36, no. 5, pp. 970-983, 2014.

[9] E. Boris, E. Ofek and Y. Wexler. "*Detecting Text in Natural Scenes with Stroke width Transform*". Computer Vision and Pattern Detection (CVPR), 2010 IEEE Conference on IEEE, 2010.

[10] T. Zhi, W. Huang, T. He, P. He and Y. Qiao. "Detecting Text in Natural Image with Connectionist Text Proposal Network". In: *European Conference on Computer Vision*. Springer, Cham, 2016.

[11] T. Shangxuan, Y. Pan, C. Huang, S. Lu, K. Yu and C. L. Tan. "*Text Flow: A Unified Text Detection System in Natural Scene Images*". Proceedings of the IEEE International Conference on Computer Vision, 2015.

[12] Z. Zheng, C. Zhang, W. Shen, C. Yao, W. Liu and X. Bai. "*Multi-oriented Text Detection with Fully Convolutional Networks*". arXiv, 2016.

[13] N. Alexander and L. Van Gool. "*Efficient Non-maximum Suppression*". Vol. 3. Pattern Detection. 18th International Conference on IEEE, 2006.

[14] Y. Cong, X. Bai1, W. Liu, Y. Ma and Z. Tu. "*Detecting Texts of Arbitrary Orientations in Natural Images*". Computer Vision and Pattern Detection (CVPR), 2012 IEEE Conference on IEEE, 2012.

[15] H. Pan, W. Huang, Y. Qiao, C. C. Loy and X. Tang. "*Reading Scene Text in Deep Convolutional Sequences*". Proceedings of the Thirtieth AAAI Conference on Artificial Intelligence (AAAI-16), 2016.

[16] H. Tong, W. Huang, Y. Qiao and J. Yao. "*Accurate Text Localization in Natural Image with Cascaded Convolutional Text Network*". arXiv, 2016.

[17] L. Minghui, B. Shi, X. Bai, X. Wang and W. Liu. "*TextBoxes: A Fast Text Detector with a Single Deep Neural Network*". Proceedings of the Thirtieth AAAI Conference on Artificial Intelligence, 2017.

[18] R. Shaoqing, K. He, R. Girshick and J. Sun. "Faster R-CNN: Towards real-time object detection with region proposal networks". *IEEE Transactions on Pattern Analysis and Machine Intelligence*, vol. 39, no. 6, pp. 1137-1149, 2017.

ORIGINAL RESEARCH ARTICLE UHD JOURNAL OF SCIENCE AND TECHNOLOGY

Review Study on Sciencedirect Library Based on Coronavirus Covid-19

Muzhir Shaban Al-Ani[1], Dimah Mezher Shaban Al-Ani[2]

[1]Department of Information Technology, College of Science and Technology, University of Human Development, Sulaymaniyah, Iraq, [2]Department of Pharmacy, College of Pharmacy, University of Philadelphia, Amman, Jordan

ABSTRACT

Several years ago, China and the United States of America began experimenting with the coronavirus, which lives in the bat. It is not known until now how the virus spread and how it extended to all countries of the world. However, it is certain that this virus first appeared and spread was at the end of 2019 and in the Chinese city of Wuhan, especially in markets close to laboratories that are working on this virus. At the beginning of the year 2020, this virus began to spread very widely all over the world and began killing thousands of people every day. The world economy was destroyed until the World Health Organization considered it a pandemic. As for the research aspect, the researchers started the research work on this pandemic from many aspects, including medical, statistical, managerial, healthcare, and others. A statistical analysis depends many key factors that have been studied. This study was conducted on April 11, 2020, where a large number of research papers were downloaded using the keywords coronavirus disease (COVID)-19, which were applied in the Sciencedirect library that was examined on 100 research papers only. The obtained results indicated that most of the research papers that worked on the subject of COVID-19 confirmed that this virus infects the human respiratory system, which in turn leads to shortness of breath and death. Here, it must be noted that the human immune system has a major role in the process of overcoming this virus and gradual recovery. The obtained analysis indicated that the main fields of coronavirus are: Medicine 42%, statistics 21%, healthcare 19%, and management 18%. Through this study, it became clear that China is the first country in terms of the number of researchers and also in terms of the number of research papers related to the COVID-19.

Index Terms: Coronavirus, Coronavirus Disease-19, Diagnosis, Human Immune System, Coronavirus Disease-19 Published Papers.

1. INTRODUCTION

Coronaviruses are a large group of viruses that may cause disease in animals and humans. It is known that a number of coronaviruses cause human respiratory infections that range from common colds to more severe diseases such as the Middle East Respiratory Syndrome and severe acute respiratory syndrome (SARS). The newly discovered coronavirus causes the Covid-19 virus. Coronavirus disease (COVID)-19 is an infectious disease caused by the newly discovered coronavirus. There was no knowledge of this virus and this emerging disease before the outbreak of outbreak in the Chinese city of Johan in December 2019. The most common symptoms of COVID-19 disease are fever, fatigue, and dry cough. Some patients may experience pain and aches, nasal congestion, cold, sore throat, or diarrhea. These symptoms are usually mild and begin gradually. Some people become infected without showing any symptoms and without feeling ill. Moreover, the severity of the disease intensifies in approximately one person out of every six people who develop COVID-19 infection, who suffer from

Access this article online

DOI: 10.21928/uhdjst.v4n2y2020.pp46-55

E-ISSN: 2521-4217

P-ISSN: 2521-4209

Corresponding author's e-mail: Muzhir Shaban Al-Ani, Department of Information Technology, College of Science and Technology, University of Human Development, Sulaymaniyah, Iraq. E-mail: Muzhir.al-ani@uhd.edu.iq

Received: 26-06-2020 Accepted: 28-07-2020 Published: 06-08-2020

difficulty breathing. The risk of the elderly and people with basic medical problems such as high blood pressure, heart disease, or diabetes is severe. About 2% of people who have contracted the disease have died. People with fever, cough, and difficulty breathing should seek medical care. The term "incubation period" refers to the period from infection with the virus to the onset of symptoms of the disease. Most estimates of the incubation period for COVID-19 disease range from 1 to 14 days, usually lasting 5 days. These estimates will be updated as more data becomes available.

A section of Kingston University's Microbiologists has concluded that a coronavirus attacks two specific groups of cells in the lungs. One of these cells is called a goblet cell, and the other is called a ciliated cell. They explain that the goblet cells produce the mucus that forms a moisturizing layer on the respiratory canal, which is important to help maintain the moisture of the lungs, and thus maintain health. The ciliary cells are cells with hairs that point upward, and their function is to shovel any harmful substance suspended in mucus, such as bacteria, viruses, and dust particles, toward the throat to get rid of them. Coronavirus, on the other hand, infects these two groups of cells, which is observed with SARS, Professor Felder says. Felder added that the coronavirus infects these cells and begins to kill them, and its tissues begin to fall and collect in the lungs, and the lungs begin to become obstructed, which means that the patient has pneumonia. Then, the body's immune system is trying to respond because it realizes that the body is under attack, and this may lead to an overload of immunity, and then the immune system makes a major attack that damages healthy tissues in the lung, and this also may make breathing more difficult. The virus not only attacks the lungs but also the kidneys, which may lead to kidney failure and later death. The World Health Organization considered COVID-19 as a pandemic disease which means an epidemic that has spread over a large area that is prevalent through an entire county, continent, or the whole world.

This work aims to introduce a brief study of COVID-19, in addition to analysis the published papers in this field.

2. MATERIALS AND METHODS

This section including: COVID-19 mechanism, published papers on COVID-19, results, and analysis.

2.1. COVID-19 Mechanism

COVID-19 virus get in the human body via many ways: Eyes, nose, and mouth (Fig. 1):

- Via eyes: In this case, the virus has two main pathways that exit through tears or enter the lacrimal sac, then reach the nasal cavity and mouth, then go to the stomach and end with gastric juices or enter the respiratory system.
- Via nose: In this case, the virus is either expelled through the mucus or enters the respiratory system.
- Via mouth: In this case, the virus enters the stomach and kills them, or enters the respiratory system.

When the virus enters the respiratory system, it settles into the lung, where it begins to attack cells there. At that time, the immune system begins to attack the virus, and this leads to many accumulations in the lung that lead to a deficiency in the work of the lung. This means shortness of breath and sometimes leads to death.

2.2. Published Papers on COVID-19

COVID-19 key word is used is applied on Sciencedirect library at April 11, 2020 in which appeared 1741 published papers, all these papers are published in 2020. To determine this this work, 100 papers were focused onto be studied as shown in Fig. 2. To analyze these hundreds published papers, the first look at them was as follows: Eighty-nine (89%) papers have been downloaded and the study has been done on it, eight (8%) papers we could not download, two

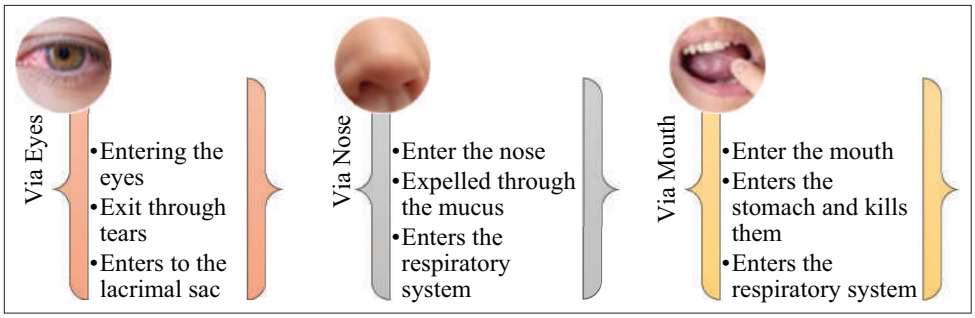

Fig. 1. Coronavirus disease-19 virus entering the human body.

duplicated (2%) papers, and finally one repeated (1%) paper. In general, 11% of the papers are canceled and 89% of the papers are considered to be studied.

3. RESULTS AND ANALYSIS

Table 1 includes data on the published research papers that have been studied. This table was divided into several fields to clarify the quality of research and on any topic in which it was focused, these fields are paper ID, topic of the paper, applied method, and applied database, in addition to the country, in which the study was conducted and the country to which the researcher belongs.

Whatever was the area of interest, they are related to the medical part of COVID-19. The field of research area regarding to the score is divided into four main categories: Medicine 37 (42%), statistics 19 (21%), healthcare 17 (19%), and management 16 (18%). Medicine category including: Treatment 22 (60%), diagnosis 6 (16%), clinical 5 (14%), emergency 1 (2.5%), hepatic 1 (2.5%), surgical 1 (2.5%), and arrhythmia 1 (2.5%). Statistical category including many fields in statistical analysis. Health-care category including: Health approach 5 (30%), health workers 3 (17%), personal health 3 (17%), community pharmacies 2 (12%), health-care provider 2 (12%), global health 1 (6%), and national care 1 (6%). Management category including: Recommendation 6 (38%), patient management 3 (19%), control 2 (13%), pharmaceutical care management 1 (6%), internet hospital 1 (6%), emergency 1 (6%), clinical management 1 (6%), and reorganization 1 (6%).

The most important categories are related to the country in which the study was conducted and the country to which the researcher belongs. The country to which the researcher belongs is focusing on 25 countries and China settles on the top, as shown in Fig. 3. The score of the researchers by country related to COVID-19 is sorted top to bottom: China 37%, USA 12%, France 7%, Taiwan 7%, Canada 5%, UK 5%, Italy 5%, India 4%, and Spain 2%, and the rest of countries are 1%.

The country in which the study was conducted is focusing on 20 countries and also China settles on the top, as shown in Fig. 4. The score of the published research papers by country related to COVID-19 is sorted top to bottom: China 37%, Global 27%, USA 12%, France 7%, Taiwan 7%, Canada 5%, UK 5%, Italy 5%, India 4%, and Spain 2%, and the rest of countries are 1%.

As a result of the previous research and studies obtained, it was found that the coronavirus has effected various places in the human body, and this virus has many different effects, including its effect on the lung and respiratory system. In general, its effect on heart murmurs, as well as on microvascular clots, in addition to other effects such high temperatures, intestinal disturbances, vomiting, and other disorders.

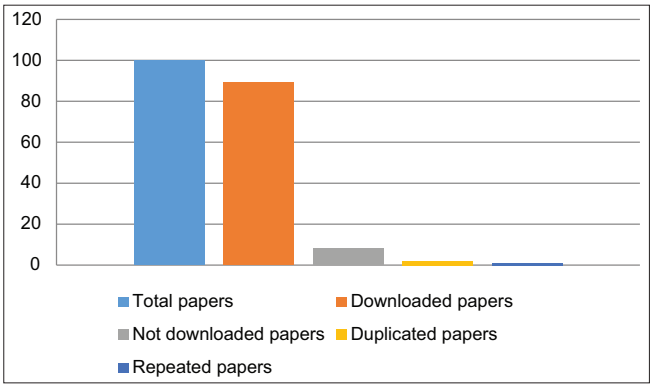

Fig. 2. Published papers on coronavirus disease-19.

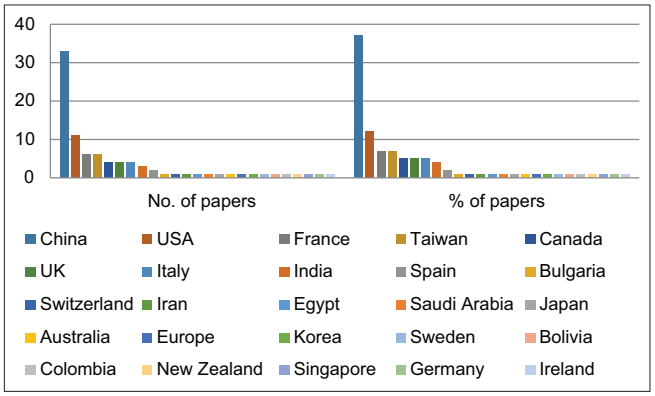

Fig. 3. Country to which the researcher belongs.

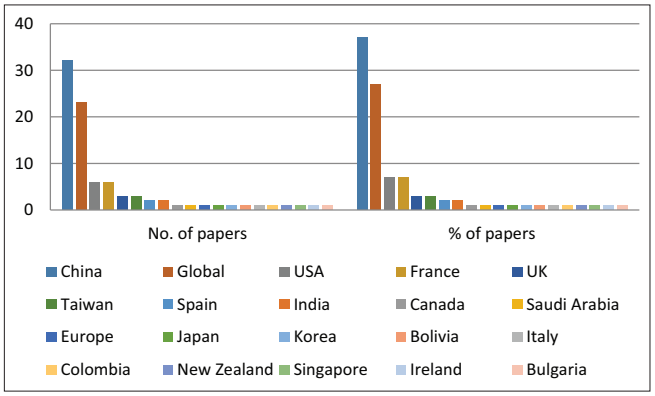

Fig. 4. Country in which the research was conducted.

TABLE 1: Search applied in Sciencedirect library at April 7, 2020.

Paper ID	Topic	Applied method	Applied database	Researcher by country	Search by country
Akram *et al*. [1]	Statistical analysis	Systematic review immunotherapy for COVID-19	Web of Science, PubMed, Scopus	Iran	Global
Kai *et al*. [2]	Medicine (clinical trial)	Effects of muscle relaxation on anxiety in patients with COVID-19	Chest CT using hypnotic drugs	China	China
Tianmin *et al*. [3]	Statistical analysis	Characteristics of COVID-19	Data collected from Chinese Center for Disease	China	China
[Sherief *et al*. [4]	Medicine (Hepatic and gastrointestinal involvement)	Characteristics of liver biochemical with COVID-19	Published COVID-19 case studies	Egypt	Global
Riyanti *et al*. [5]	Statistical analysis	Building resilience against COVID-19	Published works on COVID-19	Japan	Global
Zhenyu *et al*. [6]	Statistical analysis	Vicarious traumatization	Published works on COVID-19	China	Global
Andrew *et al*. [7]	Medicine (surgical)	Modification of head and neck treatment paradigms	Collected data	USA	USA
Cheng *et al*. [8]	Medicine (Arrhythmia)	COVID-19 and inherited arrhythmia syndromes	ECG collected data	Europe	Europe
Verónica *et al*. [9]	Management (Recommendations of pandemic)	COVID-19 and kidney transplant patients	Data collected from Nephrology Clinical Management Unit,	Spain	Spain
Jun *et al*. [10]	Medicine (Clinical progression)	COVID-19 and radiological COVID improvement	Data collected from Clinical and laboratory (CT images)	China	China
Rosa *et al*. [11]	Management (Recommendations of pandemic)	Techniques and Transplantation and Nursing areas	Data collected from (SEPAR) and (AEER)	Spain	Spain
Juan *et al*. [12]	Management (Recommendations of pandemic)	Impact of the COVID-19 pandemic in the population.	Collected cases from Hospitals and the Ministry of Health	Bolivia	Bolivia
Siyuan *et al*. [13]	Management (Recommendations of pandemic)	Management of burn wards	Data collected from Institute of Burn Research	China	China
Li *et al*. [14]	Medicine (diagnosis and treatment of COVID-19)	Internet of things-aided diagnosis and treatment of coronavirus	Collected existing data and questionnaires	China	China
Arnaud *et al*. [15]	Medicine (diagnosis and treatment of COVID-19)	CCAFU recommendations on the management of cancer during the COVID-19 epidemic	Data collected from many French associations	France	France
Li-sheng *et al*. [16]	Medicine (treatment and prevention of knowledge surrounding COVID-19)	Systematically summarizes	Data collected from current published evidence	China	China
Kai *et al*. [17]	Statistical analysis	A randomized controlled study	Data collected from two groups before and after intervention	China	China
Cuiping *et al*. [18]	Statistical analysis	Systematic Review	Collected data from PubMed database	China	Global
Andrew *et al*. [19]	Medicine (diagnosis)	Use of Cardiac Computed Tomography for COVID-19 Pandemic	Data collected from US Centers	USA	Global
Priya *et al*. [20]	Healthcare (health workers)	Challenges for the Allergist/ Immunologist	Data collected from health-care resources	USA	USA
Xinyao *et al*. [21]	Medicine (Clinical Trials on COS- COVID	clinical trials on COVID-19	Collected clinical trial protocols on COVID-19	China	China
Domenico *et al*. [22]	Statistical analysis	Application of the ARIMA model	COVID -2019 epidemic dataset	Italy	Global
Zuhua *et al*. [23]	Medicine (Chest diagnosis COVID-19)	Compare chest HRCT lung signs	Collected Chest HRCT images	China	China

(*Contd*...)

TABLE 1: (*Continued*).

Paper ID	Topic	Applied method	Applied database	Researcher by country	Search by country
Jing *et al*. [24]	Statistical analysis	Systematic review	PubMed, EMBASE, and Web of sciences databases	China	Global
Qanta *et al*. [25]	Management (Recommendations of pandemic)	Hajj through the situation with COVID-19	Literature data collected	USA	Saudi Arabia
Stéphane *et al*. [26]	Healthcare (Personal health)	Changes in care of home artificial nutrition patients during the COVID-19	Collected data treating COVID-19 patients	France	France
Wenjun *et al*. [27]	Statistical analysis	Cluster sampling of students via COVID-19 epidemic	Medical College in China	China	China
Shio-Shin *et al*. [28]	Medicine (treatment)	Treatment options for COVID-19	Collected cases	Taiwan	Taiwan
Christian *et al*. [29]	Medicine (treatment)	Effects of chloroquine against COVID-19	Collected cases	France	France
Aparna at al. [30]	Healthcare (Personal health)	Respiratory medics or ICU	Collected data from NSAIDs in COVID-19	UK	UK
Xiaoping *et al*. [31]	Medicine (treatment)	Nucleic acids testing and chest CT examination	Collected case study	China	China
Shao *et al*. [32]	Medicine (treatment)	Pneumonia and COVID-19	Collected Chest X-ray and Chest CT images	Taiwan	Taiwan
Qianying *et al*. [33]	Statistical analysis	Conceptual model for (COVID-19	Collected cases	USA	UK
Kai *et al*. [34]	Statistical analysis	Clinical features of COVID-19	Comparison young and middle-aged patients	China	China
Philippe *et al*. [35]	Medicine (treatment)	Using Hydroxychloroquine and azithromycin	Collected data from patients	France	France
Dandan *et al*. [36]	Medicine (treatment)	Responses in cytokine	Collected severe cases	USA	USA
Pedro *et al*. [37]	Healthcare (community pharmacies)	Health system from the community pharmacies	Collected cases	Colombia	Colombia
Wei-Hsuan *et al*. [38]	Medicine (treatment)	Novel COVID	Two cases are collected	Taiwan	Taiwan
Jason *et al*. [39]	Medicine (treatment)	Impact of the virus on the individual	Collected severe cases and deaths	Canada	China
Lana *et al*. [40]	Healthcare (health-care provider)	Specialist Palliative Care Service	care clinicians data collected	New Zealand	New Zealand
Muhammad *et al*. [41]	Medicine (treatment)	Drug development process	GISAID database	China	China
Wang *et al*. [42]	Management (pharmaceutical care management)	Drug Supply Management	Data collected	China	China
Alexis *et al*. [43]	Medicine (treatment)	Medicine in Drug Discovery	Historical data of intensive care unit	USA	USA
Weston *et al*. [44]	Management (Recommendations of pandemic)	predict The COVID-19 epidemic	Collected data cases	Canada	China
Nan-Yao *et al*. [45]	Medicine (treatment)	Clinical course of COVID-19	Collected data cases	Taiwan	China
Kiesha *et al*. [46]	Statistical analysis	Reducing the magnitude of the COVID-19 outbreak	Collected data cases in Wuhan	China	China
Pradip *et al*. [47]	Medicine (treatment)	Pandemic and Pregnancy	Data collected from National University of Singapore	Singapore	Singapore

(*Contd*...)

TABLE 1: (*Continued*).

Paper ID	Topic	Applied method	Applied database	Researcher by country	Search by country
Tuech *et al*. [48]	Medicine (treatment)	Digestive and oncological surgery during the COVID-19	Data collected from PMSI	France	France
Muh-Yong *et al*. [49]	Management (control)	Interrupting COVID-19 transmission	Collected data	Taiwan	Global
Claudio *et al*. [50]	Management (control)	Survive via pandemic	Collected data	Italy	Italy
Elissa *et al*. [51]	Healthcare (health approach)	Healthcare system through COVID-19	Collected data from PubMed	USA	China
Yichun *et al*. [52]	Statistical analysis	Kidney disease with death of patients with COVID-19	Data from Chinese National Health Commission	China	China
Dmitry *et al*. [53]	Statistical analysis	Simulation-based analysis on the coronavirus outbreak	Selected cases	Germany	Global
Shuangyi *et al*. [54]	Management (Internet hospital)	Fighting against COVID-19	Selected cases	China	Global
Lixiang *et al*. [55]	Statistical analysis	Propagation analysis and prediction	Data collected from many areas	China	Global
Chih-Cheng *et al*. [56]	Statistical analysis	Epidemic and the challenges	Data collected	Taiwan	Global
Weiyi *et al*. [57]	Statistical analysis	Cardiovascular burden of coronavirus	Literature data	USA	Global
Shuai *et al*. [58]	Management (Emergency)	Emergency Procedures	Data from 4 hospitals in Wuhan	China	China
Xiaoyang *et al*. [59]	management (clinical management)	Role in the treatment	ECMO database	China	China
Kai *et al*. [60]	Healthcare (health workers)	Protect healthcare workers from COVID-19	Collected data	China	China
Zaiwei *et al*. [61]	Healthcare (community pharmacies)	Guidance from clinical experience	Chinese database	China	China
Matthias *et al*. [62]	Medicine (common clinical scenarios)	Lung cancer radiotherapy during the COVID-19 pandemic	Collected data of six lung cancer cases	Switzerland	Global
Russell *et al*. [63]	Management (Recommendations of pandemic)	Systematic review	Literature data from WHO	UK	Global
Kaustuv *et al*. [64]	Healthcare (health approach)	Impact of COVID-19 epidemic	Infected cases data	India	India
Pascal *et al*. [65]	Medicine (treatment)	Literature review	Radiological data	Italy	Global
Geoffrey *et al*. [66]	Management (Patient Management)	Role of Chest Imaging	Collected data	Canada	Global
Ali *et al*. [67]	Healthcare (personal health)	Emergency cases	Several dental cases	Saudi Arabia	Global
Tao *et al*. [68]	Medicine (treatment)	Probable Pangolin with COVID-19	Data collected from RNA-seq	China	China
Razvigor [69]	Medicine (treatment)	Dermatologic aspects of COVID-19 infection	Collected skin data	Bulgaria	Bulgaria
Jiajia *et al*. [70]	Medicine (treatment)	Clinical Study of Mesenchymal Stem Cell Treatment	Collected imaging scan	China	China
Murray *et al*. [71]	Healthcare (health workers)	Recommends healthcare workers	Collected MRI	Ireland	Ireland
Stephen *et al*. [72]	Medicine (emergency)	Unprecedented disruption of lives	Data collected from STATA 16.0	Australia	China
Alice *et al*. [73]	Management (Reorganization)	Survey	Data collected from CIPOMO	Italy	Global
Praveen *et al*. [74]	Medicine (treatment)	Baricitinib as a potential drug	Biochemical data collected	India	India
Sung-Wan *et al*. [75]	Medicine (treatment)	Using psychoneuroimmunity against COVID-19	Data collected	Korea	Korea
Ritesh *et al*. [76]	Management (patient management)	Review of treatment of coronavirus	Collected current literature	India	Global
Huai-liang *et al*. [77]	Healthcare (health approach)	Public health measures	Collected data Facemask with COVID-19	China	China

(*Contd*...)

TABLE 1: (*Continued*).

Paper ID	Topic	Applied method	Applied database	Researcher by country	Search by country
Rupsa *et al.* [78]	Healthcare (health approach)	MFM Guidance for COVID-19	Collected common indicators of MFM	USA	USA
Annelies *et al.* [79]	Healthcare (Global health)	Contain the COVID-19 outbreak	Collected cases	UK	Global
Tianshi *et al.* [80]	Management (patient management)	Expert consensus during COVID-19	Data collected from Interventional Oncology Branch of China	China	China
Sheng *et al.* [81]	Statistical analysis	data-driven analysis	Official website Ministry of Health, Japan	China	Japan
Chun *et al.* [82]	Medicine (diagnosis)	Evaluation on Thin-Section CT	CT collected images	China	China
Ronan *et al.* [83]	Healthcare (Nutritional care)	Expert opinion to manage hospitalized patients	Expert opinion	France	France
Chunqin *et al.* [84]	Medicine (diagnosis)	Diagnosis of COVID-19	CT images data collected	China	China
Metcalfe *et al.* [85]	Medicine (treatment)	Mesenchymal stem cells	Clinical data collected	UK	UK
Marvi *et al.* [86]	Medicine (treatment)	Keratoconjunctivitis and COVID-19	Collected cases	Canada	Canada
Ronald *et al.* [87]	Healthcare (health approach)	Health belief model	Collected cases	USA	USA
Mohamed *et al.* [88]	Healthcare (health approach)	Unknown COVID-19	Collected data	Sweden	Global
Nan *et al.* [89]	Statistical analysis	Pregnant women with COVID-19	Collected data from Tongji Hospital in Wuhan	China	China

We know that coronavirus (COVID-19) started in China, so most of the research must begin and continue in this country to find a treatment for this disease. In spite of all the ongoing research papers on this subject, so far there is no effective treatment for this disease, on the other hand, all efforts are combined to achieve this goal and overcome this pandemic.

4. CONCLUSIONS

December 2019 was the start of an outbreak of coronavirus (COVID-19) in Wuhan, China. Then, at the beginning of the year 2020, this virus began to spread across the countries of the world gradually, as it appeared in all countries within only 2 months. During the spread of the coronavirus, researchers began working on this virus in different aspects and disciplines. This paper is based on a number of key factors that have been studied such as: Topic, applied method, applied database, researcher by country, and search by country. This search was applied on Sciencedirect library and conducted on April 11, 2020. In this work, a focus was placed on a hundred research papers, including 899 downloaded and 11 research papers that we could not download, so this work is focused on research papers that were obtained only. As a conclusion of this work, a huge number of research papers are published in these 2 months and this research papers has been divided into four main categories: Medicine 42%, statistics 21%, healthcare 19%, and management 18%. Each of these categories also was divided into many sub-categories that related to narrow fields. Furthermore, it is clear that China settles on the top of the country in which the study was conducted and also on the top of the country to which the researcher belongs.

5. ACKNOWLEDGMENT

On this occasion, we would like to extend our sincere thanks and appreciation to the Sciencedirect database that contributed to supporting the research of COVID-19 by providing research papers without fees.

REFERENCES

[1] A. A. Jafari and S. Ghasemi. "The possible of immunotherapy for COVID-19: A systematic review". *International Immunopharmacology*, vol. 83, p. 106455, 2020.

[2] K. Liu, Y. Chen, D. Wu, R. Lin and L. Pan. "Effects of progressive muscle relaxation on anxiety and sleep quality in patients with COVID-19". *Complementary Therapies in Clinical Practice*, vol. 39, p. 101132, 2020.

[3] T. Xu, C. Chen, Z. Zhu, M. Cui and Y. Xue. "Clinical features and

dynamics of viral load in imported and non-imported patients with COVID-19". *International Journal of Infectious Diseases*, vol. 94, pp. 68-71, 2020.

[4] S. Musa. "Hepatic and gastrointestinal involvement in coronavirus disease 2019 (COVID-19): What do we know till now"? *Arab Journal of Gastroenterology*, vol. 21, no. 1, pp. 3-8, 2020.

[5] R. Djalante, R. Shaw and A. DeWit. "Building resilience against biological hazards and pandemics: COVID-19 and its implications for the Sendai framework". *Progress in Disaster Science*, vol. 6, p. 100080, 2020.

[6] Z. Li, J. Ge, M. Yang, J. Feng and C. Yang. "Vicarious traumatization in the general public, members, and non-members of medical teams aiding in COVID-19 control". *Brain, Behavior, and Immunity*, vol. 88, pp. 916-919, 2020.

[7] A. T. Day, D. J. Sher, R. C. Lee, J. M. Truelson and E. A. Gordin. "Head and neck oncology during the COVID-19 pandemic: Reconsidering traditional treatment paradigms in light of new surgical and other multilevel risks". *Oral Oncology*, vol. 105, p. 104684, 2020.

[8] C. I. Wu, P. G. Postema, E. Arbelo, E. R. Behr and A. A. M. Wilde. "SARS-CoV-2, COVID-19 and inherited arrhythmia syndromes". *Heart Rhythm*, vol. 2020, p. 24, 2020.

[9] V. López, T. Vázquez, J. Alonso-Titos, M. "Cabello and Grupo de Estudio GREAT. "Recommendations on management of the SARS-CoV-2 coronavirus pandemic (Covid-19) in kidney transplant patients". *Nefrología*, vol. 40, no. 3, pp. 265-271, 2020.

[10] J. Chen, T. Qi, L. Liu, Y. Ling and H. Lu. "Clinical progression of patients with COVID-19 in Shanghai, China". *Journal of Infection*, vol. 80, no. 5, pp. e1-e6, 2020.

[11] R. C. Pérez, S. Álvarez, L. Llanos, A. N. Ares and D, Díaz-Pérez. "Recomendaciones de consenso separ y aeer sobre el uso de la broncoscopia y la toma de muestras de la via respiratoria en pacientes con sospecha o con infeccion confirmada por Covid-19". *Archivos de Bronconeumología*, vol. 56, no. 2, pp. 19-26, 2020.

[12] J. P. Escalera-Antezana, N. F. Lizon-Ferrufino, A. Maldonado-Alanoca, G. Alarcón-De-la-Vega and LANCOVID. "Clinical features of cases and a cluster of coronavirus disease 2019 (COVID-19) in Bolivia imported from Italy and Spain". *Travel Medicine and Infectious Disease*, vol. 35, p. 101653, 2020.

[13] S. Ma, Z. Yuan, Y. Peng, J. Chen and G. Luo. "Experience and suggestion of medical practices for burns during the outbreak of COVID-19". *Burns*, vol. 46, no. 4, pp. 749-755, 2020.

[14] L. Bai, D. Yang, X. Wang, L. Tong and F. Tan. "Chinese experts' consensus on the Internet of Things-aided diagnosis and treatment of coronavirus disease 2019 (COVID-19)". *Clinical eHealth*, vol. 3, pp. 7-15, 2020.

[15] A. Mejean, M. Rouprêt, F. Rozet, K. Bensalah and Le Comité de Cancérologie de l'Association Française d'Urologie. "Recommandations CCAFU sur la prise en charge des cancers de l'appareil urogénital en période d'épidémie au Coronavirus COVID-19". *Progrès en Urologi*e, vol. 30, no. 5, pp. 221-231, 2020.

[16] L. S. Wang, Y. R. Wang, D. W. Ye and Q. Q. Liu. "A review of the 2019 novel coronavirus (COVID-19) based on current evidence". *International Journal of Antimicrobial Agents*, vol. 55, no. 6, p. 105948, 2020.

[17] K. Liu, W. Zhang, Y. Yang, J. Zhang and Y. Chen. "Respiratory rehabilitation in elderly patients with COVID-19: A randomized controlled study". *Complementary Therapies*, vol. 39, p. 101166, 2020.

[18] C. Bao, X. Liu, H. Zhang, Y. Li and J. Liu. "COVID-19 computed tomography findings: A systematic review and meta-analysis". *Journal of the American College of Radiology*, vol. 17, pp. 701-709, 2020.

[19] A. D. Choi, S. Abbara, K. R. Branch, G. M. Feuchtner and R. Blankstein. "Society of cardiovascular computed tomography guidance for use of cardiac computed tomography amidst the COVID-19 pandemic". *Journal of Cardiovascular Computed Tomography*, vol. 14, no. 1, pp. 101-104, 2020.

[20] P. Bansal, T. A. Bingemann, M. Greenhawt, G. Mosnaim and M. Shaker. Clinician wellness during the COVID-19 pandemic: Extraordinary times and unusual challenges for the allergist/immunologist. *The Journal of Allergy and Clinical Immunology*, vol. 8, no. 6, pp. 1781-1790, 2020.

[21] X. Jin, B. Pang, J. Zhang, Q. Liu and B. Zhang. "Core outcome set for clinical trials on coronavirus disease 2019 (COS-COVID)". *Engineering*, vol. 1, pp. 2-6, 2020.

[22] D. Benvenuto, M. Giovanetti, L. Vassallo, S. Angeletti and M. Ciccozzi. "Application of the ARIMA model on the COVID-2019 epidemic dataset". *Data in Brief*, vol. 29, p. 105340, 2020.

[23] Z. Chen, H. Fan, J. Cai, Y. Li and J. Sun. "High-resolution computed tomography manifestations of COVID-19 infections in patients of different ages". *European Journal of Radiology*, vol. 126, p. 108972, 2020.

[24] J. Yang, Y. Zheng, X. Gou, K. Pu and Y. Zhou. "Prevalence of comorbidities in the novel Wuhan coronavirus (COVID-19) infection: A systematic review and meta-analysis". *International Journal of Infectious Diseases*, vol. 94, pp. 91-95, 2020.

[25] Q. A. Ahmed and Z. A. Memish. "The cancellation of mass gatherings (MGs)? Decision making in the time of COVID-19". *Travel Medicine and Infectious Disease*, vol. 34, p. 101631, 2020.

[26] S. M. Schneider, V. Albert, N. Barbier, D. Barnoud and P. Déchelotte. "Adaptations de la prise en charge des patients en nutrition artificielle a domicile au cours de l'épidémie virale COVID-19 en France: Avis du comite de nutrition a domicile de la societe francophone de nutrition clinique et metabolisme (SFNCM)". *Nutrition Clinique et Métabolism*e, vol. 34, no. 2, pp. 105-107, 2020.

[27] W. Cao, Z. Fang, G. Hou, M. Han and J. Zheng. "The psychological impact of the COVID-19 epidemic on college students in China". *Psychiatry Research*, vol. 287, p. 112934, 2020.

[28] S. S. Jean, P. I. Lee and P. R. Hsueh. "Treatment options for COVID-19: The reality and challenges". *Journal of Microbiology, Immunology and Infection*, vol. 53, no, 3, pp. 436-443, 2020.

[29] C. A. Devaux, J. M. Rolain, P. Colson and D. Raoult. "New insights on the antiviral effects of chloroquine against coronavirus: What to expect for COVID-19"? *International Journal of Antimicrobial Agents*, vol. 55, no. 5, p. 105938, 2020.

[30] A. Viswanath and P. Monga. "Working through the COVID-19 outbreak: Rapid review and recommendations for MSK and allied heath personnel". *Journal of Clinical Orthopaedics and Trauma*, vol. 11, no. 3, pp. 500-503, 2020.

[31] X. Yin, L. Dong, Y. Zhang, W. Bian and H. Li. "A mild type of childhood Covid-19 a case report". *Radiology of Infectious Diseases*, in press, 2020.

[32] S. C. Cheng, Y. C. Chang, Y. L. Fan Chiang, Y. C. Chien and Y. N. Hsu. "First case of coronavirus disease 2019 (COVID-19) pneumonia in Taiwan". *Journal of the Formosan Medical Association*, vol. 119, no. 3, pp. 747-751, 2020.

[33] Q. Lin, S. Zhao, D. Gao, Y. Lou and D. He. "A conceptual model for the coronavirus disease 2019 (COVID-19) outbreak in

Wuhan, China with individual reaction and governmental action". *International Journal of Infectious Diseases*, vol. 93, pp. 211-216, 2020.

[34] K. Liu, Y. Chen, R. Lin and K. Han. "Clinical features of COVID-19 in elderly patients: A comparison with young and middle-aged patients". *Journal of Infection*, vol. 80, no. 6, pp. e14-e18, 2020.

[35] P. Gautret, J. C. Lagier, P. Parola, V. T. Hoang and D. Raoult. "Hydroxychloroquine and azithromycin as a treatment of COVID-19: Results of an open-label non-randomized clinical trial". *International Journal of Antimicrobial Agents*, vol. 56, no. 1. p. 105949, 2020.

[36] D. Wu and X. O. Yang. "TH17 responses in cytokine storm of COVID-19: An emerging target of JAK2 inhibitor Fedratinib". *Journal of Microbiology, Immunology and Infection*, vol. 53, no. 3. pp. 368-370, 2020.

[37] P. Amariles, M. Ledezma-Morales, A. Salazar-Ospina and J. A. Hincapié-García. "How to link patients with suspicious COVID-19 to health system from the community pharmacies? A route proposal". *Research in Social and Administrative Pharmacy*, vol. 23, pp. 30248-30249, 2020.

[38] W. H. Huang, L. C. Teng, T. K. Yeh, Y. J. Chen and P. Y. Liu. "2019 novel coronavirus disease (COVID-19) in Taiwan: Reports of two cases from Wuhan, China". *Journal of Microbiology, Immunology and Infection*, vol. 53, no. 3, pp. 481-484, 2020.

[39] J. A. Tetro. "Is COVID-19 receiving ADE from other corona viruses"? *Microbes and Infection*, vol. 22, pp. 72-73, 2020.

[40] L. Ferguson and D. Barham. "Palliative care pandemic pack: A specialist palliative care service response to planning the COVID-19 pandemic". *Journal of Pain and Symptom Management*, vol. 60, no. 1, pp. e18-e20, 2020.

[41] M. T. ul Qamar, S. M. Alqahtani, M. A. Alamri and L. L. Chen. "Structural basis of SARS-CoV-2 3CLpro and anti-COVID-19 drug discovery from medicinal plants". *Journal of Pharmaceutical Analysis*, vol. 1, pp. 1-9, 2020.

[42] W. Ying, Y. Qian and Z. Kun. "Drugs supply and pharmaceutical care management practices at a designated hospital during the COVID-19 epidemic". *Research in Social and Administrative Pharmacy*, vol. 1, pp. 1-4, 2020.

[43] A. Nahama, R. Ramachandran, A. F. Cisternas and H. Ji. "The role of afferent pulmonary innervation in poor prognosis of acute respiratory distress syndrome in COVID-19 patients and proposed use of resiniferatoxin (RTX) to improve patient outcomes in advanced disease state: A review". *Medicine in Drug Discovery*, vol. 5, p. 100033, 2020.

[44] W. C. Roda, M. B. Varughese, D. Han and M. Y. Li. "Why is it difficult to accurately predict the COVID-19 epidemic"? *Infectious Disease Modelling*, vol. 52020, pp. 271-281, 2020.

[45] N. Y. Lee, C. W. Li, H. P. Tsai, P. L. Chen and W. C. Ko. "A case of COVID-19 and pneumonia returning from Macau in Taiwan: Clinical course and anti-SARS-CoV-2 IgG dynamic". *Journal of Microbiology, Immunology and Infection*, vol. 53, no. 3, pp. 485-487, 2020.

[46] K. Prem, Y. Liu, T. W. Russell, A. J. Kucharski and P. Klepac. "The effect of control strategies to reduce social mixing on outcomes of the COVID-19 epidemic in Wuhan, China: A modelling study". *The Lancet*, vol. 1, pp. 1-6, 2020.

[47] P. Dashraath, W. J. L. Jeslyn, L. M. X. Karen, L. L. Min and S. L. Lin. "Coronavirus disease 2019 (COVID-19) pandemic and pregnancy". *American Journal of Obstetrics and Gynecology*, vol. 222, no. 6, pp. 521-531, 2020.

[48] J. J. Tuech, A. Gangloff, F. Di Fiore, P. Michel and L. Schwarz. "Strategy for the practice of digestive and oncological surgery during the Covid-19 epidemic". *Journal of Visceral Surgery*, vol. 157, pp. S7-S12, 2020.

[49] M. Y. Yen, J. Schwartz, S. Y. Chen, C. C. King and P. R. Hsueh. "Interrupting COVID-19 transmission by implementing enhanced traffic control bundling: Implications for global prevention and control efforts". *Journal of Microbiology, Immunology and Infection*, vol. 53, no. 3, pp. 377-380, 2020.

[50] C. Guerci, A. Maffioli, A. A. Bondurri, L. Ferrario and P. Danelli. "Covid-19: How can a department of general surgery survive to a pandemic? *Surgery*, vol. 167, no. 6, pp. 909-911, 2020.

[51] E. Driggin, M. V. Madhavan, B. Bikdeli, T. Chuich and S. A. Parikh. "Cardiovascular considerations for patients, health care workers, and health systems during the coronavirus disease 2019 (COVID-19) pandemic". *Journal of the American College of Cardiology*, vol. 75, no. 18, pp. 2352-2371, 2020.

[52] Y. Cheng, R. Luo, K. Wang, M. Zhang and G. Xu. "Kidney disease is associated with in-hospital death of patients with COVID-19". *Kidney International*, vol. 97, no. 5, pp. 829-838, 2020.

[53] D. Ivanov. "Predicting the impacts of epidemic outbreaks on global supply chains: A simulation-based analysis on the coronavirus outbreak (COVID-19/SARS-CoV-2) case". *Transportation Research Part E: Logistics and Transportation Review*, vol. 136, p. 101922, 2020.

[54] S. Sun, K. Yu, Z. Xie and X. Pan. "China empowers Internet hospital to fight against COVID-19". *Journal of Infection*, vol. 81, no. 1, pp. e67-e68, 2020.

[55] L. Li, Z. Yang, Z. Dang, C. Meng and Y. Shao. "Propagation analysis and prediction of the COVID-19". *Infectious Disease Modelling*, vol. 52020, pp. 282-292, 2020.

[56] C. C. Lai, T. P. Shih, W. C. Ko, H. J. Tang and P. R. Hsueh. "Severe acute respiratory syndrome coronavirus 2 (SARS-CoV-2) and coronavirus disease-2019 (COVID-19): The epidemic and the challenges". *International Journal of Antimicrobial Agents*, vol. 55, no. 3, 105924, 2020.

[57] W. Tan and J. Aboulhosn. "The cardiovascular burden of coronavirus disease 2019 (COVID-19) with a focus on congenital heart disease". *International Journal of Cardiology*, vol. 309, pp. 70-77, 2020.

[58] S. Zhao, K. Ling, H. Yan, L. Zhong and X. Chen. "Anesthetic management of patients with COVID 19 infections during emergency procedures". *Journal of Cardiothoracic and Vascular Anesthesia*, vol. 34, no. 5, pp. 1125-1131, 2020.

[59] X. Hong, J. Xiong, Z. Feng and Y. Shi. "Extracorporeal membrane oxygenation (ECMO): Does it have a role in the treatment of severe COVID-19"? *International Journal of Infectious Diseases*, vol. 94, pp. 78-80, 2020.

[60] K. Xu, X. Lai and L. Zheng. "Suggestions on the prevention of COVID-19 for health care workers in department of otorhinolaryngology head and neck surgery". *World Journal of Otorhinolaryngology Head and Neck Surgery*, vol. 1, pp. 1-3, 2020.

[61] Z. Song, Y. Hu, S. Zheng, L. Yang and R. Zhao. "Hospital pharmacists' pharmaceutical care for hospitalized patients with COVID-19: Recommendations and guidance from clinical experience". *Research in Social and Administrative Pharmacy*, vol. 1, pp. 1-27, 2020.

[62] M. Guckenberger, C. Belka, A. Bezjak, J. Bradley and D. Palma. "Practice recommendations for lung cancer radiotherapy during the COVID-19 pandemic: An ESTRO-ASTRO consensus statement".

Radiotherapy and Oncology, vol. 146, pp. 223-229, 2020.

[63] R. M. Viner, S. J. Russell, H. Croker, J. Packer and R. Booy. "School closure and management practices during coronavirus outbreaks including COVID-19: A rapid systematic review". *The Lancet Child and Adolescent Health*, vol. 1, pp. 1-16, 2020.

[64] K. Chatterjee, K. Chatterjee, A. Kumar and S. Shankar. "Healthcare impact of COVID-19 epidemic in India: A stochastic mathematical model". *Medical Journal Armed Forces India*, vol. 76, pp. 147-155, 2020.

[65] P. Lomoro, F. Verde, F. Zerboni, I. Simonetti and A. Martegani. "COVID-19 pneumonia manifestations at the admission on chest ultrasound, radiographs, and CT: single-center study and comprehensive radiologic literature review". *European Journal of Radiology Open*, vol. 7, p. 100231, 2020.

[66] G. D. Rubin, C. J. Ryerson, L. B. Haramati, N. Sverzellati and A. N. Leung. "The Role of chest imaging in patient management during the COVID-19 pandemic: A multinational consensus statement from the fleischner society". *Chest*, vol. 158, pp. 106-116, 2020.

[67] A. Alharbi, S. Alharbi and S. Alqaidi. "Guidelines for dental care provision during the COVID-19 pandemic". *The Saudi Dental Journal*, vol. 32, pp. 181-186, 2020.

[68] T. Zhang, Q. Wu and Z. Zhang. "Probable pangolin origin of SARS-CoV-2 associated with the COVID-19 outbreak". *Current Biology*, vol. 30, no. 76, pp. 1346-1351, 2020.

[69] R. Darlenski and N. Tsankov. "Covid-19 pandemic and the skin what should dermatologists know"? *Clinics in Dermatology*, in press, 2020.

[70] J. Chen, C. Hu, L. Chen, L. Tang and L. Li. "Clinical study of mesenchymal stem cell treatment for acute respiratory distress syndrome induced by epidemic influenza a (H7N9) infection: A hint for COVID-19 treatment". *Engineering*, vol. 1, pp. 1-6, 2020.

[71] O. M. Murray, J. M. Bisset, P. J. Gilligan, M. M. Hannan and J. G. Murray. "Respirators and surgical facemasks for COVID-19: Implications for MRI". *Clinical Radiology*, vol. 75, no. 6, pp. 405-407, 2020.

[72] S. X. Zhang, Y. Wang, A. Rauch and F. Wei. "Unprecedented disruption of lives and work: Health, distress and life satisfaction of working adults in China one month into the COVID-19 outbreak". *Psychiatry Research*, vol. 288, p. 112958, 2020.

[73] A. Indini, C. Aschele, D. Bruno, L. Cavanna and F. Grossi. "Reorganization of medical oncology departments during COVID-19 pandemic: A nationwide Italian survey". *European Journal of Cancer*, vol. 132, pp. 17-32, 2020.

[74] D. Praveen, P. R. Chowdary and M. V. Aanandhi. "Baricitinib a januase kinase inhibitor not an ideal option for management of covid 19. *International Journal of Antimicrobial Agents*, vol. 55, no, 5, p. 105967, 2020.

[75] S. W. Kim and K. P. Su. "Using psychoneuroimmunity against COVID-19". *Brain, Behavior, and Immunity*, vol. 87, pp. 4-5, 2020.

[76] R. Gupta and A. Misra. "Contentious issues and evolving concepts in the clinical presentation and management of patients with COVID-19 infection with reference to use of therapeutic and other drugs used in Co-morbid diseases (hypertension, diabetes etc)". *Diabetes and Metabolic Syndrome*, vol. 14, no. 3, pp. 251-254.

[77] H. L. Wu, J. Huang, C. J. P. Zhang, Z. He and W. K. Ming. "Facemask shortage and the novel coronavirus disease (COVID-19) outbreak: Reflections on public health measures". *EClinicalMedicine*, vol. 21, p. 100329, 2020.

[78] R. C. Boelig, G. Saccone, F. Bellussi and V. Berghella. "MFM guidance for COVID-19". *American Journal of Obstetrics and Gynecology*, vol. 2, no. 2, p. 100106, 2020.

[79] A. Wilder-Smith, C. J. Chiew and V. J. Lee. "Can we contain the COVID-19 outbreak with the same measures as for SARS"? *The Lancet Infectious Diseases*, vol. 1, pp. 1-10, 2020.

[80] T. Lyu, L. Song, L. Jin, Y. Zou and Interventional Oncology Branch of China Anti-Cancer Association. "Expert consensus on the procedure of interventional diagnosis and treatment of cancer patients during the COVID-19 epidemic". *Journal of Interventional Medicine*, vol. 3, no. 2, pp. 61-64, 2020.

[81] S. Zhang, M. Diao, W. Yu, L. Pei and D. Chen. "Estimation of the reproductive number of novel coronavirus (COVID-19) and the probable outbreak size on the Diamond Princess cruise ship: A data-driven analysis". *International Journal of Infectious Diseases*, vol. 93, pp. 201-204, 2020.

[82] C. S. Guan, Z. B. Lv, S. Yan, Y. N. Du and B. D. Chen. "Imaging features of coronavirus disease 2019 (COVID-19): Evaluation on thin-section CT". *Academic Radiology*, vol. 27, no. 5, pp. 609-613, 2020.

[83] R. Thibault, D. Quilliot, P. Seguin, F. Tamion and P. Déchelotte. "Stratégie de prise en charge nutritionnelle à l'hôpital au cours de l'épidémie virale Covid-19: Avis d'experts de la societe francophone de nutrition clinique et metabolisme (SFNCM)". *Nutrition Clinique et Métabolism*e, vol. 34, no. 2, pp. 97-104, 2020.

[84] C. Long, H. Xu, Q. Shen, X. Zhang and H. Li. "Diagnosis of the coronavirus disease (COVID-19): rRT-PCR or CT"? *European Journal of Radiology*, vol. 126, p. 108961, 2020.

[85] S. M. Metcalfe. "Mesenchymal stem cells and management of COVID-19 pneumonia". *Medicine in Drug Discovery*, vol. 5, p. 100019, 2020.

[86] M. Cheema, H. Aghazadeh, S. Nazarali, A. Ting and C. Solarte. "Keratoconjunctivitis as the initial medical presentation of the novel coronavirus disease 2019 (COVID-19): A case report". *Canadian Journal of Ophthalmology*, vol. 1, pp. 1-7, 2020.

[87] R. R. Carico, J. Sheppard and C. B. Thomas. "Community pharmacists and communication in the time of COVID-19: Applying the health belief model". *Research in Social and Administrative Pharmacy*, vol. 1, pp. 1-11, 2020.

[88] N. Yu, W. Li, Q. Kang, Z. Xiong, W. M. E. El Zowalaty and J. D. Järhult. "From SARS to COVID-19: A previously unknown SARS related coronavirus (SARS-CoV-2) of pandemic potential infecting humans call for a one health approach". *One Health*, vol. 9, p. 100124, 2020.

[89] N. Yu, W. Li, Q. Kang, Z. Xiong, S. Wang, X. Lin, Y. Liu, J. Xiao, H. Liu, D. Deng, S. Chen, W. Zeng, L. Feng and J. Wu. "Clinical features and obstetric and neonatal outcomes of pregnant patients with COVID-19 in Wuhan, China: A retrospective, single-center, descriptive study". *The Lancet Infectious Diseases*, vol. 1, pp. 1-6, 2020.

ORIGINAL RESEARCH ARTICLE UHD JOURNAL OF SCIENCE AND TECHNOLOGY

Elastic and Inelastic Electron-Nucleus Scattering Form Factors for Be^9 Nucleus

Hawar Muhamad Dlshad, Aziz Hama-Raheem Fatah, Adil Mohammed Hussain

Department of Physics, College of Science, University of Sulaimani, Sulaymaniyah, Kurdistan Region, Iraq

ABSTRACT

The computations of the elastic and inelastic Coulomb form factors for the electron-nucleus scattering of beryllium nucleus Be^9 have performed with core polarization (CP) effects including the realistic Michigan sum of three range Yukawa (M3Y) interaction and the other residual interaction which is modified surface delta interaction (MSDI). In the calculations, root mean square charge density and charge radii include for the ground states. The perturbation theory is adopted to compute the CP using the harmonic oscillators potential to calculate single-particle radial wave functions. The comparison has been done between the theoretical calculations of Coulomb form factors by MSDI interaction, realistic M3Y interaction, and the experimental results that measured by other workers, it noticed that the Coulomb form factors for the (M3Y) interaction gave a reasonable depiction of the measured data.

Index Terms: Beryllium Nucleus, Core Polarization Effect, Electron Scattering, Form Factor, Harmonic Oscillator.

1. INTRODUCTION

There are two essential reasons why electron-nucleus scattering is such a successful apparatus used for studying nuclear structure. The primary one belongs to the reality that the main interaction occurring between the electron and the nucleus is well known [1]. The origin of the second reason that makes electron scattering is a valuable method in examining the properties of nuclear structure comes from its ability to identify the excited states, spins, and parities, through the calculations of the reduced matrix elements of nuclear transitions. Basically, in the electron scattering with a relatively weak interaction, the interactions of the electron with charge and the nuclear current density occur where they described by the theory of quantum electrodynamics [2].

Access this article online

DOI: 10.21928/uhdjst.v4n2y2020.pp56-62

E-ISSN: 2521-4217

P-ISSN: 2521-4209

One of the great (standard) effective interactions for light nuclei is the Cohen-Kurath [3], for 1p-shell ($1p_{1/2}$, $1p_{3/2}$) nuclei with core $_2He^4$. In addition, different macroscopic and microscopic theories have been used to analyze excitation states in Be nucleus. The form factor calculations were done by utilizing the model space (MS) wave functions alone which were not sufficient for duplicating the experimental data of the electron-nucleus scattering [4]. Therefore, the electron scattering Coulomb form factors in the p-shell nucleus (Be^9) have been investigated by taking into account higher energy configurations outside the p-shell MS which are named core polarization effects [5].

Many research studies have focused their efforts on the improvement and development of the electron scattering. Starting with Hofstadter who was the primary to utilize high-energy electron beams given by the Stanford linear electron accelerator to discover electron scattering and an old work of Sir Nevill Mott which was used electrons against point nuclei in his experiment as the relativistic scattering of Dirac particles. Then, he established a series formulation for the cross-section of the elastic scattering, also he allowed to estimating formula [6], [7].

Corresponding author's e-mail: Hawar Muhamad Dlshad, Department of Physics, College of Science, University of Sulaimani, Sulaymaniyah, Kurdistan Region, Iraq. E-mail: hawar.muhamaddlshad@gmail.com

Received: 05-04-2020 Accepted: 13-08-2020 Published: 17-08-2020

Elastic and inelastic electron scattering for the light nuclei using Born approximation had performed by Uberall and Ugincius [8]. In the last decades, the single-particle quadrupole transitions of Coulomb electron-nucleus scattering form factors studied in the B^{10} which is the p-shell nucleus by Majeed [9], whereas the studies included a microscopic theory in the core polarization (CP) effects for the excitation states up to 2ħω by employing the modified surface delta interaction (MSDI).

The charge density distributions and charge radii of the nucleus were distinguished from the investigation of elastic electron scattering data [10]. However, Sharrad *et al.* [11] have used the charge density distributions of the ground state for determining the Coulomb form factors using the approximation rule which is the plane wave Born approximation with the two-body short range correlation. Consequently, Radhi *et al.* [12] presented inelastic Coulomb and electromagnetic form factors for F^{19} in each positive parity and negative parity states by applying the single-particle states shell model and Hartree–Fock method.

At present, Raheem *et al.* [13] have been calculated the elastic Coulomb C_0 form factors for a few sd-shell nuclei using nucleon-nucleon effective interaction, which is two-body (Michigan sum of three range Yukawa [M3Y]) as residual interactions with considering the CP matrix elements.

This work is devoted to calculate the theoretical Coulomb electron scattering form factors for Be^9 by considering the role of the MS besides the CP effects using MSDI and the realistic interaction named M3Y including root mean square charge density along with charge radii for the ground states. The harmonic oscillator (HO) wave function will be adopted as a single particle wave function. To do this, first needed to use shell model code (OXBASH) to calculate the one-body density matrix (OBDM) elements [14], [15].

Finally, the theoretical calculations of Coulomb form factors by MSDI, M3Y interactions are compared with the experimental results.

2. THEORY

2.1. Coulomb Form Factor

The Coulomb electron scattering form factors of a given multipolarity (J) is a function of transfer momentum (q) and it can be described in term of reduced matrix elements (in spin state) of the transition operator [16]:

$$F_J(q)=\sqrt{\frac{4\pi}{Z^2(2J_i+1)}}\left\langle J_f\left\|T_J(q)\right\|J_i\right\rangle \quad (1)$$

Where, J_i and J_f are, respectively, the initial and final total angular momentum, while Z is the number of proton (atomic number), $T_J(q)$ is the multipole operator of electron scattering, and $\left\langle J_f\left\|T_J(q)\right\|J_i\right\rangle$ is the reduced many body matrix element.

The best description of the experimental form factors requires to correct the form factor in Equation (1) corresponding to the center of mass correction and the finite size correction of the nucleon [17]:

$$F_J(q)=\sqrt{\frac{4\pi}{Z^2(2J_i+1)}}\left\langle J_f\left\|T_J(q)\right\|J_i\right\rangle e^{\frac{q^2\left(b^2-0.43A\right)}{4A}} \quad (2)$$

Here, b is the HO size parameter that obtained from the experiment, A is the nuclear mass number, and the final term in the above equation is the correction coefficient. The reduced matrix element in Equation (1) can be expressed in two terms, the first one is MS term and the other is CP term [18].

$$\left\langle J_f\left\|T_{J\tau_z}(q)\right\|J_i\right\rangle=\left\langle J_f\left\|T_{J\tau_z}(q)\right\|J_i\right\rangle_{MS}+\left\langle J_f\left\|\delta T_{J\tau_z}(q)\right\|J_i\right\rangle \quad (3)$$

The MS reduced matrix element in the spin and isospin spaces of the transition operator T_J is performed as the sum of the product of the (OBDM) elements which are in neutron-proton formalism $OBDM(\beta, \alpha, J, \tau_z, i, f)$ multiplied by the single-particle reduced matrix elements as follow [18]:

$$\left\langle J_f\left\|T_{J\tau_z}(q)\right\|J_i\right\rangle_{MS}=\sum_{\beta,\alpha}OBDM\left(\beta,\alpha,J,\tau_z,i,f\right)\left\langle\beta\left\|T_{J\tau_z}\right\|\alpha\right\rangle \quad (4)$$

In addition, the CP reduced matrix element can be represented as:

$$\left\langle f\left\|\delta T_{J\tau_z}(q)\right\|J_i\right\rangle J_{CP}=\sum_{\beta,\alpha}OBDM\left(\beta,\alpha,J,\tau_z,i,f\right)\left\langle\beta\left\|\delta T_{J\tau_z}\right\|\alpha\right\rangle \quad (5)$$

Where, α and β are, respectively, the initial and final single-particle states for the MS when isospin included, the index

τ_z is the third component of nucleons Pauli isospin which used to identify the nucleons with $\tau_z = 1, -1$ for protons and neutrons, respectively, and the OBDM determined macroscopically for the elastic scattering by the initial and final nuclear wave functions, while it obtained from OXBASH code for inelastic scattering. The single-particle matrix element is determined from:

$$\left\langle \beta \left\| T_{J\tau_z} \right\| \alpha \right\rangle = \left\langle j_\beta \left\| \mathrm{Y}_{J\tau_z} \right\| j_\alpha \right\rangle \left\langle n_\beta, l_\beta | j_J (qr) | n_\alpha l_\alpha \right\rangle, \qquad (6)$$

Where, $\langle n_\beta, l_\beta | j_J (qr) | n_\alpha l_\alpha \rangle$ is the radial part matrix element of the spherical Bessel function $j_J (qr)$ which is calculated in [19, Equation (23)] of our published article; and $\left\langle j_\beta \left\| \mathrm{Y}_{J\tau_z} \right\| j_\alpha \right\rangle$ represents the reduced matrix element of the spherical Harmonics $\mathrm{Y}_{J\tau_z}$.

The single-particle matrix element can represent according to the first-order perturbation theory as [20]:

$$\left\langle \beta \left\| \delta T_\Lambda \right\| \alpha_{CP} \right\rangle = \left\langle \beta \left\| V \frac{Q}{E_a - H_o} T_\Lambda \right\| \alpha \right\rangle + \left\langle \beta \left\| T_\Lambda \frac{Q}{E_b - H_o} V \right\| \alpha \right\rangle \qquad (7)$$

The single-particle matrix element $\left\langle \beta \left\| \delta T_{J\tau_z} \right\| \alpha \right\rangle$ in the above equation obtained from the particle hole excitation with the first-order perturbation including residual interaction (V) for the MSDI and M3Y interaction [20].

$$\left\langle \beta \left\| V \frac{Q}{E_b - H_o} O_\Lambda \right\| \alpha \right\rangle = \sum_{\Gamma,\alpha_1,\alpha_2} \frac{\left\langle \beta\alpha_2 | V | \alpha\alpha_1 \right\rangle_\Gamma \left\langle \alpha_1 || O_\Lambda || \alpha_2 \right\rangle}{e_\alpha - e_\beta + e_{\alpha_1} - e_{\alpha_2}} (-1)^{\alpha+\alpha_2+\Gamma} (2\Gamma+1) \times \sqrt{(1+\delta_{bp})(1+\delta_{ab})} \begin{Bmatrix} \beta & \alpha & \Lambda \\ \alpha_1 & \alpha_2 & \Gamma \end{Bmatrix} + \text{terms with exchanged } \alpha_1 \text{ and } \alpha_2 \text{ by an overall minus sign} \qquad (8)$$

Here, H_o is the unperturbed Hamiltonian, E_a, E_b are the initial and final states of energy, the Q operator projects the outside space of the MS, both the indices α_1 and α_2, are, respectively, run over particle and hole states, $\begin{Bmatrix} \beta & \alpha & \Lambda \\ \alpha_1 & \alpha_2 & \Gamma \end{Bmatrix}$ is the six-*j* symbol and e is the single-particle energy. Every matrix element in the Equation (7) is obtained in iso-scalar ($T = 0$) and isovector ($T = 1$) formalism with $\Lambda = JT$ and $\Gamma = J'T'$.

The single-particle energies are calculated by [21]:

$$e_{nlj} = \left(2n + l - \frac{1}{2}\right)\hbar\omega + \begin{cases} -\frac{1}{2}(l+1)\left\langle f(r) \right\rangle_{nl} \text{ for } j = l - \frac{1}{2}, \\ \frac{1}{2} l \left\langle f(r) \right\rangle_{nl} \text{ for } j = l + \frac{1}{2}, \end{cases}$$

Where $\left\langle f(r) \right\rangle_{nl} \approx -20\, A^{-\frac{2}{3}}$ (9), $\hbar\omega = 45\, A^{-1/3} - 25\, A^{-2/3}$.

2.2. Ground-State Form Factor and the Charge Density

It is clear that the electron scattering is one of the most powerful tools for analyzing the charge density distributions of the nucleus. Since the charge density is a measurable quantity, subsequently, it is another way of calculating the form factor. Moreover, the elastic form factor is occurring when $J = 0$ (zero spin) and is obtainable from the simple form of the Fourier transform as [22]:

$$F_0 (q) = \frac{4\pi}{Z} \int_0^\infty \rho_0 (r)\, j_0 (qr)\, r^2\, dr \qquad (10)$$

Where, $F_0 (q)$ is the ground-state form factor, r is the radius of the nucleus, and $\rho_0 (r)$ is the charge density.

The entirety of all protons point charge is the representation of operator of transition charge density $\hat{\rho}_{JM} (\vec{r})$ of a nucleus [23].

$$\hat{\rho}_{JM} (\vec{r}) = \sum_{k=1}^{Z} \frac{\delta(\vec{r} - \vec{r}_k)}{r_k^2} \tilde{\mathrm{O}}_{JM} (\grave{\mathrm{U}}_k) \qquad (11)$$

Where, J is the multipolarity of the operator, M is the projection quantum number takes $2J + 1$ values, $-J \le M \le J$, $\mathrm{Y}_{JM} (\Omega_k)$ represents the spherical Harmonic, and $\delta(\vec{r} - \vec{r}_k)$ is a Dirac delta function.

The matrix element in the reduced form of the operator $\hat{\rho}_{JM} (\vec{r})$ is gotten when the transition happens from initial nuclear spin J_i to the final nuclear spin J_f and complying the inequality $J_i \le J \le J_f$, from Equation (4) where $T_{J\tau_z} \equiv \hat{\rho}_J (\vec{r})$, then it is given by:

$$\left\langle J_f \left\| \hat{\rho}_J (\vec{r}) \right\| J_i \right\rangle = \sum_{\alpha,\beta} OBDM(\alpha, \beta, J, \tau_z, i, f) \left\langle \beta \left\| \hat{\rho}_J (\vec{r}) \right\| \alpha \right\rangle \qquad (12)$$

For the ground state ($J = 0$) as mentioned before. Moreover, $J_i = J_f$, and the charge density $\rho_J^p(r)$ define of the nucleus is getting from this matrix element [23].

$$\rho_J^p(r) = \frac{1}{\sqrt{4\pi(2J_i+1)}}\left\langle J_f \left\| \hat{\rho}_J(\vec{r}) \right\| J_i \right\rangle$$

$$= \frac{1}{\sqrt{4\pi(2J_i+1)}} \sum_{\alpha,\beta} OBDM(\alpha,\beta,J,\tau_z,i,f)\left\langle \beta \left\| \hat{\rho}_J(\vec{r}) \right\| \alpha \right\rangle \quad (13)$$

The single-particle matrix element in Equation (4) can be represented by the radial wave functions of HO $\mathcal{R}_{n_\alpha l_\alpha}(r)\mathcal{R}_{n_\beta l_\beta}(r)$ and $\langle l_\beta j_\beta \| Y_J(\Omega_r) \| l_\alpha j_\alpha \rangle$ which is the spherical Harmonic reduced matrix element.

$$\left\langle \beta \left| \left| \hat{\rho}_J(\vec{r}) \right| \right| \alpha \right\rangle = \mathcal{R}_{n_\alpha l_\alpha}(r)\mathcal{R}_{n_\beta l_\beta}(r)\left\langle j_\beta \left| \left| Y_J(\Omega_r) \right| \right| j_\alpha \right\rangle \quad (14)$$

After putting Equation (14) in Equation (13), the nuclear charge density becomes [24]:

$$\rho_J^p(r) = \frac{1}{\sqrt{4\pi(2J_i+1)}} \sum_{\alpha,\beta} OBDM(\alpha,\beta,J,\tau_z,i,f)$$
$$\mathcal{R}_{n_\alpha l_\alpha}(r)\mathcal{R}_{n_\beta l_\beta}(r)\left\langle j_\beta \left| \left| Y_J(\Omega_r) \right| \right| j_\alpha \right\rangle \quad (15)$$

For the ground-state nucleus, ($\tau_z = 1, -1$), it makes $J = 0$ and $\left\langle j_\beta \left| \left| Y_J(\Omega_r) \right| \right| j_\alpha \right\rangle = \delta_{j_\alpha, j_\beta}\sqrt{(2j_\alpha+1)/4\pi}$. After utilizing the Delta-Kronecker in Equation (15) and putting $\tau_z = 1$ for protons, the equation is rewritten as:

$$\rho_0^p(r) = \frac{1}{4\pi\sqrt{(2J_i+1)}} \sum_{\alpha} OBDM(\alpha,\alpha,0,1,i,f)$$
$$\sqrt{(2j_\alpha+1)}\left| R_{n_\alpha l_\alpha}(r) \right|^2 \quad (16)$$

the index $\alpha \equiv n_\alpha l_\alpha j_\alpha$ used for all closed shells for the ground state.

The ground-state charge radii and charge distribution considered as two great determinable quantities experimentally, meanwhile, they can be calculated theoretically. The mean square radius for the nucleus gets from the charge density integration in Equation (16) [22].

$$\left\langle r^2 \right\rangle_{ch} = \int \rho_0^p(\vec{r}) r^2 \, d\vec{r} \quad (17)$$

Under the effect of the point-proton folded charge density distribution, in Equation (10), the charge density needs to be corrected by the folding factor [25].

$$\rho_{fo}(\vec{r} - \vec{r}') = \frac{1}{\sqrt{\pi^3 a^6}} e^{-\frac{(\vec{r}-\vec{r}')^2}{a^2}}, a = 0.6532\ fm \quad (18)$$

Now, for the normalized charge density with the target nucleus atomic number Z, the root-mean-square in Equation (17) gives [24]:

$$\left\langle r^2_{ch} \right\rangle = \frac{1}{Z}\int \rho_0^p(\vec{r})\rho_{fo}(\vec{r} - \vec{r}') r^2 \, d\vec{r} \quad (19)$$

3. RESULTS AND DISCUSSION

The Beryllium nucleus has 12 known isotopes, but only one of these isotopes (Be^9) is stable and a primordial nuclide. The microscopic structure of the stable nucleus Be^9 imagined as being composed of a tightly bound core He^4 plus five loosely bound nucleons outside the core divided over the p-shell (1 p3/2, 1 p1/2). On the other way, it consists of four protons and five neutrons.

In this paper, the CP effects are calculated according to Equation (7) which include M3Y and MSDI interactions.

The potential parameters of M3Y which known as three range potential contain spin orbit, central, and tensor interactions are obtained from Bertsch *et al.* [26]. Besides, the MSDI strength parameters that used in the calculations of the CP effects are A_1, B, and C. Where T is defined as the isospin (1, 0). They have taken the values as $A_0 = A_1 = B = 25/A$ and C=0 [20], where A is the mass number of Beryllium nucleus, B and C are the correction parameters. It has the HO length parameter b = 1.791 fm [27].

FORTRAN 2008 used as a computer program for calculating CPM3Y and MSDI in the elastic and inelastic form factors. In addition, the OBDM elements calculated with the shell model code OXBASH for excitation states but is obtained from the occupation numbers for the closed-shell orbits (ground state).

Beryllium nucleus has a ground state, whereas its value is ($J_i^\pi T_i$ = 3/2 $^-$1/2) E = 0.0 MeV. Here, two transitions are under investigation representing C_2 with E = 2.43 MeV where the transition occurs to the excited state ($J_f T_f$ = 5/2 $^-$1/2) and the other excited state is ($J_f T_f$ = 7/2 $^-$1/2) E = 6.38

MeV o[28]. In all graphs, the form factors with MS and CP effects including the realistic (M3Y) interactions representing as the red lines, the form factors with MSDI interaction performs as blue lines and the small filled circles represent the experimental values for the electron scattering form factors.

3.1. Elastic Coulomb form Factor for 3/2 $^-$1/2 State

For elastic electron scattering, the scattered electron leaves the nucleus in the ground-state configuration. The ground state has (J^π T= 3/2 $^-$1/2) with E = 0.0 MeV. The multipoles entering the elastic scattering are J = 0, 2 with the corresponding Coulomb transition C_0 and C_2, respectively. The calculated form factor of sum $C_0 + C_2$ is shown in Fig. 1.

The obtained OBDM elements are shown in Table 1. The calculated root-mean-square (charge radii) for the ground state without folding is 2.629 fm but with folding is 2.505 fm, while experimentally is equal to 2.519 fm [29]. The results with M3Y interaction have a great agreement with measured data in the transfer momentum domain of $1.1 \leq q \leq 2.5$ fm^{-1}. On the contrary, the calculations with MSDI interaction have a bad deal with the experimental data excepting the area of $1.5 \leq q \leq 2$ fm^{-1} where they have similarities with each other.

3.2. Inelastic Coulomb form Factor for 5/2 $^-$1/2 State

The C_2 transition for Coulomb scattering is taking place between the ground state of (J^π T = 3/2 $^-$1/2) and the first excited state (J^π T = 5/2 $^-$1/2) with excitation energy of E = 2.43 MeV. The computed and measured Coulomb form factors of inelastic electron scattering for the Be^9 nucleus are shown in Fig. 2. The OBDM elements which calculated with OXBASH code are listed in Table 2. In this transition, the calculations with MSDI are not able to denote an adequate description of the experimental data for the region of transfer momenta (q = 0.8 fm^{-1}) and (q = 1.8 fm^{-1}), but once the CP effect with M3Y interaction is applied, making the results of the total theoretical form factors fitting the experimental data along with all regions of transfer momenta.

3.3. Inelastic Coulomb form Factor for 7/2 $^-$1/2 State

The squared inelastic scattering of Coulomb form factors for Be^9 is displayed in Fig. 3. The symbol of this transition (Coulomb transition) $C_J = C_2$, it occurs between the ground state (J^π T= 3/2 $^-$1/2) and the second excited state (J^π T= 7/2 $^-$1/2) with transition energy E = 6.38 MeV. The OBDM elements are tabulated in Table 3. Fig. 3 shows the plot of measured and calculated data for the squared inelastic Coulomb scattering form factors. The ratio of agreement between the results of both M3Y and MSDI interactions

TABLE 1: The calculated OBDM elements for the Coulomb C_0+C_2 transition of Be^9

	j_1	j_2	OBDM (n)	OBDM (p)
C_0	$1s_{1/2}$	$1s_{1/2}$	2.8284	2.8284
	$1p_{1/2}$	$1p_{1/2}$	0.5305	0.6072
	$1p_{3/2}$	$1p_{3/2}$	1.6249	2.5707
C_2	$1p_{1/2}$	$1p_{3/2}$	0.2502	0.1623
	$1p_{3/2}$	$1p_{1/2}$	−0.2502	−0.1623
	$1p_{3/2}$	$1p_{3/2}$	−0.4610	−0.2982

TABLE 2: The calculated OBDM elements for the Coulomb C_2 transition of Be^9

j_1	j_2	OBDM (n)	OBDM (p)
$1p_{1/2}$	$1p_{3/2}$	−0.4820	−0.8767
$1p_{3/2}$	$1p_{1/2}$	0.4187	0.5365
$1p_{3/2}$	$1p_{3/2}$	0.6372	0.1167

TABLE 3: The calculated OBDM elements for the Coulomb C_2 transition of Be^9

j_1	j_2	OBDM (n)	OBDM (p)
$1p_{1/2}$	$1p_{3/2}$	0.2724	0.2442
$1p_{3/2}$	$1p_{1/2}$	−0.1264	−0.1242
$1p_{3/2}$	$1p_{3/2}$	−0.7953	−0.1735

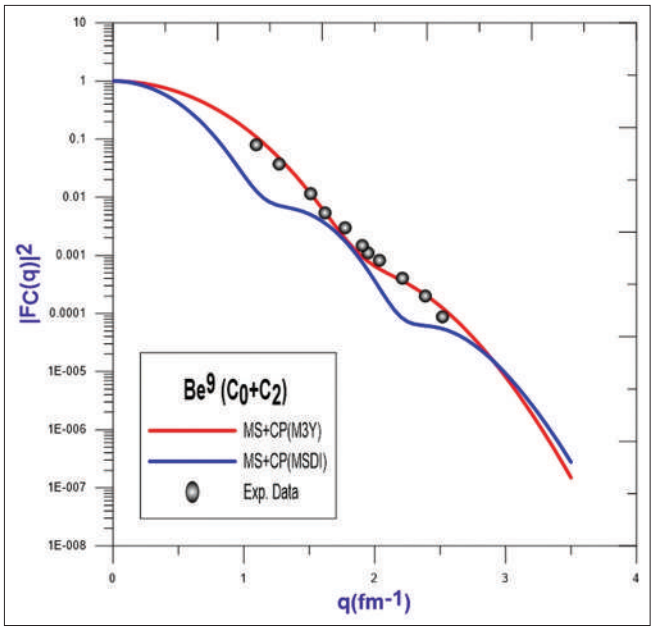

Fig. 1. Elastic Coulomb C_0+C_2 form factors for Be^9. The experimental data were taken from reference [28].

for the Be^9 form factors and the measured data are quite strong between (q = 1 fm^{-1}) and (q = 2.5 fm^{-1}). Taking into consideration that the form factors for the second excited state (J^π T = 7/2 $^-$1/2) are not substantially different from

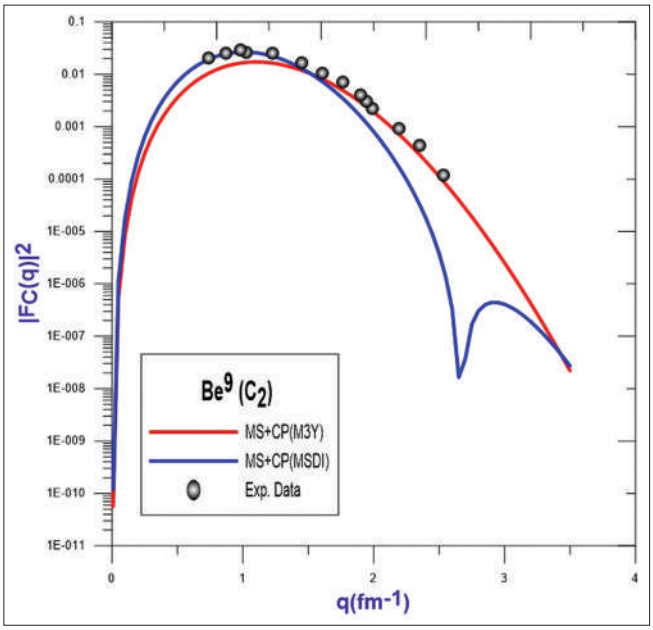

Fig. 2. Inelastic Coulomb C_2 form factors for 5/2 $^-$1/2 state of Be^9 with E = 2.43 MeV. The experimental data were taken from reference [28].

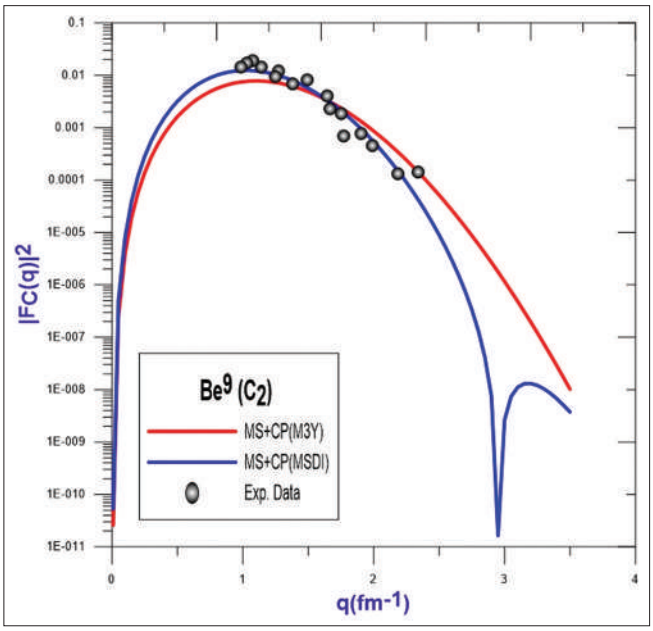

Fig. 3. Inelastic Coulomb C_2 form factors for 7/2 $^-$1/2 state of Be^9 with E = 6.38 MeV. The experimental data were taken from reference [28].

that of the first excited state (J^π T = 5/2 $^-$1/2), whence a noticeable change is observed in the computation of form factors by M3Y and MSDI interactions. The MSDI decreased faster than the M3Y during the increase of momentum transfer, especially at the point of (q = 3 fm^{-1}).

4. CONCLUSION

In the present work, it is possible to consider the following conclusions:

- The basic calculations include the Coulomb form factors for the ground state and other excitation states.
- The ground-state Coulomb form factors (C_0 transitions) for the M3Y interaction and the ground-state charge radii with folding effect give the best fit with the experimental data for beryllium (Be^9) nucleus.
- For Be^9 nucleus which is under consideration, the quality of similarity between the computed Coulomb form factors $F_C(q)$ and those of the measured data become even better in the using of the CP effects with including M3Y residual interaction for all Coulomb C_2 transitions because M3Y interaction is more realistic nucleon-nucleon interaction that adopted for the CP calculation.
- The calculation of Coulomb form factors $F_C(q)$ with (MSDI) interaction is dealing with the surface nucleons only. Therefore, it has a limited agreement with the experimental results.
- The HO succeeded to describe the wave functions completely.

5. CONFLICTS OF INTEREST

There are no conflicts of interest.

REFERENCES

[1] T. W. Donnelly and J. D. Walecka. "Electron scattering and nuclear structure". *Annual Review of Nuclear Science*, vol. 25, no. 1, pp. 329-405, 1975.

[2] D. J. Millener, D. I. Sober, H. Crannell, J. T. O'Brien, L. W. Fagg and L. Lapikas. "Inelastic electron scattering from 13C". *Physical Reviews*, vol. 39, no. 1, pp.14-46, 1989.

[3] S. Cohen and D. Kurath. "Effective interactions for the 1p shell". *Nuclear Physics*, vol. 73, no. 1, pp. 1-24, 1965.

[4] D. Salman, S. A. Al-Ramahi and M. H. Oleiwi. "Inelastic electron-nucleus scattering form factors for 64, 66, 68Zn isotopes". Vol. 2144. In: *AIP Conference Proceedings*, p. 030029, 2019.

[5] K. S. Jassim. "Longitudinal form factor for some sd-shell nuclei using large scale model space". *International Journal of Science and Technology*, vol. 1, no. 3, pp. 140-143, 2011.

[6] N. F. Mott. "*Sir Nevill Mott: 65 Years in Physics*". Vol. 12. World Scientific, Singapore, 1995.

[7] Z. Czyżewski, D. O. N. MacCallum, A. Romig and D. C. Joy. "Calculations of Mott scattering cross section". *Journal of Applied Physics*, vol. 68, no. 7, pp. 3066-3072, 1990.

[8] H. Uberall. "*Electron Scattering from Complex Nuclei V36A*". Academic Press, New York, London, 2012.

[9] F. A. Majeed. "The effect of core polarization on longitudinal form

factors in 10B". *Physica Scripta*, vol. 85, no. 6, p. 065201, 2012.

[10] G. Fricke, C. Bernhardt, K. Heilig, L. A. Schaller, L. Schellenberg, E. B. Shera and C. W. Dejager. "Nuclear ground state charge radii from electromagnetic interactions". *Atomic Data and Nuclear Data Tables,* vol. 60, no. 2, pp. 177-285, 1995.

[11] F. I. Sharrad, A. K. Hamoudi, R. A. Radhi, H. Y. Abdullah, A. A. Okhunov and H. A. Kassim. "Elastic electron scattering from some light nuclei". *Chinese Journal of Physics*, vol. 51, no. 3, pp. 452-465, 2013.

[12] R. A. Radhi, A. A. Alzubadi and E. M. Rashed. "Shell model calculations of inelastic electron scattering for positive and negative parity states in 19F". *Nuclear Physics A*, vol. 947, pp. 12-25, 2016.

[13] E. M. Raheem, R. O. Kadhim and N. A. Salman. "The effects of core polarization on some even-even sd-shell nuclei using Michigan three-range Yukawa and modified surface delta interactions". *Pramana*, vol. 92, no. 3, p. 39, 2019.

[14] B. A. Brown, A. Etchegoyen, N. S. Godwin, W. D. M. Rae, W. A. Richter, W. E. Ormand and C. H. Zimmerman. "Oxbash for windows PC". In: *MSU-NSCL Report*, pp. 1289, 2004.

[15] S. Mohammadi, B. N. Giv and N. S. Shakib. "Energy levels calculations of 24Al and 25Al isotopes". *Nuclear Science*, vol. 2, no. 1, pp. 1-4, 2017.

[16] T. de Forest and J. D. Walecka. "Electron scattering and nuclear structure". *Advances in Physics*, vol. 15, no. 57, pp. 1-109, 1966.

[17] L. J. Tassie and F. C. Barker. "Application to electron scattering of center-of-mass effects in the nuclear shell model". *Physical Review*, vol. 111, no. 3, p. 940, 1958.

[18] K. S. Jassim, A. A. Al-sammarrae, F. I. Sharrad and H. A. Kassim. "Elastic and inelastic electron-nucleus scattering form factors of some light nuclei: Na 23, Mg 25, Al 27, and Ca 41". *Physical Review C*, vol. 89, no. 1, p. 014304, 2014.

[19] H. Fatah, R. A. Radhi and N. R. Abdullah. "Analytical derivations of single-particle matrix elements in nuclear shell model". *Communications in Theoretical Physics*, vol. 66, no. 1, p. 104, 2016.

[20] P. J. Brussaard and W. M. Glaudemans. "*Shell-Model Application in Nuclear Spectroscopy*". North-Holland, Amsterdam, 1977.

[21] D. Salman, D. R. Kadhim. "Longitudinal electron scattering form factors for 54, 56 Fe". *International Journal of Modern Physics E*, vol. 23, no. 10, p. 1450054, 2014.

[22] F. I. Sharrad, A. K. Hamoudi, R. A. Radhi, Y. Abdullah, A. A. Okhunov and H. A. Kassim. "Elastic electron scattering from some light nuclei". *Chinese Journal of Physics*, vol. 51, no. 3, pp. 452-465, 2013.

[23] B. A. Brown, R. Radhi and B. H. Wildenthal. "Electric quadrupole and hexadecupole nuclear excitations from the perspectives of electron scattering and modern shell-model theory". *Physics Reports*, vol. 101, no. 5, pp. 313-358, 1983.

[24] H. M. Dlshad and A. H. R. Fatah. "Using MSDI and M3Y core polarization for the coulomb electron scattering for some ground state nuclei". *JZS (Part-A)*, vol. 21, no. 2, pp. 11-20, 2019.

[25] G. S. Anagnostatos, A. N. Antonov, P. Ginis, J. Giapitzakis and M. K. Gaidarov. "On the central depression in density of". *Journal of Physics G: Nuclear and Particle Physics*, vol. 25, no. 1, p. 69, 1999.

[26] G. Bertsch, J. Borysowicz, H. McManus and W. G. Love. "Interactions for inelastic scattering derived from realistic potentials". *Nuclear Physics A*, vol. 284, no. 3, pp. 399-419, 1977.

[27] F. A. Majeed. "Longitudinal and transverse form factors from 12C". *Physica Scripta*, vol. 76, no. 4, p. 332, 2007.

[28] J. P. Glickman, W. Bertozzi, T. N. Buti, S. Dixit, F. W. Hersman, C. E. Hyde-Wright and B. L. Berman. "Electron scattering from sup 9 be". *Physical Review C (Nuclear Physics) (USA*), vol. 43, no. 4, pp. 1740-1757, 1991.

[29] Angeli and K. P. Marinova. "Table of experimental nuclear ground state charge radii: An update". *Atomic Data and Nuclear Data Tables*, vol. 99, no. 1, pp. 69-95, 2013.

ORIGINAL RESEARCH ARTICLE UHD JOURNAL OF SCIENCE AND TECHNOLOGY

Smart University Library Management System Based on Internet of Things

Sivana Salahadin Muhamed[1,2], Aso Mohammad Darwesh[3]

[1]Department of Computer Science, College of Science and Technology, University of Human Development, Sulaymaniyah, KRG, Iraq, [2]Department of Computer, College of Science, University of Sulaimani, Sulaymaniyah, KRG, Iraq, [3]Department of Information Technology, College of Science and Technology, University of Human Development, Sulaymaniyah, KRG, Iraq

ABSTRACT

With the innovation of new technologies, many life concepts have been changed. However, libraries remain the same in many sides while the main role of libraries has been changed and new references may not need a classical library as it was 50 years ago. In the same time, library services can be improved using Internet of Things (IoT) to increase user satisfactions. In recent years, there has been arisen in the diversity of implementation based on radio-frequency identification (RFID) systems and has been successfully utilized in several areas such as health care and transportation. RFID-based library management system will let rapid transaction flow for the library and could prove instant and long-term benefits to library in traceability and security. To solve the problem that it is inconvenient to find references in the traditional library, a kind of reference positioning system using RFID technology is designed to achieve fast search references in the library. Searching and sorting misplaced references are a hard task often carried out by the librarians. In this paper, the performance of RFID reader motion and tags allows fast transaction flow and easily handling the process like references borrowing from library can be done using RFID technology and users will get notified using Global System for Mobile. Two big issues have been exposed and tried to find the best solution for them, first is the management process of any library, from user management to shelving system and the second one is the data and reference security. The results show that the system can quickly find the references that bookworms hid, and the references are not timely put back on the shelves. Furthermore, the new library hall design and IoT-based system improve the security.

Index Terms: Global System for Mobile, Internet of Things, Library Security, Library System, Radio-Frequency Identification

1. INTRODUCTION

Application of information technology in libraries has always been a boon to improve the quality and delivery of information services to the users. One technology is the radio-frequency identification (RFID) technology [1]. The technology of RFID has been innovated by Charlie Walton [2]. RFID is a technology incorporates the use of electromagnetic or electrostatic pairing within the radio frequency (RF) parcel of the electromagnetic range to uniquely identify an object, animal, or person. It is an automatic identification method where data can be stored and retrieved remotely using devices like RFID tags. The tag is also called as an "electronic label," "transponder," or "code plate," is made up of an RFID chip attached to an antenna, transmitting within the kilohertz, megahertz, and gigahertz ranges [3]. Library is an important place for

Access this article online

DOI:10.21928/uhdjst.v4n2y2020.pp63-74 | E-ISSN: 2521-4217 P-ISSN: 2521-4209

Corresponding author's e-mail: Sivana Salahadin Muhamed, Department of Computer Science, College of Science and Technology, University of Human Development, Sulaymaniyah, KRG, Iraq/Department of Computer, College of Science, University of Sulaimani, Sulaymaniyah, KRG, Iraq. E-mail: sivana.salahadin@uhd.edu.iq

Received: 09-06-2020 Accepted: 18-08-2020 Published: 20-08-2020

people to acquire new knowledge. Especially in today's era of knowledge explosion, it has become the important basic survival condition if we want to keep up with the trend of the times to gain more knowledge from references. The number and categories of library references also refresh the record in time. On the one hand, people can choose a targeted reference, on the other hand, large number of references no doubt increases the difficulty of library managers and readers when query and retrieve references. Using RFID technology in the research of library, shelf positioning system can help library information management [4]. With the maturity and popularity of the RFID technology, using the RFID technology can not only solve the contradiction between the librarians and the readers but also can improve the work efficiency of the librarians [5].

RFID is the latest technology that is used in library theft detection systems [6]. RFID-based system has been designed and developed to replace the existing library barcoding system and also the barcode can be damaged. This system allows the librarians to limit the spent time that's required for checking barcodes during charging and discharging process.

The RFID-based library management system (LMS) facilitates the quick issuing, reissuing, and returning of references with the help of RFID enabled modules. It directly provides reference information and library member data to the LMS and does not want the manual typing. It additionally provides monitoring and searching system. The monitoring module will constantly monitor the movement of references over the gates, in order that the references taken out without previous issuing will be followed out simply and will alert the librarians. The searching module gives the quick searching of references utilizing RFID reader. The physical location of the references may be simply located using this module [7]. Like any other system, this system will also have some problems that need to be solved, and these are problems such as the loss of references and the misplace of references place, the difficulty in finding the reference, also as well as stealing the references and giving them without the knowledge of the library employee, and an secure the references and users information.

2. SHELVING SYSTEM

To make library systems, efficient and successfully operational RFID solutions can be used to reduce operating costs through reducing the labor costs, enhancing automation, refining tracking and tracing, and inhibiting the loss of resources under any conditions. The system based on RFID is a unique concept by itself. Due to the fact that improved organization of references and resources becomes possible, resources are not lost, stealing is avoided, and customers are served on time and correctly [8]. Imagine a library where each reference has its own place on a particular shelf. Borrower like to take a reference off the shelf, there are some people who place back the reference in the right place, but many people either leave the references in some corner of the library or return them to the wrong places. This later situation is hard to identify and can make librarian's frightening [8]. Searching and sorting misplaced references are a difficult task often carried out by the library personnel. Quite often, librarians are busy with searching misplaced references which are left in wrong locations by library users. To overcome this, RFID-based intelligent shelving system has been proposed to provide an efficient mechanism of references management monitoring between the RFID reader and the references [9].

In this paper, we are aiming to create library system using this progressive RFID technology, which can track the references, whether they are issued or they are in library. RFID can be utilized for library circulation operations and theft detection systems.

3. SECURITY AND PRIVACY OF RFID

However, the rapid growth of RFID has raised serious privacy concerns over these years. Since RFID readers and tags communicate through a wireless channel, the messages exchanged in between, may be susceptible to eavesdropping or interception. Moreover, tags response to a reader's interrogation without the knowledge of their carriers [10]. Using encryption could be a perfect way to secure the contents of the information that is transmitted so that indeed in case an unauthorized person eavesdrops on the communication, the cipher text would not detect important information unless the key has moreover been compromised [11]. There is a need of a secure, safe, system that can facilitate the manager with the features that include monitoring the employee's communication. In this paper, we employed two different encryption algorithms, namely, triple data encryption standard (3-DES) and Message Digest 5 (MD5) to encrypt the data of system. RFID tag is used for the authentication process of verifying that identity.

4. LITERATURE REVIEW

To know the latest development in the area of RFID technology and its applications in libraries, the literature

available in primary and secondary sources of information have been meticulously scanned and summary of some of the studies has been enumerated here. Most of the articles discussed about the RFID technology, its components, and its usage in managing library activities which are still at initial stage of implementation at many libraries.

Sivasankar *et al.* (2020), in this context, the RFID technology is used to manage smooth circulation in the library, in addition to ensuring the security of the books. Furthermore, the implementation of RFID in the library area can save the time of patrons and library staff. RFID technology helps libraries improve customer satisfaction with self-service experience and increases employee efficiency by multiple value-added services. This paper illustrates the comprehensive application of RFID technology in the library domain with a case study of migration RFID systems implemented in the Scientific Information Resource Division [6].

Bomble *et al.* (2020) in this research have found that RFID is serving a variety of functions relating to stock management, security, and issuing. RFID is one such technology which can be used not only for security purpose but also in circulation operations, location of library materials, stock management, and high-speed inventorying. Moreover, the application promises to increase efficiency, productivity and enhance user satisfaction. RFID technology helps the library management to offer more secure and foolproof library services to their users. It helps a librarian in providing the users with optimum utilization of resources. The research is implementation project in Central Library, where the library staff was able to use the findings to good effect to create a business plan. It is critical to teach library staff and library users around RFID technology before implementing a program. It may be better for librarians to observe developments in RFID until the cost of tags comes [3].

Mohammed *et al.* (2019) described that a book tracking RFID-based system has been designed and developed to replace the existing library barcoding system. This system allows the librarians to limit the spent time that's required for checking barcodes during charging and discharging process. Advance, this technology has been upgraded by inserting Global System for Mobile (GSM) features to inform and alarm the borrower book with the due date of book return additionally determine the related fine if the due date is surpassed [12].

Gandu *et al.* (2019) described the deployment of smart devices in Internet of Things (IoT) applications that are expanding with huge pace causing serious security concerns, because it exchange most of private data. To counter that security issues in low-resource applications, lightweight cryptographic algorithms have been presented in recent past years. In this paper, they propose effective hardware design of piccolo lightweight algorithm uses 64 bits block size with variable key size of length 80 and 128 bits. This paper presents novel hardware architecture of piccolo-80, to supports high-speed RFID security applications. Different design procedures are there to optimize the hardware metrics trade-off for specific application [13].

Snehalatha *et al.* (2018), this paper proposes the design and implementation of smart library for digitalizing the library using IoT without any human interruption. Implementation of this framework is based on RFID technology, that is, RFID tags are placed on books and RFID reader is used to read these tags. This study is to atomize the library such as allowing fast transaction flow and easily handling the activities such as process of issuing and return of book from library can be done using RFID technology and user will get notified using GSM. RFID is used to check the availability, misplacement of book, provide anti-theft, and location of book. Book availability and location of book can be checked on webpage. Information of each user card will be maintained on database and update automatically using IoT [14].

Mahdi *et al.* (2018) examined the role of the IoT in libraries and educational centers as the new technology. Since new technologies have raised library services user expectations, so librarians should be aware of the various aspects of IoT in libraries and services. They should also be trained about IoT security issues in libraries and the lifestyles of users. The IoT will continue to affect libraries and their services through building, collection management, instruction, data security, and information literacy and so on. This study also aims to introduce readers to new IoT technology that can help libraries enhance their services and improve user satisfaction [15].

Ajay (2017) describes the potential of RFID technology in facilitating efficient library operations and demonstrates that RFID can be used in libraries to ensure security and facilitate innovative services and highlights key issues that needed to be addressed to achieve successful implementation of RFID in libraries and also examines key challenges in the deployment of the technology [16].

Santha *et al.* (2016) described that the application of GSM technology for documents identification was examined. The

mobile pervasive technology can be used by the libraries to serve their patrons to avail the library services in an effective and efficient way. The libraries should also use mobile popular technologies to support their customers as well as the patrons to allow better use of the library services. When implementing this technique, the services offered the libraries to the user will be more efficient and effective [17].

Sun *et al.* (2012) in their paper entitled "A proposed model for library stacks management" developed a new stacks management model called "parent-child-grandchild model" by changing the layout of the book stacks, the management principles, as well as by employing the RFID. In such a model, book stacks are divided into three sections, one large ("parent"), one medium "child," and one small "grandchild." The three sections comprised the entire printed collection of a library, representing different functions and use of the stacks. They pointed out that a library needs a good RFID support facility which helps the library staff to manage printed material more effectively and library users to find the physical location of books. They discussed the transaction processes, production processes, governance processes, interaction process, and facilitation process of RFID. They concluded that it is a revolutionary idea to implement the new model, which attempts to achieve not only better stack management but also a more friendly and attractive library image [18].

5. PROBLEM STATEMENT

Due to huge amount of references in libraries, working on them in terms of management and security becomes critical. Using new technologies can help solve many of these problems. Furthermore, recently, COVID-19 wakes up the world that everything must be managed differently or must be possible to manage it in classical and modern ways. Smart library systems become a new model to manage libraries. However, still some issues must be exposed. In this research, we focused on two major ones which are decreasing time consumption and save the privacy. We use IoT-based technologies to implement a modern system of LMS. Basically, we focused on using RFID and GMS. We use RFID to retrieve resources' information and find their position. Furthermore, we suggest a new design for a library to implement our system. Then, we encrypt all library data using two algorithms 3-DES and MD5 to prevent any data stolen. Finally, we design GSM system for library to direction the system and notify borrowers with a text message for important requirements.

6. NOVELTY OF WORK

1. New design for the library including different types of references each in a separate section in the library.
2. Shelve references and puts a misplaced reference in the correct place. That is by classifying the references shelves according to the types and subject of references and placing each reference in the shelf of its own class that helps put the reference in the correct place after its return by the borrower.
   Using security techniques to prevent any attacked and stolen the data of the system. We use a 3-DES and MD5 algorithm to encrypt and decrypt all stored data.
3. Using IoT to improve the library system in wasting time, shelving system, and stolen of valuable references.

7. IMPLEMENTATION OF RFID IN LIBRARY

Basically in library systems, tags ID should be compared with the database to find the reference location and its details. The database saves a set of original information that includes the tag ID, reference title, reference class number, and author name. The database of resources information is different to the borrowing one. Each user must have an RFID card which is connected to a record in the database that contains all details. Whenever the user needs borrowing any reference, employee scan his/her ID card first then select the operation (Borrow in this case) and finally scan the reference. In the software, we are maintaining the separate database for issuing or returning reissuing the references. Each user has RFIDs card and in the library software for that id is stored with the user detail. The RFID readers read the tags and it checks if the user and reference data found in the database. If both are there, then the user can issued the particular reference. Any reference not assigned to any user cannot be bringing outside the library. If not, the gate in which the non-assigned reference passed detects, issue an alarm, and informs the security and the employees by message. The library software is implemented using. NET platform using C# as a front end and Microsoft Access as back end to maintain the database.

8. METHODOLOGY

8.1. RFID Library System Design and Content

The implementation of the RFID systems has impacted on the library in various ways. In our model, we design the library system to facilitate handling references and easy to use by library employees and readers.

8.1.1. Library sections

According to the types of resources, there are three zones in the library (read only, read and copy, and borrow), as explained in Fig. 1. At the entry of each zone, there are two lights red and green informing the user and the librarian to allow/disallow entrance of the user depending on the reference type, the user can enter only that zone. In case of borrowed type of resources, the borrower will be registered by the employee of the library which allows him/her to take the resources outside the library and the exit door will opens successfully. The readers are installed in different positions at the library doors to detect the references when someone tries to steals references, as explained in Fig. 1. Fig. 2 shows the hardware implementation of the system.

8.2. The System Can Solve this Problem

8.2.1. Shelving references using RFID

With the RFID, it becomes very easy, to shelve references and put a misplaced reference in a correct place. Discharged references can easily be separated according to the class number and location number. That is by classifying the references shelves according to the types and subject of references, and placing each reference in the shelf of its own class, with a RFID reader for each shelf it is programmed for the reference class of specific shelve that helps put the reference in a correct place after its return by the borrower. The system is programmed as follows: The references are scanned through the RFID reader of the shelve when the reference is placed in the correct shelve, the green light is turned on, otherwise, the red light is turned on and an attempt is made again to search for the correct place of the reference until the green light is turned on. Thus, the state of loss of references and lack of knowing its correct location after its return is decreased. We suggest this idea of shelving reference by RFID and implement it in the system as one of our research contributions, as shown in Fig. 3.

8.2.2. Theft detection and alarm access control system

The security gates have been installed at the exit gate of the library. RFID technology is a high-performance anti-theft technology, it detects any resources that has not been checked out by librarian and cannot pass through the exit door. Fig. 4 shows the hardware implementation of exit gate.

8.2.3. Saving time at the circulation counter

Circulation includes check-out, check-in, and renewal of borrowing. It generally takes 1–2 min to complete a single transaction when the task is performed manually, while the same transaction takes place within 5–10 s with the RFID system. A further advantage is that if the user has five items to check-out or check-in the transaction can be simply completed within single cycle.

8.2.4. Save references and user privacy

The references and user information need to be secure and privacy in the database to avoid any attacked and stolen

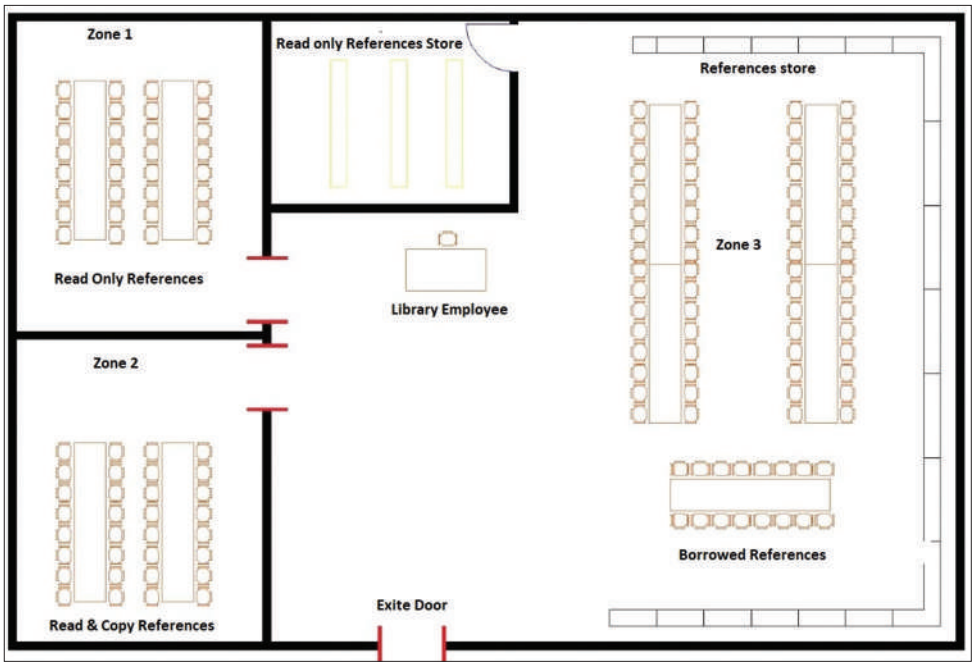

Fig. 1. The design of system.

data of the system. To prevent this issue in this system, we use 3-DES and MD5 algorithm to encrypt and decrypt stored data. The data will be encrypted and then stored in the database, and then, we need retrieve the data decrypted and display on the interface. Data encrypt and decrypt code shown in Figs. 5 and 6.

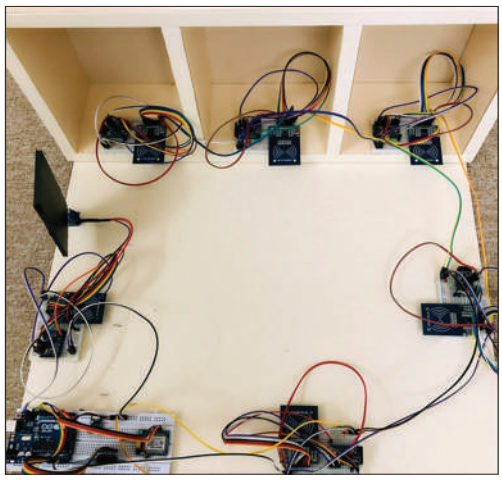

Fig. 2. Hardware implementation of the system.

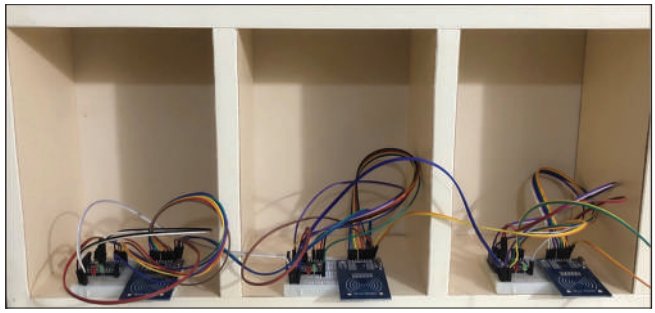

Fig. 3. Shelving references of the system.

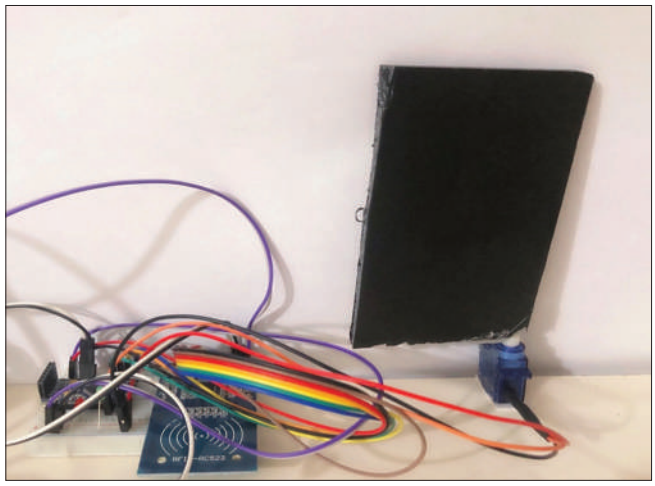

Fig. 4. Hardware implementation of exit gate.

8.2.5. Using GSM system

A GSM modem that shows in Fig. 7 is used for sending a message to the borrower regarding the last due date of returning the reference. The system will help to reduce the waiting time of users in queue for issuing and returning of references in the library. The message is shown in Fig. 8.

9. THE DESIGN OF THE SYSTEM

The RFID system includes related hardware devices and application software system, whose function and services must be connected with the library existing management system after it has been used in practice [19]. The flow diagram shown in Fig. 9 explains the functioning of the proposed library system. The librarian use RFID card for login to the system, then scan user's RFID tag. Finally, scan reference's RFID tag and set the reference as borrowed and search for another reference if user has any more reference.

9.1. The Design of the Main System Interface

Because the system consists of six modules, references information module, user information, namely, the borrowing module, the report module, history module, and the setting module, so these fife parts should be displayed in the main interface. One can understand the functions of every module clearly through the main interface. Main interface describes in Fig. 10.

9.2. The Design of References Information Module

The main function of this module is to manage the references, including add, delete or modify the information of references, display the status, or set the reference as a borrow reference for borrower user. Also can search for references by Reference tittle, Reference author, and Can search by RFID tag of reference. Reference information and details are shown in Figs. 11 and 12.

9.3. The Design of User Information Module

Each user use him/her RFID card of the university, we can use this card for library also by insert all users data in to the database and when an user need to borrow a reference s/he need just swipe him/her RFID card and display him/her information. The user information module is shown in Fig. 13.

9.4. The Design of Borrow Module

The main function of this module is to borrow references. To borrow references successfully, the borrower should swipe him/her RFID card, and click the borrow button, finally, swips RFID tag of the reference. The system will

```
private string Encrypt(string RX)
{
    if (string.IsNullOrEmpty(RX))
    {
        return string.Empty;
    }
    else
    {
        byte[] data = UTF8Encoding.UTF8.GetBytes(RX);
        using (MD5CryptoServiceProvider md5 = new MD5CryptoServiceProvider())
        {
            byte[] keys = md5.ComputeHash(UTF8Encoding.UTF8.GetBytes(hash));
            using (TripleDESCryptoServiceProvider tripDes = new TripleDESCryptoServiceProvider() { Key = keys, Mode = CipherMode.ECB, Padding = PaddingMode.PKCS7 })
            {
                ICryptoTransform transform = tripDes.CreateEncryptor();
                byte[] results = transform.TransformFinalBlock(data, 0, data.Length);
                return Convert.ToBase64String(results, 0, results.Length);
            }
        }
    }
}
```

Fig. 5. Encrypt code.

```
private string Decrypt(string RX)
{
    if(RX == string.Empty)
    {
        return string.Empty;
    }
    else
    {
        byte[] data = Convert.FromBase64String(RX);
        using (MD5CryptoServiceProvider md5 = new MD5CryptoServiceProvider())
        {
            byte[] keys = md5.ComputeHash(UTF8Encoding.UTF8.GetBytes(hash));
            using (TripleDESCryptoServiceProvider tripDes = new TripleDESCryptoServiceProvider() { Key = keys, Mode = CipherMode.ECB, Padding = PaddingMode.PKCS7 })
            {
                ICryptoTransform transform = tripDes.CreateDecryptor();
                byte[] results = transform.TransformFinalBlock(data, 0, data.Length);
                return UTF8Encoding.UTF8.GetString(results);
            }
        }
    }
}
```

Fig. 6. Decrypt code.

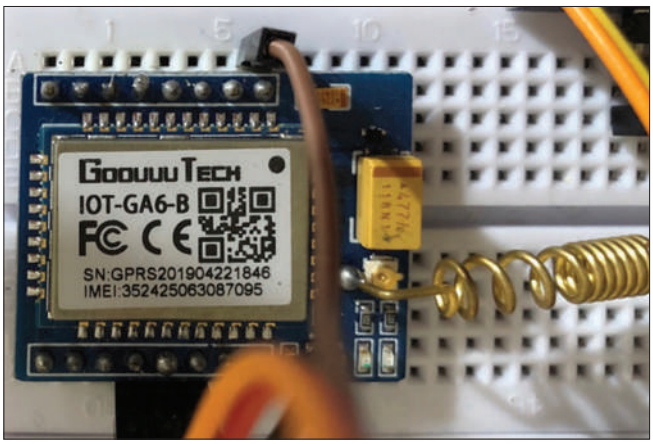

Fig. 7. GSM device.

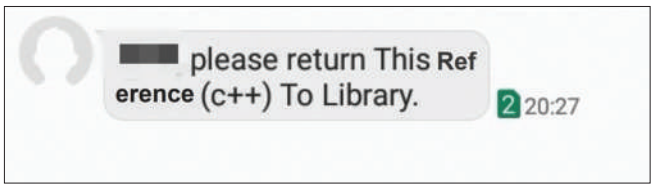

Fig. 8. System message.

build relations between the user and the borrowed references. Moreover, the references will added to list of borrowed reference, and they cannot be borrowed any more if there is only one copy of the reference in the library. Borrow module is shown in Figs. 14 and 15.

9.4.1. Return reference

The borrow module contains a return part that contains list of borrower that should return references in due date. This part shows who should return which references each day and who did not return his/her borrowed reference in specific date. If the reference returned in the current date

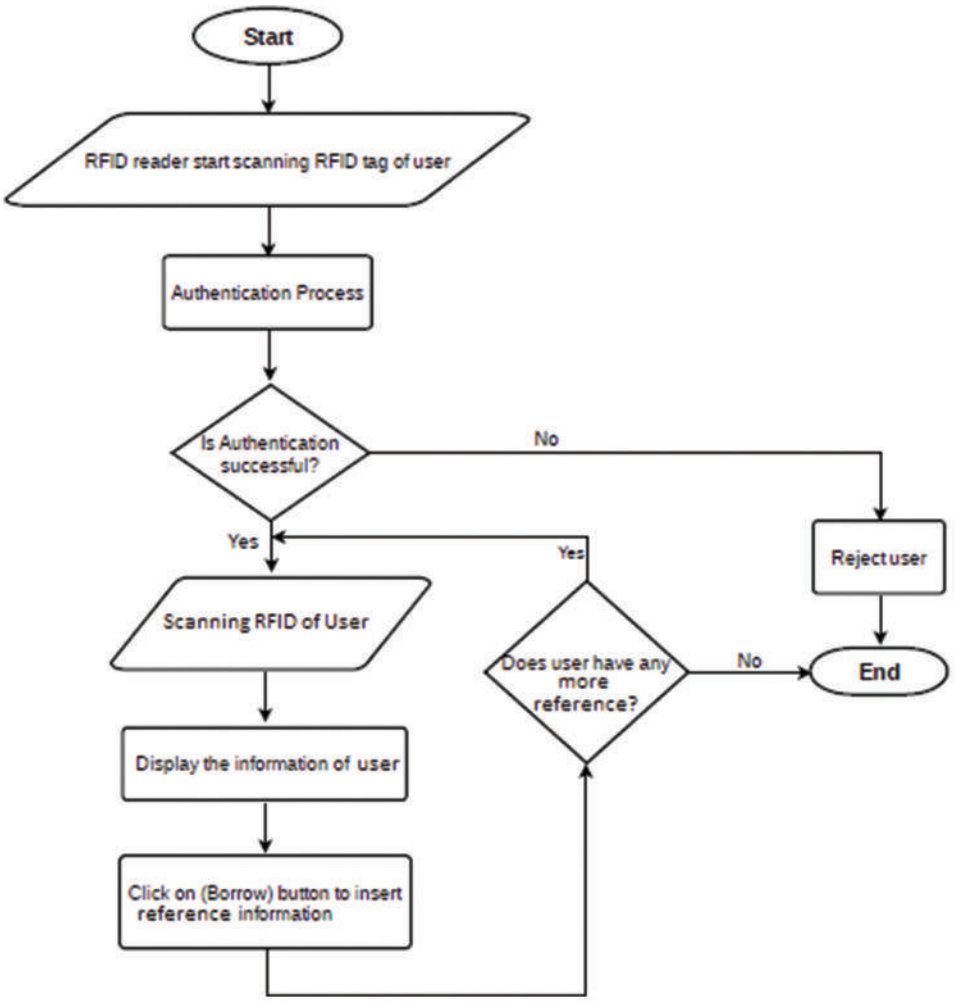

Fig. 9. The flow diagram of system.

Fig. 10. Main interface of system.

delete user from borrowed list, or the system will send SMS automatically to the user for return the reference to library. It is also possible to send SMS message again manually. The reference returning part is shown in Fig. 16.

9.5. The Design of Report Module

The report is an important part in any system. In this system, the report design shows the number of references, number of borrowed ones, top 10 of the most borrowed references and top borrowers, number of references per language, and some other reference specific data. The report module is described in Fig. 17.

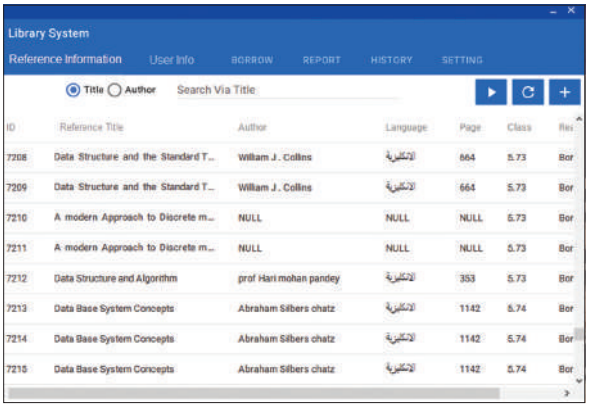

Fig. 11. List of references.

9.6. The Design History Module

This module contains all history of the system such as add reference, delete reference, borrow reference, and return

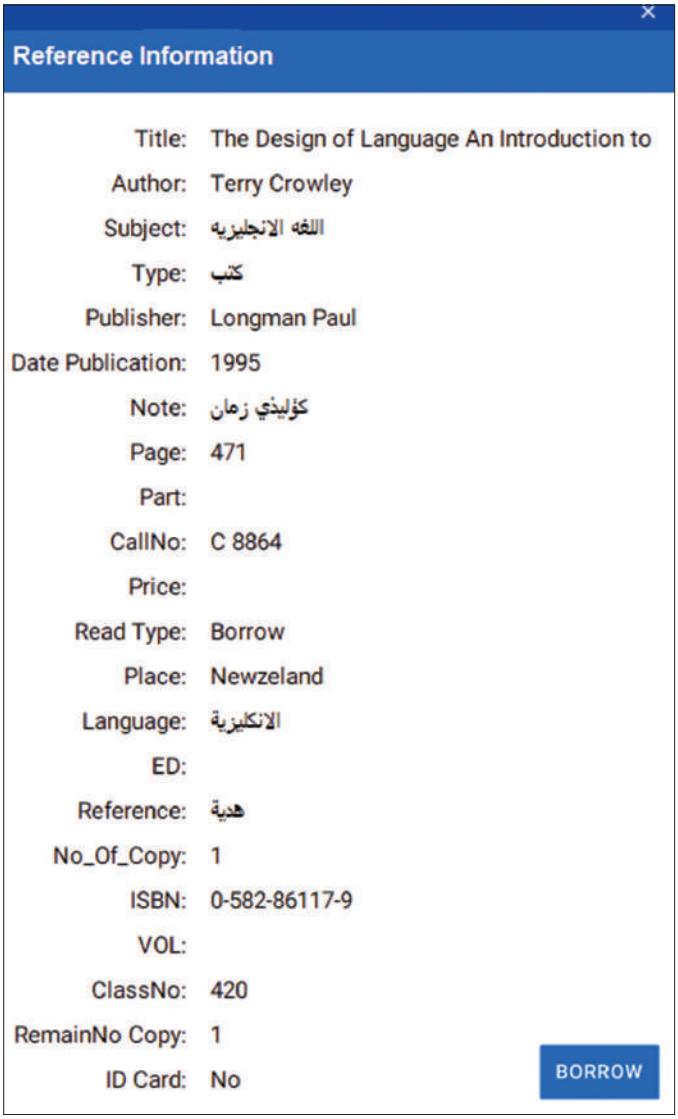

Fig. 12. Detail of reference.

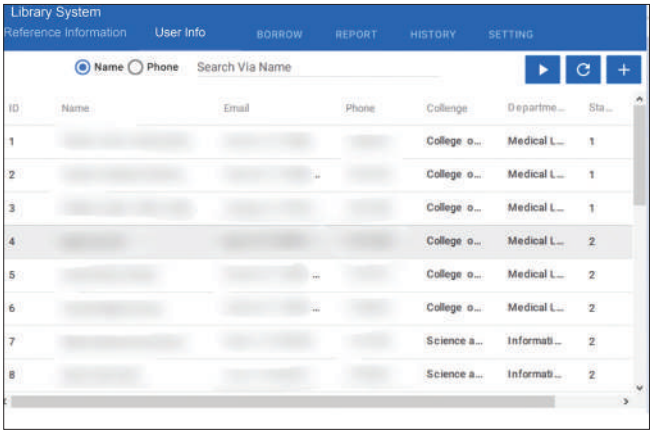

Fig. 13. List of user information.

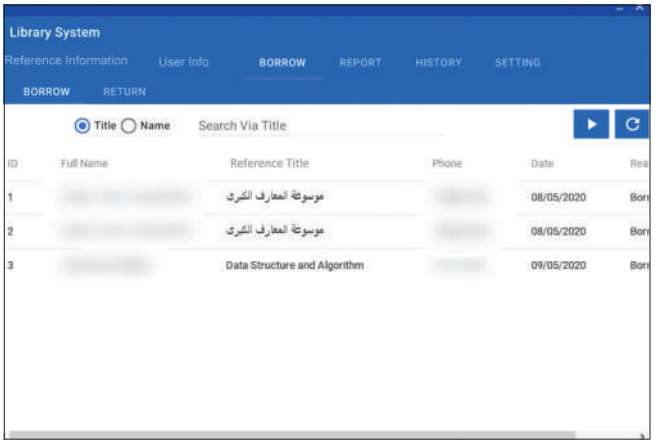

Fig. 14. List of borrowed reference.

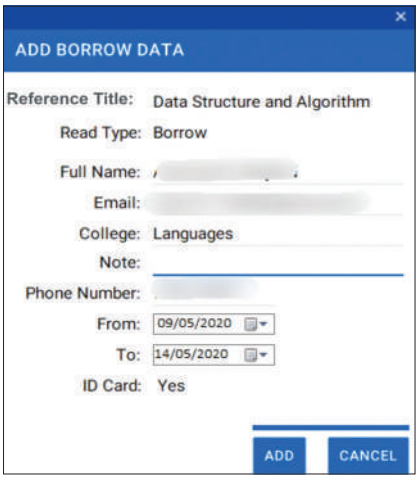

Fig. 15. Borrow process.

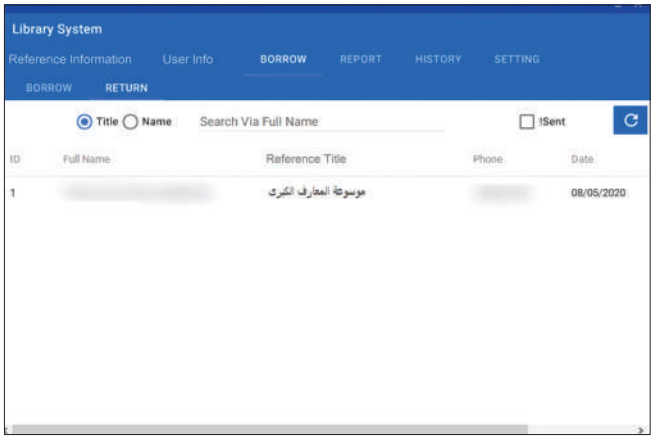

Fig. 16. Return reference part.

reference and the name of user. The history shows as monthly and we can clear all data of this month. Fig. 18 shows history module.

9.7. The Design Setting Module

The setting module contains of some part that shown in Fig. 19 that makes a system easy to control and use. Below explain parts of setting module.

9.7.1. Create user account

The employee who uses the system should have his/her user account. To create an account, we need to assign a username and password linked to an RFID tag. The login to system just needs to swipe his/her RFID card and login to the system directly without insert username and password. Create user account shown in Fig. 20.

9.7.2. Control system color

In the setting part, we can control change the system color for red, green, or blue. Moreover, can check to dark theme to enable dark theme or uncheck to disable dark theme.

9.7.3. Readering notification

We can observe what the borrower doing and where is s/he in the library. By check on readering notification, any active RFID reader in the system will be notified when the borrower use this RFID reader.

9.7.4. Auto-send SMS

By check on auto-send SMS, the system will send SMS automatically for the borrowers who does not returned reference in current day to returned reference to library.

9.7.5. Send SMS notification

If auto-send SMS does not enabled, by check on this part, the system will notify a remember notification for a librarian every day to send the message to the borrower who did not return the reference at the appointed time to library. Fig. 21 shows SMS notification.

9.7.6. Auto-connection

When check in auto-connection, all the RFID readers in the system will connected automatically and do not need to connect manually by a librarian.

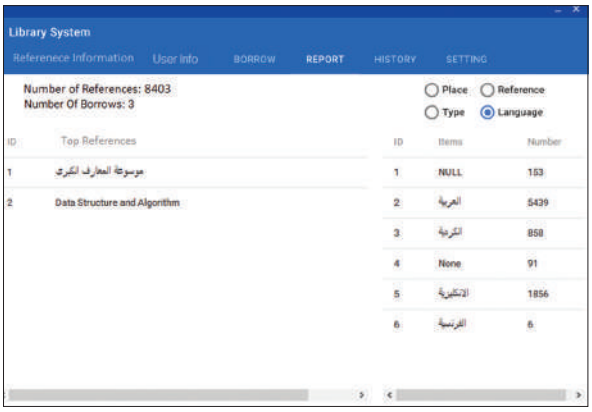

Fig. 17. Report module.

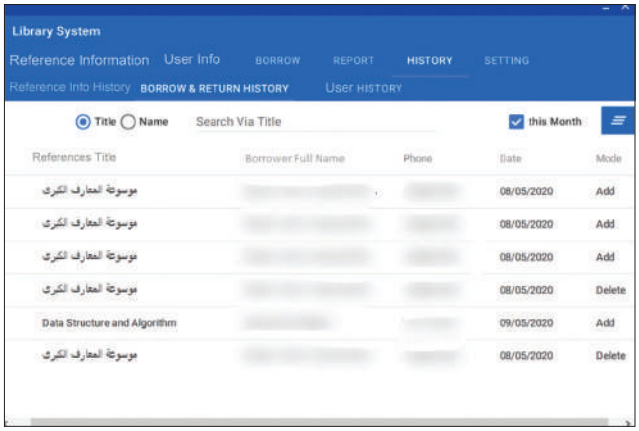

Fig. 18. History module.

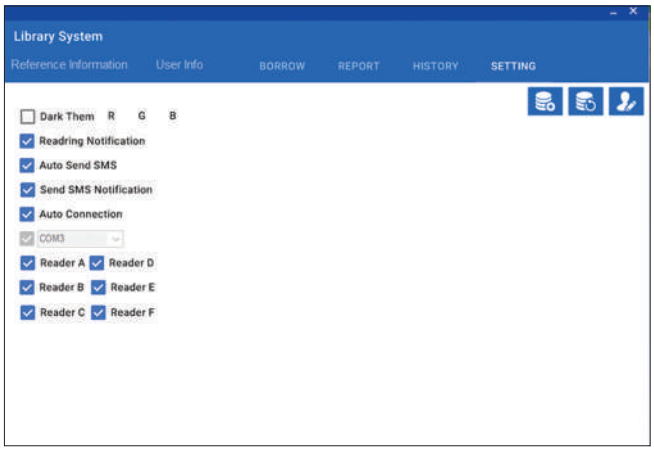

Fig. 19. Setting module.

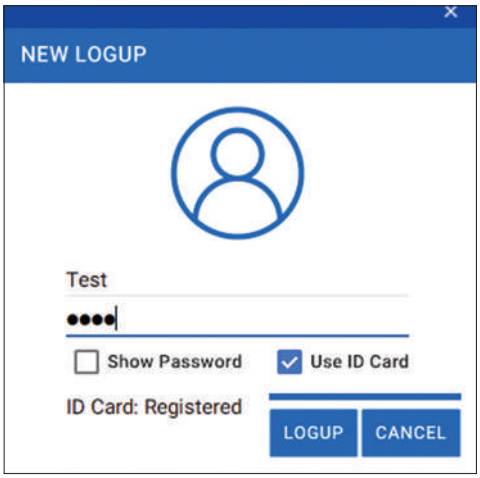

Fig. 20. Create user account.

9.7.7. RFID readers control

In the setting part, we can control all the RFID readers of the system. We decide which RFID reader is work or not. In the case, when any problem occurs in the library, we can control each RFID reader of the system to stop of working or not.

9.7.8. Backup system

The system can back up the database and by default encrypt the data. If we need to backup database without encryption, we can check to decrypt mode for did not encrypt the backup. Fig. 22 shows backup system.

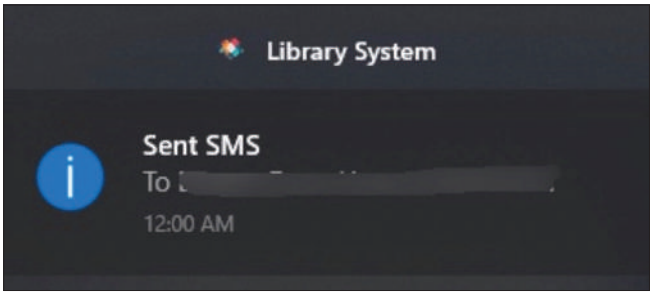

Fig. 21. Send SMS notification.

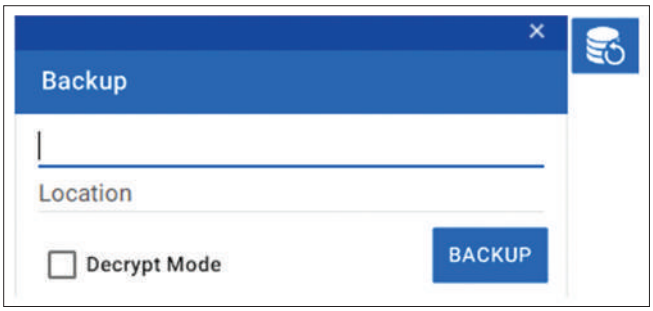

Fig. 22. Backup system.

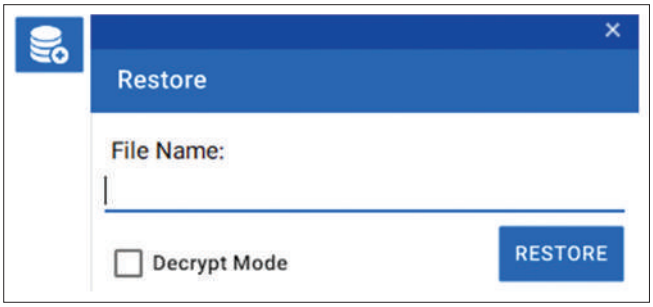

Fig. 23. Restore system.

TABLE 1: Time consumed in borrowing process of references

Borrowing process	Single reference	10 references
Manual system	1/2 min [20]	10 min [20]
Library software	1 min [20]	5 min [20]
RFID system	15 s	2.5 min

9.7.9. Restore system

We can restore the system database by choose file name and check to decrypt mode for decryption the data that we want to display on the system, which is previously encrypted. Restore system shown in Fig. 23.

10. RESULTS AND DISCUSSION

We have proposed an IoT library system using RFID and GSM technologies. This system can manage all RFID readers connected to it and detect any reference, by its RIF tag, in any position inside the library. No references without permission cab are taken outside the library. Also inside the library, references can be moved according to their category, for example, a read-only reference cannot be moved to outside the specific room. Our system helps librarian in decreasing time needed to rearrange references and also in monitoring the movement of references. Also uses can borrow references without need any librarian help, but this feature is limited to those references allowed to be borrowed outside the library. The time spent for particular reference and 10 references in others system such as manual system and library software system will describe in Table 1, also the time spent in RFID system will test. In Table 1, we find that use RFID system in library will decrease time consumed of borrowing process comparing with the other systems.

11. CONCLUSION

The smart IoT technology in libraries is in the initial stage and currently evolving, therefore, there is a need for librarians to be trained in this technology while the IoT technology is more accepted, adopted, and available easily. RFID technology is used for tracing the references location, store, and fetch information rapidly. Implementation RFID in libraries has been discussed. All the processes such as issuing, reissuing returning references, references searching processes, and finds a misplaced reference position can be done quickly using RFID in library. References are now more easily traceable; enhance using of resources, and renewing of manual reference keeping. The main advantages of implementation of RFID-based LMS are a line of sight which is not mandatory, reduces manual intervention, reduces manual errors, and accesses to references faster. RFID-based LMS would increase the speed of operation as issuing, returning back, and retrieve references information. In this paper, the

references search and location system on the library shelf are studied and designed. The hardware is designed in a new design that used for university library system. The test results of the system are demonstrated. The results show that the design of the system based on RFID can achieve easily reference searching and positioning function, and the system has a user-friendly interface. Moreover, to a certain extent, the system can help the librarian in management.

REFERENCES

[1] H. Ahmad. "Rfid technology in libraries : A case study of allama iqbal library, university of Kashmir". *Journal of Indian Library Association*, vol. 52, no. 4, pp. 109-119, 2016.

[2] A. C. Polycarpou, T. Samaras and J. N. Sahalos. *An RFID-based Library Management System Using Smart Cabinets : A Pilot Project*. The 8th European Conference on Antennas and Propagation, United States, pp. 2-4, 2014.

[3] Balasaheb, S. B. Raju, S. S. Rajabhau, A. B. Patil and P. A. Venencia. "Performance of Rfid technology at KS Goa state central library: A case study". *Studies in Indian Place Names*, vol. 40, no. 49, pp. 622-634, 2020.

[4] J. L. Liu and L. Zhu. "Library Intelligent Bookshelf Positioning System Research." In: *4th International Conference on Mechatronics, Materials, Chemistry and Computer Engineering*, Atlantis Press, Thailand, pp. 1237-1242, 2015.

[5] Y. Liu, "Design and Implementation of a Library Management System Based on RFID". In: *The 2015 International Conference on Software Engineering and Information Technology*, Indiana State University, Indiana, USA, pp. 2-4, 2016.

[6] V. Sivasankar, E. Soundararajan, and S. Rajeswari. "Challenges and impacts of RFID technology in a research library". In: *Advances in Communication Systems and Networks*, Springer, Berlin, Germany, 2020.

[7] M. Dhanalakshmi and U. Mamatha. "RFID Based Library Management System". pp. *International Journal of Innovative Research in Advanced Engineering*, vol. 1, no. 2, pp. 227-234, 2009.

[8] B. T. Venkatesh and J. Priya. "RFID: The big player in the libraries of the future". *The Electronic Library*, vol. 29, no. 1, pp. 36-51, 2011.

[9] W. M. Shamsudin, T. M. Win and M.J.E Salami. "*RFID-Based Intelligent Books*". IEEE Xplore, United States, 2007.

[10] M. Tajabadi and S. V. Azhari. "*A Hybrid Privacy-preserving Mutual Authentication Protocol for RFID Traffic Management*". ICEE, United States, pp. 1889-1894, 2019.

[11] G. Sethi and A. Dharani. "Challenges of radio frequency identification technique". *Asset Works*, vol. 3, no. 11, pp. 51-55, 2012.

[12] M. N. Mohammed, W. Muhamad, A. Wan, M. A. M. Ali, O. I. Al-Sanjary, and L. Raya. "Study on RFID based book tracking and library information system". In: *2019 IEEE 15th International Colloquium on Signal Processing and Its Applications*, IEEE, Malaysia, pp. 235-238, 2019.

[13] G. Ramu and Z. Mishra. "Hardware implementation of piccolo encryption algorithm for constrained RFID application". In: *2019 9th Annual Information Technology, Electromechanical Engineering and Microelectronics Conference*, IEEE, India, pp. 85-89, 2019.

[14] V. Pujari and B. Gadgay. "Smart library system using IoT". *International Journal for Research in Applied Science and Engineering Technology*, vol. 6, no. 7, pp. 471-476, 2018.

[15] M. Mohammadi, M. Yegane, C. Library and Q. Branch. "IOT : Applied new technology in academic libraries". In: *International Conference on Distributed Computing and High Performance Computing (DCHP 2018) 25th-27th November, 2018*, *Qom*, At University of Qom, Qom, pp. 1-12, 2018.

[16] A. K. Sharma. "Implementation of Rfid Technology in Library: A case study in UPES library". *Library Philosophy and Practice (E-Journal)*, vol. 7, pp. 70-79, 2017.

[17] L. Philosophy, R. S. Kumar and K. Kaliyaperumal. "Applications of GSM technology for documents identification in a library system". *International Journal of Academic Library and Information Science*, vol. 2, no. 1, pp. 1-6, 2016.

[18] H. Sun and K. Chen. "A proposed model for library stacks management". *Library Collections Acquisitions and Technical Services*, vol. 36, no. 1-2, pp. 24-29, 2012.

[19] L. Li. "Designing and Implementation of University Library Automatic Management System," In: *Pervasive Computing and the Networked World*, International Conference, ICPCA-SWS, Istanbul, Turkey, pp. 241-247, 2014.

[20] N. Singh. "*Deploying RFID Techniology in Management of Library Activities-a Case Study of College Library*". Tamil Nadu Agricultural University, Tamil Nadu, pp. 331-334, 2013.

ORIGINAL RESEARCH ARTICLE UHD JOURNAL OF SCIENCE AND TECHNOLOGY

Review Research of Medical Image Analysis Using Deep Learning

Bakhtyar Ahmed Mohammed[1,2], **Muzhir Shaban Al-Ani**[1]

[1]University of Human Development, College of Science and Technology, Department of Computer Science, Sulaymaniyah, KRG, Iraq, [2]University of Sulaimani, College of Science, Department of Computer, Sulaymaniyah, KRG, Iraq

ABSTRACT

In modern globe, medical image analysis significantly participates in diagnosis process. In general, it involves five processes, such as medical image classification, medical image detection, medical image segmentation, medical image registration, and medical image localization. Medical imaging uses in diagnosis process for most of the human body organs, such as brain tumor, chest, breast, colonoscopy, retinal, and many other cases relate to medical image analysis using various modalities. Multi-modality images include magnetic resonance imaging, single photon emission computed tomography (CT), positron emission tomography, optical coherence tomography, confocal laser endoscopy, magnetic resonance spectroscopy, CT, X-ray, wireless capsule endoscopy, breast cancer, papanicolaou smear, hyper spectral image, and ultrasound use to diagnose different body organs and cases. Medical image analysis is appropriate environment to interact with automate intelligent system technologies. Among the intelligent systems deep learning (DL) is the modern one to manipulate medical image analysis processes and processing an image into fundamental components to extract meaningful information. The best model to establish its systems is deep convolutional neural network. This study relied on reviewing of some of these studies because of these reasons; improvements of medical imaging increase demand on automate systems of medical image analysis using DL, in most tested cases, accuracy of intelligent methods especially DL methods higher than accuracy of hand-crafted works. Furthermore, manually works need a lot of time compare to systematic diagnosis.

Index Terms: Medical Image Analysis, Medical Image Modalities, Deep Learning, Convolutional Neural Network

1. INTRODUCTION

In the recent years, medical imaging has become the most and widest techniques to disease diagnose of human organs and anatomic vision of body. It is a broad range in digital image processing known for its effective, easiness, and safety to diagnose and follow-up diseases. Growing of huge multimodality data caused to growing of data analytics especially in medical imaging. The architecture of deep learning (DL) has depended on the neural network that includes layers to feature extraction and classification in medical image processing and includes many methods for different tasks [1]. DL has evolved in many fields such as computer-aided diagnosis (CAD), radiology, and medical image analysis which can include tasks, such as finding shapes, detecting edges, removing noise, counting objects, and calculating statistics for texture analysis or image quality [2].

In such short period, DL has owned of great role in training artificial agents to replace the complicated human manually scientific works at a reasonable time in various fields related to medical image analysis depend on public and private datasets [3]. The organs of human body vary in terms of complexity; thus some organs are more affected by the

Access this article online

DOI: 10.21928/uhdjst.v4n2y2020.pp75-90

E-ISSN: 2521-4217
P-ISSN: 2521-4209

Corresponding author's e-mail: University of Human Development, College of Science and Technology, Department of Computer Science, Sulaymaniyah, KRG, Iraq. E-mail: bakhtyar.mohammed@uhd.edu.iq

Received: 08-04-2020 Accepted: 19-08-2020 Published: 27-08-2020

process of ionization. Hence, it is important to carefully employ medical image modalities with techniques related to medical diagnosing. Furthermore, the accuracy of these modalities is too important at the first step of medical image processing [4]. The accuracy depends on different sensors or medical image devices to take images according to the ray spectrums to the modality types. Many spectrums are used to imaging body modality, some of them have too strong radiation as; gamma, while others have weak radiation to the human body, such; magnetic resonance imaging (MRI) which uses radio frequency (RF) [5]. Deep artificial neural network (Deep ANN) model was innovated in 2009, from the very beginning this branch is developing till now. In the present time, deep neural network types are the strongest machine learning methods to analyze various medical imaging [6]. In general, medical image analysis consists of five processes, such as medical image classification, medical image detection, medical image segmentation, medical image registration, and medical image localization. Furthermore, graphical processing unit (GPU) is imperative hardware part that supports improvement and acceleration of medical imaging analysis processes, such as image segmentation, image registration, and image de-noising, based on various modalities such as X-ray, CT, positron emission tomography (PET), single photon emission computed tomography (SPECT), MRI, functional MRI (fMRI), ultrasound (US), optical imaging, and microscopy images. It enables parallel acceleration medical image processing to work in harmony with DL [7].

DL is rapidly leading to enhance performance in different medical applications [8]. Some important criterions have great role in the development of medical image analysis processes, such as region of interest (ROI) which has great role of early detection and localization, in such processes as predicting the bounding box coordinates of optic disk (OD) to diagnose of glaucoma and diabetic retinopathy diseases using DL methods [9], and colonoscopy diseases such as adenoma detection rate (ADR) using convolutional neural network (CNN) [10]. Within this process, automatic analysis supports with report generation, real-time decision support, such as localization and tracking in cataract surgery using CNN [11]. Large training set is another essential element since DL methods can learn strong image features for volumetric data as 3D images for landmark detection with many good ways to train these datasets [12]. Advancements in machine learning, especially in DL, can learn many medical imaging data features resulting from the processes such as identify, classify, and quantify patterns that aid of hand-crafted processes for medical image modalities using DL methods to automate interpretations [8].

However, medical imaging data includes noise, missing values, and inhomogeneous ROI which cause inaccurate diagnose. ROI provides accurate knowledge that aids clinical decision-making for diagnostics, treatment planning, and accurate feature extraction process cause accurate diagnostic and increases the accuracy [13]. Edge detection is another key process for medical imaging applications that can be used in image segmentation, usually according to homogeneity in the way of two criterions; classification, and detection of all pixels by CNN using filters [14]. CNN method can avail local features and more global contextual features, at the same time; regardless of the different methods adopted in the architecture of CNN [15]. The architecture of CNN capable to change such as used fully connected network FCN instead of CNN method using semantic segmentation to effectively and accurately detect brain tumor in MRI images [16].

Certainly, the advancement of medical image analysis is slower than medical imaging technologies, mostly because of the study of DL for components of medical image analysis and specifically CNN is a big necessity to improve accuracy of methods for components by working on lessens obstacles such as training datasets, and declining error rate.

2. MEDICAL IMAGE MODALITIES

The essentials of data types in medical image processing are medical images. There are various cases according to the body places, organs, and different disease that became physiologists to think of different techniques to show significant features related to the medical cases. Most of the techniques that used in medical imaging rely on visible and non-visible radiations except MRI. These techniques use various body organs based on cases. Multi-variability of these modalities is necessary because of some reasons. The most significant reason is effectiveness of some of these techniques to some specific tasks, such as MRI for brain and CT for lung. Another reason is the impact of ionizing radiation to human body according to impacts of ionizing which damages DNA atom and non-ionizing rays which does not have any side effect to human body organs [5].

MRI uses radiofrequency signals with a powerful magnetic field to produce images of the human tissues. MRI is dominant among other modality types because of its safety and rich information [17]. Usually, it is used in neurology and neurosurgery of brain and spinal. It shows human anatomy in all three planes; axial, sagittal, and coronal. It is used for quantitative analysis for most of the neurological diseases as

brain [18]. Furthermore, it is able to detect streaming blood and secret vascular distortions. In spite MRI takes priority over others because of its characteristics which are superior image quality and ionizing radiation [19].

It is beneficial to process of accuracy enhancement, reduce noise, detection speed improvement, segmentation, and classification [17].

MRI of sub-cortical brain structure automatic and accurate segmentation using CNN to extract prior spatial features and train the methods on most of complicated features to improve accuracy which is effective for the processes, such as pre-operative evaluation, surgical planning, radiotherapy treatment planning, and longitudinal monitoring for disease progression [20]. It provides a wealth of imaging biomarkers for cardiovascular disease care and segmentation of cardiac structures [21]. Furthermore, it provides rich information about the human tissue anatomies so as to earn soft-tissue contrast widely. It is considered as a standard technique [17]. It provides detail and enough information about different tissues inside human body with high contrast and spatial resolution subsequently. It engages broadly to anatomical auxiliary examination of the cerebrum tissues [18]. Bidani *et al.* (2019) showed that MRI is important to diagnose dementia disease by scanning brain MRI which indicates by declining memory [22].

Geok *et al.* (2018) used MRI to brain stem and anterior cingulate cortex to classify migraine and none-migraine data using DL methods [23].

Another application of brain MRI is early detection and classification of multi-class Alzheimer's disease [24]. Suchita *et al.* (2013) showed complexity of MRI brain diagnosis which is challengeable because of variance and complexity of tumors [25]. Padrakhti *et al.* (2019) showed brain MRI useful to age prediction, as brain age estimation [26].

During MRI data acquisition group of 2-D MRI images can represent as 3-D because a lot of frame numbers, like in brain. Many different contrast types of MRI images exist, including axial-T2 cases use to edematous regions and axial-T1 cases use to the healthy tissues and T1-GD uses to determine the tumor borders, cerebrospinal fluid (CSF) uses to edematous regions in fluid-attenuated invasion recovery (FLAIR). There are several types of contrast images such as FLAIR, T2-Weighted MRI (T2), T1-Weighted MRI (T1), and T1-GD gadolinium contrast enhancement [17].

Brain MRI is one of the best imaging techniques employed by researchers to detect the brain tumors in the progression phase as a model for both steps of detection and treatment [27]. It is useful to supply information about location, volume, and level of tumor malignancy [28]. Talo *et al.* (2018) showed that traditionally the radiologists selected MRI to find status of brain abnormality. The analysis of this process was time consumer and hard, to solve this problem, utilized computer-based detection aid accurately and speedy of diagnosis process [29].

Magnetic resonance spectroscopy (MRS) is a specific modality for the evaluation of thyroid nodules in differentiation of benign from malignant thyroid tissues [30]. PET is a type of nuclear medicine images, as scintigraphy technique, it is a common and useful medical imaging technique that is used clinically in the field of oncology, cardiology, and neurology [7]. SPECT can supply actual three-dimension anatomical image using gamma ray [7]. Elastography uses to liver fibrosis, tactile imaging, photo-acoustic imaging thermography, such as passive thermography, and active thermography, tomography, conventional tomography, and computer-assisted tomography [31]. Accurate features of CT images for chest diagnosis, such as ground glass opacity to detect COVID-19 pneumonia cases, made it use in training process in improving computer-aided methods as a fast process, also it aids the clinicians especially in the diagnosis of COVID-19 infection cases [32]. Optical coherence tomography (OCT) uses low coherence light to take two and three-dimension micrometer resolution within optical scattering. It is used to early diagnosis of retinal diseases [33]. OCT images show clearly intensity variances, low-contrast regions, speckle noise, and blood vessels. [34]. Furthermore, retinal image is another modality to measure retinal vessel diameter [35]. Sun *et al.* (2017) used another sensor which is portable fundus camera used for huge datasets of retinal image quality classification which is differ from diabetic retinopathy screening systems, using CNN algorithms [36]. Papanicolaou (PAP) smear is another medical image modality used to identify the cancerous variation of uterine cervix using the learning-based method by segmenting separated PAP-smear image cells [37]. Nguyen *et al.* (2018) tested microscopic image as another type of medical image modality that took from 2D-Hela and PAP-smear datasets [38]. Confocal laser endoscopy (CLE) is another medical image modality type that relied on to diagnose and detect brain tumor for its accuracy and effectiveness in carrying out the automatic diagnosis [39]. It is a type of advanced optical fluorescence technology which undergoing application assessments in brain tumor surgery while most of the images distorted and interpreted

as non-diagnostic images [40]. In gastrointestinal diseases, new medical imaging technique innovated which known as wireless capsule endoscopy (WCE) to record WCE frame images to detect abnormal patterns [41]. It uses to diagnose of gastrointestinal diseases through a sensor which is quite small to swallow and capture every scenes of anatomical parts that pass through them [41]. Dermoscopic image is another useful modality and is dermoscopic images that use to skin lesion [42], [43]. Breast cancer (BrC) image is another type of well-known cancers that rely on such medical image modalities as mammography which known as X-ray of breast, US which is called sonogram [44]. Furthermore, histology images use to determine multi-size and discriminative patches to classify BrC [45]. Masood *et al.* (2012) determined fine-needle aspiration (FNA) data as another way to take breast sample [46]. M. hyper-spectral image (HSI) is another new modality use to diagnosis and early detection of oral cancer using CNN before surgery [47]. Dey *et al.* (2018) used it to early detect of oral cancer in habitual smokers [39]. N. Single X-ray projection uses to monitoring and radiotherapy tumor-tracking to analyze tumor motion [48].

3. MEDICAL IMAGE ANALYSIS

It is the process of analyzing medical images through medical image analysis techniques. These techniques are composed of five main components named, medical image classification, medical image detection, medical image segmentation, medical image localization, and medical image registration.

3.1. Medical Image Classification

This element of medical image analysis techniques is responsible for classifying labeled image classes based on their features. In this process, the homogeneity and heterogeneity features determine how the classes are categorized. In traditional methods, shape, color, and texture used to be key features for categorizing labeled image classes. Whereas, in modern methods, where DL is essential for labeling images, various algorithms have become fundamental tools for accurate multi-class label classification [49]. Categorization process is a technique that follows extraction process. It runs on selected features [27].

Litjens *et al.* (2017) departed classification process into two phases; either image classification and object or lesion classification. Image classification is the first medical image analysis process that depart the image into some smaller image sizes, but object classification works on the small data that identified earlier [50]. Suchita *et al.* (2013) identified different objects in the image as the main function of classification technique. Hence, she classified images into two main subdivisions; supervised; and unsupervised [25].

In supervised learning, datasets are the most significant reasons to teach the methods and increase accuracy through feature extraction process [22].

Wong *et al.* (2018) showed that MRI brain images are used to diagnose tumors and classify them according to classes as, no tumor, low grade gliomas, and glioblastomas. Those classes can also be subdivided as in gliomas which are classified to I and IV according to the World Health Organization classification [51].

Image quality determines the class of the examined images. Low image quality is considered inappropriate for diagnosis [52].

It is worth mentioning that some researchers use synonyms for classification, such as CADx. Among them, Ker *et al.* (2017) employed different terms to represent various CNN algorithms [53].

Rani (2011) explained data mining can be performed in many ways, all techniques are important in special manners and classification is an analysis technique used to retrieve important and relevant information about data. It can be applied as micro-classifications in mammograms, classification of chest X-rays, and tissue and vessel classification in MRI. When this technique in DL counts on CNN, it can come up with valuable benefits translated as proper working in noisy environments [54].

Suzuki (2017) compared between Massive Training Artificial Neural Network (MTANN) and CNN models. They are used to classifying lung nodules and non-nodules. Each has advantages that distinguish it from the other. For instance, in classification of lesions and non-lesions in CAD, MTANN scored a better result of decreasing False Positives. On the other hand, CNN is able to score higher accuracy level within areas under the ROC curve (areas under curve). For example, if MTANN manages to score 0.882 for lung nodules under ROI, then CNN will score 0.888 for seven tooth types under the same circumstances in computer vision [1].

Yamashita *et al.* (2018) explained that CAD has become a part of routine clinical work for detecting brain, breast, eye, chest, etc. For each organ, this classification process plays special role. For brain, CAD applies fMRI in two stages to detect autism spectrum disorder (ASD). During the first stage, CAD

will identify the bio markers for ASD. While in the second stage, in two subdivision steps, CAD depends on fMRI with accuracy of 70% to identify the anatomical structure.

Certainly, CNN can be used as a magic tool for classification. Another advantage for CNN in this regard is using it for processing target objects separated from medical images. However, it is not deniable that this process requires a large number of training data [55].

Ruvalcaba-Cardenas *et al.* (2018) tested that 2D-CNN 3D-CNN models are well used for small class separation using single-photon avalanche diode sensor in low-light indoor and outdoor daytime conditions as long as using noise removal algorithm with 64 X 64-pixel resolution [56].

The process of identifying labels and lesions types requires a lot of sufficiency work specially to determine early treatment [14]. The whole chain process extracts the features of microscopic image classification [38]. Table 1 illustrates some important reviews of classification process.

3.2. Medical Image Detection

Finding abnormal objects are the main goal of medical Image Detection. Usually, detecting the abnormality happens through comparing two cases on the images. Most of the time, this process takes place with the aid of computer-aided detection (CAD). This starts with identifying objects on the images through the application of detector algorithms [16]. To reduce time consumption and reach efficient detection, experts have dedicated time and efforts to find faster and accurate methods. Marginal space learning is one of the significant approaches in which more efficient and faster in function compare to traditional methods [3]. The function of CAD in this process is to de-stress the radiologists who use manual diagnosis by easily selecting the abnormality on the images. From this standpoint, CAD can take different forms based on its function. The forms are, detection regions aid of processing techniques, set of extracted features, and extracted features fed in to classifier [8]. Diagnosing brain tumor through automatic detection may face difficulties that require smart intervention [64].

Actually, MRI is multi used for diagnoses for other diseases. Alkadi *et al.* (2018) used it for prostate cancer diagnosis to provide information on, location, volume, and level of malignancy [28].

The good thing about automated diagnosis for all medical imaging fields is the attempt to increase accuracy and reduces time consumption [65]. In neurodegenerative diseases, dementia for instance which causes of lessens in memory, language, and lack of wise [22]. That can boost the performance of CNN and improve detection and localization accuracy [41]. For super-pixel image analysis, different structure detection required. This engages image augmentation to aid CNN to extract the features from the original dermoscopy image data [43].

The role of detection lies in identifying abnormal among normal cases. The whole process is called CNN-based CAD system. Ker *et al.* (2017) employed computer aided in collaboration with 2D and 3D-CNN detection for various detection purposes, especially it used for lymph node detection to diagnose infection or tumor [53]. Tajbakhsh *et al.* (2016) shaded the light on detection process which is a complicate process. He divided into two stages, polyp detection, which works on increasing the rate of misdetection by finding perception changing features such as, color, shape, and size of colon features. However, the feature of shape is more affective compare to other features. Moreover, pulmonary embolism (PE) detection, which causes of blocking pulmonary arteries because blood clots that barrier transmit blood from lower extremity source to lung using CT pulmonary angiography (CTPA) which is time consuming, and death rate of PE is 30% but it becomes 2% with right treatment with implementing the deep CNN method [52].

The advantages and disadvantages of each practical technique lie in its outcome balance between accuracy and cost of operation in edge detection. Laplacian of Gaussian edge detector, convolve image by filter of high pass filter to find edge pixels so as to analyze edge pixel places from both sides. Canny edge detector which considers optimal edge detector so as to get the lowest error rate in the detection of real edge point and 2D Gabor filter which its utilization rely on frequency and orientation representations [35]. It is agreed that CAD works on ROI in image analysis. Meaning that, detection gathers the regions of interest in one limited area. This is can be seen in MRI of brain tumor, and it determines earliest signs of abnormality. Altaf *et al.* (2019) used 3D CNN to detect BrC using automated breast US image modality using sliding window technique to extract volume of interests, then using 3D-CNN to determine the possibility of existing tumor [59].

Experts and technology development have been working hard in this field to make medical image analysis more sufficient and fruitful. The attention of experts is not limited to software only, but hardware section is also

TABLE 1: Mentions the classification methods for different body organs

Author	Type of application	Method	Modality	Used dataset	Accuracy	Advantage
Mohsen *et al.* [27]	Brain Classification	Deep Neural Network (DNN)	Brain MRI	66 private MRI	96.97%	DNN more accurate than; KNN, LDA, and SMO
Suchita *et al.* [25]	Brain Classification	ANN	brain MRI	70 MRI	98.60%	Object identification
Tajbaksh *et al.* [52]	Colonoscopy Frame Classification	Deep CNN	Colonoscopy frame images	6-colonoscopy videos; 4000 frames from ImageNet	Reduced FP by 10%, 15%, and 20%	Improved CNN method
Ahn *et al.* [57]	Skin Disease Classification	Convolutional sparse kernel network (CSKN)	X-ray, and dermoscopy images	IRMA, and ISIC 2017	95.30%	supervised CSKN classification higher than others
Ker *et al.* [53]	Classification	CNN	Multimodality	Partitioned different public dataset	Different	Compared between them
Yuqian *et al.* [45]	Breast Cancer Classification	CNN	Histology images	Breast Histology dataset	88.89%	image-wise classification
Rani [54]	Classification	ANN	Multilayer heart disease images	heart disease dataset	94%	Shows advantages of CNN
Wu *et al.* [58]	Face Skin Classification	different CNN algorithms	Clinical facial images	Xiangya-Derm	Best accuracy is 92.9%	Compared between of; ResNet-50, Inception-V3, and DenseNet-121
Suzuki [1]	Classification	MTANN	Lung nodule images	76 malignant and 413 benign	88.20%	accuracy of CNN is higher than MTANN
Altaf *et al.* [59]	Brain, breast, Diabetic Retinopathy, Chest, Abdomen, and Miscellaneous Classification	KSO, AlexNet, CNN, 3D DenseNet (3D CNN), GANs, and CNN	fMRI, mammogram, retinopathy, CT, and CT liver	Multiple datasets, 1713 of Carolina breast cancer study, MESSIDOR, public; LIDC-IDRI	68.6-85.6%, 94-95%, 90.4, and 7% improved	robust results for neurological function of biomarkers
Yamashita *et al.* [55]	Binary Classification	2D and 3D CNN	CT/MRI	Mentioned various public datasets	----	Showed importance of training dataset
Khaled *et al.* [17]	Brain tumor Classification	DL with traditional ML	Brain MRI	Mentioned many datasets	Max accuracy is 100%	----
Muthu *et al.* [18]	Classification	CNN	Brain MRI in DICOM format	Public datasets	100%	training CNN
Shahin *et al.* [42]	Skin lesion Classification	Deep NN framework	RGB dermoscopic JPEG image	ISIC 2018	up to 89.9%	Differentiate between seven skin lesion types
Nguyen *et al.* [38]	Deep learning	Proposed feature concatenation network	Microscopic image	917 images of PAP-smear, and 862 2D-HELA	92.63±1.68%, 92.57±2.46%	----
Kopoulos *et al.* [43]	Dermoscopy Image super pixel Classification	CNN	RGB dermoscopic JPEG image	ISIC	85.2%	used some beneficial filtering techniques
Murtaza *et al.* [44]	Breast cancer classification	Deep Neural Network (DNN)	Mammography	55% used public and others private	----	assess BrC classification
Ken *et al.* [51]	Brain tumor Classification, and cardiac classification	pre-trained CNNs, and VGGNet	Brain MRI, and 2D cardiac CTA	191 testing and 91 training, and 263 testing and 108 training	82%, and 86%	classify according to tumor stages and grades from magnetization
Sun *et al.* [36]	Retinal fundus image quality feature Classification	hybrid CNN	Retinal fundus image	Kaggle	97.12%	used AlexNet, Google Net, VGG-16, and ResNet-50.
Hosny *et al.* [60]	Skin lesion Classification	AlexNet transfer learning	Dermoscopic image	Derm; IS and Quest, MED-NODE, ISIC	96.86%, 97.7%, 95.91%	angle rotation with GPU
Bidani *et al.* [22]	Classification	DCNN	Brain MRI	OASIS	>80%	Indicates importance of dataset
Arevalo *et al.* [61]	Mammography mass lesion Classification	supervised CNN3	Mammography film images	BCDR-FO3	86%	compared between baseline and learned methods

(*Contd...*)

TABLE 1: (*Continued*)

Author	Type of application	Method	Modality	Used dataset	Accuracy	Advantage
Daysi *et al.* [56]	Classification	2D and 3D-CNN	SPAD image	SPAD dataset	95%	3D accuracy higher than 2D
Fauzi *et al.* [62]	brain Classification	SVM and Radiant Basics function (RBF)	T2 MRI	60 original patients	65%	Linearly combine different groups
Litjens *et al.* [50]	Classification	CNN	MRI/CT	public	----	Classified according to; Image/Exam, and Object or lesion classification
Talo *et al.* [29]	Classification	ResNet-34	MRI	5-fold of 613 images	100%	Abnormality brain detection
Geok *et al.* [23]	Classification	3D-CNN	MRI migraine	198 MR images	85%	Deep learning methods more accurate
Islam and Yanqing [24]	Multi-classification	Google Net	Brain MRI	OASIS	73.75%	Accuracy of Google Net higher than Inception
Rajan *et al.* [47]	Oral cancer classification	Partitioned CNN	Hyperspectral medical image	500 trained patterns	94.50%	Compared with conventional methods
Sajedi *et al.* [26]	Age prediction Classification	2D and 3D CNN	Brain MRI	Used many datasets	----	Show age via MRI
Hamad *et al.* [63]	Classification	hybrid	Colon endoscopy image	Mentioned some datasets	96.70%	----
Dey *et al.* [39]	Oral cancer recurrence Classification	ANN, SVM, KNN, and PNN	Confocal Laser Endoscopy (CLE)	Oral Squamous Cell Carcinoma (OSCC) DIC and PAP datasets	86%	Any task needs specific method

receiving a good share of care. Every now and then, CAD is witnessing development in one way or another. Every trail to the purposes of reduces the errors and increases the accuracy [66]. Table 2 illustrates some important reviews of detection process.

3.3. Medical Image Segmentation

It is the process of analyzing a digital image to partitioning it into multiple regions. The main purpose of segmentation is to shade lights on objects detected on the image [68]. In another definition, medical image segmentation is the process of selecting anatomy body organ outlines accurately [3].

From the given definitions, we realize that segmentation is a complicate process. Therefore, researchers have been working on developing procedures to make it easier [15]. To accelerate different applications of automated segmentation process, pre-operative assessment, surgical planning, radiotherapy treatment planning, and longitudinal monitoring are added to the process [20]. Improvement of medical image segmentation can happen in many manners. To improve the physical support of this process, GPU is the key answer to do so [7]. Segmentation is either semantic or non-semantic. Semantic segmentation links each pixel in an image to a class label, whereas, non-semantic segmentation works on the similar shapes, such as clusters [51].

In segmentation process, the methods are changeable. Yet, the quality of the process will change accordingly. In medical image segmentation, MRI plays significant role in quantity image analysis [16].

Through MRI, the image is cut into many regions sharing similar attributes [6]. Dividing the images into ROI means that the image is divided to sections including objects, adjacent regions, and similar region pixels [13]. Through the application of CNN models, brain tumor tissues will be ready to labeling any small patch around each point. The labeling process will highlight intensity information inserted by multi-channel CNN methods [69].

Certainly, a successful segmentation requires detecting object boundaries. This process is called edge detection. By looking at the name, it indicates that the process involves many other factors that affect the edge shapes including geometrical and optical properties, separation conditions, and noise, in addition use for feature detection and texture analysis [14]. Within all this complicity, CNN will be able to diagnose brain tumor through MRI and automatic segmentation simplifies [64]. Like other medical image analysis techniques, segmentation is also a process of stages. Segmentation is either organ segmentation, or lesion segmentation. The role of organ segmentation is to analyze quantity such

TABLE 2: Mentions the detection methods for different body organs

Author	Type of application	Method	Modality	Used dataset	Accuracy	Advantage
Mair *et al.* [3]	Detection	deep reinforcement learning	CT	----	----	Detected via marginal space learning
Shen *et al.* [8]	Detection	Deep learning (CNN)	Multi-modality	Mentioned a lot	Varies	Extracted morphological digital information
Ouseph and Shruti [64]	Tumor Detection	CNN	MRI	Private MRI dataset of tumorous patients	89.21%	Reduced operators and errors
Alkadi *et al.* [28]	Prostate Cancer Detection	Deep convolutional encoder-decoder	T2 MRI	19 patients from public (12 CVB)	89.40%	Used 3D Sliding window
Srivastava *et al.* [65]	Detection	Deep CNN and transfer learning	Gastrointestinal, and brain MRI	464 high resolution images (WSLs) and OASIS	97.6%, and >80%	Detected dementia disease
Lan *et al.* [41]	WCE abnormal pattern Detection	Two types of hybrid methods using CNN	WCE	WCE2017	70%	Got better accuracy
Kopoulos *et al.* [43]	Detection	CNN	RGB dermoscopy image	ISIC	85.2%	Exhibited different filters are necessary to augmentation
Litjens *et al.* [50]	Detection	Deep learning (CNN)	MRI/CT	Public	----	Detection process involved localization and detection
Yamashita *et al.* [55]	Pulmonary tuberculosis detection on chest	AlexNet and Google Net in 2D CNN	Radiographs (X-ray)	1007 chest radiographs	99%	Detected chest pulmonary tuberculosis
Ker *et al.* [53]	Detection	Google Net fine-tuned	CT lymph node	ILSVRC 2013	95%	----
Tajbaksh *et al.* [52]	Colonic Polyp, and Pulmonary Embolism Detection	AlexNet, and AlexNet	Colonoscopy, and lung CTPA	40 short colonoscopy videos to frames	P<0.05, %25, %50,	Decreased the rate of misdetection by; 4%, 12%, 25%, 10%, 50%
Masood *et al.* [46]	Breast cancer detection Type I, and Type II	CGPANN	Fine-needle aspiration (FNA)	WDBC database, 200 images for each case	99%, and 99.5%	Used FNA to feature extract
Suzuki [1]	Lymph node detection	MTANN and CNN	CT	----	----	MTANN used to enhance lesion detection
Morariu *et al.* [35]	Vessels Detection	LoG, C, G filters	Retinopathy image	18 healthy patient image, and 12 retinopathy images	varied	Trade-off between the processes of accuracy and cost
Altaf *et al.* [59]	Brain, Breast, Eye, Chest, Abdomen, Miscellaneous Detection	Inception-V4 and ResNet, 3D CNN, VGG-16, CNN	MRI, ABUS, OCT, CMR, WGD, and inner ear CT	OASIS, 171 tumors, ImageNet, 8428	99%, >95%, 98.6%, 98%, 98.51%	Used various; methods, datasets, modalities with different accuracies
Summer *et al.* [66]	Lung nodules, and Polyp Detection	Deep learning (CNN)	X-Ray and CT	MICCAI	----	Automated disease detection and organ and lesion detections
Carneiro *et al.* [67]	Detection	Deep learning (CNN)	X-ray, CT, MRI, and microscopy	mentioned some public datasets	----	Indicated performance of each technique

as volume and shape segmentation in clinical parameters. While lesion segmentation, combines object detection, organ, and substructure segmentation, and apply them in DL algorithms [50].

The outer look of segmentation is similar to quantitative assessment of medical meaningful pieces. Actually, in some functions segmentation depends on quantitative assessment for its application within a short period of time [55]. In surgical planning, segmentation is applied on 2D image slices to determine accurate boundary of the lesions to prepare them to the operation [53]. Medical image segmentation is either automatic or semi-automatic. Both work on extracting ROI, but for different body organs such as coronary angiograms, surgical planning, surgery simulations, tumor segmentation, and brain segmentation [70].

It separates and bounds different components of body organs automatically or semi-automatically to different tissue classes, pathologies, organs, and some biological criterions, according to various body organs [69]. In short, segmentation process aims to solve problems appears on regions of body organs such as brain, skin, and so on. For this purpose, medical image uses MRI, and CT to select optimal weights [71]. Another important process for medical imaging applications is edge detection which use in image segmentation usually according to homogeneity in the way of two criterions; classification, and detection of all pixels by CNN using filters [14].

Hamad *et al.* (2018) focused on pathology image segmentation as pre-requisite disease diagnosis to determine features, such as shape, size, and morphological appearances, for cancer of nuclei, glands, and lymphocytes [63]. Dey *et al.* (2018) shaded the lights on the three subdivisions of segmentation naming them, Otsu, to calculate quality of global threshold, Gradient Vector Flow Active Contour Method, to analyze dynamic or 3D image data [39].

Image quality has impact on segmentation process for it has to do with feature extraction, model matching, and object recognition [72]. Rupal *et al.* (2018) determined three soft tissues in normal brain using MRI technique, such as gray matter (GM), white matter, and CSF. He showed both of algorithms and GPU has a big role to speed up this process, with its many methods innovated to enhance the segmentation process [73].

Despite the factors that impact segmentation process, there are other reasons that enhance segmentation such as organs of body, modality image, and algorithm. On the other hand, segmentation faces challenges that hold the process back such as large variability in sensing modality, artifacts which vary from organ to organ, etc. Ngo *et al.* (2017) classified segmentation to active contour models, machine learning models, and hybrid active contour and machine learning models [74]. Table 3 illustrates some important reviews of segmentation process.

3.4. Medical Image Localization

Every method has different contour to select the location of the destination shapes from images, Wei *et al.* (2019) studied tumor localization on 3D images of three patients depending on; contour, location of tumor centroid in 3D space, and the angle of tumors to find error of tumor localization at different angles. The results showed that according to tumor motion and projection angles which exhibits that the CNN based method was more robust and accurate in real-time tumor localization [48].

Lan *et al.* (2019) explored that multiregional combination such as selective search, edge boxes, and abjectness is used to improve object localization that account as essential of the non-rigid and amorphous characteristics to improve object localization [41].

Urban *et al.* (2018) showed ADR aim of colonoscopy and accuracy according of colonoscopies for ADR. Advancements of computer-assisted image analysis especially DL models, such as CNNs which aid of making agent to perform its tasks to improve performance. It exhibits any increasing point of accuracy in manually work, as the result shows that real-time localized polyps and detection polyps higher than hand-crafted work [10].

Muthu *et al.* (2019) verified that appropriate hardware is beneficial of adequately localize brain tumor to achieve high accuracy of detection and classification using CNN [18].

Localization uses in every steps of applications while the radiology systems individually analyze and prepare reports without any human intrusion, especially in MRI and CT modality using CNN, such as CT images of neck, lung, liver, pelvis, and legs [53].

Mitra *et al.* (2018) improved localization process using OD in color retinal fundus images predicting the bounding box coordinates which work same as ROI. Some methods used to renew the frames of ROI as solitary regression predicament of image pixel values to ROI coordinates. CNN can predict bounding boxes depending on intersection of the union. It increases the chance of recovery and strengthens the detection diagnosis accuracy [9].

Oliver *et al.* (2018) proposed localizing multiple landmarks in medical image analysis to easily transfer our framework to new applications. It integrated various localizers, low test application algorithms, low amount of training data algorithms, and interoperability. The pros of this approach is detecting and localizing spatially correlated point landmarks [78].

Localization process usually comes before the detection process. Almost they are integrated together, especially in misdetection which relies on localization process [59].

Zheng *et al.* (2017) divided localization process into two steps, in the first process the abdomen area is selecting, while the

TABLE 3: Mentions the segmentation methods for different body organs

Author	Type of application	Method	Modality	Used dataset	Accuracy	Advantage
Mair *et al.* [3]	Segmentation	CNN	MRI Cardiac	----	----	Selected anatomy body organ accurately
Havaei *et al.* [15]	Segmentation	CNN	MRI brain	BRATS 2013	----	Accelerated segmentation process
Kushibar *et al.* [20]	Segmentation	CNN	Sub-cortical brain	Public MICCAI 2012 and IBSR-18	----	Increased segmentation accuracy
Eklund *et al.* [7]	General Image Segmentation	CNN	Multiple modalities	Big datasets	----	Faster than other methods
Ken *et al.* [51]	Semantic Segmentation	Deep learning	Brain	43 3D images	----	Exhibited it can track brain tumor
Kumar *et al.* [16]	Semantic Segmentation	DL and ML	MRI brain	Dataset of 15 cases	96%	Improved detection of MRI brain tumor
Selvikvag *et al.* [6]	Segmentation	Deep learning (CNN)	MRI	----	----	Quantitatively analyze images
Berahim *et al.* [13]	Segmentation	Morphological LS, RG-LS	Multimodality	Both	0.03% improved	Segmented primary boundary accurately
Zikic *et al.* [69]	Segmentation	CNN	Brain tumor	BRATS 2013-2014	83.7±9.4	Enhanced network architecture
Shen *et al.* [8]	Segmentation	3D CNN	3D brain MRI	Mentioned a lot of datasets	Different accuracies	Used to skull extraction
Mohamed *et al.* [14]	Segmentation	CNN	----	International datasets	----	Beneficial to edge detections to detect edge boundaries
Ouseph and Shruti [64]	Brain tumor Segmentation	CNN	Brain MRI	Private MRI from cancerous patients	89.21%	Improved segmentation level
Litjens *et al.* [50]	Cardiac and brain Segmentation	CNN	CT/MRI	Public	----	Useful for substructure from lesion segmentation
Mohsen *et al.* [27]	Segmentation	Fuzzy c-mean and CNN	Brain MRI	Private dataset of 66 brain MRI	----	Improved progressing process
Yamashita *et al.* [55]	Uterus malignant tumor Segmentation	CNN	MRI	ISBI	----	Quantitative assessment
Ker *et al.* [53]	Tumor Segmentation	3D CNN	Brain	22 pre-term, 35 adults	82-87%	Assisted surgical planning
Sajedi *et al.* [26]	Segmentation	Multiple methods	Brain MRI	OASIS	----	Useful to age prediction
Tajbaksh *et al.* [52]	Intima-Media Boundary Segmentation	Carotid AlexNet (CIMT)	Cardiac image	121 CTPA datasets with 326 PEs	$P < 0.0001$ segmentation error	Used to intima-media boundary (CIMT) risk stratification
Nourouzi *et al.* [70]	Knee bone Segmentation	Multi-method	MRI	----	----	Classified segmentation process according to types
Bernal *et al.* [75]	Segmentation	FCNN	Brain MRI	IBSR18, MICCAI2012, and iSeg2017	Improved accuracy by 1%	Compared between 2D and 3D
Suzuki [1]	Segmentation	DL based method	Lung tissue	Different dataset	82-95%	Neural edge enhancer
Altaf *et al.* [59]	Brain, breast, eye, chest, abdomen, miscellaneous Segmentation	CompNet (Brain)	Normal MRI image	OASIS	98%	Compared different accuracies
Dey *et al.* [71]	Segmentation	Metaheuristic; GA, PSO, ACO, ABCO	MRI	----	----	Determined suspicious various regions
Hamad *et al.* [63]	Segmentation	NN based method	Pathology	Mentioned a lot of datasets	----	Segmentation improved accuracy

(*Contd...*)

TABLE 3: (*Continued*)

Author	Type of application	Method	Modality	Used dataset	Accuracy	Advantage
Jeylan *et al.* [76]	Mass Segmentation	Kapur-ScPSO and Otsu-PSO	Mammogram	10 benchmark images	----	It assisted detection process
Padmusini *et al.* [72]	Binary retinal vascular Segmentation	OCT	Multiple modalities of retinal images	Mentioned a lot of datasets	96%	Segmenting abnormal images
Rajan *et al.* [47]	Segmentation	Partitioned CNN	Hyper-spectral machine learning	----	94.50%	Showed reasons of segmentation process
Ngo *et al.* [74]	Segmentation	Deep belief networks	Cardiac MRI	MICCAI and JSRT	10 times faster	Selected endocardium
Dhungel *et al.* [77]	Mass Segmentation	CRF, CNN, and DBN	Mammogram	DDSM-BCRP for breast	95%	Indicated obstacles of mammogram mass segmentation
Zheng *et al.* [12]	Pathology kidney Segmentation	MSL	CT	370 CT scans	Mean segmentation error is 2.6	Determined amount of abnormality of chronic kidney disease

second process is detecting and localizing the kidneys places. According to this, the body consists of three parts; above abdomen; head and thorax, abdomen, and legs. Diaphragm separates abdomen and thorax and an optimal slice index maximizing separation between abdomen and legs, second step is kidney which localize same as abdomen detection by axial image to determine the place of kidneys which use surrounding organs to determine the location of kidneys because kidney place is next to liver and spleen but the position of abdomen organs is not fixed, same as abdomen localization [12].

Banerjee *et al.* (2019) designed a framework that consists of CNN methods which implement to enhance the performance of localization, detection, and annotation of surgical tools. The proposed method can learn most of the features [11]. Table 4 illustrates some important reviews of localization process.

3.5. Medical Image Registration

Image registration involves determining a spatial transformation or mapping that relates positions in one image to corresponding positions in one or more other images. Image registration is transformation an image to the same digital image form according to the mapping points. Rigid is known as image coordinate transformation and only involves translation and rotation processes. Transformation maps parallel lines fixed with parallel lines is affine for map lines onto maps is projective and map lines on curves is curved or elastic [72].

The purpose of developing medical image modalities is to get higher resolutions and implementing multi-parametric tissue information at proper accuracy and time. It causes increasing the visually of image registration. Nowadays, it is very common to improve accuracy and speeding up in DL [6]. It involves two forms; mono-modal inside same device or multi-modal inside different devices. In general, it consists of four steps; feature detection, feature matching, transform model estimation, and image resampling and transformation [13]. Registration known as common image analysis task, its form of working is iterative framework. DL can properly increase registration performance and especially using deep regression networks to direct transformation [50]. Ker *et al.* (2017) exhibited that another benefit of medical image registration has indicated in neurosurgery or spinal surgery, to select the place of the mass or destination landmark, and to obtain systematic operation [53].

The most necessity to transmit from source to destination using appropriate method rely on; selecting modality into spatial alignment, and the fusion that is necessary for showing integrated data [72].

Marstal *et al.* created collaborative platform to registration process, as an open source for the medical algorithms which is the continuous registration challenge (CRC) that involves eight common datasets [79].

Ramamoorthy *et al.* (2019) showed that polycystic ovary syndrome is another women disease made from imbalance hormone of follicle stimulating hormone, and monitoring of cysts grow up by registration technique which apply through these steps; first step, is initial registration which inputs pre-processed US images. Second step is similarity measure–implement correlation coefficient on reference and source image. Third step is image transformation which monitors the growth of the cyst at initial stage and periodic checkups. Fourth step is final registration alignment. It

TABLE 4: Mentions the localization methods for different body organs

Author	Type of application	Method	Modality	Used dataset	Accuracy	Advantage
Wei *et al.* [48]	Lung tumor real-time Localization	CNN with MM and MM-FD with PCA	X-ray projection	3D took from three patients	<1 mm	More robust and accurate
Lan *et al.* [41]	Localization	MRC	WCE	WCE 2017	70.30%	Improved object localization and RPN
Urban *et al.* [10]	Polyp Localization	CNN	Colonoscopy images	8641 images	96.4%	Improved accuracy of CNN
Muthu *et al.* [18]	Brain Tumor Localization	CNN	MRI	Private dataset	----	Showed localization is important to detection
Ker *et al.* [53]	Localization	CNN	Axial CT	4000	99.80%	It decreased error rate after augmentation
Mitra *et al.* [9]	Distance metric Localization	Various augmenting techniques used to amplify dataset	Color retinal fundus images	MESSIDOR for test set, and Kaggle	98.78, 99.05%	Coordination bounding box as ROI
Oliver *et al.* [78]	Localization lower limbs, spine, thorax	General framework of CRE topology	X-ray, and CT	2D, 660, 302 public 3D dataset	94.3, and 84.1%	Localized spatially correlated landmarks
Altaf *et al.* [59]	Brain, breast, eye, chest, abdomen, and miscellaneous tumor Localization	Inception-V4 and ResNet, 3D CNN, fine-tuned VGG-16, CNN	MRI, ABUS, OCT, CMR, WGD, and inner ear CT	OASIS, 171 tumors, ImageNet, and 8428	maximum 99%, >95%, 98.6%, 98%, and 98.51%	Used various; methods, datasets, modalities with different accuracies
Zheng *et al.* [12]	Abdomen and kidney Localization	Caffe CNN	CT	370 CT scans	Mean segmentation error 1.7 mm	Used local context to localize kidney
Banerjee *et al.* [11]	Localization	AlexNet, VGGNet, and ResNet-18/50/152	Medical image frame	8 videos from ImageNet dataset	82%	Improved the efficiency of surgical tools
Alkadi *et al.* [28]	Prostate cancer localization	Mono-modal deep learning	T2 MRI	12CVB	89.40%	Showed its importance of treatment planning

TABLE 5: Mentions the registration methods for different body organs

Author	Type of application	Method	Modality	Used dataset	Accuracy	Advantage
Selvikvag *et al.* [6]	Registration	Deep learning and deep neural network	MRI	----	----	Improved accuracy and speed up
Berahim *et al.* [13]	Registration	Mutual information (MI)	Multimodality	----	----	Made mapping point to transform images
Litjens *et al.* [50]	Registration	Deep learning	CT/MRI	Public	----	----
Ker *et al.* [53]	Registration	LDDMM	MRI brain	OASIS	----	Improved the process in computational time
Padmusini *et al.* [72]	Registration	RANSAC method	SDOCT retinal images	----	----	Measured the size of geographic lesions
Marstal *et al.* [79]	Registration	Continuous Registration Challenge (CRC)	Lung CT, and brain MRI	POPI and DIRLAB	----	Appropriately take new datasets
Ramamoorthy *et al.* [80]	Registration	Image Registration techniques	Ultrasound abdomen scan image	Doppler scan, Pandiyan scan, Devaki scan	93.00%	Monitored PCOS using registration during reproductive cycle
Altaf *et al.* [59]	Registration	Deep CNN, FCN	Brain MRI, OCT, CT lung, 3D MRI, and MR-TRUS	ABIDE, DIRLAB, CREATIS	1.5% enhanced	Registered 2D and 3D, and speeded up reconstruction
Maier *et al.* [3]	Deformable registration	Deep learning	----	----	----	Used non-rigid registration, and point-based registration

is either mono-modal image or multi-modal images. Last step is optimization that optimizing the spatial information which is executed by changing affine point optimizer radius at various appointments that determine by gynecologists in addition to correlation coefficient similarly metrics and affine transformation [80].

In addition, registration process goes through the following steps; first is initial registration which feed them preprocessed images, second is similarity measurement in the way of correlation coefficient of reference and source image, third is image transformation which involve monitoring growth of the cyst monitoring at initial stage and periodic check-ups, fourth is final registration, and fifth is optimization [80]. Table 5 illustrates some important reviews of registration process.

4. DISCUSSION AND CONCLUSION

This study is a review over medical image modalities and most significant types. In this regard, the study focuses on medical image analysis and its components using DL. Medical image modalities clearly show how much the techniques or devices are important for medical image processing tasks, especially for medical image analysis. For a better approach, the study demonstrates the tremendous role of modalities that used in medical image processing by mentioning the most common modalities, such as MRI, SPECT, PET, OCT, CLE, MRS, CT, x-ray, WCE, BrC, PAP smear, HSI, and US. Furthermore, it exhibits how the modalities imperative to extract significant features from medical image values. Some significant diseases are reviewed after being diagnosed using some specific modalities. This is too beneficial to motivate to improve these tasks to implement those automatically using different approaches.

In medical image analysis, both medical image analysis and its components are properly introduced. It enumerates the components which are medical image classification, medical image detection, medical image segmentation, medical image localization, and medical image registration and defining them. For the sake of accurate results, the study reviewed some researches performed on each modality in various cases. Localization of anatomical structures is a prerequisite for many tasks in medical image analysis [81]. Medical image segmentation is defined in many ways according to its understanding. In simple words, image segmentation is the process of partitioning medical images into smaller parts [82].

Medical image detection is the process of localizing and detecting such important desired things inside medical imaging as objects detection, edge detection, and boundary detection [83]. Medical image classification is a process of illuminating different cases according to their similar features and selecting classes for them. It plays an essential role in clinical treatment and teaching tasks [84]. There are more than 120 types of brain and central nervous system tumors which classified as to less aggressive, such as benign: Grades I and II, aggressive, such as malignant; Grades III and IV, and the skull [73]. Early diagnosis of tumor has significant role of enhancement in increasing treatment possibilities.

The main aim of this survey study is to discuss about processing of medical image analysis and its components such as medical image classification, medical image detection, medical image segmentation, medical image localization, and medical image registration, depended on DL methods. Especially CNN is dominant model for computer vision which involves, such algorithms as; AlexNet, DenseNet, ResNet-18/34/50/152, VGGNet, Google Net, Inception-V3, pre-trained CNN, hybrid CNN, VGG-16, Inception-V4, fine-tuned VGG-16, carotid AlexNet, Inception-V4, 3D CNN, and Caffe CNN. It shows comparison between some different methods that used many public and private datasets for different medical image analysis components with different accuracies. It created table of medical image analysis components that represent many proposed methods and their process advantages. This approaches used for various human body organs with time progressing, which indicates CNN model algorithms preferred and have optimum accuracies compare to other DL methods for medical imaging. Most of the studies depend on using different medical image modalities and different public and private datasets in their types and sizes. The most accurate one among these approaches was brain MRI using CNN which imply these implemented approach that used to brain tumor were preferred. It looks the strong points, such as working on declining error rate and making strong training dataset for CNN because it is supervised learning method of these approaches and what are the weak points and how DL improved in medical image analysis.

REFERENCES

[1] K. Suzuki. "Overview of deep learning in medical imaging". *Radiological Physics and Technology*, vol. 10, no. 3, pp. 257-273, 2017.

[2] D. Ravi, C. Wong, F. Deligianni, M. Berthelot and J. Andreau-Perez. "Deep learning for health informatics". *IEEE Journal of Biomedical and Health Informatics*, vol. 21, no. 1, pp. 4-21, 2017.

[3] A. Maier, C. Syben, T. Lasser and C. Riess. "A gentle introduction to deep learning in medical image processing". *Zeitschrift für Medizinische Physik*, vol. 29, no. 2, pp. 86-101, 2019.

[4] J. K. Han. Terahertz medical imaging. In: "*Convergence of Terahertz Sciences in Biomedical Systems*". Springer, Netherlands, pp. 351-371, 2012.

[5] J. O'Doherty, B. Rojas-Fisher and S. O'Doherty. "Real-life radioactive men: The advantages and disadvantages of radiation exposure". *Superhero Science and Technology*, vol. 1, no. 1, p.

2928, 2018.

[6] A. S. Lundervold and A. Lundervold. "An overview of deep learning in medical imaging focusing on MRI". *Zeitschrift für Medizinische Physik*, vol. 29, no. 2, pp. 102-127, 2019.

[7] A. Eklund, P. Dufort, D. Forsberg and S. M. LaConte. "Medical image processing on the GPU-past, present and future". *Medical Image Analysis*, vol. 17, no. 8, pp. 1073-1094, 2013.

[8] D. Shen, G. Wu and H. Suk. "Deep learning in medical image analysis". *Review in Advance*, vol. 19, pp. 221-248, 2017.

[9] A. Mitra, P. S. Banerjee, S, Roy, S. Roy and S. K. Setua. "The region of interest localization for glaucoma analysis from retinal fundus image using deep learning". *Computer Methods and Programs in Biomedicine*, vol. 165, pp. 25-35, 2018.

[10] G. Urban, P. Tripathi, T. Alkayali, M. Mittal, F. Jalali, W. Karnes and P. Baldi. "Deep learning localizes and identifies polyps in real time with 96% accuracy in screening colonoscopy". *Gastroenterology*, vol. 155, no. 4, pp. 1069-1078.e8, 2018.

[11] N. Banerjee, R. Sathish and D. Sheet. "Deep neural architecture for localization and tracking of surgical tools in cataract surgery". *Computer Aided Intervention and Diagnostics in Clinical and Medical Images*, vol. 31, pp. 31-38, 2019.

[12] Y. Zheng, D. Liu, B. Georgescu, D. Xu and D. Comaniciu. "*Deep Learning Based Automatic Segmentation of Pathological Kidney in CT: Local Versus Global Image Context*". Springer, Cham, Switzerland, pp. 241-255, 2017.

[13] M. Berahim, N. A. Samsudin and S. S. Nathan. "A review: Image analysis techniques to improve labeling accuracy of medical image classification". *Advances in Intelligent Systems and Computing*, vol. 700, pp. 1-11, 2018.

[14] M. A. El-Sayed, Y. A. Estaitia and M. A. Khafagy. "Automated edge detection using convolutional neural network". *International Journal of Advanced Computer Science and Applications*, vol. 4, no. 10, p. 11, 2013.

[15] M. Havaei, A. Davy, D. Warde-Farley, A. Biard, A. Courville, Y. Bengio, C. Pal, P. M. Jodoin and H. Larochelle. "Brain tumor segmentation with deep neural networks". *Medical Image Analysis*, vol. 35, pp. 18-31, 2017.

[16] S. Kumar, A. Negi, J. N. Singh, H. Verman. "A Deep Learning for Brain Tumor MRI Images Semantic Segmentation using FCN". In: *2018 4th International Conference on Computing Communication and Automation*, Greater Noida, India, India, 14-15 Dec 2018, 2018.

[17] M. K. Abd-Ellah, A. I. Awad, A. A. M. Khalafd and H. F. A. Hamed. "A review on brain tumor diagnosis from MRI images: Practical implications, key achievements, and lessons learned". *Magnetic Resonance Imaging*, vol. 61, pp. 300-318, 2019.

[18] R. P. M. Krishnammal and S. Selvakumar. "Convolutional Neural Network based Image Classification and Detection of Abnormalities in MRI Brain Images". In: *2019 International Conference on Communication and Signal Processing*, Chennai, India, India, 4-6 April, 2019.

[19] H. H. Sultan, N. M. Salem and W. Al-Atabany. "Multi-Classification of Brain Tumor Images Using Deep Neural Network". *IEEE Access*, vol. 1, pp. 1-11, 2019.

[20] K. Kushibar, S. Valverde, S. Gonzalez-Villa, J. Bernal, M. Cabezas, A. Oliver and X. Liado. "Automated sub-cortical brain structure segmentation combining spatial and deep convolutional features". *Medical Image Analysis*, vol. 48, pp. 177-186, 2018.

[21] F. Guo, M. Ng, M. Goubran, S. E. Petersen, S. K. Piechnik, S. N. Bauerd and G. Wright. "Improving cardiac MRI convolutional neural network segmentation on small training datasets and dataset shift: A continuous kernel cut approach". *Medical Image Analysis,* vol. 61, p. 101636, 2020.

[22] A. Bidani, M. S. Gouider and C. M. Traviesco-Gonzalez. "Dementia Detection and Classification from MRI Images Using Deep Neural Networks and Transfer Learning". In: *International Work-Conference on Artificial Neural Networks IWANN 2019*, vol. 11506, pp. 925-933, 2019.

[23] H. N. G. Geok, M. Kerzel, J. Mehnert, A. May and S. Wermter. "Classification of MRI Migraine Medical Data Using 3D Convolutional Neural Network". *ICANN 2018*, vol. 11141, pp. 300-309, 2018.

[24] Z. J. Islam and Y. Yanqing. "A novel deep learning based multi-class classification method for Alzheimer's disease detection using brain MRI data. In: *International Conference*, BI 2017, Beijing, China, November 16-18, 2017, Beijing, China, 2017.

[25] S. Goswami and L. K. P. Bhaiya. "Brain Tumor Detection Using Unsupervised Learning Based Neural Network". In: *2013 International Conference on Communication Systems and Network Technologies*, Gwalior, India, 6-8 April 2013.

[26] H. S. A. Pardakhti. "Age prediction based on brain MRI image: A survey". *Journal of Medical Systems*, vol. 43(8), p. 279, 2019.

[27] H. Mohsen, A. E. S. A. El-Dahshan, E. S. M. El-Horbaty, A. B. M. Salem. "Classification using deep learning neural networks for brain tumors". *Future Computing and Informatics Journal*, vol. 3, no. 1, pp. 68-71, 2018.

[28] R. Alkadi, F. Taher, A. El-Baz and N. Werghi. "A deep learning-based approach for the detection and localization of prostate cancer in T2 magnetic resonance images". *Journal of Digital Imaging*, vol. 32, no. 12, pp. 793-807, 2018.

[29] M. Talo, U. B. Baloglu, O. Yildirim and U. R. Acharya. "Application of deep transfer learning for automated brain abnormality classification using MR images". *Cognitive Systems Research*, vol. 54, pp. 176-188, 2018.

[30] L. Aghaghazvini, P. Pirouzi, H. Sharifian, N. Yazdani, S. Kooraki, A. Ghadiri and M. Assadi. "3T magnetic resonance spectroscopy as a powerful diagnostic modality for assessment of thyroid nodules". *SciELO Analytics*, vol. 62, no. 5, pp. 2359-4292, 2018.

[31] A. Elangovan and T. Jeyaseelan. "Medical Imaging Modalities: A Survey. In: "*2016 International Conference on Emerging Trends in Engineering, Technology and Science*". Pudukkottai, India, 24-26 Feb, 2016.

[32] Y. Song, S. Zheng, L. Li, X. Zhang, X. Zhang, Z. Huang, J. Chen, H. Zhao, Y. Jie, R. Wang, Y. Chong, J. Shen and Y. Yang. "*Deep learning Enables Accurate Diagnosis of Novel Coronavirus* (*COVID-19*) *with CT images*". medRxiv, 2020.

[33] J. Men, Y. Huang, J. Solanki, X. Zeng, A. Alex, J. Jerwick, Z. Zhang, R. E. Tanzi, A. Li and C. Zhou. "Optical coherence tomography for brain imaging and developmental biology". *IEEE Journal of Selected Topics in Quantum Electronics*, vol. 22, no. 4, p. 6803213, 2016.

[34] L. Ngo, G. Yih, S. Ji and J. H. Han. "A Study on Automated Segmentation of Retinal Layers in Optical Coherence Tomography Images. In: *2016 4th International Winter Conference on Brain-Computer Interface* (*BCI*). Yongpyong, South Korea, 22-24 Feb, 2016.

[35] L. Moraru, C. D. Obreja, N. Dey and A. S. Ashour. *Dempster-Shafer Fusion for Effective Retinal Vessels Diameter Measurement*. Elsevier, Amsterdam, Netherlands, pp. 149-160, 2018.

[36] J. Sun, C. Wan, J. Cheng, F. Yu and J. Liu. "Retinal Image Quality

Classification using Fine-Tuned CNN. In: *OMIA 2017, FIFI 2017: Fetal, Infant and Ophthalmic Medical Image Analysis*". vol. 10554. Springer, Berlin, Germany, pp. 126-133, 2017.

[37] Y. Song, J. Z. Cheng, D. Ni, S. Chen, B. Lei and T. Wang. "Segmenting Overlapping Cervical Cell in Pap Smear Images. In: *2016 IEEE 13th International Symposium on Biomedical Imaging* (*ISBI*), Prague, Czech Republic, 13-16 April, 2016.

[38] L. D. Nguyen, D. Lin, Z. Lin and J. Cao. "Deep CNNs for Microscopic Image Classification by Exploiting Transfer Learning and Feature Concatenation. In: *2018 IEEE International Symposium on Circuits and Systems* (*ISCAS*), Florence, Italy, 27-30 May 2018.

[39] S. Dey, D.N. Tibarewala, S. P. Maity and A. Barui. "A*utomated Detection of Early Oral Cancer Trends in Habitual Smokers*. Elsevier, Amsterdam, Netherlands, pp. 83-107, 2018.

[40] M. Izadyyazdanabadi, E. Belykh, M. Mooney, N. Martirosyan, J. Eschbacher, P. Nakaji, M. C. Preul and Y. Yang. "Convolutional neural networks: Ensemble modeling, fine-tuning and unsupervised semantic localization for neurosurgical CLE images". *The Journal of Visual Communication and Image Representation*, vol. 1, pp. 10-20, 2018.

[41] L. Lan, C. Ye, C. Wang and S. Zhou. "Deep convolutional neural networks for WCE abnormality detection: CNN architecture, region proposal and transfer learning". *IEEE Access*, vol. 7, pp. 30017-30032, 2019.

[42] A. H. Shahin, A. Kamal and M. A. Elattar. "Deep Ensemble Learning for Skin Lesion Classification from Dermoscopic Images". In: *2018 9th Cairo International Biomedical Engineering Conference*, Cairo, Egypt, Egypt, 20-22 Dec. 2018.

[43] S. V. Georgakopoulos, K. Kottari, K. Delibasis, V. P. Plagianakos and I. Maglogiannis. "Improving the performance of convolutional neural network for skin image classification using the response of image analysis filters". *Neural Computing and Applications*, vol. 31, no. 6, pp. 1805-1822, 2019.

[44] G. Murtaza, L. Shuib, A. W. A. Wahab, G. Mujtaba, H. F. Nweke, M. A. Al-Garadi, F. Zulfiqar, G. Raza and N. A. Azmi. "Deep learning-based breast cancer classification through medical imaging modalities: State of the art and research challenges". *Artificial Intelligence Review*, 53, pp. 1-66, 2019.

[45] Y. Li, J. Wu and Q. S. Wu. "Classification of breast cancer histology images using multi-size and discriminative patches based on deep learning. *IEEE Access*, vol. 7, pp. 21400-21408, 2019.

[46] A. M. Ahmad, G. Muhammad and J. F. Miller. "Breast Cancer Detection Using Cartesian Genetic Programming evolved Artificial Neural Networks. In: *GECCO '12 Proceedings of the 14th Annual Conference on Genetic and Evolutionary Computation*, Philadelphia, Pennsylvania, USA, July 07-11, 2012.

[47] P. R. Jeyaraj E. R. S. Nadar. "Computer-assisted medical image classification for early diagnosis of oral cancer employing deep learning algorithm". *Journal of Cancer Research and Clinical Oncology*, vol. 145, no. 4, pp. 829-837, 2019.

[48] R. Wei, F. Zhou, B. Liu, X. Bai, D. Fu, Y. Li and B. Liang. "Convolutional neural network (CNN) based three dimensional tumor localization using single X-ray projection". *IEEE Access*, vol. 7, pp. 37026-37038, 2019.

[49] Z. Lai and H. F. Deng. "Medical image classification based on deep features extracted by deep model and statistic feature fusion with multilayer perceptron". *Computational Intelligence and Neuroscience*, vol. 2018, pp. 1-13, 2018.

[50] G. Litjens, T. Kooi, B. E. Bejnordi, A. A. A. Setio, F. Ciompi, M. Ghafoorian, J. A. W. V. Laak, B. Van Ginneken and C. S. Diagnostic. "A survey on deep learning in medical image analysis". *Medical Image Analysis*, vol. 42, pp. 60-88, 2017.

[51] K. C. L. Wong, T. Syeda-Mahmood and M. Moradi. "Building medical image classifiers with very limited data using segmentation networks". *Medical Image Analysis*, vol. 49, pp. 105-116, 2018

[52] N. T. Member, J. Y. Shin, S. R. Gurudu, R. T. Hurst, C. Kendall, M. Gotway and J. Liang. "Convolutional neural networks for medical image analysis: Full training or fine tuning". *IEEE Transactions on Medical Imaging*, vol. 35, no. 5, pp. 1299-1312, 2016.

[53] J. Ker, L. Wang, J. Rao and T. Lim. "Deep learning applications in medical image analysis". *IEEE Access*, vol. 6, pp. 9375-9389, 2017.

[54] K. U. Rani. "Analysis of heart diseases dataset using neural network approach". *International Journal of Data Mining and Knowledge Management Process*, vol. 1, no. 5, pp. 1-8, 2011.

[55] R. Yamashita, M. Nishio, R. K. G. Do and K. Togashi. "Convolutional neural networks: an overview and application in radiology". *Insights into Imaging*, vol. 9, no. 4, pp. 611-629, 2018.

[56] A. D. Ruvalcaba-Cardenas, T. Scolery and G. Day. "Object classification using deep learning on extremely low-resolution time-of-flight data". In: *2018 Digital Image Computing: Techniques and Applications* (*DICTA*), Canberra, Australia, Australia, 10-13 Dec 2018.

[57] E. Ahn, A. Kumar, M. Fulham, D. Feng and J. Kim. "Convolutional sparse kernel network for unsupervised medical image analysis". *Medical Image Analysis*, vol. 56, pp. 140-151, 2019.

[58] Z. Wu, S. Zhao, Y. Peng, X. He, X. Zhao, K. Huang, X. Wu, W. Fan, F. Li, M. Chen, J. Li, W. Huang, X. Chen and Y. Li. "Studies on different CNN algorithms for face skin disease classification based on clinical images". *IEEE Access*, vol. 7, pp. 66505-66511, 2019.

[59] F. Altaf, S. M. S. Islam, N. Akhtar and N. K. Janjua. "Going deep in medical image analysis: Concepts, methods, challenges and future directions". *IEEE Access*, vol. 7, pp. 99540-99572, 2019.

[60] K. M. Hosny, M. A. Kassem and M. M. Foaud. "Classification of skin lesions using transfer learning and augmentation with Alex-net". *PLoS One*, vol. 14, no. 5, p. e0217293, 2019.

[61] J. Arevalo, F. A. Gonzalez, R. R. Pollan, J. L. Oliveira and M. A. G. Lopez. "Convolutional neural networks for mammography mass lesion classification". In: *2015 37th Annual International Conference of the IEEE Engineering in Medicine and Biology Society* (*EMBC*), Milan, Italy, 25-29 Aug 2015.

[62] M. F. B. Othman, N. B. Abdullah and N. F. Kamal. "MRI Brain Classification Using Support Vector Machine. In: *2011 4th International Conference on Modeling, Simulation and Applied Optimization*, Kuala Lumpur, Malaysia, 19-21 April 2011.

[63] S. H. Shirazi, S. Naz, M. I. Razzak, A. I. Umar and A. Zaib. "*Automated Pathology Image Analysis*". Elsevier, Pakistan, pp. 13-29, 2018.

[64] N. C. Ouseph and K. Shruti. "A reliable method for brain tumor detection using cnn technique". *IOSR Journal of Electrical and Electronics Engineering*, vol. 1. pp. 64-68, 2017.

[65] A. Srivastava, S. Sengupta, S. J. Kang, K. Kant, M. Khan, S. A. Ali, S. R. Moore, B. C. Amadi, P. Kelly, S. Syed and D. E. Brown. "Deep Learning for Detecting Diseases in Gastrointestinal Biopsy Images. In: *2019 Systems and Information Engineering Design Symposium* (*SIEDS*), Charlottesville, VA, USA, USA, 26-26 April 2019.

[66] R. M. Summers. "*Deep Learning and Computer-Aided Diagnosis for Medical Image Processing: A Personal Perspective*". Springer International Publishing, Switzerland, pp. 3-10, 2017.

[67] G. Carnerio, Y. Zheng, F. Xing and L. Yang. *Review of Deep Learning Methods in Mammography, Cardiovascular,and Microscopy Image Analysis*. Springer, Switzerland, 2017, pp. 11-35.

[68] V. V. Kumar, K. S. Krishna and S. Kusumavathi. "Genetic algorithm based feature selection brain tumour segmentation and classification". *International Journal of Intelligent Engineering and Systems*, vol. 12, no. 5, pp. 214-223, 2019.

[69] D. Zikic, Y. Ioannou, M. Brown and A. Criminisi. "Segmentation of brain tumor tissues with convolutional neural networks". MICCAI Workshop on Multimodal Brain Tumor Segmentation Challenge (BRATS) At, Boston, Massachusetts. pp. 36-39, 2014.

[70] A. Norouzi, M. S. M. Rahim, A. Altameem, T. Saba, A. E. Rad, A. Rehman and M. Uddin. "Medical image segmentation methods, algorithms, and applications". *IETE Technical Review*, vol. 31, no. 3, pp. 199-213, 2014.

[71] N. Dey and A. S. Ashour. "*Computing in Medical Image Analysis*". Elsevier, Amsterdam, Netherlands, pp. 3-11, 2018.

[72] N. Padmasini, R. Umamaheswari and M. Y. Sikkandar. "*State-of-the-Art of Level-Set Methods in Segmentation and Registration of Spectral Domain Optical Coherence Tomographic Retinal Images*. Elsevier, United Kingdom, 2018, pp. 163-181.

[73] R. R. Agravat and M. S. Raval. "*Deep Learning for Automated Brain Tumor Segmentation in MRI Images*". Elsevier, United Kingdom, pp. 183-201, 2018.

[74] T. A. Ngo and G. Carneiro. "Fully automated segmentation using distance regularised level set and deep-structured learning and inference. In: L. Lu, Y. Zheng, G. Carneiro, L. Yang, (eds) "*Deep Learning and Convolutional Neural Networks for Medical Image Computing. Advances in Computer Vision and Pattern Recognition*". Springer, Cham, 2017, pp. 197-224.

[75] J. Bernal, K. Kushibar, M. Cabezas, S. Valverde, A. Oliver and X. Llado. "Quantitative analysis of patch-based fully convolutional neural networks for tissue segmentation on brain magnetic resonance imaging". *IEEE Access*, vol. 7, pp. 89986-90002, 2019.

[76] R. Ceylan and H. Koyuncu. "*ScPSO-Based Multithresholding Modalities for Susoicious Region Detection on Mammograms*". Elsevier, Amsterdam, Netherlands, pp. 109-135, 2018.

[77] N. Dhungel, G. Carneiro, A. P. Bradley. Combining deep learning and structured prediction for segmenting masses in mammograms. In: L. Lu, Y. Zheng, G. Carneiro, L. Yang, (eds). "*Deep Learning and Convolutional Neural Networks for Medical Image Computing. Advances in Computer Vision and Pattern Recognition*". Springer, Cham, pp. 225-240, 2017.

[78] A. O. Mader, C. Lorenz, M. Bergtholdt, J. von Berg, H. Schramm, J. Modersitzki and C. Meyer. "Detection and localization of spatially correlated point landmarks in medical images using an automatically learned conditional random field". *Computer Vision and Image Understanding*, vol. 176-177, pp. 45-53, 2018.

[79] K. Marstal, F. Berendsen, N. Dekker, M. Staring and S. Klein. "The Continuous Registration Challenge: Evaluation-as-a-Service for Medical Image Registration Algorithms". In: *2019 IEEE 16th International Symposium on Biomedical Imaging* (*ISBI 2019*), Venice, Italy, Italy, 8-11 April 2019.

[80] S. Ramamoorthy, R. Vinodhini and R. Sivasubramaniam. "Monitoring the growth of Polycystic Ovary Syndrome using Mono-modal Image Registration Technique". In: *International Conference on Data Science and Management of Data* (*CoDS-COMAD'19*), Kolkata, India, January 03-05, 2019.

[81] B. D. de Vos, J. M. Wolterink, P. A. de Jong, T. Leiner, M. A. Viergever and I. Isgum. "Conv net-based localization of anatomical". *IEEE Transactions on Medical Imaging*, vol. 36, no. 7, pp. 1470-1481, 2017.

[82] U. Bagci. "*Medical image computing CAVA: Computer Aided Visualization*". University of Central Florida, Florida, 2017.

[83] M. M. Murray, M. L. Rosenberg, A. J. Allen, M. Baranoski, R. Bernstein, J. Blair, C. H. Brown, E. Caine, S. Greenberg and V. M. Mays. "*Violence and Mental Health: Opportunities for Prevention and Early Detection: Proceedings of a Workshop*". The National Academies Press, Washington, DC, 2018.

[84] S. S. Yadav and S. M. Jadhav. "Deep convolutional neural network based medical image classification for disease diagnosis". *Journal of Big Data*, vol. 6, p. 113, 2019.

ORIGINAL RESEARCH ARTICLE UHD JOURNAL OF SCIENCE AND TECHNOLOGY

Fall Detection Using Neural Network Based on Internet of Things Streaming Data

Zana Azeez Kakarash[1,2], Sarkhel H. Taher Karim[3,4], Mokhtar Mohammadi[5]

[1]Department of Engineering, Faculty of Engineering and Computer Science, Qaiwan International University, Sulaymaniyah, Iraq, [2]Department of Computer Engineering and Information Technology, Faculty of Engineering, Razi University, Kermanshah, Iran, [3]Department of Computer Science, College of Science, University of Halabja, Halabja, Iraq, [4]Department of Computer Network, Technical College of Informatics, Sulaimani Polytechnic University, Sulaymaniyah, Iraq, [5]Department of Information Technology, Lebanese French University, Erbil, Kurdistan Region, Iraq

ABSTRACT

Fall event has become a critical health problem among elderly people. We propose a fall detection system that analyzes real-time streaming data from the Internet of Things (IoT) to detect irregular patterns related to fall. We train a deep neural network model using accelerometer data from an online physical activity monitoring dataset named, MobiAct. An IBM Cloud-based IoT data processing framework is used to manage streaming data. About 96.71% of accuracy is achieved in assessing the performance of the proposed model.

Index Terms: Fall Detection, Internet of Things, Artificial Neural Networks, Machine Learning

1. INTRODUCTION

These days, we can see a quick increment in people using wearable devices for more different purposes and reasons in their lives. According to the previous studies, the employment of connected wearable detector devices is expected to extend from 325 million in 2016 to 1105 million in 2022 [1]. In this way, where an unmeasurable number of wearable devices is connected together will produce a huge amount of information consistently, at that time, we face or interaction with a critical test of storing, handling, and processing that information's to produce usable information and to make a keen world. Distinguishing regularities and abnormalities or inconsistencies in gushing information from that measure of usable information, we previously produced subsequent to putting away and preparing it can give us an encounter and can possibly give experiences, and is useful in human services, money, security, web-based social networking, and numerous applications [2], [3].

Over the most recent few years, totally different types of methodologies and techniques have been proposed for identifying regularities and irregularities pattern in streaming data for fall detection, which may be a wearable tool based, ambiance sensor-based, and vision-based [4]. Above all, wearable devices typically take some different benefit of embedded sensors to observe the movement and placement of the body, such as measuring system, accelerometer, magnetometer, and gyroscope [5], [6]. As well as the value of wearable tool based any methodologies or techniques are very low, also because the installation and operation are not complex, and the task is not difficult for the elderly [7], [8]. If from now the physician could not specifically monitoring and identify falls, then there is no chance to save or protect you in future to preventing an accident. For such reasons, fall identification and anticipation have turned into a significant issue then must be find and propose a good way to solve

Access this article online

DOI:10.21928/uhdjst.v4n2y2020.pp91-98 E-ISSN: 2521-4217 P-ISSN: 2521-4209

Corresponding author's e-mail: Zana Azeez Kakarash, Department of Software Engineering Faculty of Engineering and Computer Science, Qaiwan International University Sulaimani, Iraq. E-mail: zana.azeez@kti.edu.krd

Received: 10-03-2020 Accepted: 28-09-2020 Published: 25-10-2020

in the method of detecting regularities and irregularities in streaming data for fall detection [9], [10].

Fall in the human daily life is one of the main health risks and dangerous, mostly for the older community in our today's society, because of the rose growing in mortality, morbidity, incapacity, disability, and frailty [11]. Nearly for fall initiate injuries as collected and represented, over 80% of all damage related clinic confirmations among peoples for more than 65 years [12], [13]. According to the reasons as we mentioned before, falls affect a huge number of the elderly all through the world. For instance, falls some of the aged cost the National Health Service more than £4.6 million every day as indicated by a report by the Centre for Social Justice UK [14].

The notable studies and researches in this filed are detecting fall or anomaly in real streaming data [15]-[20] and outliers [21], [22]. We will probably investigate the circumstance of unpredictable human development identification, for example, fall, by utilizing continuous sensor information. At that point, we map that issue as sporadic example location issue, thinking about a fall as a capricious action with respect to standard human action and attempt to perceive the exceptional fall situations from ordinary development or human activities, for example, walking, sitting, lying (LYI), sleeping, standing, and every other movement such as playing, cooking, and running.

In general, Artificial Neural Networks (ANN) have systematically achieved higher results in the detection falls from physical activity observation knowledge. Ozdemir and Barshan have used a pair of 2520 trials to make a huge amount of dataset [23]. Their fall detection system achieved 95% accuracy by employing a multi-layer perceptron (MLP) for binary classification between activities of daily living (ADL) and fall. Kerdegari *et al*. recorded 1000 movement acceleration data collection using a waist-worn measuring system and obtained 91.6% accuracy for binary classification for ADL against fall using MLP [24]. Nukala *et al*. collected knowledge from 322 tests achieved 98.7% accuracy with MLP victimization scaled conjugate graduate learning [25].

Theodoridis *et al*. [26] developed two long short-term memory (LSTM) models, one with easy measuring system data collection associated another with accelerometer data revolved at an angle, using a published dataset referred to as UR Fall Detection. The LSTM model with rotation obtained the most effective results with 98.57% accuracy.

The work by class Musci *et al*. used one public dataset (SisFall) dataset implementing Recurrent Neural Network with underlying LSTM blocks for developing online fall detection system [27]. They achieved 97.16% accuracy victimization associate best window breadth of w = 256. Ajerla *et al*. [42] slightly changed the preprocessing done by Vavoulas *et al*. on other public dataset (MobiAct) dataset and achieved quite 90% accuracies on most of their experiments victimization MLP and LSTM [28], [29]. They also obtained 99% accuracy victimization LSTM in two of their experiments. Table 1 shows the compares performance of the ANN techniques.

Nowadays, there are a lot of wearable sensors devices exist which may observe falls automatically and send a notification to the caregivers, machine services, or ambulance offerings. However, most of them are expensive or need a subscription of month-to-month service. A large number of studies and research has been done on fall detection the usage of sensors such as accelerometers and gyroscopes, because of low cost and incorporated into a large number of cell phones accessible todays in the world such as smartphones and tablets. Rather than fall identification, there is a dire need for prediction and prevention systems [30], [31].

In this paper, we propose a system for detecting abnormal pattern of falling behavior in real-time streaming data in internet of things (IoT). The data were obtained from wearable sensor systems used for human health and activity tracking and control. In our research, we focus on how to train the proposed system to recognize and distinguish irregular activity pattern related to specific kinds of fall according to three different annotated published datasets: MobiAct, using Vavoulas *et al*. in 2016 [32], SisFall, using Sucerquia *et al*. in 2017 [33], and UMAFALL by way of Eduardo *et al*. in 2018 [34] for implementing our framework from streaming data for fall detection, we used an ANN model for fall recognition giving (96.71%) accuracy. At that point, we integrate our system for that huge amount of data recordings from streaming sensor (online) into free IBM Streams to fabricate an IBM Cloud-based IoT information preparing structure.

TABLE 1: Comparison of the ANN techniques

Research paper	Technique	Accuracy
Ozdemir *et al*., 2014 [35]	MLP	95%
Kerdegari *et al*., 2013 [36]	MLP	91.6%
Nukala *et al*., 2014 [37]	MLP	98.7%
Theodoridis *et al*., 2018 [38]	LSTM	98.57%
Abbate *et al*., 2012 [39]	Feed-forward ANN	100%
Musci *et al*., 2018 [40]	RNN with LSTM	97.16%
Ajerla *et al*., 2018 [41]	MLP and LSTM	99% (LSTM)

MLP: Multi-layer perceptron, RNN: Recurrent Neural Network, LSTM: Long short-term memory, ANN: Artificial Neural Networks

2. METHODOLOGY

We proposed a profound learning model to recognize fall and in this manner, another structure for utilizing the model with steaming information from wearable sensor frameworks is proposed. Simulated fall detection is used due to the scarcity of actual fall data, as fall is a dangerous event. We consider a framework that includes ANN as one of the evaluating procedure.

ANN has ceaselessly achieved better outcomes in fall recognition from physical checking spilling information. The architecture comprises three essential layers (I) gathering stream for information ingestion, (ii) streaming extract, transform, and load engine for real-time query processing, and (iii) Online Analytical Processing backend for taking care of long-running inquiries. The means of the proposed framework are as per the following data collection

2.1. Dataset

All open datasets or we can say public data sets for wearable fall detection frameworks are distinguished that the selection criteria for any datasets should give priority to the experimental subjects, the quantity of tests and sorts of ADL and falls included in the study [42].

Based on that, we have chosen three different datasets, MobiAct, SisFall, and UMAFall, to evaluate our framework dependent on the number of subjects and number of exercises secured by each dataset.

It is possible to collect data from one or several sources. For instance, in an IoT workload, data are ingested simultaneously from thousands of separate data sources. Each source submits fresh tuples to a stream (likely to send them through a socket), which a data collector mechanism then receives. This data collector mainly act as a queue for messaging [43].

As we explained in Table 2, MobiAct dataset contains labeled data for four differing kinds of falls and nine completely different ADLs were collected from 70 subjects (Male/Female) and quite a pair of 2500 trials buy using so many different kind of a smartphone. The activities are depicted employing a time stamp, raw measuring system values, raw rotating mechanism values, and orientation information. Table 3 shows the activities covered within the MobiAct dataset. In the MobiAct dataset is that it does not embrace fall data from any old people [44]. SisFall remedies this situation by mixing with information from 15 old people aged between 60 and 75 years. Still, in these two datasets real fall data it does not available or do not included.

SisFall contains annotated data for 15 differing kinds of falls and 19 different types of ADLs were collected from 38 subjects and quite 4500 trials using a custom measuring instrument containing two completely different models of 3D accelerometers and a rotating mechanism positioned on a buckle. Furthermore, UMAFall datasets include 12 different types of fall and 15 types of ADLs were collected from 2600 trials by using so many kinds of smartphone and remote accelerators. Like first dataset as I mention above these activities are also depicted employing a time stamp, raw measuring system values, raw rotating mechanism values, and orientation information

2.2. Data Preprocessing

2.2.1. Segmentation

Using the same procedure given by Aziz *et al.* [45], the raw data are segmented into 200 blocks and then the feature sets for each block are generated.

2.2.2. Feature extraction

List of features A: A sum of 54 features were created in include setA [46]. For every pivot (x, y, and z) of the quickening, 21 highlights were determined from the mean, middle, Standard Deviation (STD), slant, kurtosis, least, and most extreme. Utilizing the outright estimations of every hub (x, y, and z) of the quickening, another 21 highlights were determined from the mean, middle, STD, slant, kurtosis, least, and most extreme. Incline, another component, was determined utilizing Eq. 1, one for the given tomahawks esteems (x, y, and z) and another for the supreme qualities (|x|, |y|, |z|).

TABLE 2: Activites covered in datasets

Code	Activity	Description
FALL		
FOL	Forward-lying	Fall forward from standing, use of hands to dampen fall
FKL	Front-knees-lying	Fall forward from standing, first impact on knees
SDL	Sideward-lying	Fall sideward from standing, bending legs
BSC	Back-sitting-chair	Fall backward while trying to sit on a chair
ADL		
STD	Standing	Standing with subtle movements
WAL	Walking	Normal walking
JOG	Jogging	Jogging
JUM	Jumping	Continuous jumping
STU	Stairs up	10 stairs up
STN	Stairs down	10 stairs down
SCH	Sit chair	Sitting on a chair
SCI	Car step in	Step in a car
SCO	Car step out	Step out of a car

TABLE 3: Datasets used for training

Dataset	No. of subjects (male/female)	Age range	No. of activities ADLs/falls	No. of samples (ADLs/falls)
MobiAct [32]	70 (45/25)	20–47	9/4	2526 (1879/647)
SisFall [33]	60 (30/20)	19–30, 60–75	19/15	4505 (2707/1798)
UMAFall [34]	55 (35/15)	30–47	15/12	2650 (1700/950)

ADL: Activities of daily living

$$\text{Slope} = \sqrt{\begin{matrix}(\max_x - \min_x)^2 + (\max_y - \min_y)^2 \\ +(\max_z - \min_z)^2\end{matrix}} \quad (1)$$

Four different features were determined utilizing mean, STD, slant, and kurtosis of the tilt edge (TAi) between the gravitational vector and the Y-axis utilizing Eq. 2.

$$TAi = \sin^{-1}(yi / (\sqrt{xi^2 + yi^2 + zi^2})) \quad (2)$$

Where i denotes the sequence of the sample.

Utilizing the magnitude of the acceleration vector, six features were resolved from the mean, STD, least, greatest, contrast among most extreme and least, and zero-intersection rate. The size was determined utilizing Eq. 3.

$$Magnitude = \sqrt{xi^2 + yi^2 + zi^2} \quad (3)$$

Where i denotes the sequence of samples.

For each of the three axes (x, y, and z), the average absolute difference was calculated [47]. Furthermore, the average resultant acceleration of all the three axes was generated using Eq. 4.

$$Average\ resultant\ acceleration = \left(\frac{1}{n}\right) * \sum_i \sqrt{xi^2 + yi^2 + zi^2} \quad (4)$$

Where i denotes the sequence of samples.

Combined Feature Set. The feature sets A, B, and C are merged to generate the dataset with the combined features. We had 7670 samples in the dataset. After feature extraction, each sample had one of six classification values and 58 extracted features. Class values include four kinds of falls and two kinds of non-falls as defined in the MobiAct dataset. The two non-fall classes denote Standing (STD) and LYI positions.

2.2.3. Normalization

The extracted features were normalized using Matlab R2017b with the min-max scaling formula given in Eq. 5.

$$X = \frac{x - Min(feature)}{Max(feature) - Min(feature)} \quad (5)$$

2.2.4. Data balancing

The obtained dataset after normalization was very unbalanced containing 5830 non-fall and 1840 fall data. We made data balanced for our dataset using Matlab R2017b as follows: The various fall data categories were merged into a single fall data classification while the two non-fall data categories were merged into a single non-fall data classification. Then, the fall data were oversampled to create 2000 samples and the non-fall data were under-sampled to create 2000 samples to create a combined balanced dataset containing 4000 samples.

2.2.5. Feature selection

Selection of discriminable features affects the performance of the classification in terms of accuracy and complexity. Among different feature selection methods, the relief-F method is used for feature selection, the relief-F method in python is used with number of neighbor set to two and number of features to be kept set to four. The relief-F compared to the relief method is more robust and can deal with incomplete and noisy data [48].

2.3. Predictive Modeling

We created a simple predictive Deep Neural Network (DNN) model consisting of five layers including three hidden layers to detect fall based on data stream sensor.

The structure of DNN is displayed in Fig. 1. The model was constructed and designed using offline datasets and then was implemented in our streaming data processing system.

We are building a streaming data processing system with IBM tools, and then we tested and validated our prediction model with a static fall data.

2.4. Streaming Data Processing Framework

After finalizing, testing and approving our proposed model using specific static data for fall detection, we build up a streaming data processing and handling structure with IBM devices. The framework structure is appeared in Fig. 2.

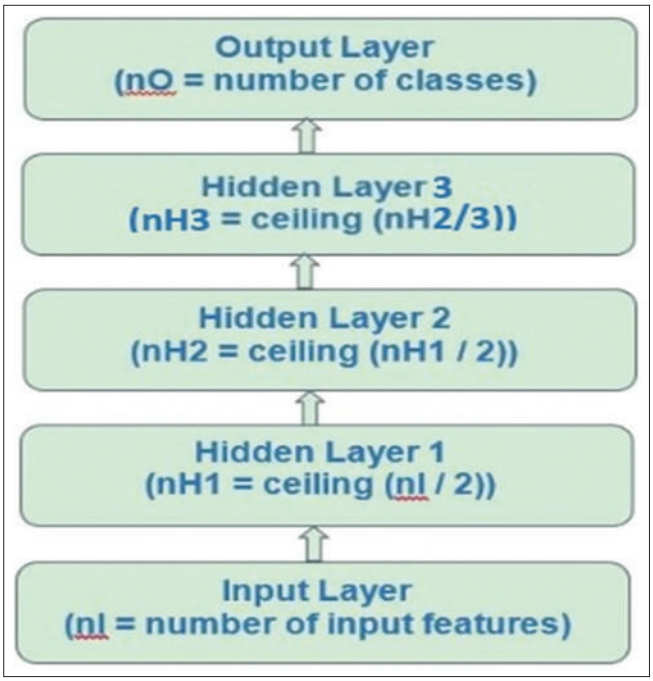

Fig. 1. Deep learning model utilized for the proposed framework.

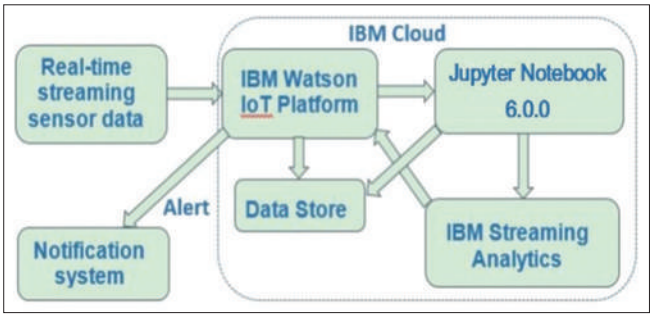

Fig. 2. The framework of the data stream processing system to detect irregular patterns for internet of things streaming data.

2.5. Architecture and Components

- Data source: Sensor information is recovered from the cell phone or any wearable devices must be fixed in the patient body.
- Data ingestion system: To receiving the sensor data from a smartphone or a wearable sensor and go about as the Message Queuing Telemetry Transport [49] message broker, we used IBM Watson IoT Platform. And also Apache Kafka [50] is used here as an open source alternative, which uses depends on its own protocol.
- Data stream processing: To start with we utilized Jupyter Notebook with IBM Cloud [51] as appeared in Fig. 3, for offline information preparing to run the element extraction and to execute the AI model utilizing the sample data. The Python code utilized in Jupyter Notebook and the middle information records have been posted on Github. We had an arrangement to utilize the IBM Streaming Analytics [52], an organization for IBM Streams on IBM cloud, to continually screen the sensor information from mobile phone or wearable sensors and send an admonition to the watching application to alert human services suppliers about the crisis care required by patients in the unexpectedly occasion or some other of a fall.
- Data store: We have the plan to use IBM Cloud [53] as the NoSQL database to store the sensor information from the Watson IoT platform and classification of that streaming data which are obtained from Watson Studio.
- Data sink: The framework will have different output channels:
  - Knowledge base.
  - Visualization
  - Monitor
  - IBM cloud.

1. Implementation: The tests were run on a framework with the accompanying least equipment and programming prerequisites:
   - Platform: Keras with tensor flow backend
   - CPU: Intel Core i5-2467M, 1.6 GHz
   - RAM: 10 GB
   - Hard disk: 128 GB
   - OS: Windows 10 64 bit .

To actualize the framework, we utilized a free IBM cloud account and the relevant services. We included the following accompanying assets.

- Jupyter notebook 6.0.0
- Cloud object storage
- Streaming analytics
- IoT platform.

3. RESULTS AND DISCUSSION

The machine learning model for the complete feature set was first tried on MobiAct as explained in Section 2.1. This resulted in our model in an accuracy of (96.71%) for binary classification, fall and ADL (non-fall) using Eq 6. The model was lept running for 200 epochs.

$$ACC = (\text{True positive} + \text{True negative}) / \text{Number of all samples} \quad (6)$$

The normalized and un-normalized confusion matrices were implemented for classifying fall and non-fall (ADL) cases out of 7670 samples are appeared in Fig. 4. This shows the

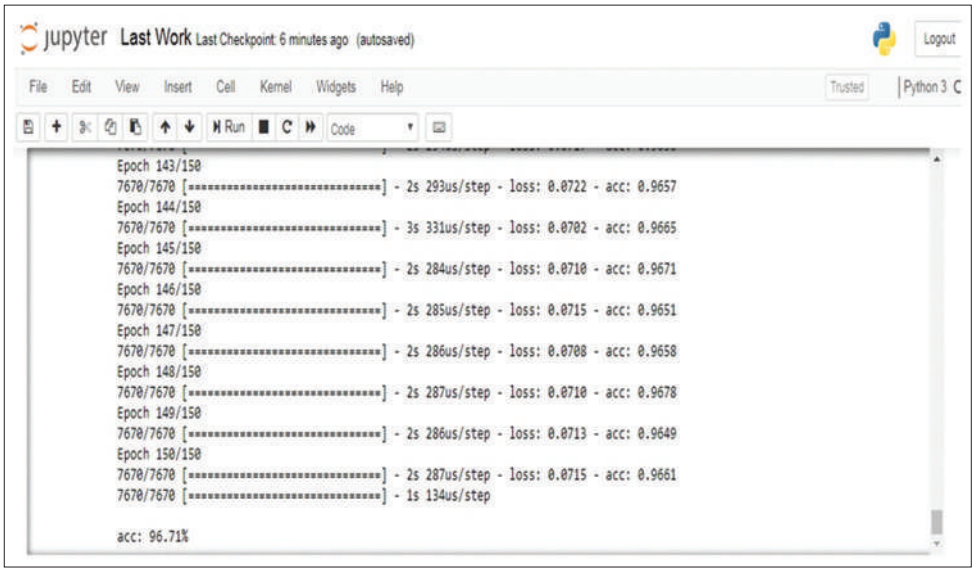

Fig. 3. Machine learning model executed using Jupyter Notebook.

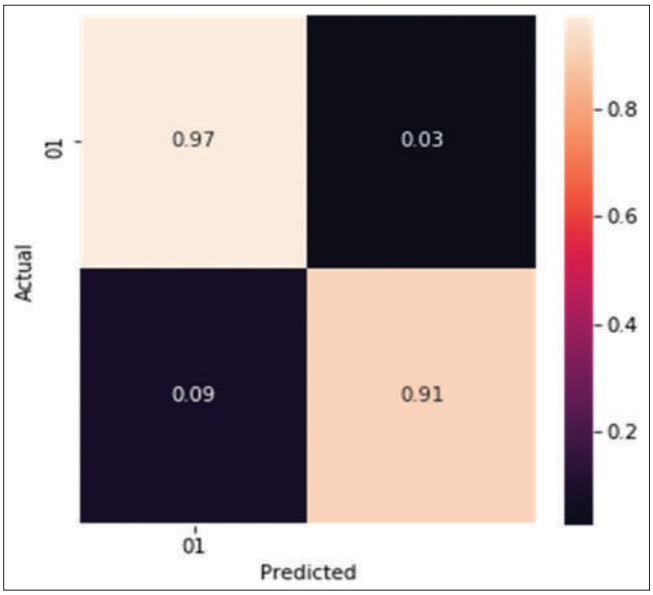

Fig. 4. Normalized confusion matrix for the trained model.

created model performs incredible and can be utilized to develop the proposed framework.

4. CONCLUSION

In this paper, we addressed the problem of irregularity pattern detection from online streaming data. Here, we especially focused on detecting fall as an irregular human activity which is common amongst elderly people. We implemented a DNN model that can classify fall from non-fall activities based on the dataset MobiAct and two more datasets with an accuracy of 96.71%. For future, we plan to compare the proposed system with other systems that use open source streaming data analytics tools to evaluate the functionality and performance of the IBM tools used in our framework.

REFERENCES

[1] H. Tankovska. "Statistic", 2020. Available from: https://www.statista.com/statistics/487291/global-connected-wearable-devices.

[2] Mahfuz. "Detecting Detecting Irregular Patterns in IoT Streaming Data for Fall Detection Irregular Patterns in IoT Streaming Data for Fall Detection". 2018 IEEE 9th Annual Information Technology, Electronics and Mobile Communication Conference (IEMCON), 2018.

[3] E. Bahmani, M. Jamshidi and A. Shaltooki. "Breast cancer prediction using a hybrid data mining model". *International Journal on Informatics Visualization*, vol. 3, no. 4, pp. 327-331, 2019.

[4] J. Liu. "Development and evaluation of a prior-to-impact fall event detection algorithm". *IEEE Transactions on Biomedical Engineering*, vol. 61, no. 7, pp. 2135-2140, 2014.

[5] P. Pierleoni. "A high reliability wearable device for elderly fall detection". *IEEE Sensors Journal*, vol. 15, no. 8, pp. 4544-4553, 2015.

[6] R. Freitas. "*Wearable Sensor Networks Supported by Mobile Devices for Fall Detection*". SENSORS, IEEE, 2014.

[7] X. Zhuang. "*Acousticfalldetection Using Gaussian Mixture Models and Gmm Super Vectors*". 2009 Ieee International Conference on Acoustics, Speech and Signal Processing, 2009.

[8] Y. Li. "Efficient source separation algorithms for acoustic fall detection using a microsoft kinect". *IEEE Transactions on Biomedical Engineering*, vol. 61, no. 3, pp. 745-755, 2014.

[9] R. Hamedanizad, E. Bahmani, M. Jamshidi and A. M. Darwesh. "Employing data mining techniques for predicting opioid withdrawal

in applicants of health centers". *Journal of Science and Technology*, vol. 3, no. 2, pp. 33-40, 2019.

[10] A. Shaltooki and M. Jamshidi. "The use of data mining techniques in predicting the noise emitted by the trailing edge of aerodynamic objects". *International Journal on Informatics Visualization*, vol. 3Z, no. 4, pp. 388-393, 2019.

[11] A. S. Cook. "Falls in the Medicare population: incidence, associated factors, and impact on health care". *Physical Therapy*, vol. 2009, no. 2, pp. 324-332, 2009.

[12] P. Kannus. "Fall-induced injuries and deaths among older adults". *JAMA*, vol. 281, no. 20, pp. 1895-1899, 1999.

[13] Y. Cheng. "*A Fall Detection System Based on SensorTag and Windows 10 IoT Core*". 15th International Conference on Mechanical Science and Engineering, pp. 238-244, 2015.

[14] O. Ojetola, E. I. Gaura and J. Brusey. "*Fall Detection with Wearable Sensors Safe* (*Smart Fall Detection*)". Intelligent Environments, 2011 7th International Conference on, pp. 318-321, 2011.

[15] S. M. S. Forbes. "Fall prediction using behavioural modelling from sensor data insmarthomes". *Artificial Intelligence Review*, vol. 53, pp, 1071-1091, 2019.

[16] S. K. Gharghan. "Accurate fall detection and localization for elderly people based on neural network and energy-efficient wireless sensor network". *Energies*, vol. 11, pp. 1-32, 2018.

[17] D. Yacchirema. "Fall detection system for elderly people using IoT and big data". *Procedia Computer Science*, vol. 130, pp. 603-610, 2018.

[18] C. C. H. Hsu. "*FallCare+: An IoT Surveillance System for Fall Detection*". Proceedings of the 2017 IEEE International Conference on Applied System Innovation IEEE-ICASI 2017 Meen, pp. 921-922, 2017.

[19] Ahmad S. "*Real-Time Anomaly Detection for Streaming Analytics*". arXiv, 2016.

[20] S. C. Tan. "*Fast Anomaly Detection for Streaming Data*". Proceedings of the 22nd International Joint Conference on Artificial Intelligence, pp. 1511-1516, 2011.

[21] M. Gupta. "Outlier detection for temporal data: A survey". *IEEE Transactions on Knowledge and Data Engineering*, vol. 26, no. 9, pp. 2250-2267, 2014.

[22] S. Sadik and L. Gruenwald. "*Research Issues in Outlier Detection for Data Streams*". Vol. 15. SIGKDD Explorations, pp. 33-40, 2013.

[23] T. Özdemir and B. Barshan. "Detecting falls with wearable sensors using machine learning techniques". *Sensors*, vol. 14, no. 6, pp. 10691-10708, 2014.

[24] H. Kerdegari, K. Samsudin, A. R. Ramli and S. Mokaram. "Development of wearable human fall detection system using multilayer perceptron neural network". *International Journal of Computational Intelligence Systems*, vol. 6, no. 1, pp. 127-136, 2013.

[25] T. Nukala, N. Shibuya, A. Rodriguez and J. Tsay. "An efficient and robust fall detection system using wireless gait analysis sensor with artificial neural network (ANN) and support vector machine (SVM) algorithms". *Open Journal of Applied Biosensor*, vol. 3, pp. 29-39, 2014.

[26] T. Theodoridis, V. Solachidis, N. Vretos and P. Daras. "Human fall detection from acceleration measurements using a recurrent neural network". In: *Precision Medicine Powered by pHealth and Connected Health*. Springer, Berlin, Germany, pp. 145-149, 2018.

[27] M. Musci, D. De Martini, N. Blago, T. Facchinetti and M. Piastra. "*Online Fall Detection using Recurrent Neural Networks*". arXiv, 2018.

[28] G. Vavoulas, C. Chatzaki, T. Malliotakis, M. Pediaditis and M. Tsiknakis. "*The MobiAct Dataset: Recognition of Activities of Daily Living Using Smartphones*". ICT4AgeingWell, pp. 143-151, 2016.

[29] D. Dharmitha, M. Sazia and Z. Farhana. "Fall Detection from Physical Activity Monitoring Data". Presented at the International SIGKDD workshop on Big Data, Streams and Heterogeneous Source Mining: Algorithms, Systems, Programming Models and Applications (BigMine), London, 2018.

[30] D. Ajerla, S. Mahfuz and F. H. Zulkernine. "A Real-Time Patient Monitoring Framework for Fall Detection". Queen's University, Kingston, Ontario, Canada, 2018.

[31] D. Ajerla. "*Fall Detection from Physical Activity Monitoring Data*". BIGMINE, London, UK, 2018.

[32] T. Xu, Y. Zhou and J. Zhu. "New advances and challenges of fall detection systems: A survey". *Applied Science*, vol. 8, no. 3, p. 418, 2018.

[33] H. Chen, (Eds.). "*Ngu3Fall Detection Using Smartwatch Sensor Data with Accessor Architecture*". Springer International Publishing, Berlin, Germany, pp. 81-93, 2017.

[34] E. C. J. Santoyo-Ramón. "*UMAFall: Fall Detection Dataset* (*Universidad deMalaga*)". Available from: https://www.figshare.com/articles/UMA_ADL_FALL_Dataset_zip/4214283. [Last accessed on 2018 Jun 04].

[35] S. Ahmad, A. Lavin, S. Purdy and Z. Agha. "Unsupervised real-time anomaly detection for streaming data". *Neurocomputing*, vol. 262, pp. 134-147, 2017.

[36] M. Ahmed, A. N. Mahmood and M. R. Islam. "A survey of anomaly detection techniques in financial domain". *Future Generation Computer Systems*, vol. 55, pp. 278-288, 2016.

[37] S. Ahmad and S. Purdy. "*Real-time Anomaly Detection for Streaming Analytics*". arXiv, 2016.

[38] M. Mohammadi, A. Al-Fuqaha, S. Sorour, and M. Guizani, "Deep Learning for IoT Big Data and Streaming Analytics: A Survey," *IEEE Communications Surveys & Tutorials,* 2018.

[39] J. Meehan, C. Aslantas, S. Zdonik, N. Tatbul and J. Du. "Data *Ingestion for the Connected World*". Classless Inter-Domain Routing, 2017.

[40] S. Sadik and L. Gruenwald. "Research issues in outlier detection for data streams". *ACM SIGKDD Explorations Newsletter*, vol. 15, no. 1, pp. 33-40, 2014.

[41] M. Gupta, J. Gao, C. C. Aggarwal and J. Han. "Outlier detection for temporal data: A survey". *IEEE Transactions on Knowledge and Data Engineering*, vol. 26, no. 9, pp. 2250-2267, 2014.

[42] E. Casilari, J. A. Santoyo-Ramón and J. M. Cano-García. "Analysis of public datasets for wearable fall detection systems". *Sensors*, vol. 17, no. 7, p. 1513, 2017.

[43] J. Meehan. "*Data Ingestion for the Connected World*". Creative Commons Attribution License, 2017.

[44] M. P. G. Vavoulas. "The mobiFall dataset: Fall detection and classification with a smartphone". *International Journal of Monitoring and Surveillance Technologies Research*, vol. 2, no. 1, p. 13, 2014.

[45] O. Aziz, M. Musngi, E. J. Park, G. Mori and S. N. Robinovitch. "A comparison of accuracy of fall detection algorithms (threshold-based vs. machine learning) using waist-mounted tri-axial accelerometer signals from a comprehensive set of falls and non-fall trials". *International Federation for Medical and Biological Engineering*, vol. 55, no. 1, pp. 45-55, 2017.

[46] G. Vavoulas1. "*The MobiAct Dataset: Recognition of Activities of Daily Living using Smartphones*". In" International Conference on Information and Communication Technologies for Ageing Well and e-Health, 2016.

[47] J. R. Kwapisz, G. M. Weiss and S. A. Moore. "Activity recognition using cell phone accelerometers". *SIGKDD Explorations*, vol. 12, no. 2, pp. 74-82, 2010.

[48] Y. Z. Z. Wang. "*Application of Relieff Algorithm to Selecting Feature Sets for Classification of High Resolution Remote Sensing Image*". 2016 IEEE International Geoscience and Remote Sensing Symposium, pp. 755-758, 2016.

[49] MQTT. Available from: https://www.mqtt.org/getting-started. [Last accessed on 2020 Jan 01].

[50] A. Kafka. Available from: https://www.kafka.apache.org/intro. [Last accessed on 2020 Jan 05].

[51] IBM. "IBM Watson Studio IBM Watson and Cloud Platform Learning Center", 2020. Available from: https://www.developer.ibm.com/technologies/data-science.

[52] IBM. "*IBM Streaming Analytics IBM Watson and Cloud Platform Learning Center*". 2016-07-18 2016

[53] IBM. "IBM Cloudant-IBM Watson and Cloud Platform Learning Center", 2020. Available from: https://www.developer.ibm.com/components/cloud-ibm.

ORIGINAL RESEARCH ARTICLE UHD JOURNAL OF SCIENCE AND TECHNOLOGY

Temporal Variation of Drinking Water Quality Parameters for Sulaimani City, Kurdistan Region, Iraq

Jwan Bahadeen Abdullah and Yaseen Ahmed Hamaamin*

Department of Civil Engineering, College of Engineering, University of Sulaimani, KRG, Iraq

ABSTRACT

Water is vital for all forms of life on earth. Assessing the quality of water especially drinking water is one of the important processes worldwide which affect public health. In this study, the quality of drinking water in Sulaimani City is monitored for a study period of 1 year. A total number of 78 water samples were collected and analyzed for 17 physical and chemical properties of water supply system to the city. Samples of water are collected from the three main sources of drinking water for Sulaimani City (Sarchnar, Dukan line-1, and Dukan line-2) from February to August 2019. The results of physical and chemical parameters of collected water samples were compared with the World Health Organization and Iraqi standards for drinking water quality. The results of this study showed that mostly all parameters were within the standards except the turbidity parameter which was exceeded the allowable standards in some cases. This research concluded that, in general, the quality of drinking water at the three main sources of Sulaimani City is suitable and acceptable for drinking.

Index Terms: Seasonal, Variation, Water, Quality, Sulaimani

1. INTRODUCTION

One of the most critical and important natural resources to sustain life is water. Therefore, there is an increasing awareness that assessing the quality of water is essential for abundant activities such as drinking, agricultural, industrial, hydropower generation, and recreational purposes [1], [2] and [3]. Worldwide impaired quality, scarcity, and pressure on water resources due to the growing demands, requires the critical researches on quantity and quality of water [1], [4] and [5]. Consequently, the necessary step in national water planning and management is assessing the quality of water [6], [7], [8] and [9]. Global water resource contamination is increasing due to diverse human activities and population growth, which raised international alarm about quality of water [6]. Regular monitoring the quality of water and advising ways for protecting water resources are necessary in all countries, especially in developing countries which have a rapid urbanization [10], [11] and [12]. Water quality can be defined in terms of its chemical, physical, and biological characteristics which show the suitability of water for different uses such as drinking, industrial, agricultural, and domestic. Observing water quality parameters for annually (or with any intervals) sampled water are the key for detecting information about the pollution level and the quality variation in water over trends of time [2], [3], [5], [7] and [8]. According to the reports conducted by the World Health Organization (WHO) in Iraq show that 25% of childhood deaths are due to the water borne diseases that can be prevented. In terms of obtaining safe water and sanitation, the condition in Kurdistan region is better compared with the other cities in Iraq but still problems

Access this article online

DOI: 10.21928/uhdjst.v4n2y2020.pp99-106

E-ISSN: 2521-4217
P-ISSN: 2521-4209

Corresponding author's e-mail: Yaseen Ahmed Hamaamin, Department of Civil Engineering, College of Engineering, University of Sulaimani, KRG, Iraq. Email: yassen.amin@univsul.edu.iq

Received: 25-08-2020 Accepted: 30-10-2020 Published: 05-11-2020

with environmental issues are existing [13]. Issa and Alrawi [14] developed water quality index for Erbil's three water treatment plants, they found that the quality of water fallen within the good level of water quality.

According to the official directorate of water, the quality of drinking water in Sulaimani City is acceptable in terms of physiochemical and biological properties, but one of the concerned problems of the city's water supply is the yellow tint occurred in a certain time in the years, especially in spring and autumn [15]. The main sources of municipal drinking water in Sulaimani city are Sarchnar, Dukan line-1, and Dukan line-2, due to unexpected growth population in the city and economic problems, continuous water supply does not exist in the city, it has intermittent water supply of about few hours each 2 days [16]. The main objective of this study is monitoring and assessing the quality of municipal drinking water supply for the Sulaimani City by evaluating the chemical and physical characteristics of water sampled from the main sources of drinking water in the city.

2. MATERIALS AND METHODS

2.1. Study Area

Sulaimani City is located in the north part of Iraq which is one of the major cities in the Iraqi Kurdistan region with a population of over 1 million. The city is stretched between two mountains at the intersection point of Longitude 45.44312° and Latitude of 35.55719° with average level of about 850 m above the sea level. The weather of the city is dry and warm in summer with an average temperature of 31.5°C, while the weather is cold and wet during winter season with average temperature of 7.6°C [16] and [17]. Fig. 1 shows water treatment plant and sampling locations which are both in Sulaimani Governorate.

2.2. Water Quality Parameters

In this study, 17 physical and chemical water parameters were used to measure the quality of drinking water for Sulaimani City. Temperature, electrical conductivity (EC), total dissolved solids (TDS), salinity, PH, turbidity, free chlorine, total chlorine, total alkalinity, hardness, calcium, ammonia, ammonium, chloride, fluoride, nitrate nitrogen, and nitrate parameters were measured in the study.

Temperature as one of important water quality parameters has a great effect on growth and activity of aquatic life. Temperature affects the solubility of oxygen in water which consequently affects the life of aquatic organisms. Furthermore, biochemical reactions of aquatic bacteria can be doubled for each 10°C, to a certain limit of temperature [18] and [19].

EC of water measures the ionic content of a water sample which indicates the range of alkalinity and hardness of water. This parameter affects the acceptability of water for drinking purpose because it impacts the taste of water significantly. The amount of conductivity in any sample of water is influenced by the amount of TDS concentration which is another important parameter in monitoring the quality of water. However, lime scaling and buildup can be occurred from high alkaline water. Dissolve solids can occur in water from dissolving of soil minerals while it is in touch with soil layers. Runoff from residential areas and farming, leaching pollutant from soil and industrial or sewage treatment to water resources can be other sources of TDS [9] and [20]. Salinity is a parameter that related to the presence of salt content in water. Suitability of water may be rendered by the amount of salt content in it [21], [22]and [23].

PH is a parameter that indicates whether the water is acid or basic. Furthermore, it shows if the water is suitable or not for various purposes. PH has a direct relation with every phase of water treatment processes. Low pH cause corrosion in water distribution systems, on the other hand, high pH affects the palatability of water [21] and [22].

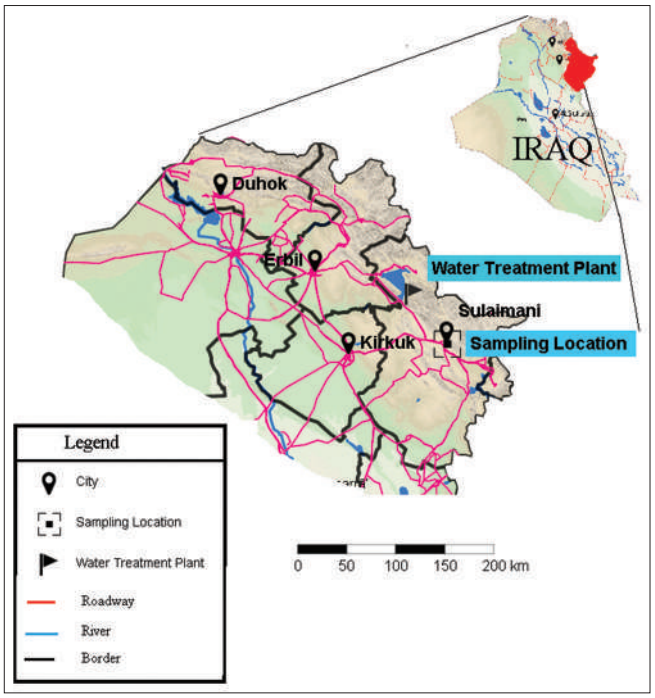

Fig. 1. Study area.

Turbidity of water is occurred by the presence of suspended solids such as clay, silt, and other microscope organisms that are the very fine hard to be removed by routine water treatment methods. This parameter affects the acceptability of consuming water for drinking or other uses especially in certain industries [19].

Chlorination is the most universal method of water disinfection, which is efficient and powerful way in the treatment process. After completion of the disinfection process, extra chlorine can remain in the form of residual chlorine which is very important, because it insures protecting water from recontamination especially in old water distribution systems [21].

Total alkalinity is the size of water response with H+ ions and sometimes is indicated as alkali level. Alkalinity relates with the scale deposition and corrosion in distribution systems. This parameter can be attributed to carbonates and hydroxides in natural water. The unit used for expressing alkalinity is mg/l $CaCO_3$ [24].

Ammonia and ammonium concentration express as mg/l N and mg/l NH_3, respectively. These parameters indicate the possibility of pathogenic micro-organisms presence in water and sewage pollution of water. In water treatment, presence of ammonia with high level can impair the chlorination process of water [19] and [21].

The characteristic of water that improves its palatability and shows the suitability of water for drinking purpose is hardness (mg/l $CaCO_3$) which is the soap destroy capacity of water. The main constituents of hardness are calcium and magnesium which are the widespread abundance metals in the formation of rocks [23].

Calcium is the most important element which ensures the normal growth and health of human body. Water with high amount of calcium consider as very palatable and acceptable water. Calcium is the primary constituent of hardness and it is very beneficial to health. Its concentration in water expressed as mg/l Ca [20].

Naturally, fluoride occurs rarely in waters, main sources of this element in water are public water supply fluoridation and industrial discharges. Fluoride should be added to water supply because of its importance for growing children teeth and reducing tooth decay. Fluoride concentration is expressed as mg/l F. Chloride (mg/l Cl) is the parameter which can be consider for accepting the palatability of water and it does not have hazard to human health. High amount of chloride raises the salty taste of water [16].

Nitrate nitrogen (mg/l N) and nitrate (mg/l NO_3) can be found in natural water due to the organic wastes, sewage discharges, farming fertilizer, runoff from surfaces, plants nitrogen fixing, and bacterial oxidation. High level concentration of nitrate is hazardous to human, especially infants because of its reaction with blood hemoglobin which causes methemoglobinemia [21].

2.3. Sample Collection and Data Analysis

Water samples were collected from the three main water distribution pipes on weekly bases and after rainfall events from three main sources of drinking water in Sulaimani City, Sarchnar, Dukan line 1, and Dukan line 2. Water samples were obtained at the same time and location from the main Sarchnar Control station where the three main distribution lines located which feed the city with drinking water supply. The date and time of samplings were altered by rainfall events and any other expected changes which can affect the quality of water.

Sarchnar water is natural spring water source, is pumped to the city without any treatment process except chlorination. The other two water supply main lines Dukan 1 and 2 are from the city's water treatment plant-1 and plant-2 which are located in Peer Qurban (N 35.88808° and E 44.99651°), receive water from lesser Zab River downstream of water from Dukan Lake. In year of 2018, Sulaimani City received following average amount of water from each source: 32535559 m^3/year from Sarchanr, 16721500 m^3/year from Dukan1, and 58893329 m^3/year from Dukan 2. Water samples were collected for winter, spring, and summer seasons between months February and August 2019. The samples were preserved in clean plastic bottles, and transferred to laboratory for analyzing physical and chemical parameters according to the defined methods in the standard methods for examination water and wastewater [25]. Physical parameters such as temperature, PH, conductivity, TDS, and salinity were analyzed and recorded *in situ* immediately after running the water tabs for about 1 min and collecting the samples using Palintest Multi-Parameter Pocket meter (PT162). As soon as water samples were arrived laboratory, turbidity test and free chlorine and total chlorine test were conducted using Hanna Turbidity meter (HI98703-02) and Palintest spectrophotometer 7500 (7500 2180072). After that the remained water parameters were conducted using Palintest spectrophotometer 7500 (7500 2180072). Water samples lab results of the tests were evaluated and

compared with the WHO water standards [19] and Iraqi water standards [26] for drinking water (Table 1).

3. RESULTS AND DISCUSSION

In this study, a total of 78 samples were collected and analyzed for 17 physical and chemical properties of water from the three main sources of drinking water in Sulaimani city (Sarchnar, Dukan line1, and Dukan line2) from February to August 2019. Table 2 shows the descriptive statistics of all water quality parameters test results obtained in the study.

In this study, the value of temperature for water samples collected from Sarchnar was close to the value of Dukan 2 which was ranged between 15.8 and 20.4°C. The temperature of samples from Dukan 1 was lower in winter season (14°C) and higher in summer season (23.1°C). In general, the average value temperature of collected samples during the period of study was 17.8°C for Sarchnar, 19°C for Dukan 1, and 18.6 for Dukan 2 (Fig. 2), while Sarchnar source is a spring and the intake from this source located at the source location which makes it is less affected by temperature rise during summer season compared to the other sources which are from Lesser Zab River.

While there were some strong correlations between the three parameters (TDS, EC, and salinity), only TDS changes shown in Fig. 3. The TDS values starting with the minimum value in the middle period of winter season and continuous rising until March and then falling again to the minimum value in the beginning of April during the intensive rainfall occurred in Kurdistan region and finally rising the values to the maximum value in August and continuous approximately with the same level to the end of summer season. This fluctuating of TDS may be due to contribution of groundwater during dry season to the river water, while it was low during flood season because of more rainfall runoff contribution to the river flow during spring months.

According to the WHO standards [19] and Iraqi standards [26], the range of PH should be between 6.5 and 8.5. In this study, minimum value of PH for all samples was 7.32 for Sarchnar source and the maximum value was 8.23 for Dukan 2. Fig. 4

TABLE 1: Drinking water standards [19] and [26]

Parameter	WHO standards	Iraqi standards
PH	6.5–8.5	6.5–8.5
Conductivity (µs/cm)	600	1500
TDS (mg/l)	1000	1000
Alkalinity (mg/l $CaCO_3$)	600	--
Turbidity (NTU)	5	5
Free Chlorine (mg/l)	5	5
Hardness (mg/l $CaCO_3$)	500	500
Calcium (mg/l Ca)	75	50
Ammonia (mg/l NH_3)	1.5	--
Fluoride (mg/l F)	0.7–1.5	--
Chloride (mg/l Cl)	250	250
Nitrate Nitrogen (mg/l N)	10	--
Nitrate (mg/l NO_3)	50	50

TABLE 2: Descriptive statistics of water quality parameters for samples collected from main sources of drinking water of Sulaimani City; Sarchnar, Dukan line 1, and Dukan line 2

Parameter	Sarchnar					Dukan Line 1					Dukan Line 2				
	Min.	Max.	Mean	Med.	Std. dev.	Min.	Max.	Mean	Med.	Std. dev.	Min.	Max.	Mean	Med.	Std. dev.
Temperature	15.8	19.6	17.8	18	0.84	14	23.1	19.0	19.6	2.90	15.8	20.4	18.6	19.15	1.32
Conductivity	357	562	461	455	79.23	342	566	466	452	78.79	333	537	435	437	75.56
TDS	251	398	327	322	55.29	245	402	331	321	56.15	235	381	309	310	53.70
Salinity	168	269	220	217	38.15	163	271	223	217	39.80	157	258	208	210	38.01
PH	7.32	8.1	7.7	7.6	0.21	7.63	8.05	7.66	7.71	0.29	7.44	8.28	7.72	7.66	0.24
Turbidity	0.28	10.5	1.9	1.41	2.23	0.26	11.6	1.93	0.88	2.69	0.31	14.1	2.43	1.15	3.11
Free chlorine	0.15	0.92	0.64	0.69	0.15	0.11	0.53	0.33	0.36	0.12	0.65	1.96	1.05	0.96	0.34
Total chlorine	0.17	0.94	0.67	0.72	0.14	0.17	0.53	0.35	0.37	0.11	0.66	1.98	1.07	1	0.33
Alkalinity	135	220	190	203	26.98	130	235	191	200	28.79	135	200	169	173	19.60
Ammonia	0	0.08	0.03	0.02	0.02	0	0.04	0.02	0.02	0.01	0	0.05	0.02	0.02	0.01
Ammonium	0	0.08	0.03	0.03	0.02	0	0.05	0.03	0.03	0.02	0	0.06	0.02	0.03	0.02
Hardness	121	175	152	151	17.55	124	193	153	154	17.39	128	171	145	144	12.42
Calcium	48	70	61	63	6.62	50	78	62	62	7.03	52	68	59	58	4.65
Fluoride	0	0.61	0.2	0.19	0.18	0.01	0.54	0.21	0.18	0.17	0	0.49	0.21	0.2	0.14
Chloride	0	18	5	5	3.75	0	15	4	4	3.13	0	9	4	2	2.62
Nitrate (N)	2.3	5.24	3.5	3.16	1.01	2.34	5.14	3.4	3.03	0.9	2.24	6.3	3.6	3.11	1.23
Nitrate (NO_3)	10.4	23.6	15.4	14	4.46	10.4	22.8	15.0	13.60	4.0	10	28	16.1	14	5.40

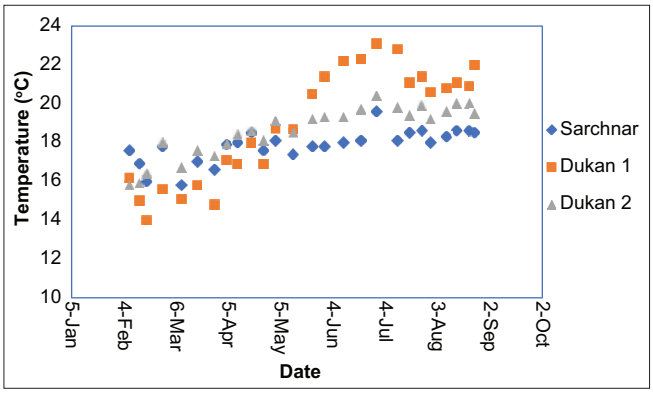

Fig. 2. Temporal variation of temperature.

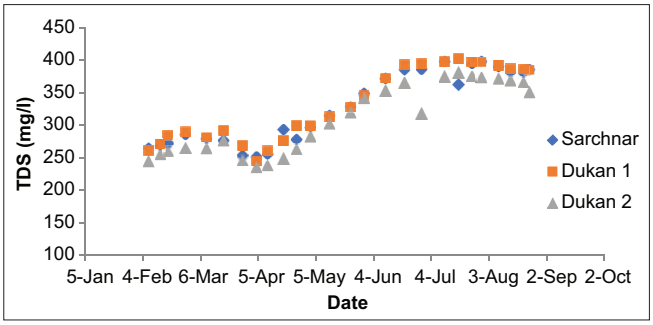

Fig. 3. Temporal variation of total dissolved solids.

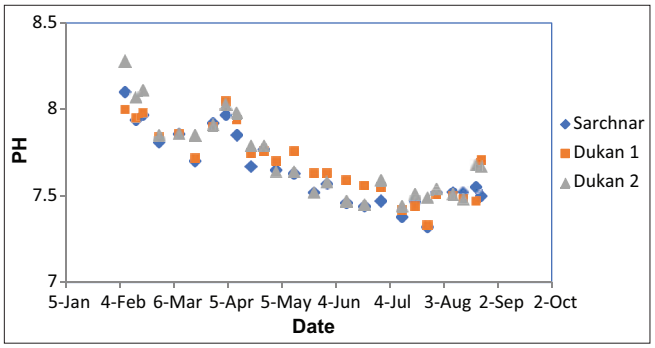

Fig. 4. Temporal variation of PH.

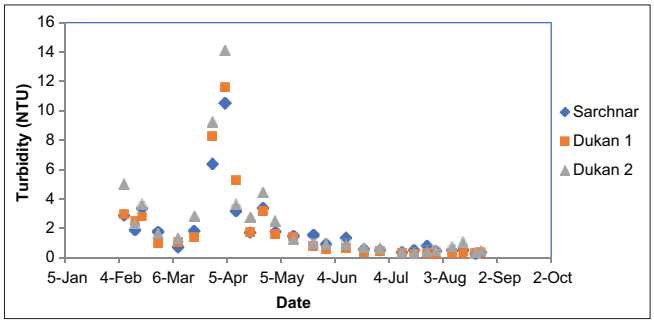

Fig. 5. Temporal variation of turbidity.

shows that the results of PH for the three sources were close, and the results were raised during the flood events occurred in February and March. The average value of PH for Sarchnar, Dukan 1, and Dukan 2 was 7.7, 7.66, and 7.72, respectively. As the alkalinity has a high correlation to pH through buffering water against excessive change of PH, the same trend of pH is observed in its plot against time.

Maximum permissible limit of total alkalinity according to the WHO standards is 600 mg/l. In the current study, total alkalinity with the range of 130–235 mg/l was recorded for all water samples. The value of total alkalinity was lower in rainy seasons than in the arid one. Furthermore, the results of Sarchnar water samples were close to Dukan 1, but Dukan 2 water samples recorded lower results.

Turbidity as one of important parameter for drinking water should be under 5 NTU, the average results of turbidity were within the standards which were 1.9 NTU for Sarchnar and Dukan 1 and 2.43 NTU for Dukan 2. However, the value of turbidity was raised significantly to the highest value which was 10.5, 11.6, and 14.1 NTU for Sarchnar, Dukan Lane 1, and Dukan lane 2, respectively, because of the storm occurred in the beginning of April. In summer season, the value of turbidity reached the minimum value of 0.26 NTU and it remains around this value until the end of the study without significant change (Fig. 5).

Fig. 6 shows that the amounts of free chlorine residual in the collected samples from Dukan 1 have the lower values ranged between 0 and 0.5 mg/l, samples from Sarchnar ranged between 0 and 1 mg/l and Dukan 2 have the higher values (0.5–2 mg/l). Because the Dukan 2 source feeds water to the far neighborhoods in the city, the amount of free chlorine was higher than the other sources so as to insure obtaining safe water to the residential. The results of free chlorine residual concentration in the water samples were ranged between 0.11 and 1.96 mg/l which were within the recommended value in the WHO standards [19] and Iraqi water specifications [26].

The mean concentration of ammonia and ammonium in this study was very low (0.02 and 0.03 mg/l) for all water sources which were below the standard limit (1.5 mg/l). The results of ammonia and ammonium for the three sources were close to each other during the period of the study except in several data for Sarchnar which were higher than the other with the value around (0.08 mg/l). Fig. 7 shows temporal variation of ammonia in the three sources of water.

According to the drinking water quality standards, the limit of hardness should be within the limit of 500 mg/l. The value of hardness for all water samples was between 120 and 200 mg/l $CaCO_3$ which was below the permissible value. Fig. 8 represents that the range of hardness for the water samples from Sarchnar and Dukan1 was close and the average range was around 150 mg/l $CaCO_3$. The average value of hardness in Dukan 2 was 145 mg/l $CaCO_3$.

In this study, the average value of calcium concentration for the three sources was around 60 mg/l which was within the recommended limit (75 mg/l). As shown in Fig. 9, most of the calcium concentration results for the three sources were close and all values during the study were below the standard limit except in two data recorded for Dukan 1 water samples which exceeded the standard limit with the value of 78 mg/l.

According to the WHO guidelines for drinking water standards [19], fluoride concentration should be under 1.5 mg/l. In the current study, fluoride mean value was 0.21 mg/l for all sources of drinking water. At the beginning of the study, minimum results were recorded which were sometimes near zero. The value of fluoride concentration continued rising until August, this rising was continued in Sarchnar water samples but Dukan 1 and 2 water samples started falling until the end of the study (Fig. 10). The fluoride level all the time is below the recommended level of 0.7 mg/l for healthy teeth enamel.

Minimum observed that results of chloride for the three water sources during the study were recorded in winter season which were between 0 and 1mg/l. Most of the chloride values were ranged between 1 and 10 mg/l, but in May 12 the concentration of chloride for water samples from Sarchnar and Dukan 1 reached maximum value which was 18 mg/l and 15 mg/l, respectively (Fig. 11). The average value of chloride concentration in the study was 5 mg/l which was below the permissible value of 250 mg/l. In this study, the mean values of nitrate nitrogen and nitrate were 3.5 mg/l N and 15.6 mg/l NO_3, respectively, which were below the

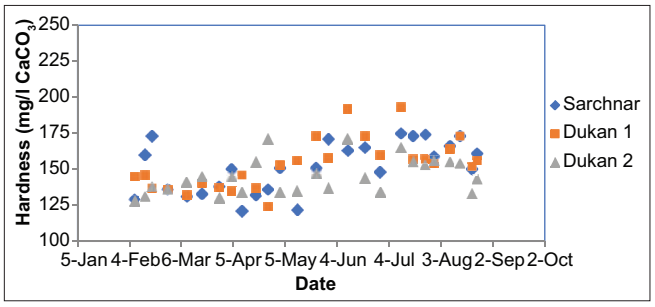

Fig. 8. Temporal variation of hardness.

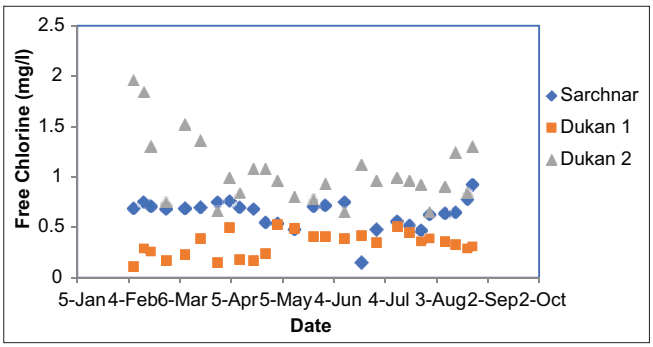

Fig. 6. Temporal variation of free chlorine.

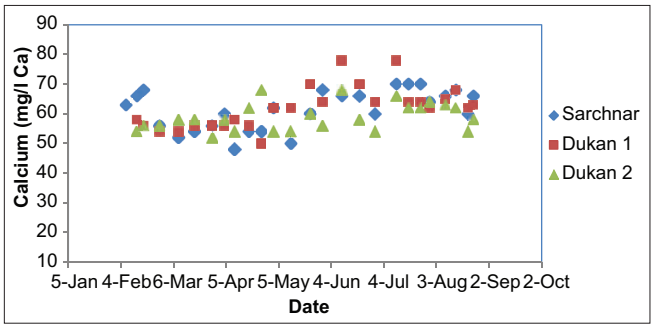

Fig. 9. Temporal variation of calcium.

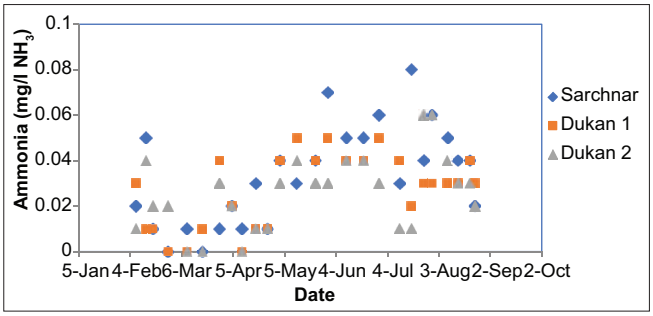

Fig. 7. Temporal variation of ammonium.

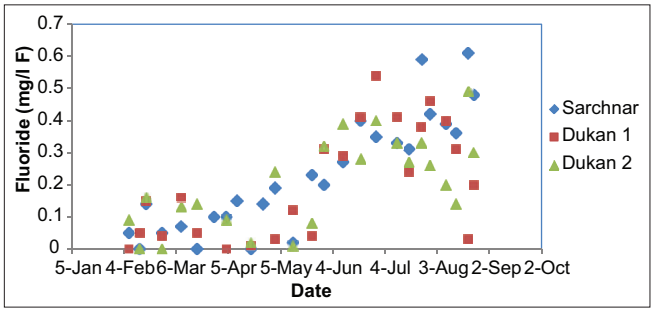

Fig. 10. Temporal variation of fluoride.

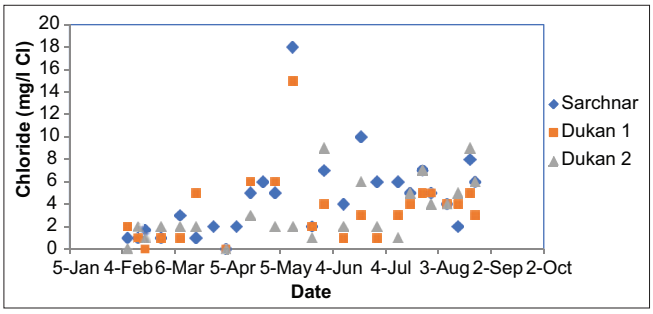

Fig. 11. Temporal variation of chloride.

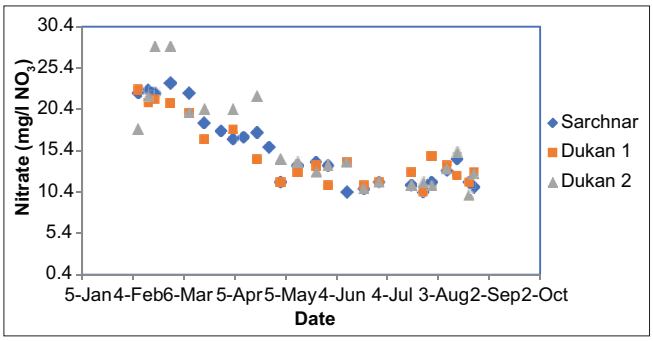

Fig. 12. Temporal variation of nitrate (NO_3).

permissible limits according to standards (10 mg/l of nitrate nitrogen and 50 mg/l of nitrate).

Fig. 12 shows that the results of nitrate concentration in the three water sources are similar starting from highest value in the winter season and then decreasing to the lower values in summer season. The reason of increasing the amount of nitrate during the rainy season may be due the agricultural runoff which is one of the main sources of occurring nitrate in water [19], and [21].

4. CONCLUSIONS

From the results of this study, it can be concluded that, in general, the quality of water at the sources of Sulaimani City is suitable for drinking purpose, because the analyzed physical and chemical parameters of water samples during the period of the study were mostly within the standards recommended by the WHO guidelines [19] and Iraqi specifications [26]. However, there was some turbidity exceedance of the permissible level during flood events and high rainfall events. Furthermore, the level of fluoride exists in the water is below the standard level for healthy teeth which is between 0.7 mg/l and 1.5 mg/l. Even though, the Sarchnar source is natural spring and different from the other sources, but high differences were not observed in the results of measurements between the sources. This may be because of huge amount of water in lake this year due to the significant high amount of rainfall during the period of study which can dilute contaminants in the impounded water. Finally, this study recommends addition a pretreatment unit to be used during flood events to reduce the turbidity and addition of fluoride to the drinking water to restore and strengthening the users' teeth enamel. Furthermore, it is crucial and important for future researches and water quality monitoring to include heavy metal and disinfection water quality parameters.

REFERENCES

[1] C. Prakirake, P. Chaiprasert and S. Tripetchkul. "Development of specific water quality index for water supply in Thailand". *Songklanakarin Journal of Science and Technology*, vol. 31, no. 1, pp. 91-104, 2009.

[2] A. H. M. Alobaidy, H. S. Abid and B. K. Maulood. "Application of water quality index for assessment of Dokan lake ecosystem, Kurdistan region, Iraq". *Journal of Water Resource and Protection*, vol. 2, no. 9, p. 792, 2010.

[3] A. C. AL-Shammary, M. F. AL-Ali and K. H. Yonuis. "Assessment of Al-Hammar marsh water by uses Canadian water quality index (WQI)". *Mesopotamia Environmental Journal*, vol. 1, no. 2, pp. 26-34, 2015.

[4] E. D. Ongley. Water quality management: Design, financing and sustainability considerations-II. In: Invited Presentation at the World Bank's Water Week Conference: Towards a Strategy for Managing Water Quality Management. World Bank, United States, 2000.

[5] A. Sargaonkar and V. Deshpande. "Development of an overall index of pollution for surface water based on a general classification scheme in Indian context". *Environmental Monitoring and Assessment*, vol. 89, no. 1, pp. 43-67, 2003.

[6] K. Mosimanegape. Integration of Physicochemical Assessment of Water Quality with Remote Sensing Techniques for the Dikgathong Damin Botswana. Master's Dissertation, University of Zimbabwe, Harare, 2016.

[7] H. J. Vaux. "Water quality (book review)". *Environment*, vol. 43, no. 3, p. 39, 2001.

[8] A. Parparov, K. D. Hambright, L. Hakanson and A. Ostapenia. "Water quality quantification: Basics and implementation". *Hydrobiologia*, vol. 560, no. 1, pp. 227-237, 2006.

[9] A. H. M. Alobaidy, B. K. Maulood and A. J. Kadhem. "Evaluating raw and treated water quality of Tigris River within Baghdad by index analysis". *Journal of Water Resource and Protection*, vol. 2, no. 7, pp. 629, 2010.

[10] H. C. Kataria, M. Gupta, M. Kumar, S. Kushwaha, S. Kashyap, S. Trivedi and N. K. Bandewar. "Study of physico-chemical parameters of drinking water of Bhopal city with reference to health impacts". *Current World Environment*, vol. 6, no. 1, pp. 95-99, 2011.

[11] H. Q. Khan. Water quality index for municipal water supply of Attock city, Punjab, Pakistan. In: Survival and Sustainability. Springer, Berlin, Heidelberg, 2010.

[12] M. Alsawalha. "Assessing drinking water quality in Jubail industrial city, Saudi Arabia". *American Journal of Water Resources*, vol. 5,

no. 5, pp. 142-145, 2017.

[13] N. Othman, T. Kane, and K. Hawrami. Environmental health assessment in Sulaymaniyah city and Vicinity. Tech Report, United States, 2017.

[14] H. M. Issa and R. A. Alrwai. "Long-term drinking water quality assessment using index and multivariate statistical analysis for three water treatment plants of Erbil City, Iraq". *UKH Journal of Science and Engineering*, vol. 2, no. 2, pp. 39-48, 2018.

[15] F. Salih, N. Othman, F. Muhidin and A. Kasem. "Assessment of the quality of water in Sulaimaniyah city, Kurdistan region: Iraq". *Current World Environment*, vol. 10, no. 3, pp. 781-791, 2015.

[16] D. A. M. Barznji and D.G.A. Ganjo. "Assessment of the chemical water quality in Halabja-Sulaimani, Kurdistan region of Iraq". *Asian Journal of Water Environmental and Pollution*, vol. 11, no. 2, pp. 19-28, 2014.

[17] Y. A. Hamaamin. "Developing of rainfall intensity-duration-frequency model for Sulaimani city". *Journal of Zankoy Sulaimani*, vol. 19, no. 3-4, p10634, 2017.

[18] S. M. Razuki and M. A. Al-Rawi. Study of some physiochemical and microbial properties of local and imported bottled water in Baghdad city. *Iraq Journal of Market Research and Consumer Protection*, vol. 2, no. 3, pp. 1-7, 2010.

[19] World Health Organization. Guidelines for Drinking-water Quality: First Addendum. 4th ed. World Health Organization, Geneva, 2017.

[20] C. E. Boyd. Water Quality: An Introduction. 3rd ed. Springer, Berlin, Germany, 2015.

[21] Environmental Protection Agency. Parameters of Water Quality: Interpretation and Standards. Environmental Protection Agency, United States, 2001.

[22] M. V. Ahipathy and E. T. Puttaiah. "Ecological characteristics of Vrishabawathi River in Bangalore (India)". *Environmental Geology*, vol. 49, no. 8, pp. 1217-1222, 2006.

[23] H. Boyacioglu and H. Boyacioglu. "Surface water quality assessment by environmetric methods". *Environmental Monitoring and Assessment*, vol. 131, no. 1-3, pp. 371-376, 2007.

[24] World Health Organization. Guidelines for Drinking-water Quality: Incorporating First and Second Addenda. 3rd ed., Vol. 1, World Health Organization, Geneva, 2008.

[25] L. Apha, A. Clesceri and A. Greenberg. Standard Methods for the Examination of Water and Wastewater. 20th ed. American Public Health Association, Washington, DC, 1998.

[26] ICSD, WCL. Iraqi Criteria and Standards for Drinking Water, Chemical Limits. ICS: 13.060.20, IQS: 417, 2nd Update 2009 for Chemical and Physical Limits. ICSD, WCL, United States, 2009.

ORIGINAL RESEARCH ARTICLE UHD JOURNAL OF SCIENCE AND TECHNOLOGY

Adaptive Software-defined Network Controller for Multipath Routing based on Reduction of Time

Hemin Kamal[1,2], **Miran Taha**[2,3]

[1]*University of Human Development, College of Science and Technology, Department of Computer Science, Sulaymaniyah, Iraq,* [2]*College of Science, Department of computer, University of Sulaimani, Sulaymaniyah, Iraq,* [3]*Integrated Management Coastal Research Institute, Universitat Politécnica de Valencia, Valencia, Spain*

ABSTRACT

Software-defined network (SDN) is a new paradigm in the networking that makes a programmability and intelligence the networks. The main SDN characterize is separating network management (control plane) from the forwarding device (data plane). SDN logically centralizes the network with the programmable controller which collects global knowledge about the network. The SDNs can improve the performance of the routing packets in the networks because of agility and the ability to create a policy for a driven network. In the multipath routing, the SDNs controller is responsible to calculate the routes of optimum path and alternative path wherever a link is failed. However, a high delay time calculation of selecting optimum and alternative paths in multipath routing by the SDN controller is observed in the recent investigations. In this paper, we propose an efficient algorithm for SDN multipath routing controller. The mechanism of the proposed approach calculates the best path from the source to the destination which is based on using adaptive packet size and observing network link capacity. The proposed algorithm considers reducing delay time of the link handling when the flow traffic switches from the main path to the recovery path. As a result, this approach is compared to some state of the arts according to the delay time of choosing the best path and alternative paths in a given network topology. SDN based on the proposed algorithm consumed approximately 1 ms for selecting recovery routes. On the other hand, the proposed algorithm can be integrated to an SDN controller which provides better consolidation of transmission for sensitive applications as video streaming.

Index Terms: Adaptive algorithm, Multipath routing, Mininet, Software-defined network, Simulation

1. INTRODUCTION

The universal connectivity network that we use today is built on different network topology such as the Internet of Things, data center network, and mobile caller network provides pervasive global coverage on a scale [1]. In addition, the multipurpose network which uses different types of the data video stream, Voice over Internet Protocol, User Datagram Protocol, and Transmission Control Protocols flow of data is significantly more cost efficient than specialized or dedicated network solutions [2]. There is an amount of data through the network with the very difficult process of routing which is hugely important in networking. Data should be transferred continuously without any interruption which is one of the most performed functions of the network [3].

The modern network usually suffers link failures and topology changes. Link failure is a common phenomenon in computer networks that may occur anytime due to network configuration change, network device error, power outage, or many other reasons and results in the disruption of service distribution. This disruption results in unimaginable losses in critical networks [4]. Multipath routing protocols could be addressing

Access this article online

DOI:10.21928/uhdjst.v4n2y2020.pp107-116 E-ISSN: 2521-4217 P-ISSN: 2521-4209

Corresponding author's e-mail: Hemin Kamal, University of Human Development, College of Science and Technology, Department of Computer Science, Sulaymaniyah, Iraq; College of Science, Department of computer, University of Sulaimani, Sulaymaniyah, Iraq. E-mail: hemin.kakahama@uhd.edu.iq

Received: 05-09-2020 Accepted: 05-11-2020 Published: 15-11-2020

this problem. Thus, efficient algorithm should be presented to handle link failures to keep the flow of the interrupted networks. For handling link failure, network systems keep redundant links for each path so that in case of a link failure, the network systems may calculate a new backup path and keep the system uninterrupted. Keeping redundant links may create loops in computer networks [5]. On the one hand, the most problem of multipath routing is selecting the optimal path on the network and divide the traffic amongst the paths [6]. On the other hand, to overcome this limitation of traditional networks in handling link failure of critical networks, one possible solution can be software-defined network (SDN) which is a new paradigm in computer networking. SDN makes computer networks programmable and more manageable by separating the control and forwarding components of the network where the centralized SDN controller programs and manages the network devices (e.g., switches and routers) by secured communication channel [7]. The controller detects the link failure by receiving messages from the data plane and it can handle link failure both proactively and reactively [8]. In the reactive approach, the SDN controller provides alternative paths on-demand in the SDN switches which is time consuming. In the proactive approach, the controller installs redundant paths in the switches initially and the switches handle link failures locally by directing the flow to the alternative path [9].

In this paper, we propose an algorithm for SDN controller which based on using adaptive packet to calculate multipath routing. The algorithm chooses the optimal path from some available paths on the network. The parameters of the proposed algorithm include the shortest/longest path, link capacity (bandwidth), and number of the hops. Whenever flow of main path is down, the controller switched over the traffic from main to backup path in a short period of time.

The structure of this paper is organized as follows. We review some related works in section 2 while section 3 presents an introduction to the SDN architecture and comparing with the traditional network architecture. Therefore, section 4 explains the problem statements. Section 5 presents the proposed algorithm for multipath routing based SDN. Section 6 explains the experiments and the test results. Finally, the conclusion and future works are given in section 7.

2. RELATED WORK

Delay calculating routes in the SDN controller are one of the main issues. There are numerous articles that investigated how the SDN controllers were decided to select the optimum path and alternative paths. However, the issue investigated in both academic and industrial areas. In this section, we review some related works in detail to explain the existing gaps regarding the delay time of calculating paths by the SDN controllers.

Sharma *et al*., 2011 [10], detected the decision time problem for multipath routing which are hard timeout and idle timeout while the links failed or topology changed. They proposed the fast link restoration mechanism on multipath routing architecture. The proposed mechanism based on the new Address Resolution Protocol (ARP) request and the controller able to restore the path to an alternative path within 12 ms regardless of any timeout of traffic flow. This mechanism decentralized because based on the ARP request on the local switch.

Sgambelluri *et al*., 2013 [11], determined the link failures in the SDN, designed the mechanism to enhance the OpenFlow architecture to protect the segment on the network. The novel mechanism provides an effective network by providing the different priorities of resource utilization for main path and backup path based on OpenFlow segment protection. The presented mechanism implemented the OSP scheme enabling fast recovery in networks composed of OpenFlow-based Ethernet switches. The OSP scheme does not require a full-state controller and, on failure, it does not involve the controller in the recovery process. The implementation results showed that the controller can decide to active the backup path on around 64 ms.

Dorsch *et al*., 2016 [12], outstanding the technical issue in link recovery time in dynamic topology. They suggested the technique for improving fault tolerant to link failure based on the SDN controller. The controller use a centralized approach for both failure detection and traffic recovery bidirectional forwarding detection and OpenFlow allow to saving the delay time on switching the connection. Bidirectional forwarding detection protocol for local link failure is detected between two switches, the drawback of this technique is the negotiation module needs to spend a time period in notifying the failure detection result, the proposed mechanism needs 4.5 ms to change the path to another path.

Lin *et al*., 2016 [13], detected the link failure and link conduction problem in datacenter network link congestion which occurs when a link is carrying too much data. A typical effect is packet loss which caused an actual reduction in network throughput. They proposed the mechanism for link handling for SDN enabled data center network for the traffic recovery. The SDN controller calculates the main and backup path based on a link weighting function. The experiment results showed the recovery time <100 ms. The

proposed mechanism designed for data center network and they did not address the scalability issue.

Dloryhu *et al.*, 2016 [14], focused on controller response time under normal consideration and presence the outage, which is generally impact by network latency. They presented the mechanism to deal with link fail handling issues. Depend on this mechanism, controller pre-establishes the multipath routing from the source to destination. When the current path downed on the SDN, the controller can switchover the traffic to another active path averagely in 40 ms.

Aldwyan and Sinnott, 2019 [15], investigated on the delay issue on multipath routing mechanism which raised a problem to sensitive application. They introduced the new approaches to improve the responsibility of the applications to provide latency aware of the failed link. They proposed an algorithm for path selection in the datacenter based on the SDN. Their work utilizes container technologies and microservice-based application architecture. The approach autonomously generates latency aware failover capabilities by providing deployment plans for micro services and their redundant placement across multiple datacenter networks, with the goal of minimizing the amount switchover time as per implementation result the link handling time reduced to 40 ms.

Hsieh and Wang, 2019 [16], determined the timeout issue for SDN multipath routing when the main link failed and the packet traffic not arrive to destination on time. The authors proposed an efficient mechanism to handle link failure detection and recovery. They explained an efficient mechanism to handle link failure detection and recovery. The proposed method based on a multicontroller in SDN architecture. The topology contains local and global controller to decide to find the best path by calculating the link cost weight based on switch controller propagation delay and load standard division. The experiment results in the implemented mechanism can handle the failed link only 7 ms of delay time.

Therefore, the proposed algorithm for the SDN controller is different from the aforementioned approaches, which uses adaptive packet size to select recovery routes in a given network topology further it reduces that the delay time is taken to select the paths compared to those recent works.

3. STATEMENT OF THE PROBLEM

Routing algorithms and protocols are one of the most important processes of selecting routes in static and dynamic networks. Although internet services utilized by end users, the users are suffered due to inefficient designation of routing algorithms and the quality of service parameters such as bandwidth, delay, packet loss, and jitter. Further, SDN controllers can be programmed to control the packets flows and this programmable approach used to provide multipath routing, however, the controller decided to specify a path to integrate the transmission. The decision process of multipath routing takes time, which called delay time, this time can be dynamic when the controller selects main path and recovery path for the routing packets. However, the problem becomes complex when the controller used insufficiently designed algorithms; thus, the delay time to retrieve the paths to end user takes longer time and end users unsatisfied with the service. For instance, one of the issues is calculating link capacity based on packet size and number of the packets, however, insufficient packets also introduced inaccurate path selection. It is important to take into consideration the number of parameters to design an efficient algorithm for the SDN controller. How the adaptive packet can be selected to test the capacity of the links and how long the sniffing of link capacity needed. To answer those questions, we design an adaptive algorithm for the SDN controller which can reduce the delay time of path selection.

4. SDN ARCHITECTURE

In the traditional network, control plane routing protocols have been implemented together with data plane forwarding functions, monolithically, within a router as depicted in Fig. 1. In network communication, the data is transmitted from the source to the destination and vice versa. Generally, forwarding and routing processes are two important functions in the network layer [17]. The local process of the router executes the delivery of arrived packets from the input interface to the output interface. This is a simple hardware-based operation and takes a short period of time which can be finished on a few nanoseconds [18]. Another function is routing which is a network-wide process to provide end-to-end packet delivery from the source to destination. Routing process is more complex than forwarding and it takes a long time typically about the seconds, as well it implemented in software [19]. The routing algorithm calculates the paths from source to destination and it finds the best path to integrate the routing. Conventionally, a routing algorithm runs in each and every router, and both forwarding and routing functions. The routing algorithm function in one router communicates with the routing algorithm function in other routers to compute the values for its forwarding table. The forwarding table

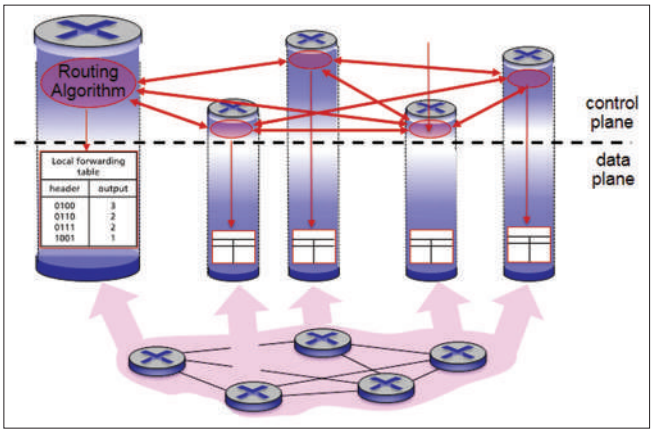

Fig. 1. Forwarding table in traditional networks.

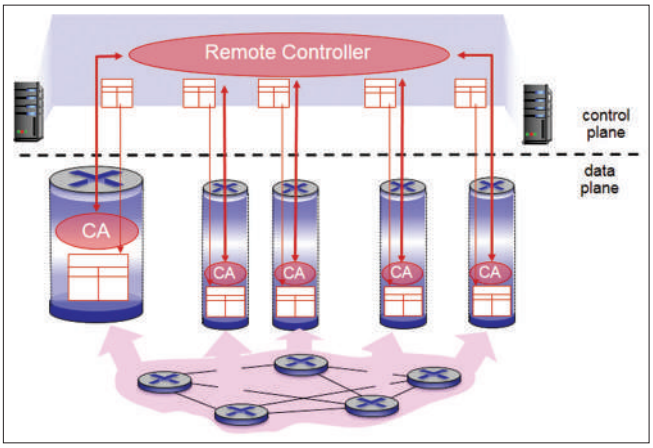

Fig. 2. Forwarding table in software-defined networks.

contains the values of the outgoing link interface to decide which packet should be forwarded [20]. SDN makes a clear separation between the data and control planes, implementing control plane functions in a separate "controller" service that is distinct, and remote, from the forwarding components of the routers it controls. The routing device performs forwarding only, while the remote controller computes and distributes forwarding tables [21]. The routers and the remote controller communicate by exchanging messages containing forwarding tables and other pieces of routing information. The control plane approach is at the heart of SDN, as shown in Fig. 2, where the network is "software defined" because the controller that computes forwarding tables and interacts with routers is implemented in software [22].

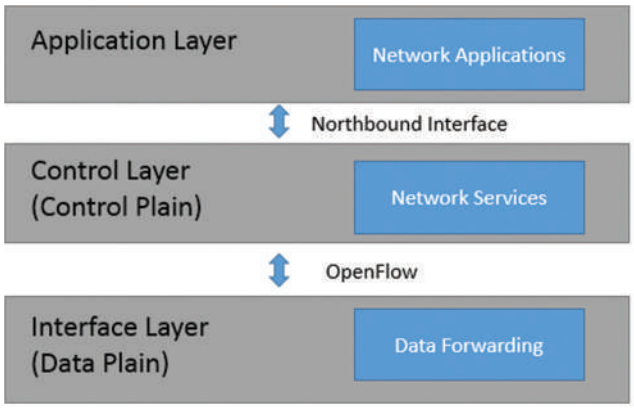

Fig. 3. Architecture of software-defined networks

The data plane also is a part of a network its functionality only forwards the network packets instructed by the controller. This data plane cannot take any forwarding decision [23]. The communication between the data plane and the control plane is performed by OpenFlow messages. The secured channel is used to connect the switches to the controller [24]. Fig.3 illustrates the general description of the SDN layered architecture. The architecture generally compromised three different layers, the button layer is the infrastructure layer that is where the network forwarding equipment, it relies on new layer the control layer to provide it with its configuration and its forwarding instructions, the middle layer or control layer is responsible for configuring that infrastructure layer it does that by receiving service requests from the third layer (the application layer), the control layer maps the service requests on to the infrastructure layer in the most optimal manner possible dynamically configuring that infrastructure layer, the third layer where cloud (internet) applications or management applications place their demands for the network on to the control layer. In SDN, each of these layers and the application program level interfaces between them is designed to be open and provides agility by logically centralizing the full configuration of the networks.

5. PROPOSED ALGORITHM

In this section, the description of the proposed algorithm, select the main and the backup multipaths, and choosing adaptive packet size to reduce delay time of the multipath routing, will explain in details. The decision of path selection in multipath routing is one of the most important parts for the SDN controller, the application layer multipath routing algorithm should be designed in SDN to provide adequate path selection with minimum cost. To provide best path selection, we propose an algorithm which uses important metrics to calculate the paths. The proposed mechanism for multipath routing describes the simple method to select a path set for multipath OpenFlow controller (OFC), which calculates the best main and backup path from source to

destination, it is based on topology discovery information from the controller, as shown in Fig. 1.

The SDN controller's algorithm chooses one best path as the main path, although two important metrics are considered to select the main path, respectively, included; availability of the links bandwidth and the paths length (number of hops). The mechanism calculates the link by sending series of adaptive packets with minimum cost. The controller's algorithm sets the main and backup path in the corresponding table of the individual OpenFlow switches. If there is no failure during the transfer, the incoming packet uses the main path to transfer flow to the destination. When the main path is failed, the OFC obtains notification from the OpenFlow switch of the failure and the controller automatically switches the flow to the backup path to transfer the packet to the destination. The description of proposed system algorithm is shown in Fig. 4.

To manipulate and develop multipath mechanism that can reduce network failure, the configured backup path traces the existence of the main path record in the flow table. Under normal conditions, the backup path stays in standby mode. When there is no any failure or any change of network circumstance, the timeout of selected backup path is automatically expired, and as soon as the recording is forcibly removed from the flow table, the backup path will be inactive mode and continue to run traffic, which guarantees the minimum network failed time.

The mechanism implemented using the following algorithm. The proposed algorithm used depth first search to achieve the feature of finding the multipath between two nodes.

After finding all the paths between source and destination, depth first search path finding algorithm explores possible vertices in a graph by finding the deepest vertex in the graph

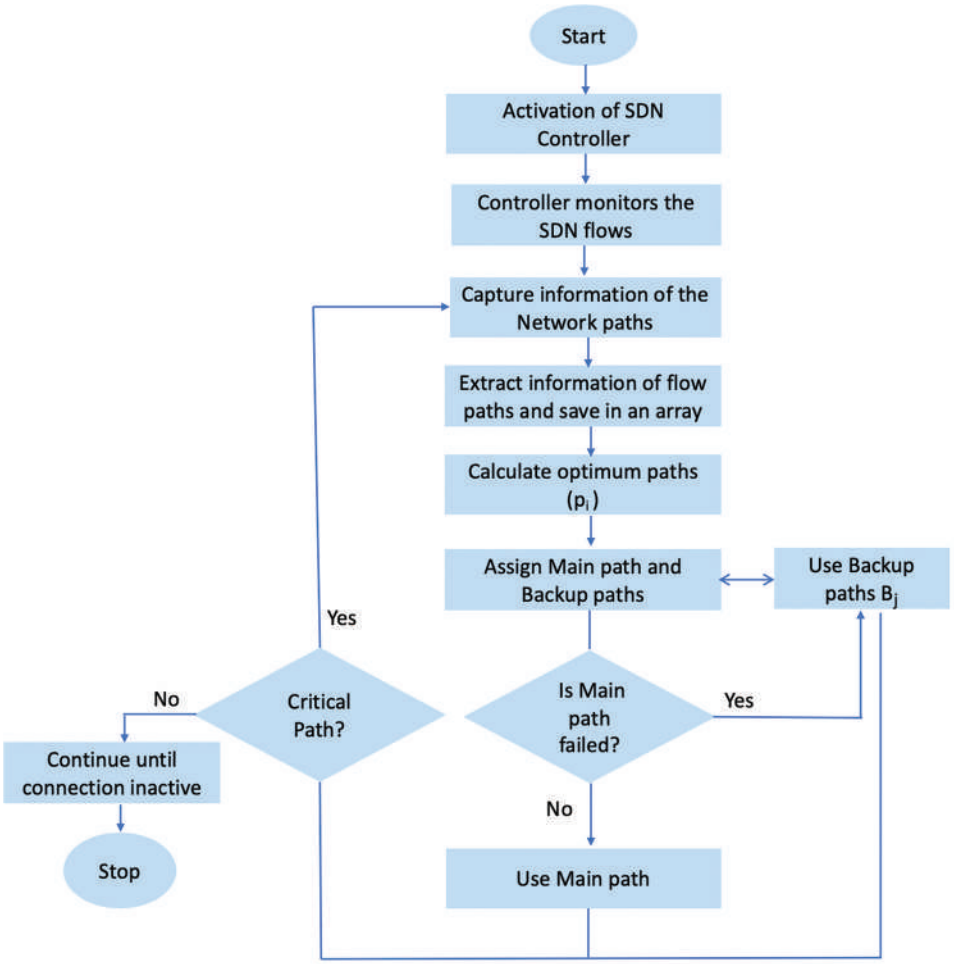

Fig. 4. Description of proposed algorithm function.

first before it backtracks to find other possible vertices using a stack also evaluate those paths to find the best path for the transmission. This part is rather simple first calculate the link cost between two nodes, logically a packet might be having more delay in passing throw lower link capacity than higher link. Respectively, it will take less time in crossing a higher bandwidth link than a lower bandwidth link. The proposed algorithm uses this logic to calculate the cost. Higher link capacity has a lower cost. Lower link capacity has a higher cost. Proposed algorithm uses this formula to calculate the cost as explained in Equation (1).

$$Cost = \left(\frac{Refereces\ link\ capcity}{Interface\ link\ capacity\ in\ bps}\right) \quad (1)$$

Reference (link capacity) bandwidth was defined as arbitrary value in SDN which define as Fast Ethernet uses 100 Mbps (10^8) bandwidth as reference bandwidth. With this bandwidth, our equation would be (Cost = 10^8/interface bandwidth in bps). For instance, if the link capacity is 10 Mbps, the link cost is (10) and think capacity is 100 Mbps, the link cost equal 1, then adds the link cost of the path to get the cost and get the optimal according to the cost of the path. Considering the OSPF, calculating the interface cost is an indication to compute maximum number of the packets across a certain interface. The cost of an interface is inversely proportional to the bandwidth of that interface. A higher bandwidth indicates a lower cost. There is more overhead (higher cost) and time delays. After that, the controller defined property of packets for every switch to execute specific actions such as forward or drop the packets. After getting all available paths, controller adds them into the SDN switch. The state of the selection path algorithm configuration is external to OpenFlow. The proposed algorithm based on bucket weights which provide equal load sharing. When a specified port or link goes down instead of the packet dropping, controller decides to switchover the traffic to backup path. This process reduces the disconnection time of a downed link or switch. Equation (2) explains the weight calculation for the proposed algorithm.

$$weight = \left(\left(1 - \frac{pw}{\sum pw}\right) * 10\right) \quad (2)$$

Where *Weight* represents the bucket weight and *pw* is cost of path. Furthermore, detail of the Pseudo code is explained in Algorithm 1. The link failure handling with SDN is an emerging concept, different fast failover mechanisms have been proposed as explained in the state of the art. We propose

ALGORITHM 1: Multipath routing algorithm in SDN

```
Input: Host x, y = h1,h2,h3,...h_n, Data transfer between Host x and
Host y
Output:
1: SDN_C → SDN Controller
2: N → Switch Number (SrcSwitch, DesSwitch)
3:Cost → 0
4:Datapath →Path[]
5: While SDN_C do:
6:For j in N do
7: j.setFirstSwitch (SrcSwitch)
8: While (nextSwitch! = DesSwitch)
9:For i in range(len(path) - 1):
10:Cost += get_link_cost(path[i], path[i+1])//calculate link cost
11:Return cost
12:End for
13: nextSwitch= Random(N)
14: If (nextSwitch in datapath)
15: nextSwitch = Random(N)
16: Else
17: j.append(nextSwitch)
18: End if
19:End while
22:Path. append(j)
23:End for
24: OptPath = getLestCost(datapath) //Evaluate the link cost and
    choose best path
26: End while
27:ReturnOptPath
```

adaptive failover mechanism for the controller of SDN to make it more efficient and applicable when a delay of few milliseconds can be challenged. The proposed mechanism for handling path failures and restoration involves the controller calculates all available paths from the source to the destination and installs the flow entries on the switches. The controller contains information about the complete topology. In case of any path or link failure, a switch informs the controller. When the controller is notified about a path or link change, controller checks each calculated path P whether it is affected by the link change or not. If any path is affected, the transition rate adaptively decreases by the controller, further, the controller changes the current link to the backup link considering the minimum rate. It also checks that if the flow adds to the entries in OpenFlow switches for older path. If so, then, the controller removes all flow entries from OpenFlow switches for older path and adds in the switches for the new path. The connection of hosts might be recovered in short time and controller overloading also reduced.

6.EXPERIMENTS AND TEST RESULTS

6.1.Testbed Description

We used different tools for conducting our experiments, creating the experimental network, implementing multipath

routing mechanisms, observing the network's behavior, and calculating the delay. We install the SDN environment using virtualization install Ubuntu 18.04 which is one of newest Ubuntu version to implement SDN scenarios [25]. Mininet has been used for implementing the research in SDN and OpenFlow [26]. We can run unmodified code on virtual hardware on a simple PC using Mininet to simulate the SDN and make a centralized network with centralized controller which can use both command line and API [27]. For writing our scripts, we use the API provided by Ryu SDN controller for multipath routing. Furthermore, ping tool is used to observe the path of the packets. The ping is common and quick tool to measurement the latency and how long it takes one packet to get from source to destination [28]. This time measured by the local clock in the pinging device, from the sending the request to get reply. The interval time between each packet is 1 ms and the default packet size is 56 byte with 8 byte from the packet header. In addition, we use VLC application to generate the video streaming which is very sensitive traffic through the network [29]. To apply the tests, we use a workstation with these characteristics; HP workstation, processor: 2, 4 GHZ Core i7, Memory: 8 GB, graphics card: Nvidia 1 GB, and Hard disk: 500 GB.

6.2.Experiments

To achieve our goal of implementing the multipath routing and reduce the link handling time in SDN environment using OpenFlow protocol and flow tables, we implement the proposed algorithm as described in Section 5. Therefore, we apply different experiments to evaluate the proposed algorithm, we demonstrate that our system performs using proof of concept tests to manifest the controller which can find the best path from some available path on the network and the controller can handle the link failed in shortest time without any packet lost. Therefore, to show accuracy and efficiency of the proposed algorithm in the test results, we provide a video streaming test, the videos are streamed over VLC application from source to destination using multipath routing. The received video compares to the original one to realize that how link handling is affected on the quality of the videos.

6.2.1. Network topology

The scenario tested for the multipath network topology. We implemented the SDN using python script with the APIs of Mininet and Ryu to create the data plane and the controller. The network topology consists of two hosts' h1 and h2 with the IP address 10.0.0.1 and 10.0.0.2, respectively. The network topology provided six switches such such as s1, s2, s3, s4, s5, s6, s7, and s8. The switches are enabled with OpenFlow version 1.3 and one remote SDN controller c0. There are seven available paths between the hosts. The fast path capacity is10, 20, 30, 40, 50, 60, and 70 Mbps. This simple scenario is used to observe that if the presented solution is working correctly, as well as to observe the effect of the parameter values on the proposed algorithm. In addition, Fig. 5 depicts the general description of the proposed network topology to find and calculate the link handling time.

6.2.2. Multipath routing based on video streaming

In this experiment, we apply video stream test on the implemented SDN topology not only to evaluate network performance of different network services but also to determine the network path which the controller detects the traffic of the links throughout the network. In this test, we use VLC application to provide video streaming from h1 as a video stream server and sending the video stream (broadcast) to the network and h2 receives the video stream as a client. The result of this experiment showed that the link handling time of streamed video traffic from the main path to backup path do not make any effect on the video stream service or frame frozen from client side and the video streaming could be transferred through the network without any delay or interruption. Therefore, in the another test, the video stream is transmitted over the network, the main link is down manually and monitoring the flow traffic to observe that the controller's activity, the controller flows the traffic from the fast path to slow path (compared with each other) without any disruption in the video streaming. Fig. 6 explains the change of the traffic strategy path from the proposed multipath network topology.

6.2.3. Link handling time

In this scenario, we test with ICMP protocol between h1 and h2 with different packet size (32, 64, and 128 bit) (8-bit header in each packet and the remaining are datagram) and time interval (0.5, 1, and 2 ms). The experiment results are stored in text file. In this experiment, the main path is downed in the special timestamp and we compare the time in this time stamp. The result presented in Table 1, in the first test,

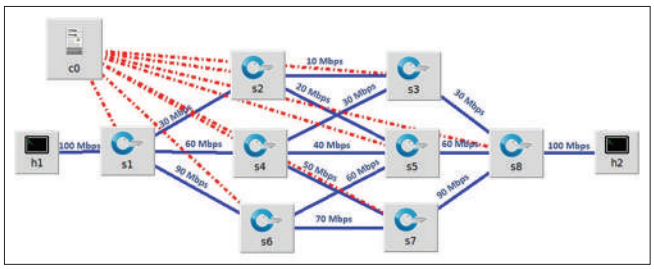

Fig. 5. Multipath network topology.

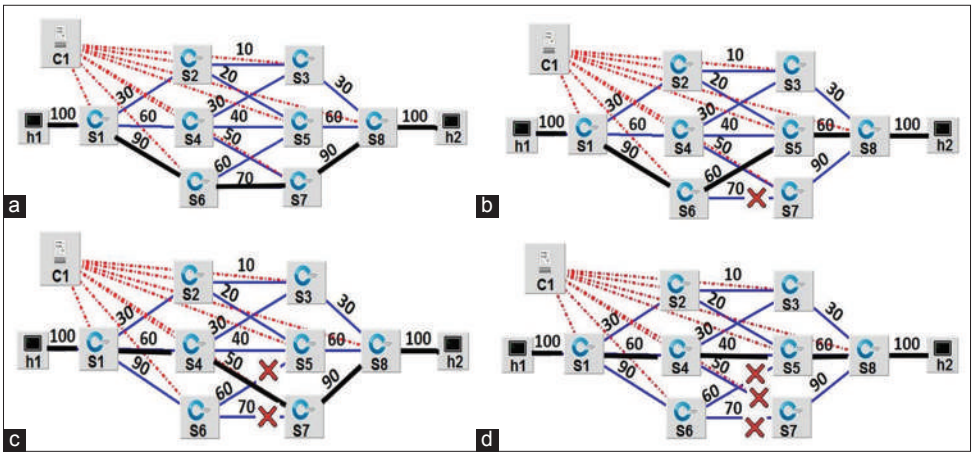

Fig. 6. Path failing and handling for the proposed network topology. (a) Flow over S1-S6-S7-S8, (b) flow over S1-S6-S5-S8, (c) flow over S1-S4-S7-S8, (d) flow over S1-S4-S5-S8.

TABLE 1: Relation between packet size and link handling time

Test No.	Packet size (Byte)	Interval(s)	Number of packets	Link handling time (ms)
1	32	0.5	20	0.82
2	32	1 (Default)	20	0.87
3	32	2	20	1.23
4	64 (Default)	0.5	20	1.14
5	64 (Default)	1 (Default)	20	1.28
6	64 (Default)	2	20	1.11
7	128	0.5	20	1.23
8	128	1 (Default)	20	1.26
9	128	2	20	2

the obtained result is 0.82 ms and I is a minimum delay time of link handling also the packet size for this test was 32 bit and time interval between two packets is 0.5 ms, which is the optimal data transfer for multipath routing.

The experiments results showed that the link handling time according to proposed algorithm approximately 1 ms which the proposed algorithm provides minimum link handling time compare to the papers mentioned on related work. Fig.7 illustrates the comparison the link handling time between proposed and related works algorithms.

6.2.4. Video stream test experiment

In this test experiment, we develop the testbed to be ready for streaming videos. Purpose of this test is to show time of path recovery between the proposed mechanism and traditional mechanism. We use 40 s of BigBuckBunny [30], with x.264 tool [31], the video is encoded to SD quality resolution further average of the streamed video bitrate approximately reaches to 1000 kb/s, the bitrate of the

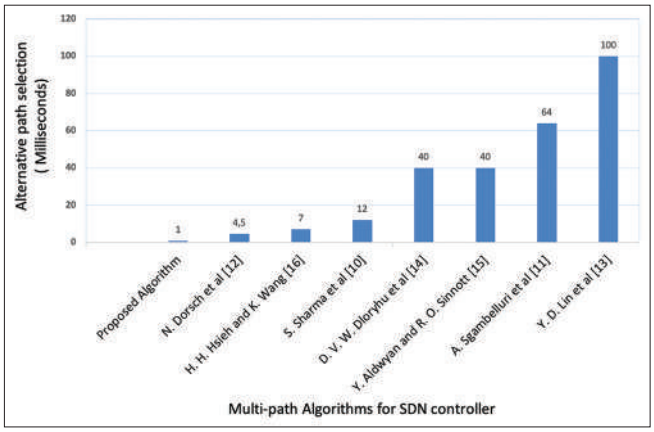

Fig. 7. Comparing the link handling time on proposed and related works algorithm.

video is dynamic which means the bitrate can be less or high than 1000 kb/s that is depended on the size of each i-frame. Therefore, time of path recovery of multipath routing is observed for streaming video between the sender and the receiver. When a path is failed, the recovery paths are used. To save the result experiment, we monitor the network throughput and bitrate of the streamed video, the information is captured in the entrance of receiver side and the information extracted for analyzing. As shown in Fig. 8, when the process initiated, the video is streamed to the receiver (end user), the received video at client side is received through VLC application. In this experiment, the current path is failed at the 10th s of video time, the programmed SDN controller is taken optimum path to integrate the transmission. The process through using proposed algorithm took 3 s, it means that the video is frozen 3 s at the client side also this value can be changed

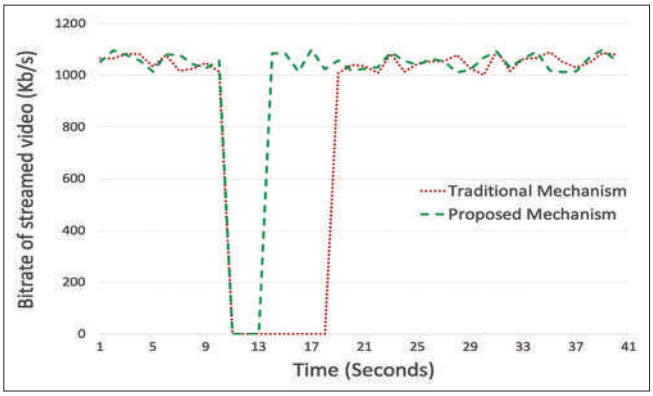

Fig. 8. Comparing path recovery time in proposed and traditional mechanisms.

according to the network conditions, however, in the traditional approach, the process takes 8 s, which means video is frozen for 8 s and the client is waited for a long time until the buffer's client application received entire packets. This test presents that using previous programmable SDN controller (traditional) for multipath routing makes end users unsatisfactory with sensitive applications. On the other hand, the proposed mechanism can provide better result and less time consumption for path recovering.

7. CONCLUSION AND FUTURE WORK

In this paper, we proposed a multipath routing algorithm for the programmable SDN Ryu controller using Mininet network emulator. The proposed algorithm is based on important metrics such as adaptive packet size and observing the network state. The SDN controller based on proposed algorithm decided to switch the flow traffic from the main path to optimal backup path when the main link is down. The proposed algorithm provided the efficient result for selecting routes for critical network infrastructures as well as for any network systems intolerant of delays. As a result, the experimental results showed that the link handling time approximately equal to 1 ms which is the best result presented than other recent researches as mentioned in the related works.

On the other hand, the proposed mechanism also provided better quality of experience for the sensitive applications like video streaming.

In future work, we plan to apply the reinforcement learning approach to the proposed algorithm to deploy an accurate decision of selecting recovery path.

8. ACKNOWLEDGMENTS

This work has done at the University of Sulaimani and Human Development University.

9. DECLARATION OF CONFLICTING INTEREST

The author(s) declared no potential conflicts of interest with respect to the research, authorship, and/or publication of this article.

REFERENCES

[1] M. Amiri, A. Sobhani, H. Al Osman and S. Shirmohammadi. "SDN-enabled game-aware routing for cloud gaming datacenter network". *IEEE Access*, vol. 5, no. c, pp. 18633-18645, 2017.

[2] M. Taha, L. Garcia, J. M. Jimenez and J. Lloret. "SDN-Based Throughput Allocation in Wireless Networks for Heterogeneous Adaptive Video Streaming Applications". In: *2017 13th International Wireless Communications and Mobile Computing Conference (IWCMC)*, pp. 963-968, 2017.

[3] P. Faizian, M. A. Mollah, Z. Tong, X. Yuan and M. Lang. "A Comparative Study of SDN and Adaptive Routing on Dragonfly Networks". In: *Proceedings of the International Conference for High Performance Computing, Networking, Storage and Analysis 2017*, 2017.

[4] S. N. Hertiana, Hendrawan and A. Kurniawan. "A Joint Approach to Multipath Routing and Rate Adaptation for Congestion Control in Open Flow Software Defined Network". In: *2015 1st International Conference on Wireless and Telematics (ICWT)*, pp. 1-6, 2016.

[5] W. Jiawei, Q. Xiuquan and N. Guoshun. "Dynamic and adaptive multi-path routing algorithm based on software-defined network". *International Journal of Distributed Sensor Networks*, vol. 14, no. 10, pp. 1-10, 2018.

[6] R. Baruah, P. Meher and A. K. Pradhan. *Efficient VLSI Implementation of CORDIC-Based Multiplier Architecture*. Springer, Singapore, 2019.

[7] F. Rhamdani, N. A. Suwastika and M. A. Nugroho. "Equal-cost Multipath Routing in Data Center Network Based on Software Defined Network". In: *2018 6th International Conference on Information and Communication Technology (ICoICT)*, pp. 222-226, 2018.

[8] M. F. Ramdhani, S. N. Hertiana and B. Dirgantara. "Multipath Routing with Load Balancing and Admission Control in Software-Defined Networking (SDN)". Vol. 4. In: *2016 4th International Conference on Information and Communication Technology (ICoICT)*, pp. 4-9, 2016.

[9] R. Wang, S. Mangiante, A. Davy, L. Shi and B. Jennings. "QoS-aware Multipathing in Datacenters using Effective Bandwidth Estimation and SDN". In: *2016 12th International Conference on Network and Service Management (CNSM)*, pp. 342-347, 2017.

[10] S. Sharma, D. Staessens, D. Colle, M. Pickavet and P. Demeester. *Enabling Fast Failure Recovery in OpenFlow Networks*. pp. 164-171, 2011.

[11] A. Sgambelluri, A. Giorgetti, F. Cugini, F. Paolucci and P. Castoldi. "Open flow-based segment protection in Ethernet networks".

Journal of Optical Communications and Networking, vol. 5, no. 9, pp. 1066-1075, 2013.

[12] N. Dorsch, F. Kurtz, F. Girke and C. Wietfeld. Enhanced Fast Failover for Software-Defined Smart Grid Communication Networks". In: *2016 IEEE Global Communications Conference (GLOBECOM)*, pp. 1-6, 2016.

[13] Y. D. Lin, H. Y. Teng, C. R. Hsu, C. C. Liao and Y. C. Lai. "Fast Failover and Switchover for Link Failures and Congestion in Software Defined Networks". In: *2016 IEEE International Conference on Communications (ICC)*, 2016.

[14] R. H. Hwang and Y. C. Tang. "*Fast Failover Mechanism for SDN-Enabled Data Centers*." International Computer Symposium, Chiayi, Taiwan, pp. 171-6, 2016.

[15] Y. Aldwyan and R. O. Sinnott. "Latency-aware failover strategies for containerized web applications in distributed clouds". *Future Generation Computing Systems*, vol. 101, pp. 1081-1095, 2019.

[16] H. H. Hsieh and K. Wang. "A Simulated Annealing-based Efficient Failover Mechanism for Hierarchical SDN Controllers". In: *IEEE Region 10 Annual International Conference, Proceedings/ TENCON*, pp. 1483-1488, 2019.

[17] F. Y. Okay, S. Ozdemir and M. Demirci. "SDN-Based Data Forwarding in Fog-Enabled Smart Grids". In: *2019 1st Global Power, Energy and Communication Conference (GPECOM)*, pp. 62-67, 2019.

[18] A. Tariq, R. A. Rehman and B. S. Kim. "Forwarding strategies in NDN-based wireless networks: A survey". *IEEE Communications Surveys and Tutorials*, vol. 22, no. 1, pp. 68-95, 2020.

[19] Y. Zhang, Z. Xia, A. Afanasyev and L. Zhang. A note on routing scalability in named data networking." In: *2019 IEEE International Conference on Communications Workshops (ICC Workshops*), pp. 1-6, 2019.

[20] A. Jayaraman. *Comparative Study of Virtual Machine Software Packages with Real Operating System*, 2012.

[21] J. F. Kurose, R. Rose. *Computer Networking a Top-Down Approach.* 7th ed. Pearson, United Kingdom, 2017.

[22] J. Ali, S. Lee and B. H. Roh. "Performance Analysis of POX and Ryu with Different SDN Topologies". *ACM International Conference Proceedings Series*, pp. 244-249, 2018.

[23] Y. Shi, Y. Cao, J. Liu, and N. Kato. *A Cross-Domain SDN Architecture for Multi-Layered Space-Terrestrial Integrated Networks*. Vol. 33. IEEE Network, Piscataway, pp. 29-35, 2019.

[24] M. Alsaeedi, M. M. Mohamad and A. A. Al-Roubaiey. *Toward Adaptive and Scalable Open Flow-SDN Flow Control: A Survey*. Vol. 7. *IEEE Access*, Piscataway, pp. 107346-107379, 2019.

[25] F. Keti and S. Askar. "Emulation of Software Defined Networks Using Mininet in Different Simulation Environments". In: *2015 6th International Conference on Intelligent Systems, Modelling and Simulation*, pp. 205-210, 2015.

[26] S. Lee, J. Ali, and B. H. Roh. "Performance Comparison of Software Defined Networking Simulators for Tactical Network: Mininet vs. OPNET". In: *2019 International Conference on Computing, Networking and Communications (ICNC)*, pp. 197-202, 2019.

[27] C. Fernandez and J. L. Muñoz. *Software Defined Networking (SDN) with Open Flow 1.3, Open v Switch and Ryu*, pp. 183, 2016.

[28] Z. H. Zhang, W. Chu and S. Y. Huang. "The Ping-Pong Tunable Delay Line in a Super-Resilient Delay-Locked Loop". In: *2019 56th ACM/IEEE Design Automation Conference (DAC)*, pp. 90-91, 2019.

[29] M. Taha, J. Lloret, A. Canovas and L. Garcia. "Survey of transportation of adaptive multimedia streaming service in internet". Network Protocols and Algorithms, vol. 9, no. 1-2, pp. 85, 2017.

[30] Available from: https://www.peach.blender.org. [Last accessed 2020 Jun 01].

[31] Available from: https://www.videolan.org/developers/x264.html. [Last accessed on 2020 Jun 20].

ORIGINAL RESEARCH ARTICLE UHD JOURNAL OF SCIENCE AND TECHNOLOGY

Serological and Molecular Detection of Hepatitis B virus among patients referred to Kurdistan Center for Hepatology and Gastroenterology in Sulaimani City/Kurdistan Region of Iraq

Raz Sirwan Abdullah[1], Salih Ahmed Hama[1,2]

[1]Department of Biology, College of Science, University of Sulaimani, Kurdistan Region, Sulaymaniyah, Iraq, [2]Department of Medical Laboratory Science, College of Health Sciences, University of Human Development, Kurdistan Region, Sulaymaniyah, Iraq

ABSTRACT

Hepatitis B virus infection is caused by the hepatitis B virus, a major global health problem. This infection can lead to chronic conditions, followed by cirrhosis and hepatocellular carcinoma (HCC). The current study was aimed to detect HBV using serological and molecular techniques. During 2019, 300 blood samples were collected from Kurdistan Center for Hepatology and Gastroenterology in Sulaimani city. Enzyme-linked immunosorbent assay (ELISA) and real-time polymerase chain reaction (RT-PCR) techniques were used for the detection of HBsAg and HBV DNA, respectively. Obtained results were revealed that 92 out of 300 tested patients (30.66%) seropositive for HBsAg. Among 92 seropositive patients, 53 were shown positive results for HBV DNA by RT-PCR. Dental clinic visiting and dialysis were among the important risk factors for HBV transmission. The vast majority of positive results were among males. Smokers showed relatively high rates of positive results. One-third of the referred patients who had liver complaints were positive for HBsAg. More than half of the seropositive patients showed RT-PCR positive results. It was concluded that the molecular method (RT-PCR) is more sensitive and gives a more accurate result than serology (ELISA). Therefore, it can be used as a diagnostic tool for HBV detection.

Index Terms: Hepatitis B Virus, Hepatitis B Surface Antigen, Enzyme-linked Immunosorbent Assay, Gold In-tube, Real-time Polymerase Chain Reaction

1. INTRODUCTION

Hepatitis B virus (HBV) is a small DNA virus with a spherical structure and lipid coat membrane, a *Hepadnaviridae* family member. Cause acute liver inflammation in acute and chronic forms is followed by liver failure, cirrhosis, and hepatocellular carcinoma (HCC). More than 90% of patients with acute HBV infection recover although they have severe symptoms, whereas in chronic forms (can be asymptomatic); patients are unable to clear the virus [1]. Several transmission routes are now known, including tattooing, piercing, exposure to the infected blood and body fluids, saliva, vaginal discharge, and semen, perinatal transmission. However, it was noticed that HBV infection in infancy and early childhood could lead to chronic hepatitis in about 95% of cases [2].

It was reported that the sexually transmitted HBV infection also could lead to chronic hepatitis in 5% of unvaccinated men and women. Moreover, studies revealed that HBV could

Access this article online

DOI:10.21928/uhdjst.v4n2y2020.pp117-122 | E-ISSN: 2521-4217 P-ISSN: 2521-4209

Corresponding author's e-mail: Raz Sirwan Abdullah, Department of Biology, College of Science, University of Sulaimani, Kurdistan Region, Sulaymaniyah, Iraq. E-mail: razbio89@gmail.com

Received: 12-10-2020 Accepted: 08-11-2020 Published: 26-11-2020

survive outside the body for at least seven days [2], [3]. It was confirmed that HBV infection is a global health problem, and more than 400 million people worldwide suffering from chronic HBV infections [4]. Hepatitis B surface antigen (HBsAg) is one of the essential antigens of the virus, located on the lipid membrane of the virus [1], [4]. It was reported that Hepatitis B e antigen (HBeAg) negative and anti-HBe positive results in the laboratory could be considered as evidence of chronic HBV infection [4]. Other investigators concluded that HBsAg and Anti-HBsAg antibodies are more likely indicators of detecting HBV infection [5]. The absence of HBsAg and detection of anti-HBsAg among HBV patients can be considered a sign of recovery from the disease, whereas if HBV DNA is still detected during this stage, this could be an indicator for chronic infection [4]. The vast majority of chronic cases may lead to HCC [6].

It was reported that the seropositive patients for HBsAg, HBeAg, and HBV DNA were more likely suspected with the chronic infection of HBV. Several mechanisms were known to lead to the conversion of chronic HBV infection to HCC [6]. Researches showed that if the immune system fails to clear HBV, the cycles of necrosis, inflammation, and reconstruction will repeat, causing hepatocytes may suffer from potentially epigenetic changes and carcinogenic mutations [7]. As a subsequence, the HBV genome may find in almost liver tumor cells, which may alter liver cell function. This can lead to changes in carcinogen-related genes, including cyclin A, telomerase reverse transcriptase, platelet-derived growth factor beta-receptor, and mitogen-activated protein kinase 1 [6], [7]. It was good understood that smoking and alcohol are risk factors for HBV infection [8]. HBV replication is a relatively complex mechanism. The HBV genome is converted to a relaxed circular DNA or a double-stranded linear DNA during replication. Each of them can be converted to covalently closed circular DNA (cccDNA) [9]. RNA pre-genome and HBV mRNAs are produced by cccDNA. The RNA pre-genome acts as the template for the synthesis of the negative-sense DNA strand and the positive-sense DNA strand is finally made based on the DNA negative-strand [9], [10]. As laboratory markers, the HBsAg, anti-HBs, HBeAg, anti-HBe, Hepatitis B core antigen HBcAg, and anti-HBc IgM/IgG are the most critical serological markers for the diagnosis of HBV [11]. HBsAg is the most significant marker for detecting HBV by ELISA [5], [6], [9], [10], [11]. Molecular methods for identifying HBV DNA according to the WHO standards include the quantitative polymerase chain reaction (qPCR) and the real-time polymerase chain reaction (RT-PCR) [10], [11]. The current study aims to determine the percentage rates of HBsAg seropositivity and HBV nucleic acid detection by RT-PCR among patients (who are enormously suffered from liver complaints) referred to Gastroenterology Center in Sulaimani City.

2. MATERIALS AND METHODS

2.1. Study Population

The study's population included people visiting the Kurdistan Center for Hepatology and Gastroenterology in Sulaimani city from June to November 2019. All patients had liver problems, and they had experienced specific symptoms included fever, chills, abdominal pain, nausea, diarrhea, dark urine, loss of appetite, jaundice, and fatigue. The sample size of the current study was 300 patients included 160 males and 140 females.

2.2. Sample Collection

Fresh venous blood samples were collected and transferred to the laboratory using cool boxes for the desired Lab. investigation. Serum samples were kept until HBsAg and HBV DNA detection by ELISA RT-PCR.

2.3. HBsAg Detection by ELISA

Sandwich-ELISA method was depended to detect HBsAg using a special ELISA kit (Elab-Science, China) with a pre-coated microtiter plate well with recombinant HBsAb. All preserved sera samples were transferred to room temperature for about 30 min. 100 µL of each sample, standard, and blank were added to the desired wells. The plate was covered with sealer and incubated for 90 min at 37°C. The wells were aspirated and washed by an ELISA washer as directed by the supplied company. 100 µL of Biotinylated Detection Ab Working Solution were added to each well, and the plate was covered and incubated for 60 min at 37°C. The plate was washed. To each well, 100 µL of HRP Conjugate Working Solution was added except for the blank control and incubated q for 30 min at 37°C. The plate was washed after that, 90 µL of Substrate Solution was added to each well and mixed, then incubated at 37 °C for 15 min. 50 µL of stop solution were added for the wells and mixed thoroughly. The optical density was measured at 450 nm using ELISA Microplate Reader.

2.4. Viral DNA Extraction and Amplification

High molecular weight genomic viral DNA was extracted by a fully automated magnetic beat nucleic acid extraction system (Zinexts, Taiwan). The viral nucleic acid extraction kit (Zinexts) was used to separate viral genomic viral DNA using 400 µl of serum and 100 µl Elute volume. The

extracted viral DNA was stored at -80°C until the day of examination by RT-PCR using an RT-PCR machine (Line Gene 9600 PLUS -Bioer, China-). A special Kit (Fluorion HBV QNP 2-0 -Inotek, Turkiye) was used for the detection of HBV DNA.

2.5. PCR Reaction

A total volume of PCR Mix, internal control, aH2O, and Extracted viral DNA (25 µl) was prepared as directed by the supplied company as summarized below:

Items	Volume
PCR Mix	12.5 µl
Detection Mix 1	1.4 µl
Detection Mix 2	1.1 µl
Internal Control	1 µl
dH2O	4.0 µl
Extracted viral DNA/Standard/ Negative/Positive Control	5 µl
Total Volume	25.0 µl

The process of PCR programming for detecting HBV nucleic acid was performed starting with the denaturation step, renaturation, annealing, elongation, and data collection as summarized in the below table.

Step	Temperature (°C)	Duration	Cycle
Initial denaturation	95	15 min	1
Denaturation	95	30 s	50
Annealing, elongation, and data collection	54	1:30 min	
Infinite hold	22	∞	

2.6. Statistical Analysis

The results were analyzed using Chi-square and Mann–Whitney U-tests through SPSS V. 25 software (SPSS Inc., Chicago, IL, United States). Statistically, the *P*-value was considered to be <0.05 ($P < 0.05$) significant.

3. RESULTS

The patients who participated in this study who suffered from health complaints were distributed on males (160) and females (140). The mean age of them was 38.16 ± 15.24 years. All patients who were referred to the GIT center were clinically suspected of having hepatitis and liver complaints. Several symptoms were depended and recorded among the tested patients who were submitted for serologic and molecular detection of the Hepatitis B virus. Pre-diagnosed liver caser patients, blood transfusion also was included in addition to their residency (Table 1).

TABLE 1: Distribution of the tested patients according to the different variables

Variable		Number (%)
Gender	Males	160 (53.33)
	Females	140 (46.67)
Smoking	Smokers	180 (60.00)
	Non-smokers	120 (40.00)
Age mean	Mean±SD	38.16±15.24
Clinical Symptoms	Fever	260 (86.67)
	Chills	249 (83.00)
	Abdominal pain	171 (57.00)
	Nausea	133 (44.33)
	Diarrhea	120 (10.00)
	Loss of appetite	110 (36.67)
	Jaundice	73 (24.33)
	Dark urine	35 (11.67)
	Fatigue	30 (10.00)
Liver cancer (HCC)	Yes	6 (2.00)
	No	294 (98.00)
Residency	Urban	130 (43.33)
	Rural	170 (56.67)
Blood transfusion	Yes	13 (4.33)
	No	287 (96.67)

Serologic tests by ELISA revealed that out of 300 tested patients, 92 (30.66%) were seropositive for HBsAg. The vast majority of positive results were among males (50 patients - 54.34%), whereas the percentage rates of seropositive cases were lower among females (42 patients - 45.66%). When the results were analyzed statistically, it was noticed that gender has a valuable effect on the seropositive results. The majority of the seropositive cases were smokers (67.4%). There was a significant difference between smokers and non-smokers ($P < 0.05$), whereas it has appeared that the marital status has no significant effects on the HBsAg seropositive results ($P > 0.05$).

Studying several risk factors for HBV transmission indicated that visiting dental clinics and dental surgery (927.17%), followed by dialysis (21.73%), were among the highest risk factors. Statistical analysis showed that dental visiting and dialysis significantly affect the seropositive results ($P < 0.05$). Although relatively a large number of the seropositive patients were within uncertain transmission routes, 39 patients out of 92 (42.4%). Finally, it has appeared that seropositive results were higher (58.7%) outside Sulaimani city center (rural) while the percentage was lower (41.3%) in the city center (urban). It was concluded that the patient's residency has valuable effects on the obtained results ($P < 0.05$) (Table 2).

Depending on HBV DNA detection by RT-PCR, it was noticed that out of the 92 seropositive patients, 53 (57.6%) were positive for HBV DNA (Table 3). Positive results

were higher among males (62.26%) when compared with females (37.74%). Similarly, DNA detection among smokers was relatively higher (64.15%) comparing to non-smokers (35.85%). The positive results among married patients were elevated (56.6%) if compared with single patients (43.4%). Half of the patients with liver cancer were seropositive for HBsAg, whereas two-third of them was HBV DNA positive. Moreover, patient's residency showed significant effects on the positive results where the percentage rates of positive results were higher among patients outside Sulaimani city center (Rural) (58.5%) comparing to those from the city center (41.5%) (Urban). Statistical analysis indicated that gender, smoking, marital status, and liver cancer have significant effects on HBV DNA detection results ($P < 0.05$) (Table 3). Studying the modes of transmission indicated that dental clinics and dental visiting have a significant effect on the positive results of RT-PCR ($P < 0.05$) and can be considered as an important risk factor for HBV transmission, followed by dialysis, which is also can be considered as a risk factor after dental clinic visiting (Table 3).

TABLE 2: Represents different risk factors for HBsAg seropositivity by ELISA

Variable		Number (%)	*P* value
Gender	Males	50 (54.34)	<0.05
	Females	42 (45.66)	
Smoking	Smoker	62 (67.4)	<0.05
	Non-smoker	30 (32.6)	
Marital status	Married	48 (52.17)	>0.05
	Single	44 (47.83)	
Liver Cancer	Yes	3 (50%)	>0.05
	No	3 (50%)	
Mode of Transmission	Dental visiting	25 (27.17)	<0.05
	Surgery	1 (1.88)	
	Dialysis	20 (21.73)	
	Blood transfusion	2 (2.16)	
	Sexual route	2 (2.16))	
	Animals modes	1 (1.08)	
	Barbershop	1 (1.08)	
	Familial history	1 (1.08)	
	Uncertain	39 (42.4)	
Residency	Urban	38 (41.3)	<0.05
	Rural	54 (58.7)	

TABLE 3: Studying risk factor for HBV DNA detection by RT-PCR

Variables	Explanation	Number (%)	*P* value
Gender	Male	33 (62.26)	<0.05
	Female	20 (37.74)	
Smoking	Smokers	34 (64.15))	<0.05
	Non-smokers	19 (35.85))	
Marital state	Married	30 (56.6)	<0.05
	Single	23 (43.4)	
Liver cancer	No	1 (33.33)	<0.05
	Yes	2 (66.67)	
Modes of transmission	Dental visiting	16 (30.18)	<0.05
	Dialysis	7 (13.2)	
	Surgery	2 (3.77)	
	Blood transfusion	2 (3.77)	
	Sexual	1 (1.88)	
	Animals	1 (1.88)	
	Barbershop	1 (1.88)	
	Familial	1 (1.88)	
	Unknown	22 (41.5)	
Residency	In City center	22 (41.5)	<0.05
	Outside the city center	31 (58.5)	

The positive results were relatively higher among males for HBsAg and DNA detection (54% and 62.26%), respectively, when compared to female patients who showed lower positive results (46% and 37.74%), respectively. It was noticed that relatively a large number of patients were seropositive for HBsAg while they were negative for HBV DNA detection by RT-PCR (Fig. 1).

4. DISCUSSION

Life-threatening infection by HBV stills a global cause of health concern. It was estimated worldwide that over 257 million people are under the risk of liver cirrhosis and HCC due to chronic hepatitis B virus (HBV) infection [12]. The high seropositivity rates of HBV infection among studied cases in the current study can be explained where all patients submitted to this research were with a chronic history of liver problems. All of them were previously referred by their specialist physicians to the gastroenterology center for checking and laboratory investigations. They were suspected of having hepatitis. Several studies and investigators reported a lower prevalence of HBV infections than our observation. In a previous study, it was reported that the prevalence of HBsAg seropositivity among a population of 345 tested cases was relatively lower [13]. In the current study, blood transfusion was considered as an important

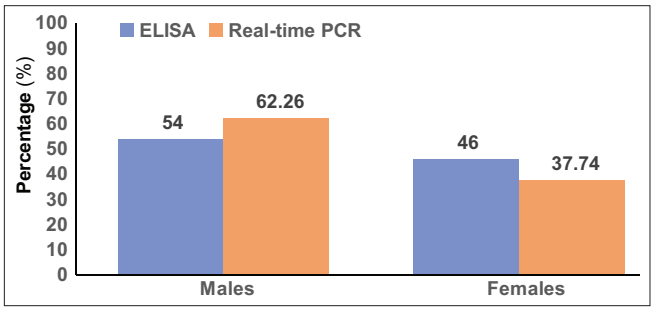

Fig. 1. Comparison between positive results of HBV using ELISA (seropositivity) and RT-PCR techniques.

risk factor for HBV transmission, which was also common among thalassemic patients. These observations were agreed with observation reported by others [14]. In another study done in Sulaimani, it was found that occupation, education level, history of jaundice, smoking, and alcohol drink had a significant effect on viral hepatitis infections, especially HCV infection [15]. Our observations were parallel with their conclusion considering some factors, including smoking. The results of the current study were different from the results reported by the Iranian research group who reported a relatively lower prevalence of HBV infection (7.4%) [16]. Moreover, our conclusions agreed with results reported in a study in Switzerland who reported relatively high HBV prevalence (32.4%) [17]. Ott *et al.* in 2012 found that the global HBeAg prevalence varied between 20 and 50% [18]. The current observations were in this range and agreed with their results. Similar to our results, a high prevalence of HBV infections (30.4%) were reported in Spain [19].

Studies done in Italy reported higher prevalence rates (52.7%) [20] than our observations. Moreover, studies done in Australia reported lower HBV prevalence in comparison to the current results, although it was relatively high compared to other related studies in other countries [21].

The high prevalence rates of HBV seropositivity among males in our study may be due to that they engaged in a range of parenteral (sharp objects sharing), especially in barbershops, which expose them to HBV infection. Our results were agreed with conclusions reported by other investigators in 2018 [9]. The risk of HBV infection among males was agreed with other epidemiological studies conducted in different areas among different groups and populations who observed that HBV infection is strongly associated with increased age among males [22], [23], [24], [25].

Results reported in the current study suggested that occupational transmission of HBV infections in dental settings, which sometimes found frequently, and high prevalence of HBV seropositivity among dental clinics and patients who referred to these clinics may be due to inadequate sterilization of the surgical tools used in dental clinics, and sharing some tools between the patients [26]. Similarly, inadequate sterilization and cleaning of materials and machines used in hemodialysis might be directly contributed to the prevalence of HBV infection among patients with hemodialysis.

The current study showed that not all HBsAg seropositive patients were positive for HBV DNA detection by RT-PCR, which was agreed with observations reported by a study done in Nairobi (Kenya) in 2017 by Mathai *et al.* [27]. They reported that the seropositive results of HBsAg and HBV DNA detection are totally different, and none of ELISA and RT-PCR cannot be alternative for each other [28]. Unlike conclusions of the current study, other researchers found that HBsAg detection and quantification by ELISA is more sensitive and gives more accurate results in detection of HBV infection, and they found that ELISA can be considered as an acceptable or adequate method in the diagnosis of HBV infection and HBsAg detection [29].

5. CONCLUSION

The percentage rates of HBsAg were relatively high (30.66%) among patients referred to the Gastroenterology center in Sulaimani who have suffered from liver complaints. More than half of the seropositive patients showed RT-PCR positive results for HBV nucleic acid detection. The gender, smoking, and marital status, and living places were significantly increased the incidence rate of HBV infection. Visiting dental clinics, dental surgery, and dialysis were among significant risk factors that facilitate the transmission of HBV infection.

6. ACKNOWLEDGMENTS

Our thanks, due to all patients involved in this study, we want to thank specialist physicians in the Sulaimani Gastroenterology center.

REFERENCES

[1] T. J. Liang. "Hepatitis B: The virus and disease". *Hepatology*, vol. 49, no. 5 Suppl, pp. S13-S21, 2009.

[2] World Health Organization. "*Hepatitis B: Fact Sheet*", World Health Organization, Geneva, 2020.

[3] S. Lanini, V. Puro, F. N. Lauria, F. M. Fusco, C. Nisii and G. Ippolito. "Patient to patient transmission of hepatitis B virus: A systematic review of reports on outbreaks between 1992 and 2007". *BMC Medicine*, vol. 7, p. 15, 2009.

[4] G. Fattovich. "Natural history of hepatitis B". *The Journal of Hepatology*, vol. 39, no. Suppl 1, pp. S50-S58, 2003.

[5] G. Raimondo, T. Pollicino and G. Squadrito. "Clinical virology of hepatitis B virus infection". *The Journal of Hepatology*, vol. 39, no. Suppl 1, pp. S26-S30, 2003.

[6] M. G. Peters. "Hepatitis B virus infection: What is current and new". *Topics in Antiviral Medicine*, vol. 26, no. 4, pp. 112-116, 2019.

[7] J. E. Song and D. Y. Kim. "Diagnosis of hepatitis B". *Annals of Translational Medicine*, vol. 4, no. 18, p. 338, 2016.

[8] S. K. K. Mani and O. Andrisani. "Hepatitis B virus-associated

hepatocellular carcinoma and hepatic cancer stem cells". *Genes* (*Basel*), vol. 9, no. 3, p. 137, 2018.

[9] X. Liu, A. Baecker, M. Wu, J. Y. Zhou, J. Yang, R. Q. Han, P. H. Wang, Z. Y. Jin, A. M. Liu, X. Gu, X. F. Zhang, X. S. Wang, M. Su, X. Hu, Z. Sun, G. Li, L. Mu, N. He, L. Li, J. K. Zhao and Z. F. Zhang. "Interaction between tobacco smoking and hepatitis B virus infection on the risk of liver cancer in a Chinese population". *International Journal of Cancer*, vol. 142, no. 8, pp. 1560-1567, 2018.

[10] C. Seeger and W. S. Mason. "Molecular biology of hepatitis B virus infection". *Virology*, vol. 479-480, pp. 672-686, 2015.

[11] J. E. Song and D. Y. Kim. "Diagnosis of hepatitis B". *The Annals of Translational Medicines*, vol. 4, no. 18, p. 338, 2016.

[12] World Health Organization. "*Hepatitis B"*. World Health Organization, Geneva, 2017.

[13] M. Asad, F. Ahmed, H. Zafar, S. Farman. "Frequency and determinants of Hepatitis B and C virus in general population of Farash Town, Islamabad". *Pakistan Journal of Medical Sciences*, vol. 31, no. 6, pp. 1394-1398, 2015.

[14] S. A. Hama and M. I. Sawa. "Prevalence of hepatitis B, C, and D among thalassemia patients in sulaimani governorate". *Kurdistan Journal of Applied Research*, vol. 2, no. 2. pp. 137-142, 2017.

[15] S. A. Hama. "Hepatitis C seropositivity and RNA detection among Type2 diabetic patients in sulaimani governorate-Iraqi Kurdistan Region". *Journal of Zankoy Sulaimani A*, vol. 18, no. 4, pp. 1-8, 2016.

[16] Z. Nokhodian, M. R. Yazdani, M. Yaran, P. Shoaei, M. Mirian, B. Ataei, A. Babak, M. Ataie. "Prevalence and risk factors of HIV, syphilis, hepatitis B and C among female prisoners in Isfahan, Iran". *Hepatitis Monthly*, vol. 12, pp. 442-447, 2012.

[17] L. Gétaz, A. Casillas, C. A. Siegrist, F. Chappuis, G. Togni, N. T. Tran, S. Baggio, F. Negro, J. M. Gaspoz and H. Wolff. "Hepatitis B prevalence, risk factors, infection awareness and disease knowledge among inmates: A cross-sectionalstudy in Switzerland's largest pre-trial prison". *Journal of Global Health*, vol. 8, no. 2, pp. 020407, 2018.

[18] J. J. Ott, G. A. Stevens, S. T. Wiersma. "The risk of perinatal hepatitis B virus transmission: hepatitis B e antigen (HBeAg) prevalence estimates for all world regions. *BMC Infectious Diseases*, vol. 12, p. 131, 2012.

[19] P. S. Hoya, A. Marco, J. García-Guerrero, A. Rivera. "Hepatitis C and B prevalence in Spanish prisons". *European Journal of Clinical Microbiology and Infectious Diseases*, vol. 30, pp. pp. 857-862, 2011.

[20] S. Babudieri, B. Longo, L. Sarmati, *et al*. "Correlates of HIV, HBV, and HCV Infections in a prison inmate population: results from a multicentre study in Italy". *Journal of Medical Virology*, vol. 76, pp. 311-317, 2005.

[21] J. M. Reekie, M. H. Levy, A. H. Richards, *et al*. "Trends in prevalence of HIV infection, hepatitis B and hepatitis C among Australian prisoners 2004, 2007, 2010". *MJA*, vol. 200, pp. 277-280, 2014.

[22] A. C. Stief, R. M. Martins, S. M. Andrade, M. A. Pompilio, S. M. Fernandes, P. G. Murat, G. J. Mousquer, S. A. Teles, G. R. Camolez, R. B. L. Francisco and A. R. C. Motta-Castro. "Seroprevalence of hepatitis B virus infection and associated factors among prison inmates in state of Mato Grosso do Sul. Brazil". *Revista da Sociedade Brasileira de Medicina Tropical*, vol. 43, no. 5, pp. 512-515.

[23] F. J. Souto. "Distribution of hepatitis B infection in Brazil: The epidemiological situation at the beginning of the 21st century". *Revista da Sociedade Brasileira de Medicina Tropical*, vol. 49, pp. 11-23, 2016.

[24] J. Paoli, A. C. Wortmann, M. G. Klein, V. R. Z. Pereira, A. M. Cirolini, B. A. de Godoy, N. J. R. Fagundes, J. M. Wolf, V. R. Lunge and D. Simon. "HBV epidemiology and genetic diversity in an area of high prevalence of hepatitis B in Southern Brazil". *The Brazilian Journal of Infectious Diseases*, vol. 22, no. 4, pp. 294-304, 2018.

[25] P. F. Belaunzaran-Zamudio, J. L. Mosqueda-Gomez, A. Macias-Hernandez, S. Rodríguez-Ramírez, J. Sierra-Madero and C. Beyrer. Burden of HIV, syphilis, and hepatitis B and C among inmates in a prison state system in Mexico. AIDS Research and Human Retroviruses, vol. 33, no. 6, pp. 524-533, 2017.

[26] M. A. A. Al Kasem, M. Al-Kebsi Abbas, M. M. Ebtihal and A. A. S. Hassan. "Hepatitis B virus among dental clinic workers and the risk factors contributing for its infection". *Online Journal of Dentistry and Oral Health*, vol. 1, no. 2, pp. 1-6, 2018.

[27] F. Mathai, M. O. Ngayo, S. M. Karanja, A. Kalebi and R. Lihana. "Correlation of quantitative assay of HBsAg and hepatitis B virus DNA levels among chronic HBV patients attending pathologist lancet laboratory in Nairobi, Kenya". *Archives of Clinical Infectious Diseases*, vol. 12, no. 4, pp. e13306, 2017.

[28] M. Gencay, A. Seffner, S. Pabinger, J. Gautier, P. Gohl, M. Weizenegger, D. Neofytos, R. Batrla, A. Woeste, H. S. Kim, G. Westergaard, C. Reinsch, E. Brill, P. T. T. Thuy, B. H. Hoang, M. Sonderup, C. W. Spearman, G. Brancaccio, M. Fasano, G. B. Gaeta, T. Santantonio and W. E. Kaminski. "Detection of *in vivo* hepatitis B virus surface antigen mutations a comparison of four routine screening assays". *Journal of Viral Hepatitis*, vol. 25, no. 10, pp. 1132-1138, 2018.

[29] H. J. Lee, S. Y. Kim, S. M. Lee, J. Heo, H. H. Kim and C. L. Chang. "Elecsys hepatitis B surface antigen quantitative assay: Performance evaluation and correlation with hepatitis B virus DNA during 96 weeks of follow-up in chronic hepatitis B patients". *Annals of Laboratory Medicine*, vol. 32, no. 6, pp. 420-425, 2012.

ORIGINAL RESEARCH ARTICLE UHD JOURNAL OF SCIENCE AND TECHNOLOGY

Intelligent Traffic Congestion Control System using Machine Learning and Wireless Network

Mohammed Abdulmaged Faraj[1,2]*, Najmadin Wahid Boskany[2]

[1]University of Human Development, College of Science and Technology, Department of Computer Science, Sulaymaniyah, Iraq, [2]College of Science, Department of computer, University of Sulaimani, Sulaymaniyah, Iraq

ABSTRACT

Traffic congestion has become a big problem for most people because it increases noise, air pollution, and wasting time. Current normal traffic light system is not enough to manage the traffic problematic congestions because they operate on a fixed-time length plan. In recent years, internet of things led to introducing new models of intelligent traffic light systems; by utilizing different techniques such as predictive-based model, radiofrequency identification, and ultrasonic-based model. The most essential one of these techniques is depends of image processing and microcontroller communications. In this paper, we propose an intelligent, low cost, and efficient microcontroller circuit-based system for controlling cars in traffic light. This system can manage car traffics smarter than traditional approaches, it is capable to dynamically adjust timings of traffic signal. It can rapidly respond to traffic conditions to reduce traffic congestion. For implementing this system, a server, microcontroller board, cameras, as hardware and wireless network between traffic lights as infrastructure for communication are used. The system uses machine learning technique (i.e.,Yolov3 model and OpenCV) for decision depending on existence of emergency cars and number of cars. The experiment results show higher accuracy in managing traffic lights and recognizing the emergency cars.

Index Terms: Machine Learning, Intelligent Traffic Control, Yolov3, Wireless Communication, Internet of Things

1. INTRODUCTION

Transportation is one of the basic human activities for the development of societies. Ground transportation is done by all types of vehicles such as cars, motorcycles, bicycles, or public transportation. These regulations or rules set by government institutions. Traffic systems are designed to uphold the lives and safety of people, whether they are drivers or walkers as well as regulate and monitor pedestrian traffic. Traffic lights are tradition system used to manage the flow of traffic, also the walkers pass streets in safe way. However, the traditional traffic lights are not that good and it may cause additional traffic delays [1].

Different road traffic problems have appeared around the world as a result of population growth and increasing the number of cars in traffic lights, especially in large urbanized areas. Road safety mainly depends on drivers' decisions, and these depend only on what drivers see and hear [2]. People also face other problems like traffic jam which is becoming riskier every day and led to traffic accidents. Traffic jam is a very serious problem, for that many researchers have paid attention to intelligent transportation system, for example, predicting traffic flow according to monitoring the traffic light. This mission stays as a challenge for computer vision, several methods have been implemented in previous years with some drawbacks such as difficulties in implementation due to using large number of hardware and high cost [3].

Access this article online

DOI:10.21928/uhdjst.v4n2y2020.pp123-131

E-ISSN: 2521-4217
P-ISSN: 2521-4209

Corresponding author's e-mail: Mohammed Abdulmaged Faraj, University of Human Development, College of Science and Technology, Department of Computer Science, Sulaymaniyah, Iraq; College of Science, Department of computer, University of Sulaimani, Sulaymaniyah, Iraq. E-mail: mohammed.abdulmaged90@gmail.com

Received: 11-09-2020 Accepted: 30-11-2020 Published: 10-12-2020

There are many ways of detecting vehicles and emergencies cars on road such as motion detection, installing lasers sensors. On both sides of the road, etc. [3], smart traffic light system is an essential part in smart cities to decrease traffic congestion [4].

There are some simple traffic management systems that have uses Global Positioning System and infrared (IR) for detecting the ambulance and can also count cars and detect the real-time density of traffic light, and some other technologies have been used radiofrequency identification tags to identify emergency vehicles and loop inductive methods to determine the number of vehicles [5].

In this paper, an intelligent system is proposed for managing traffic light. This system has capability of managing traffic light in smart way using image processing and machine learning to detect number of vehicles in the traffic light and ambulance as emergency car. The proposed system mainly uses Yolov3 as a perfect algorithm for car detection, it is faster than other algorithm for detecting objects in real time and the accuracy is high, for example, the accuracy of faster Region-based Convolutional Neural Network algorithm is high, but it is slow for detecting objects in real time.

The remainder of this paper is organized as follows. Related works are illustrated in section 2. System description explained in section 3. The detail of the proposed system is presented in section 4. System algorithm and flowchart are illustrated in section 5. Experiment result is explained in section 6. Finally, conclusions are presented in last section.

2. RELATED WORKS

There have been many researches in developing intelligent traffic lights algorithms by researchers using different methods. Some of them are presented below:

M. M. Elkhatib and A. S. Alsamna (2019), designed a system consists of two part of implementation; first, to control traffic light more effective using embedded system and image processing and second used wireless and Bluetooth connection from android application to control traffic light signals, using image processing and embedded system, the system capable to detect the number of vehicles simultaneously in each lane, the green light will be longer where there are more cars in one lane than the other, in this method as a system controller, they used Arduino and for detection and counting cars used C++ environment and OpenCV library [6].

El. H. Imad (2019), proposed some solutions such as machine learning, internet of things, and closed-circuit television system, the first step is determined the number of outgoing and incoming cars in the traffic light by installing sensors in the roads and collecting data from them, also there are other sensors installed on the roads to determine emergency cars (for example, ambulances, polices, etc.) also an agent installed at each traffic light, which collect data from sensors that installed in the roads of an traffic light a pan–tilt–zoom camera installed at each traffic light it takes images of that roads and send them to the agent [7].

L. F. P. Oliveira *et al.* (2019), in their work developed a controller of traffic light and centralized it, able to communicate with other traffic lights through wireless network, it has been used magnetic IR sensors and digital camera to determine number of vehicles in that lane of intersection, also several wireless sensors installed, it allows creating strategic plans to control traffic and synchronizes it and prioritizes certain traffic that has more vehicles and maintains stability, vehicle speed. Two control circuits designed, one for direct current lamps and the other for alternating current lamps, are designed to control the different types of traffic lights. Control the traffic light period, collect data from sensors, and communicate with the RF module for that microcontroller circuit have been used [8].

T. A. Kareem and M. K. Jabbar (2018), proposed the system which is consists of hardware and software part. The first circular hardware part is a model which includes four lanes of a traffic light, also it has Global System for Mobile Communications (GSM) system. The lamps of the traffic light and GSM are connected to Arduino UNO. All signals that are coming from the GSM to software and converted to lamps of traffic lights are controlled by Arduino, second circular hardware part is same model of the first part except GSM it replaced with IR remote. The goal of their paper is to open the traffic light in the emergence cases, using GSM system and IR it control the closing and opening of the traffic light, designed for emergency vehicles, especially with ambulances by opening the traffic light in the lane which the ambulance came using IR system or GSM [9].

M. B. Natafgi *et al.* (2019), have used reinforcement learning to implement traffic light system and Lebanese traffic used as a real data for testing. It used a software simulation tool for testing and training. This tool can simulate the traffic lane and interact with neural network. On the roads, the sensors installed to detect cars. The controller have used the data of sensors to calculate the number of vehicles and time delays in those traffic lights it saves that data every hour in the database.

Q-learning has been used to train the network. The proposed system tested using the traffic simulator SUMO [10].

M. Z. Ismail *et al.* (2019), developed a system for traffic light for emergency cars to pass the traffic intersection where the traffic road jammed with long queue of cars and change traffic light from red to green. The main tools have been used are Arduino and sensors through Bluetooth. Sensors with Bluetooth are located at emergency car and at the traffic light the Arduino and Bluetooth are located. The controller is Arduino mega and Bluetooth module is HC-05. The advantage of this system is saving time when emergency car comes to the traffic then the traffic light will change the light to green [11].

N. Diaz *et al.* (2018), developed an autonomous traffic light system using PIR sensor and Raspberry Pi, based on the PIR sensor (passive infrared sensor) the microcontroller control lighting of the traffic intersection based on the times that programmed with Python code which sends a signal to the microcontroller when in the traffic light the PIR sensors detect IR radiation. The Raspberry pi was programmed using the Python, the structure built with several parts: Python Code, Circuit Schematic, simple design of the traffic light, and printed circuit board [1].

A. H. Akoum (2017), designed a system in which filter method was used, this method filter the image only show the vehicles and separate all waste, after that display the number of cars in the image. According to the number of boxes that detected around the vehicles it gives the number of vehicles, the web browser used as a graphical user interface, many future improvements can be used to the counting vehicles, tracking and detection system can be expanded to real-time live video [3].

3. SYSTEM DESCRIPTION

In this section, required hardware and software components are described briefly.

3.1. System Hardware

System hardware parts are packaged to be embedded with normal traffic light to changed it to intelligent traffic light. Below brief description of required hardware are defined one by one:

3.1.1. Control unit

The controller is based on ESP32 Nodemcu which it is electronic platform and open source. ESP32 Nodemcu is a microcontroller board module Chip with built-in WiFi: Standard 802.11 B/G/N, operating in the range of 2.4–2.5GHz, modes of operation: Client, access point, station + access point, dual core microprocessor, operating voltage: 3.3 VDC. It has 36 GPIOs. It has Bluetooth v4.2 BR/EDR and BLE, implemented in C. It can get power through micro-USB port and also it connected and programmed from computer through the on-board micro-USB connector, as shown in Fig. 1 [12]. In this research, ESP32 Nodemcu has been used to control the traffic light based on the data received from the server (i.e., number of cars and detecting ambulance). Moreover, it is used to communicate with next traffic light through wireless communication.

3.1.2. LED

For traffic lights LED with three colors, red, green, and yellow are used for this purpose. LED that collects the three color in one are designed for traffic light, it has 3 pins connected with control unit (ESP32 Nodemcu) to receive high voltage to turn on the lights and 1 pin for ground connected to ground pin of Arduino, as shown in Fig. 2.

Connection between ESP32 and traffic light is depicted by Fritzing open-source software, as shown in Fig. 3.

3.1.3. Powerful server

For this work fast server computer required, the important part is GPU, whenever GPU is increased the training and

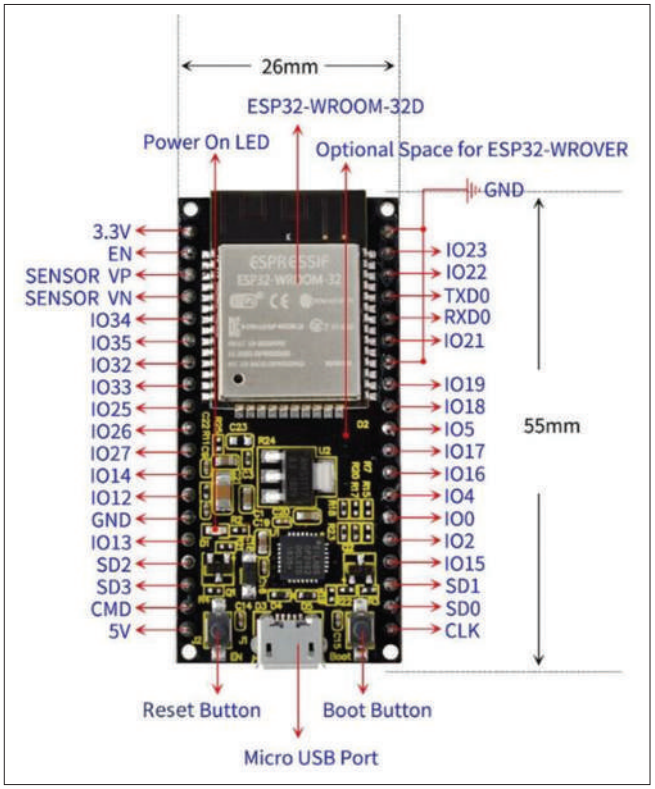

Fig. 1. On-board micro-USB connector.

Fig. 2. LED traffic light.

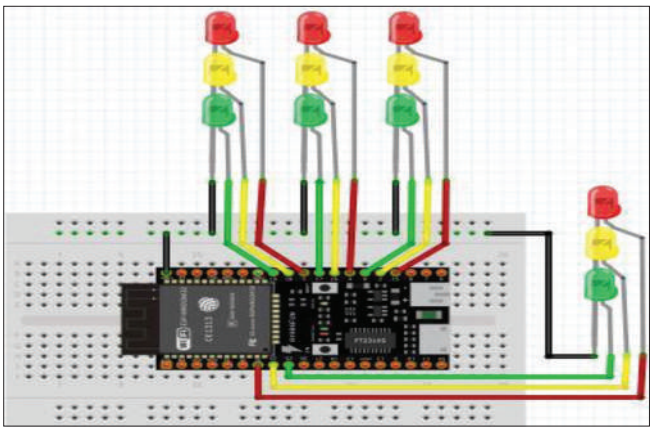

Fig. 3. Connection between ESP32 and traffic light.

testing will be faster. The minimum requirements are RAM 16GB, GPU Nvidia Geforce 1060 6GB. Fast and high-quality computer is important for training available dataset. Furthermore, it is used for process the video that received from cameras for detecting the cars and ambulance. Received data then send to microcontroller to make decision to open the lane or no.

3.1.4. Camera

Many cameras (i.e., IP camera or webcam camera) installed on each lane of traffic light to record video and send real live of traffic light to server in this research, webcam camera (i.e., resolution 800×600, frame rate up to 15 frame/s (VGA), automatic white balance and manual balance) has been used which is connected to computer through USB, as shown in Fig. 4.

Fig. 4. USB camera.

3.1.5. Benchmark board

Instead of real traffic light and to avoid some difficulties in real-life traffic light environment, simulated board is used for tests which is very close to real one. All required components exist, roads and intersections build on the board dimension which is 120×60 cm (Fig. 5).

3.2. System Software

System software consists of different parts which are combined together, below a brief description of required software is defined one by one:

3.2.1. Yolo

Yolov3 "You Only Look Once" is an algorithm that uses CNN for object detection. YOLO is one of the fastest object detection algorithms. This algorithm applies a single neural network to the full image, it is accurate as SSD but 3 times faster it can be installed on Windows and Linux [13]. YOLOv3 as an algorithm that is a single convolutional neural network that predicts the bounding boxes with the class probabilities from the single check. This sort of algorithm is used mainly within the real-time application, this algorithm has been used because of it is faster algorithm for detecting objects in real time and the accuracy is high.

YOLO is made up of 24 convolutional layers, with two fully connected layers. Moreover, the input image is separated into M×M grid cells. Grid cell that includes the midpoint of the object is responsible for predicting the object. The output tensors of YOLO model will be a vector of N*N*(M*5 + C) in which M indicates the predicted bounding boxes with the confidence score by each grid cell. C is the class probabilities

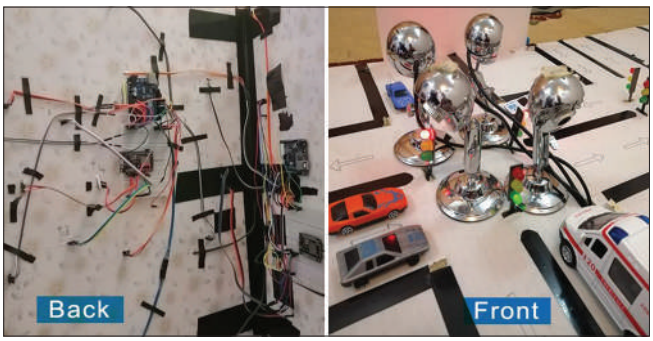

Fig. 5. Benchmark board.

for the predicting bounding boxes. Every bounding box M has five components within which are x, y, w, and h and the confidence score C. The coordinate (x, y) represents the object's midpoint with regard to grid cell location and offsets (w, h) represents the bounding box's width and height concerning image dimensions. YOLOv3 foresees multiple bounding boxes per grid cell. However, those bounding boxes have highest Intersection over Union and ground truth to this which is known as non-maxima suppression [14].

An example of detection using YOLO is license plate detection for non-helmeted motorcyclist [15] and there are more examples for detecting different objects using YOLO.

3.2.2. Esp-now

For network communication among traffic light ESP-NOW used), ESP-NOW is developed by Espressif that allows various devices to communicate with each other. The protocol is like the low-power 2.4GHz. It needs before their communication to pairing between devices. Once the matching is complete, in a straight line it managed to communicate up to 165.47 m, the connection is secure and peer to peer. It used the MAC address of the microcontroller for linking for the purpose of joining in the right direction [16].

4. PROPOSED MODEL

A brief description of the entire system is given in this section. The proposed model consists of hardware entities and software entities. The whole system (as one package) should be embedded to any traffic light to be changed from normal traffic light to intelligent traffic light.

The proposed system mainly works based on relation between a server computer and ESP32 ModeMcu open-source microcontroller. The server receives car videos through attached cameras, to be used for car identification and counting car numbers in each lane at the same time. The microcontroller side controls all the operations of the electronic circuits connected to its digital input and output pins.

Video cameras are used for inputting real-time video to the server, image processing starts by car identification, feature extraction, matching with available dataset images, and detecting ambulance car. The microcontroller, in turn, reacts depending on emergency car existence on the road sides by changing light sign to green and send command to next neighbor traffic light via wireless communication to change it to green sign.

Yolov3 in turn starts to do fast image processing on already prepared dataset which consist of 2000 images of normal car and 2000 images of ambulance.

The decision will be trigger in two cases: First, in case, if ambulance is detected on a side, the system automatically decides to open this side (i.e., change the light from red to green) to let it pass the traffic light soon and it communicates with next traffic light through wireless network to change the light to green too. Second, also in case, if the amount of waiting cars in one side exceeded 10 cars and other sides are empty automatically change this side light to green. Fig. 6 shows general description of the proposed system.

5. SYSTEM ALGORITHM

In this section, an algorithm for managing the system is described in steps as follows: First step, the model sets its parameters. Then, continually images sent to the server through attached camera and image processing in the server side will start. Later, image detection begins by distinguishing emergency car from normal car, if received image was for emergency car (i.e., ambulance) or number of cars at a lane reached 10 then the server notifies the microcontroller to change the traffic light to green. In the same time, it communicates with next traffic light to change light to green to let the emergency car pass overall interactions. Otherwise, the system continues in a loop and gets new images. All steps are explained in Fig. 7 using below flowchart.

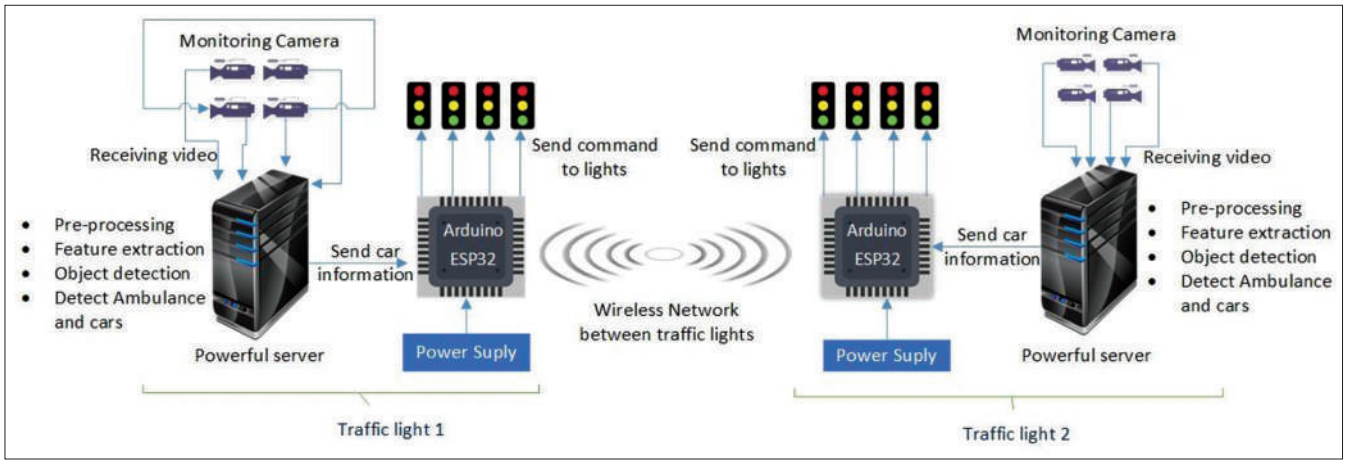

Fig. 6. General description of the proposed system.

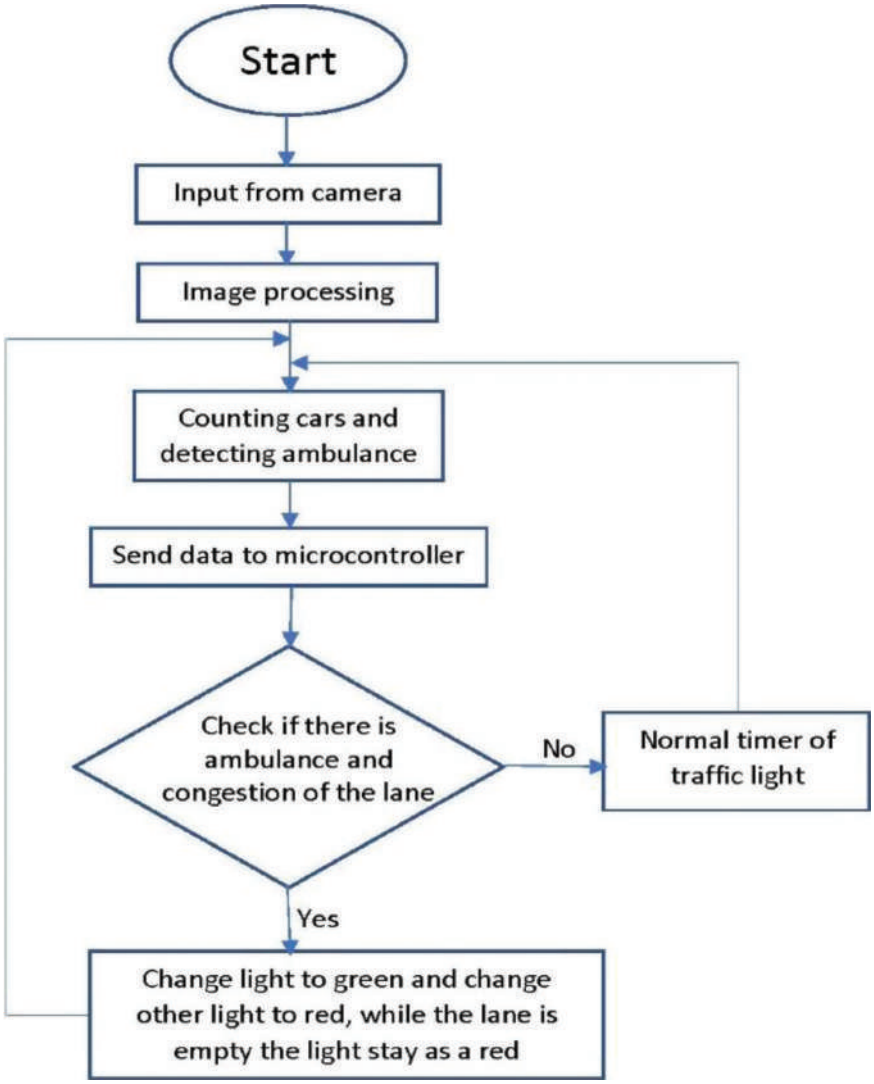

Fig. 7. Flowchart of system algorithm.

6. EXPERIMENT RESULT

Experiment steps start with downloading images and selecting object in each image one by one that we want to recognize it. Then making an XML file for each image that contain coordination of that object in the image to be ready for YOLOv3 this done by python code, to be ready for training. For training this model, GPU used for around 1 day duration with graphics card NVIDIA GTX 1060.

After the model has been implemented and tested many times, possible results were obtained. As it appears, the system works normally and continues getting images from camera that installed in the traffic light, as shown in Fig. 8.

It tested with different in number of images for training, and it tested with the image, the accuracy and time of training were different. As shown in Table 1 and Fig. 9 dataset for training, 4000 images have been used (2000 normal cars and 2000 ambulance).

As its clear from Table 1, we have 500 images for car with duration of 40 min the result is 97%, if we increase training time to 6 h and number of images to 4000 the system accuracy reaches maximum value 100% to detect normal cars and ambulance, while when the training time is short and number of images lesser the accuracy of detecting the ambulance starts from 65%.

As shown in Fig. 10 in the second test, the system implemented on a video for detecting ambulance the results shows different accuracy and time of training, as shown in Table 2 and Fig. 11.

TABLE 1: Accuracy with different dataset

Number of images / Accuracy	500 Image	1000 Image	2000 Image	3000 Image	4000 Image
Car (%)	97	94	98	98	100
Ambulance (%)	65	72	95	96	100
Time of training	40 min	55 min	110 min	210 min	360 min

Fig. 8. Simulated system.

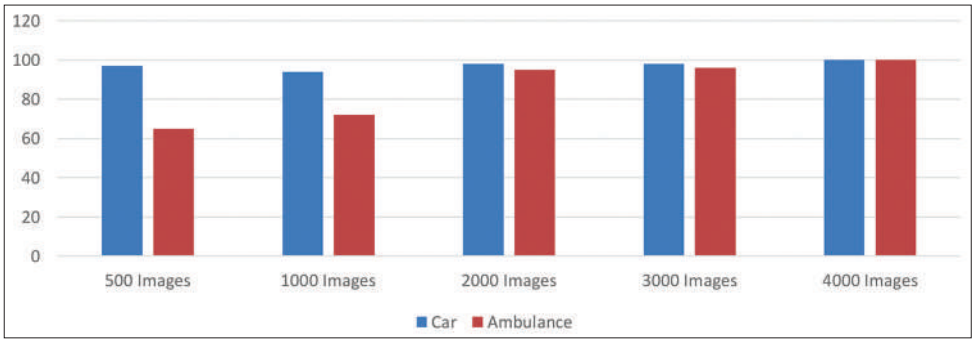

Fig. 9. Accuracy with different dataset.

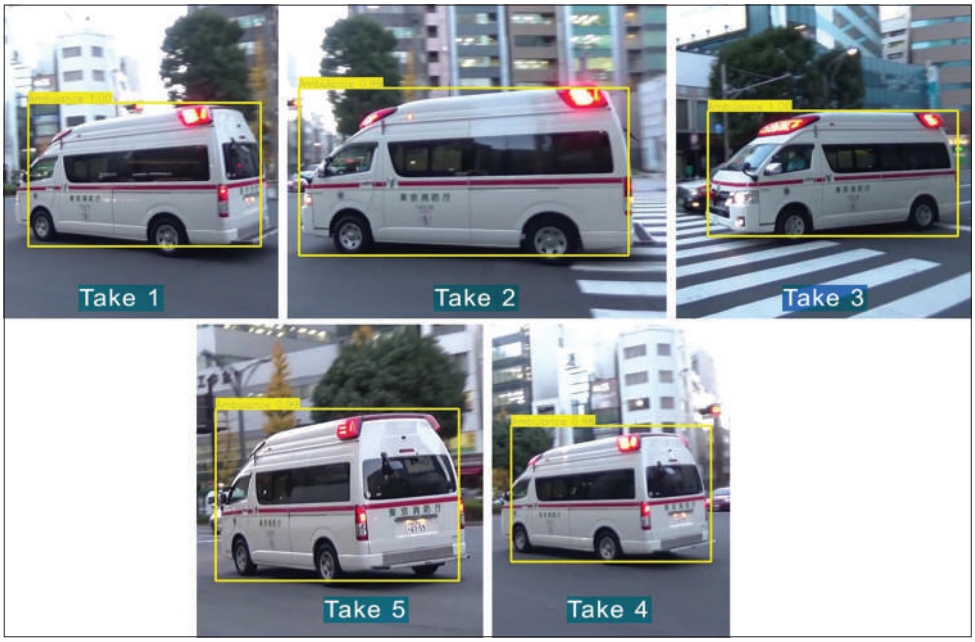

Fig. 10. Different takes of video for detecting ambulance.

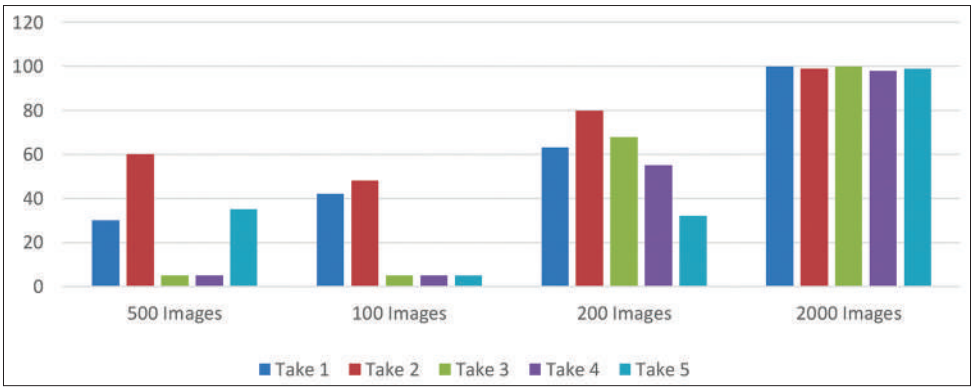

Fig. 11. Accuracy of ambulance with different dataset (Video).

TABLE 2: Accuracy of ambulance with different dataset (Video)

Different takes / Number of images	Take 1	Take 2	Take 3	Take 4	Take 5
500 Image	0.30	0.60	0.05	0.05	0.35
1000 Image	0.42	0.48	0.05	0.05	0.05
2000 Image	0.63	0.80	0.68	0.55	0.32
4000 Image	1.00	0.99	1.00	0.98	0.99

7. CONCLUSION

In this paper, we developed an intelligent approach to solve traffic lights congestion problems using machine learning with image processing models. The system mainly depends on Yolov3 model and OpenCV for decision. The traffic information is received from cars and vehicles in traffic light intersections. The system can recognize two types of car information, one of them is car type and the other is number of cars. Car type is used for distinguishing emergency car from normal car and number of cars is used for comparison among cars in each lane. In both cases, the system uses gathered information and gives priority to emergency cars over normal car and crowded lane to empty lane. To handle the complex traffic cases in our problem, the system uses image processing and Yolov3 algorithm. Another feature of this system is that the traffic lights communicate together through wireless medium to gives priority to emergency car. Tests experiments

presented that the system can reduce over 55% of the average waiting timing for cars in traffic intersection and process emergency car as soon as possible. The above capabilities have good impact and effect in smart city's traffic lights.

REFERENCES

[1] N. Diaz, J. Guerra, and J. Nicola. "Smart Traffic Light Control System". In: *2018 IEEE 3rd Ecuador Tech. Chapters Meet*, *ETCM 2018*, 2018.

[2] I. Santos-González, P. Caballero-Gil, A. Rivero-García, and C. Caballero-Gil. "Priority and collision avoidance system for traffic lights". *Ad Hoc Networks*, vol. 94, pp. 101931, 2019.

[3] A. H. Akoum. "Automatic traffic using image processing." *Journal of Software Engineering and Applications*, vol. 10, no. 9, pp. 765-776, 2017.

[4] H. Joo, S. H. Ahmed and Y. Lim. "Traffic signal control for smart cities using reinforcement learning". *Computer Communications*, vol. 154, pp. 324-330, 2020.

[5] A. Dumka and A. Sah. *Smart Ambulance Traffic Management System (SATMS)-a Support for Wearable and Implantable Medical Devices*. Elsevier Inc., Amsterdam, 2020.

[6] M. M. Elkhatib and A. S. Alsamna. "Smart Traffic Lights using Image Processing Algorithms". In: *2019 IEEE 7th Palestinian International Conference on Electrical and Computer Engineering,* pp. 1-6, 2019.

[7] E. L. H. Imad. "Proposed Solutions for Smart Traffic Lights using Machine Learninig and Internet of Thing". In: *2019 International Conference on Wireless Networks and Mobile Communications*, pp. 1-6, 2019.

[8] L. F. P. Oliveira, L. T. Manera and P. D. G. Luz. "Smart Traffic Light Controller System". In: *2019 Sixth International Conference on Internet of Things: Systems, Management and Security*, pp. 155-160, 2019.

[9] T. A. Kareem and M. K. Jabbar. *Design and Implementation Smart Traffic Light Using GSM and IR*. pp. 1-5, 2018.

[10] M. B. Natafgi, M. Osman, A. S. Haidar and L. Hamandi. Smart Traffic Light System Using Machine Learning". In: *2018 IEEE International Multidisciplinary Conference on Engineering Technology*, pp. 1-6, 2019.

[11] M. Z. Ismail, A. Z. A. Lutfi and M. A. M. Roslan. "Smart traffic light for emergency vehicle by using arduiono". *AIP Conference Proceedings*, vol. 2129, pp. 1-6, 2019.

[12] Andreas, C. R. Aldawira, H. W. Putra, N. Hanafiah, S. Surjarwo and A. Wibisurya. "Door security system for home monitoring based on ESp32". *Procedia Computer Science*, vol. 157, pp. 673-682, 2019.

[13] J. Redmon and A. Farhadi. *YOLOv3: An Incremental Improvement*, 2018.

[14] Y. Jamtsho, P. Riyamongkol and R. Waranusast. "Real-time Bhutanese license plate localization using YOLO". *ICT Express*, vol. 6, no. 2, pp. 121-124, 2019.

[15] Y. Jamtsho, P. Riyamongkol and R. Waranusast. *Real-time License Plate Detection for Non-helmeted Motorcyclist using YOLO*. *ICT Express*, Amsterdam, 2020.

[16] F. Koyanagi. *ESP32 With ESP-Now Protocol*, 2019.

ORIGINAL RESEARCH ARTICLE UHD JOURNAL OF SCIENCE AND TECHNOLOGY

A Traceable and Reliable Electronic Supply Chain System Based on Blockchain Technology

Shaniar Tahir Mohammed*, Jamal Ali Hussien

Department of Computer, College of Science, University of Sulaimani, Sulaymaniyah, Iraq

ABSTRACT

Electronic supply chain (ESC) is a network among the parties of a supply chain system, such as manufacturers, suppliers, and retailers. It recodes all the processes involved in the distribution of specific products until transported to final customers. Blockchain (BC) technology is a decentralized network that records all the transactions in real-time and is used in many areas such as cryptocurrency. In this paper, we work on an ESC system that records all the transactions based on BC technology using a drug supply chain system as a case study. The recording of the transactions consists of three main stages. First, all the parties of the ESC system are represented in the BC network as clients with unique identities. Second, all the information related to a specific drug is recorded inside the transaction and each transaction has its own signature. Finally, all the transactions of the drug from the manufacture to the patient are recorded inside a block with a unique identity for each block. These steps inside the BC are performed based on security cryptography mechanisms, such as rivest-shamir-adleman (RSA) and secure hash algorithm SHA. The results illustrate that the proposed approach protects the drugs from counterfeiting, ensures the reliability, and provides a real-time tracking system for the transactions that have occurred among ESC parties.

Index Terms: Blockchain, Block, Electronic Supply Chain, Monitoring, Reliability, Traceability

1. INTRODUCTION

Supply chains can be defined as a series of interconnected activities between manufacturers and customers, which include the coordination, planning, and controlling of products and services [1]. The classical supply chain has many issues such as need for paperwork; speed limits; and lack of traceability, security, and reliability [2]. The ESC records all the activities and transactions of supply chains electronically [1], [2], [3]. In the logistics process in an ESC, the products can be transported in a way that the parties (manufacture, supplier, distributor, wholesaler, retailer, and customer) of the network can ensure the quality of goods [1], [4], [5].

The blockchain (BC) is a decentralized peer-to-peer (p2p) network distributed ledger, with unlimited digital transactions across the network without the need of third-parties. This technology can be used in different areas such as cryptocurrency, since it has a useful number of features such as reliability and traceability [6], [7], [8]. BC has different types depending on the organization or the company that uses it or on the architecture of the network [6]. In BC technology, every single node or client has a copy of the ledger in the network after a consensus from all participants [2], [6]. BC has four basic features: Decentralization, openness, security, and privacy [2], [4]. BC and distributed databases (DBs) are different in their structures. In addition, in BC systems the transactions are controlled and managed by all the participants while in database system DBs the transactions are managed by a single entity [6].

Access this article online

DOI:10.21928/uhdjst.v4n2y2020.pp132-140

E-ISSN: 2521-4217
P-ISSN: 2521-4209

Corresponding author's e-mail: Shaniar Tahir Mohammed, Department of Computer, College of Science, University of Sulaimani, Sulaymaniyah, Iraq. E-mail: shaniar.mohammed@univsul.edu.iq

Received: 28-08-2020 Accepted: 03-12-2020 Published: 14-12-2020

Many researchers have worked on the process of merging the electronic supply chain (ESC) with BC using different approaches. However, either the researches stay theoretical and have not been implemented [4] or it does not fully benefit from all the security features of BC for improving reliability, traceability, and the monitoring process of the ESC systems [9].

In this paper, BC technology is used to create a reliable architecture for the ESC process and solves the problem of supply chain systems, such as reliability and traceability. Regarding the drug safety issues, the aim of this research was to help authorities in Iraqi Kurdistan to monitor and trace drug transportation from the manufacturers all the way to the patients in a secure and reliable way. In particular, this model is helpful in reducing paperwork, monitoring drug flow between ESC clients, protecting the drug from counterfeiting, tracing the transactions, reducing cost, and protecting the information flow between clients.

The proposed model is based on three main parts of BC technology used in ESC architecture: *Clients*, *Transactions,* and *Blocks*. The *Clients* represent the ESC parties, such as suppliers and manufacturers. Each client has a unique *identity* based on the security mechanism *RSA-1024*. The *Transactions* hold the drug flow information in ESC between all parties. The proposed model generates a *signature* for each transaction based on *RSA-1024* algorithm, for protecting the ESC from unknown transactions and also from modification. The *Blocks* hold the transaction between the ESC parties, each block holds five transactions from the manufacturer to the final destination, the patient. Each block has a unique *identity* based on the *SHA-256* algorithm. The information flow of drug ESC model is decentralized and shared between all the clients and recorded in real-time enabling tracking and monitoring of the activities by all the participants.

1.1. Problem Statement

The classical supply chain has some problems such as depending on paperwork to exchange information; high cost; and lack of reliability, traceability, and trust. While in the ESC, all the information and processes are captured and recorded in an electronic way, which is helpful in eliminating paperwork, reducing cost, and increasing reliability, since all processes can be monitored by all parties of the ESC system.

BC is a helpful technology that can be used with an ESC to record all the information in a decentralized way. Then, the processes of the ECS and can be monitored by all participants of the network without needing a third party. In addition, it increases reliability because in BC various security mechanisms are used when recording supply chain processes. Furthermore, traceability can be improved based on BC technology, since the encryption of the information prevents unknown transactions and unknown clients protecting the data from modification. All the transactions that have occurred in the ESC can be monitored in real-time.

In Iraqi Kurdistan, there does not exist an electronic system for recording and monitoring drug information and the transactions between the parties of the supply chain system. Therefore, it is difficult to establish reliability and provides an efficient traceability of drugs. For our case study, we work on the pharmaceutical system for drug transportation from manufacturers to final destination patients in Iraqi Kurdistan using ESC with BC technology.

The proposed system allows us to protect the drug from counterfeiting, enables traceability of drugs, and increase reliability between all parties in the ESC system. The information flow between all parties is held in BC in a secure way without a third-party involvement; therefore, the authorities can easily monitor drug transportation and transactions.

2. BACKGROUND

2.1. The Structure of ESC Systems

The ESC is a network between the producer of the specific product and the supplier to record the information about all the processes of product transportation and improving health and safety, speed, cost, scalability, and transparency while distributing to consumers [10], [11], [12]. In this network, there exist various entities, such as people, resources, and information that need to be recorded in a fast and secure way. The general structure of the ESC includes the following participants:

a) Provider: It provides raw materials to the suppliers, such as the raw materials used in producing drugs, food ingredients, and automobile parts [13].
b) Supplier: It is somebody who is responsible for the actions of producing the raw materials, like a *farmer*.
c) Manufacturer: The manufacturer performs various actions to produce specific products.
d) Distributor: The distributor is responsible for moving the product to the retailers.
e) Retailer: It is responsible for marketing the goods, such as local stores, supermarkets, pharmacies, or car shops [3], [14].

f) Consumer: The consumer buys a product and checked it to ensure originality. For instance, a patient who buys the drug in a pharmacy [13].

Fig. 1 illustrates all the stages of the general ESC process:

2.2. BC Architecture

BC technology was conceptualized for the first time by Satoshi Nakamoto in 2008 and used in various areas especially for cryptocurrencies like "Bitcoin" [15], [16], [17]. This technology is a decentralized p2p mesh network of nodes linked to each other and contains blocks without the need to be managed by a third-party. Several layers govern BC operations and generate the protocols for BC applications.

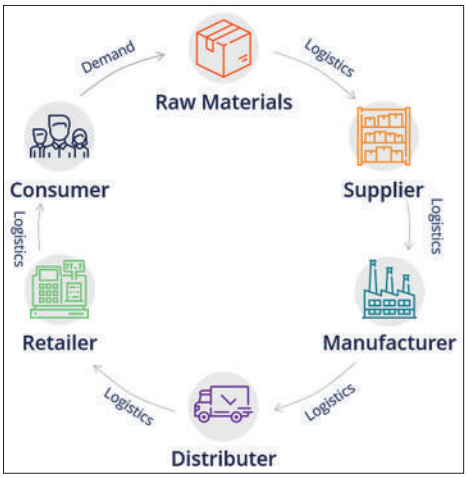

Fig. 1. General structure of the electronic supply chain.

BC generally has two main types: Public BC and private BC. Public BC is decentralized where parties can access the current and previous records. While private BC is a centralized network that is privately available for organizations that have a limited number of participants. Private BC is less secure than public BC. Fig. 2 shows an overall structure of the BC architecture [18]:

The BC contains a sequence of techniques that are used to recording transactions in real-time between the parties of the network (*sender* and *recipient*). The information is held inside blocks and each block links to a previous block, as shown in Fig. 2. The BC provides security features such as cryptographic hash, digital signature, and distributed consensus mechanism [13], [18], [19].

Fig. 3 illustrates the general architecture of BC in the Bitcoin process [15]. Each transaction that occurs in a BC encapsulates the phases is shown in Fig. 3. In the case of supply chain systems, all logistic processes from producing a specific good until delivering it to customers are recorded.

The Bitcoin cryptocurrency process consists of the following six stages. The same stages are used for our proposed system.

1. The Transaction: The transaction holds information, for example, in an ESC transaction; it includes the sender and receipt identity, date and time, the quantity of the goods, name of the product, location, and so on.

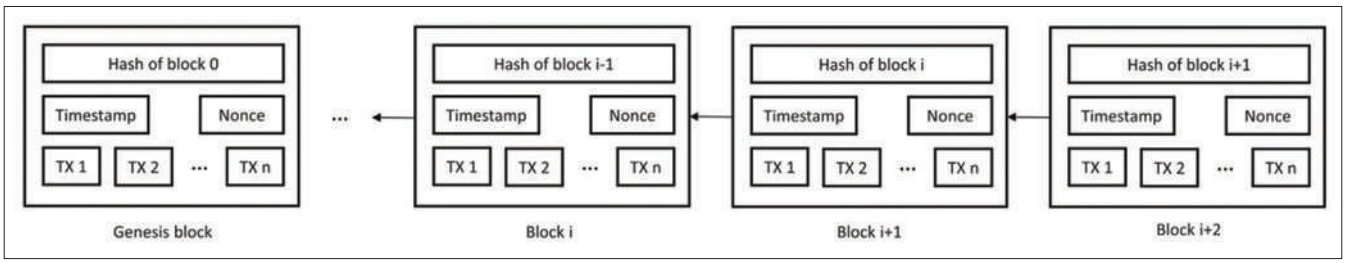

Fig. 2. Block structure in the blockchain technology.

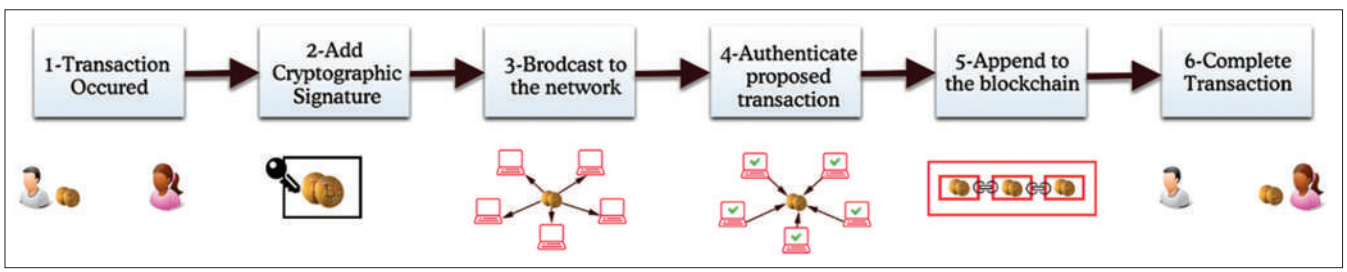

Fig. 3. Cryptocurrency with blockchain architecture.

2. A cryptographic signature is the second stage of the BC architecture to provide a secure algorithm function to implement a cryptographic signature to both sender and receipt identity using cryptographic algorithms, such as SHA256, SHA512, and RSA.
3. Broadcasting the Transaction: In this stage, the transaction must be broadcasted to the network for the authentication process.
4. The transaction verification: The transaction must be authenticated and verified by all the parties inside the decentralized network.
5. Digital ledger: After notifying all the parties of the BC of the new transactions, they are added to the digital ledger and appended to the BC.
6. Transaction completion: Finally, the transaction is completed and the money or the information related to it is transferred to the receipt and added to the block. Each block is linked to the previous one.

2.3. Cryptographic Algorithms

The secure hash algorithm SHA is one of the cryptographic hash functions designed to hold data securely by transforming the data into hash code using its own family of types such as SHA1, SHA224, SHA256, and SHA512. Each of them has a different size in bytes [20].

The RSA cryptographic system is used for data encryption and decryption with two keys (private key and public key), when the private key is only known to the owner and the public key is publicly available and can be accessed by everyone [21], [22]. The size of the key of RSA should be 1024 bits or higher. The public key is used for encryption while the private key is used for decryption [21].

3. THE RUNNING EXAMPLE

We describe the supply chain process in an earlier section. We show a small example of a supply chain process between two clients known as the *manufacturer* and the *supplier* for transporting a drug between them. Table 1 shows the information related to one transaction occurred between two clients in the supply chain. This transaction is taken from a large set of transactions from the pharmaceutical system in the Iraqi Kurdistan. We use the information about a specific drug to demonstrate various transactions in our proposed ESC with BC. In the upcoming sections, we show more transactions about a specific drug. The structure of the transactions contains all the information needed for the drug supply chain process, such as *drug_id, drug name, sender_id, recipient_id, location, size,* and *date and time*.

TABLE 1: A simple transaction information occurred between two clients in a supply chain system

Manufacturer name	Sanofi
Supplier name	Awafi
Drug name	Plavix
Drug Id	3622554532
Date and time	October 10, 2019, 02:00:13

In ESC systems, the information can be stored electronically with a centralized system without real-time recording of the process, which is not secure. However, public BC systems with ESC are secure since they are decentralized and there is no need for third-parties to manage the process. Public BC systems are reliable and transactions can be traced at each stage of the ESC in real-time.

4. RELATED WORK

Randhit kumar and *Rakish Tripathi* [9] proposed a traceability structure for supply chain based on BC technology to medicine system or drug manufacturing to protect the drug while transported from the manufacturer to the consumer, they used BC to encrypt the QR code of the drugs to protect the drug from counterfeiting. The methodology of this research provides a structure to protect the medicine supply chain from a man-in-the-middle attack.

BC in various case studies and different sectors of industry such as the pharmaceutical supply chain is used by *S. Aich*, *S. Chakraborty*, *M. Sain*, *H. Lee*, and *H. Kim* [13] to ensure the tractability of drugs and to improve the efficiency of supply chain network. They mentioned the problems occurred in different sectors of the conventional supply chain and find solutions. They compare the traditional supply chain to a digital supply chain based on BC and Internet of Things (IoT) for pharmaceutical process to track and protect drugs from counterfeiting. IoT was used to record digital identification for all products to provide trustworthiness in the digital supply chain system. All the participants of the system in the network can ensure the transparency of the information recorded in the BC.

M. P. Caro, *M. S. Ali*, *M. Vecchio*, and *R. Giaffreda* [23] proposed a new agriculture food supply chain based BC architecture with IoT to keep the system from data tampering. The integrity of the data and traceability of the process is

conducted using various BC mechanisms such as ethereum and hyperledger sawtooth.

A three-tier architecture based on BC was proposed by *S. Malik* [10] to ensure data availability to consumers and to provide scalability for handling transaction loads while keeping the history and confidential information safe when delivering to other parties of a supply chain process.

5. BC -BASED ESC SYSTEM

In this section, we propose an ESC model, which enables traceability, reliability, monitoring of drug transactions in the Iraqi Kurdistan based on the BC technology. We worked on the pharmaceutical supply chain by recording logistic steps of the ESC to transport a drug from the *manufacturer* to a *patient* using BC technologies. Fig. 4 shows a block diagram of the proposed model.

In our proposed system, transactions occur among supply chain parties in pharmaceutical process according to these instructions:

1. Capturing the transaction *n* in the pharmaceutical supply chain system between client A and client B.
2. Based on the *RSA-1024* algorithm, generating a unique identity for each one of the five different types of clients. The identities are shared between all the participants of the BC. Table 2 shows the client identities.
3. Build a unique transaction *signature* using RSA-1024, which facilitates traceability and the identification of the drug transported between the clients.
4. Each transaction holds the *sender and recipient identities*, *item information*, *date and time,* and other related information.
5. Typically, each drug requires *five* transactions between the *clients* to be delivered from the *manufacturer* to the *patient* in the supply chain process. These transactions are added to a single block *m*.

TABLE 2: Client identity while applied RSA-1024 algorithm in ESC

Client Type	Client Name	Client Identity
Manufacturer	*Sanofi*	30819f300d06092a864886f70d 01010105000381…….
Supplier	Awafi Medicine Store	06c48043be02d767f023a62ff5 b7ec7c0bc08e9bd…….
Wholesaler	KMCA	c873e055bf23971a944882e78 eb82ed0045af93c2…….
Retailer	Shar	f3a6765fb8755bfc8543ef2d691 d3799ec281cda96…….
Patient	Ahmed	0dfb14bfb66ada3c097353d2cc 58608e8659cbbe9…….

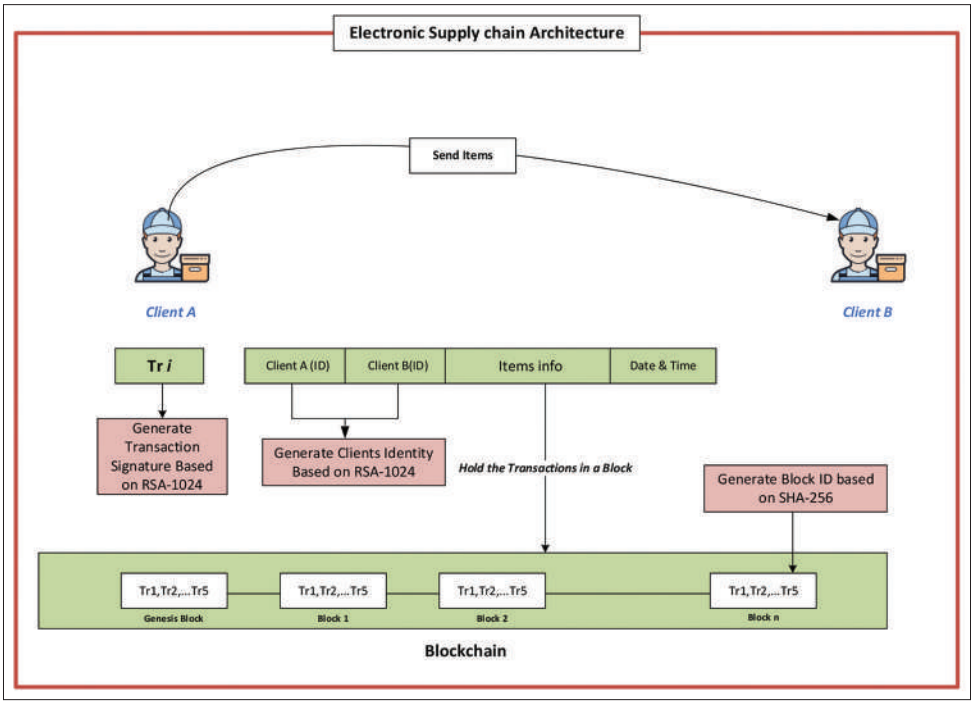

Fig. 4. Block diagram of the electronic supply chain process using blockchain technology.

6. Before adding them to the BC, a *unique identity* based on the *SHA-256* algorithm is generated for each block.
7. The block *m* added to the BC and each block linked to the previous one. This makes blocks to be easily traceable and reliable, and facilitate real-time monitoring.

In Fig. 5, the main parts of the proposed ESC system are illustrated. The system records any transaction that has occurred inside the ESC using BC. The ESC includes five types of clients: *Manufacturer*, *supplier*, *wholesaler*, *retailer*, and *patient*. Drugs are produced by the manufacturer, transported to the supplier, wholesaler, and then to the warehouse or the retailer. Finally, the drugs will be delivered to the patient. All these transactions can be tracked and recorded securely without need to third-party's involvement.

5.1. Transaction Processes

Each transaction has its own *signature*; they are created with RSA-1024 algorithm. With these signatures, we can protect our ESC transactions from any *unknown transactions*. Fig. 6 depicts a small transaction between two clients in the ESC.

We hold five transactions inside each block of the BC, one transaction between each two clients starting from the *manufacturer* and ending with the *patient*. Table 3 shows three transaction *signatures* as an example.

5.2. The Block Structure of Our BC System

In this research, another main part is the generation of a *unique* block for the ESC's transactions before adding it to the BC. Block identities are generated with the *SHA-256* algorithm.

In general, inside the BC, we have an unlimited number of blocks, which means that the system can generate any number of blocks, but in the proposed approach worked on 2000 blocks, each block holds five transactions in the pharmaceutical supply chain process in Iraqi Kurdistan. The size of each block is between 830 and 890 bytes depending on the amount of information saved inside each transaction and held in a block, the BC is not reseted after holding the transaction, and the transactions history remain inside the blocks. Each block in the BC system is protected from modification because these blocks are shared in a decentralized network and each block is linked to the previous block with its own *identity*. Only the participants of the supply chain system can see the information inside the blocks, which enables the clients to easily *monitor* the processes of ESC. The average time duration between the current block and the previous block is 0.0056 ms. Table 4 shows four blocks with current and previous identities.

6. RESULTS AND DISCUSSION

In the proposed system, we can ensure drug quality and the correctness of information related to the drug manufacturing process. Our system creates a secure channel among parties based on BC technology, which provides *traceability* of drugs, reduces *cost*, enhances *reliability,* eliminates *paperwork, and facilitates monitoring* by all clients in the pharmaceutical process.

Table 5 contains a chain of five transactions inside a single block *(#block112)* regarding the transportation of a specific drug from the manufacturer all the way to the patient. The

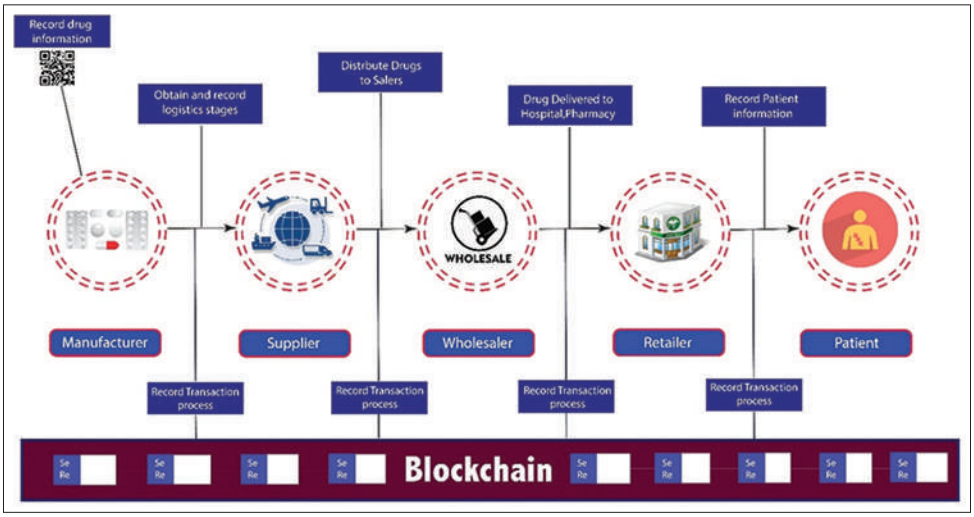

Fig. 5. Pharmaceutical supply chain process in ESC.

TABLE 3: Three transaction signature while applied RSA-1024 algorithm in ESC

1bee9567d03e61c48e748cb2983ee4bfd308009555e45d6fe9bbbed051e338055e9950a664e280048268b8457a16ce22a8b699b3e11e0f8d553e
23541b328e949f18c7db20cd44a9c60153d3dff3538984aae8eb1fa117d54fe84e2cfd261a659cc05c97e87e7b7078c101d81595ebcf4610f
ca0172799935f82df0125b04e82
6f606e75128216b1562ca131ffdc6bae4d9967636244cac72478ea5e8764bf86824f6ad9ed250b7c031896604e969dd3cceb5989a556bf31
e0a39aca8d84d69e41740221592f4b0c0feacb34f0068c5ef5d731108cbe8e6c36503d1d158332eeb6b6cd62b734dd147409d11d085eb65
dccb4d0874c384ddbf2b0495aec858c8c
8b3c55fbe861e80937fb1ac70fa7781c041bd7af30249b0e42f7f6553e265a260a87d00d44a5942a34f3cbf168a7a54a1afb9dc40e946ff43d0
d6a7e69d72eea8c96b8da2306e7e334597cc7192e5f040318bfeea61af225c2b0da26b68b6195ef4066c6b8a9f65c9d49607bf68b340359ae
bb8e464de7d1b6c87f687851bb70

TABLE 4: Block identity in our blockchain system generating based on SHA-256

Block number	Block current identity (SHA-256)	Block previous identity (SHA-256)
#Block112	6ad6d74005e15af42 18b693b3c……	0a6b88cb1c75ab 970fd11e4……
#Block251	23075fc5076b836 136a3a92e9……	a9f893431c9c961 bfb7896483……
#Block512	97fb8026b07ed4f1 f73d23f31……	1ca161f2094af3f6e fba34h11……
#Block600	906886c8477237b 80b0de1fb2……	aa45b1772c74e330 74d0c061a……

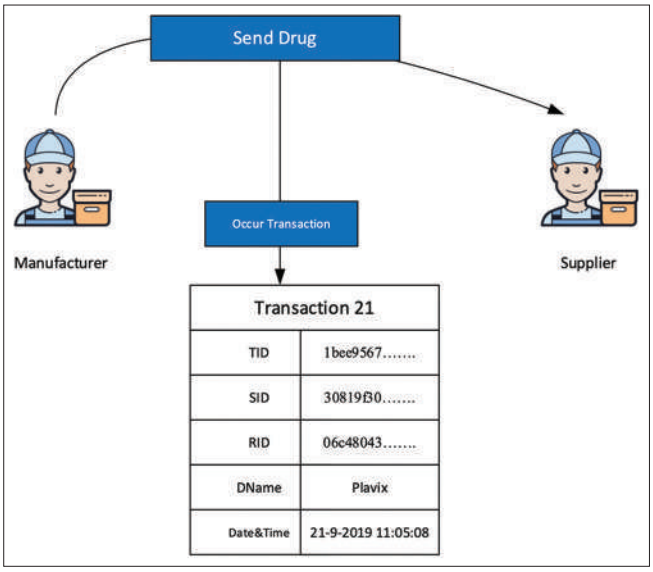

Fig. 6. Transaction structure and signature in ESC.

drug has its own unique identifier. There are unique identifiers for each of the sender and the receiver per transaction along with the date and time of the transaction.

In Table 6, we choose a transaction **(***#transaction21)* among the five transactions of the block *(#block112)* between the supplier, *RASAN,* and the wholesaler, *KMCA,* showing all the information of that transaction. The detail about the transaction includes the *location, date, and time*, and *size*.

6.1. Traceability

In our proposed system, each *block* contains the transactions that are related to one single drug. Each drug has a *unique identifier*, for example, *#block112* is encrypted with the *SHA-256* cryptography algorithm and linked to the previous block (Table 6). In this way, we can *trace* the transaction between these two clients. We can determine when the transaction has started (*DateTime*), which clients participate in the transaction (*Sender and Recipient IDs*), where is the current location of the drug (*Supplier and Wholesaler locations*), and whether the transaction has *occurred* or it is in a waiting state.

The information is recorded in real-time, which means we can *trace* each drug transported between the clients in real-time. The transactions can be monitored by all the participants, without modification by an *unknown* client or user. Since the network is decentralized, we do not need a third-party for managing the information of the transactions that are held inside the blocks.

6.2. Reliability and Monitoring

The reliability of the information is another feature of the proposed approach. Since our system uses several security mechanisms with BC technology, such as RSA-1024 and SHA-256 algorithms. These algorithms are used for generating a unique identity for each participant (sender identity and recipient identity), transaction (transaction identity), and block (block identity) of the ESC system, as shown in Table 5. With these identities, we can trust the transactions. BC has an important process called consensus algorithm, which provides agreements among clients of the BC network about the data. Based on the consensus algorithm a participant can generate new blocks that must be accepted by the other parties of the system. This is useful for improving the reliability and ensuring the traceability of the system.

There is an important feature inside the transactions, which is the *transaction type*. Its value is either *verified* or *unverified*. If a client notices that some *identities* have been changed or the

TABLE 5: Simple drug information for five transactions inside one block in the blockchain system

#Block112					
Drug Name: Omeprazole_Cap E/C 10mg,			**Drug ID: 0103050P0AAAFAF**		
Tr	**Sender name**	**Sender ID**	**Receiver name**	**Receiver ID**	**Date time**
20	Sanofi (Manufacturer)	30819f300d06…	RASAN (Supplier)	300d06092a86…	2020-02-04 17:25:48
21	RASAN (Supplier)	08b1058b43….	KMCA (Wholesaler)	dbded6379261…	2020-02-05 11:15:22
22	KMCA (Wholesaler)	002b6bd609e7...	Zhin (Warehouse)	10af53600f2c…	2020-04-11 9:08:40
23	Zhin (Warehouse)	6a2744af1447…	Lia (Retailer)	236a2744af14…	2020-04-21 16:21:54
24	Lia (Retailer)	49ad4dbd1e…	Ahmed (Patient)	a6a8c08fc87cd...	2020-04-29 06:22:11

TABLE 6: One transaction inside a block in our BC system from the ESC

#Block112	
#Transaction21	
Transaction ID	1bee9567d03e61c48e748cb2983ee4bfd 308009555e45d6f……..
Sender ID	08b1058b43……..
Recipient ID	300d06092a86……..
Supplier Location	Iraq
Wholesaler Location	Iraq
DateTime	10-1-2020 08:22:12
Drug ID	0103050P0AAAFAF
Drug Name	Omeprazole_Cap E/C 10mg
Size in Block	150 Byte
Block_Id	6ad6d74005e15af4218b693b3cb1fb79538 159d5db568f7528c……
Block _Prev_Id	0a6b88cb1c75ab970fd11e49f1db8d237d9 bf819ef1165fdb0fb……
Transaction Type	Verified
Situation	Occurred

drug information has been modified, then the value of the field *transaction type* is changed from *verified* to *unverified* and all the participants of the network are notified about this modification. This prevents the transaction to be faked and protects the drug from counterfeiting. This process enables the reliability of the ESC system and establishes trust among the participants of the network. Since all the transactions happen in real-time, all participants as well as the authorities can *monitor* the process of drug transportation between all the clients of the ESC system.

7. CONCLUSIONS AND FUTURE WORK

In this research work, BC technology is used for recording information flow between supply chain parties using the pharmaceutical supply chain system in Iraqi Kurdistan as a running example. The proposed system generates unique identifiers for the clients and the transactions regarding a specific drug and stores them along with the drug information inside a block of the BC system. The generation of identifiers and storing of information happen in real-time when the transactions occur. Therefore, the authorities and supply chain parties can easily monitor or track the transactions to protect the drug from counterfeiting and information from modification, thus establishing trust and reliability of the process. In addition, the process of recording and monitoring supply chain transactions electronically reduces cost and time and eliminates paperwork.

In the future, we want to implement our proposed model in other sectors, such as food and clothes, to provide reliability and traceability among vendors and customers. Furthermore, the Internet of Things IoT can be used to hold transaction information about physical things that are included in the ESC systems.

8. ACKNOWLEDGMENT

We would like to express thanks to Dr. Firdous Nuri, Dr. Dana Sardar, and Sulaimani Health Center for providing information about the drug manufacturer companies and pharmaceutical parties in Iraqi Kurdistan.

REFERENCES

[1] K. Korpela and T. Dahlberg. "*Digital Supply Chain Transformation Toward Blockchain Integration*". Hawaii International Conference on System Sciences (HICSS)At: Big Island, Hawaii, pp. 4182-4191, 2017.

[2] D. Schniederjans, C. Curado and M. Khalajhedayati. "Supply chain digitisation trends: An integration of knowledge management". *International Journal of Production Economics*, vol. 220, p. 107439, 2020.

[3] S. Chen, R. Shi, Z. Ren, J. Yan, Y. Shi and J. Zhang. "A *Blockchain-Based Supply Chain Quality Management Framework*". IEEE 14th International Conference on e-Business Engineering (ICEBE), Shanghai, pp. 172-176, 2017.

[4] D. Tse, B. Zhang, Y. Yang, C. Cheng and H. Mu. "*Blockchain Application in Food Supply Information Security*". IEEE International Conference on Industrial Engineering and Engineering Management (IEEM), Singapore, pp. 1357-1361, 2017.

[5] W. Kenton. "*Supply Chain*". Available from: https://www.investopedia.com/terms/s/supplychain.asp. [Last accessed on 2020 Apr 01].

[6] N. B. Al Barghuthi, H. J. Mohamed and H. E. Said. "*Blockchain in Supply Chain Trading*". 5th HCT Information Technology Trends (ITT), Dubai, United Arab Emirates, 2018, pp. 336-341, 2018.

[7] H. Min. "Blockchain technology for enhancing supply chain resilience". *Business Horizons*, vol. 62, no. 1, pp. 35-45, 2019.

[8] M. Nofer, P. Gomber, O. Hinz and D. Schiereck. "Blockchain". *Business and Information Systems Engineering*, vol. 59, no. 3, pp. 183-187, 2017.

[9] R. Kumar and R. Tripathi. "*Traceability of Counterfeit Medicine Supply Chain through Blockchain*". 11th International Conference on Communication Systems and Networks (COMSNETS), Bengaluru, India, pp. 568-570, 2019.

[10] S. Malik, S. S. Kanhere and R. Jurdak. "*ProductChain: Scalable Blockchain Framework to Support Provenance in Supply Chains*". IEEE 17th International Symposium on Network Computing and Applications (NCA), Cambridge, MA, pp. 1-10, 2018.

[11] G. Büyüközkan and F. Göçer. "Digital supply chain: Literature review and a proposed framework for future research". *Computers in Industry*, vol. 97, pp. 157-177, 2018.

[12] S. Kamble, A. Gunasekaran and S. Gawankar. "Achieving sustainable performance in a data-driven agriculture supply chain: A review for research and applications". *International Journal of Production Economics*, vol. 219, pp. 179-194, 2020.

[13] S. Aich, S. Chakraborty, M. Sain, H. Lee and H. Kim. "*A Review on Benefits of IoT Integrated Blockchain based Supply Chain Management Implementations across Different Sectors with Case Study*". 21st International Conference on Advanced Communication Technology (ICACT), PyeongChang Kwangwoon Do, Korea (South), pp. 138-141, 2019.

[14] S. R. Niya, D. Dordevic, A. G. Nabi, T. Mann and B. Stiller. "*A Platform-independent, Generic-purpose, and Blockchain-based Supply Chain Tracking*". IEEE International Conference on Blockchain and Cryptocurrency (ICBC), Seoul, Korea (South), pp. 11-12, 2019.

[15] V. Morkunas, J. Paschen and E. Boon. "How blockchain technologies impact your business model". *Business Horizons*, vol. 62, no. 3, pp. 295-306, 2019.

[16] C. Schmidt and S. Wagner. "Blockchain and supply chain relations: A transaction cost theory perspective". *Journal of Purchasing and Supply Management*, vol. 25, no. 4, p. 100552, 2019.

[17] D. Macrinici, C. Cartofeanu and S. Gao. "Smart contract applications within blockchain technology: A systematic mapping study". *Telematics and Informatics*, vol. 35, no. 8, pp. 2337-2354, 2018.

[18] S. S. Hazari and Q. H. Mahmoud. "*A Parallel Proof of Work to Improve Transaction Speed and Scalability in Blockchain Systems*". IEEE 9th Annual Computing and Communication Workshop and Conference (CCWC), Las Vegas, NV, USA, pp. 916-921, 2019.

[19] A. A. Maksutov, M. S. Alexeev, N. O. Fedorova and D. A. Andreev, "*Detection of Blockchain Transactions Used in Blockchain Mixer of Coin Join Type*," 2019 IEEE Conference of Russian Young Researchers in Electrical and Electronic Engineering (EIConRus), Saint Petersburg and Moscow, Russia, pp. 274-277, 2019.

[20] S. Gueron. "*Speeding Up SHA-1, SHA-256 and SHA-512 on the 2nd Generation Intel® Core™ Processors*". 9th International Conference on Information Technology New Generations, Las Vegas, NV, pp. 824-826, 2012.

[21] A. Karakra and A. Alsadeh. "*A-RSA: Augmented RSA*". SAI Computing Conference (SAI), London, pp. 1016-1023, 2016.

[22] S. A. Nagar and S. Alshamma. "*High Speed Implementation of RSA Algorithm with Modified Keys Exchange*". 6th International Conference on Sciences of Electronics, Technologies of Information and Telecommunications (SETIT), Sousse, pp. 639-642, 2012.

[23] M. P. Caro, M. S. Ali, M. Vecchio and R. Giaffreda. "*Blockchain-based Traceability in Agri-food Supply Chain Management: A Practical Implementation*". IoT Vertical and Topical Summit on Agriculture Tuscany (IOT Tuscany), Tuscany, pp. 1-4, 2018.

ORIGINAL RESEARCH ARTICLE UHD JOURNAL OF SCIENCE AND TECHNOLOGY

Fusion Method with Mean-discrete Algorithm in Feature level for Identical twins Identification

Bayan Omar Mohammed

Department of Information Technology, College of Science and Technology, University of Human Development, Sulaymaniyah, KRG, Iraq.

ABSTRACT

The study on twins is an important form of study in the forensic and biometrics field as twins share similar genetic traits. A biometric is one of the common types of pattern recognition which acquires biometric data from a person. From these data, a feature is established and extracted where these features can be used to identify individual. Exiting works in biometric identification concentrate on unimodal biometric identification. The high similarity in a pair of twin's biometric may lead to miss performance. Hence, due to their great accurateness, multimodal biometric systems have become more favored than unimodal biometric systems in identical twins identification. However, these systems are highly complex. We proposed Mean-Discrete feature based fusion algorithm for Kurdish handwriting and fingerprint for identical twins detection. Its viability and advantage over the unimodal biometric systems are highlighted. This paper employed 800 images from 50 pairs of identical twins from Kurdistan Region to carry out the experiment.

Index Terms: Mean-discrete Algorithm, Multi-biometric, Feature Based Fusion, Twins Identification, Kurdish Handwriting-fingerprint.

1. INTRODUCTION

Biometric-based identification and systems of verification are among the integral technologies today [1-3], and their applications are rather common in access controls (e.g., building entry and computers), electronic commerce (elimination of fake transactions), as well as illegal immigration's reduction [4]. Notably, biometric identification system for identical twins poses greater challenge as opposed to that which identifies non-twins due to the considerable resemblance that twin individuals have with each other [4,5]. For this reason, researchers of pattern recognition and computer vision have shown their interest in identifying the biometric of a twin. Furthermore, due to its high level of accurateness, in certain situation, this method was the one which could recognize a specific person's biometric pattern from a collection of individuals [6-8].

The unimodal biometric identification systems for identical twins are now significantly more accurate and reliable [9], and in this respect, good performance can be seen in a number of traits. Still, technological issues remain to be addressed. Among the available unimodal biometric systems include Wonder Ears (Identification of Identical Twins based on images of ear) [10], 3D face recognition (Identification of Identical Twins based on faces) [11], double trouble (Identification of Identical Twins based on Face Recognition) [12], analysis of facial marks [5], and aside from identification of identical twins based on handwriting individuality [13]; these systems have all been scrutinized. Nonetheless, it should be noted that these studies were

Access this article online

DOI:10.21928/uhdjst.v4n2y2020.pp141-150 | E-ISSN: 2521-4217 P-ISSN: 2521-4209

Corresponding author's e-mail: Bayan Omar Mohammed, Department of Information Technology, College of Science and Technology, University of Human Development, Sulaymaniyah, KRG, Iraq. E-mail: bayan.omar@uhd.edu.iq

Received: 28-10-2020 Accepted: 15-12-2020 Published: 27-12-2020

all considering the physiological aspects [14] implying the unlikely occurrence of change.

Sharing one zygote causes identical twins to have similar genetic composition, increasing the difficulty in identifying them [15]. More than one biometric trait would thus be used in identifying these twins, making multimodal biometric system suitable due to the use of both physical and behavioral traits in its application [16]. Multimodal biometric system combines many biometric traits from multitude of sources. In the context of enrolment, the use of this system enables the enrolment of users even though they have no identified biometric identifier. Such ability becomes a solution to the problems of enrolment, and these abilities therefore prove the universality of multimodal biometric system. To affirm sound performance in a twin's biometric identification, good and thorough features have to be used as input to a classifier. Accordingly, in a multi-biometric system, an individual is represented by various features. For this reason, a single feature extracted directly for the multi-biometric itself is not representative of a unique feature for a twin biometric.

There are countless of representations in multi-biometric systems, which have led to the presence of vast variance between features for one individual. Somehow, there is small variance in the context of twins' comparison, making it necessary to engage one more process. This is to enable the unique features to be represented from the pool of multi-biometric features. During the process, many representations obtained from multi-biometric representations of a twin are merged and converted into a uni-representation. The merging and conversion are done before the execution of the identification task. As a result, the level of variance in the data between the twins is decreased. However, the majority of past researches were focusing on the discrete feature extraction methods of each twin's biometric. Hence, this study presents the application of Mean-Discrete feature based fusion algorithm to combine these features with twins' Kurdish handwriting-fingerprint.

2. RESEARCH FRAME WORK

Features extracted from a feature extraction method comprise an ensemble of global features. In the context of this study, the features, which are usually classed individually, are representatives of the twin's Kurdish handwriting-fingerprint particularly, with respect to word and shape. Furthermore, the individual classification of features allows the identification of an individual within a twin or a group of individuals. Accordingly, this study presents the feature-based fusion that the performance of identification in the arena of twin biometric identification can be improved.

For the purpose, twin's exclusive individual features would be needed, whereas the extracted features are often in multi-representations. For this reason, individual features for each individual within a set of twins are employed together. Arguably, such usage will increase the performance of twin identification. These are called a Mean-Discrete feature vector and this method is used following the process of feature extraction. Mean-discrete feature vector carries the generalized features of global features possessed by individuals. In the model of twin identification, the features are generalized before the classification task. This generates better outcome. Relevantly, the framework proposed in this study is shown in summarized form in Fig. 1.

3. FEATURE EXTRACTION

Aspect United Moment Invariant (AUMI) allows the extraction of global features from the region and boundary (word or shape) in a separate and continuous manner to represent an individual [17]. Here, the fusion embedded scaling factor of aspect is created [18] into the United Moment Invariant [19], as shown in Fig. 2.

This instantly combines the capacities of these two functions of moment into the proposed AUMI. The [19] United Moment Invariant has an association with the geometrical representation that considers the normalized central moment equations of Geometric Moment Invariant (GMI) [20] and the boundary representation of Improved Moment Invariant (IMI) [21]. Finally, [17] AUMI comprises eight features with the construction of the [19] United Moment Invariants (UMI), as shown below:

$$\theta_1 = \frac{\sqrt{\varnothing_2}}{\varnothing_1} \quad (1)$$

$$\theta_1 = \frac{\sqrt{\varnothing_2}}{\varnothing_1} \quad (2)$$

$$\theta_3 = \frac{\sqrt{\varnothing_5}}{\varnothing_4} \quad (3)$$

$$\theta_4 = \frac{\varnothing_3}{\varnothing_2 \varnothing_4} \quad (4)$$

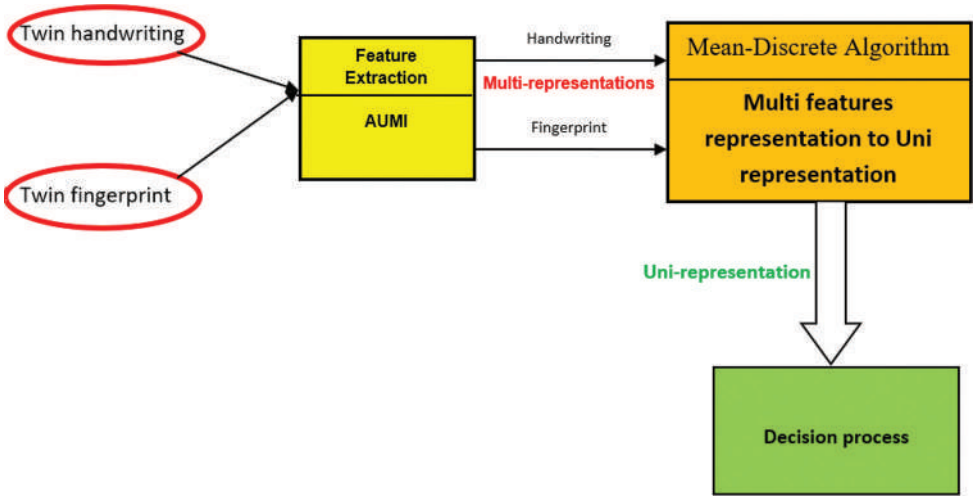

Fig. 1. Proposed framework for twin multi-biometric.

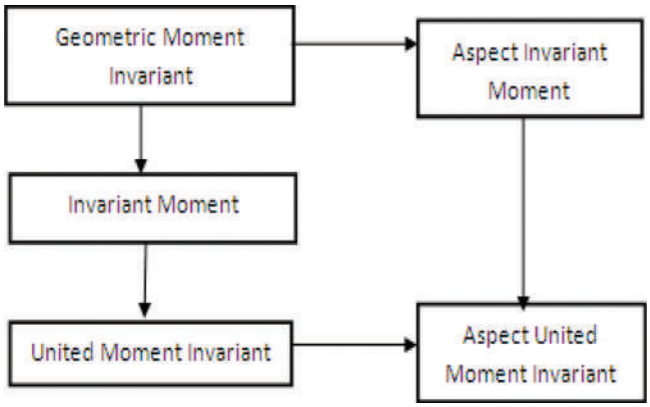

Fig. 2. Aspect united moment invariant structure by Mohammed and Shamsuddin [14], Hu [20].

$$\theta_5 = \frac{\varnothing_1 \varnothing_6}{\varnothing_2 \varnothing_4} \tag{5}$$

$$\theta_6 = \frac{\left(\varnothing_1 + \sqrt{\varnothing_2}\right)\varnothing_2}{\varnothing_6} \tag{6}$$

$$\theta_7 = \frac{\varnothing_1 \varnothing_5}{\varnothing_3 \varnothing_4} \tag{7}$$

$$\theta_8 = \frac{\varnothing_3 + \varnothing_4}{\sqrt{\varnothing_5}} \tag{8}$$

As ϕ_i denotes large values, the natural logarithm is employed. As such, below is obtained for $i = 1$ to 7; $\theta_i \leftarrow \log 10\ \phi_i$.

The features of the AUMI satisfy the individuality of the concept of the twin's handwriting-fingerprint [22,23], and the outcomes demonstrate a lower intra-class value for the variance between features for the mean absolute error (MAE) in comparison to the value for the inter-class. This is the reason why the features of the AUMI were explored and employed in the domain of twin biometric identification in this study. The AUMI presents the striking individual features in the extracted invariant feature. In the context of a twin's biometric identification, getting features that denote the twin's handwriting-fingerprint from numerous writing styles and shapes are the main purpose [23,24]. The AUMI is primarily concerned with obtaining the twin's handwriting-fingerprint's unique features. The purpose of employing algorithms is to extract individual features. Eventually, such use accurately reflects the handwriting-fingerprint of the twin. Conversely, for a multi-biometric representing an individual belonging to a twin, the directly extracted individual features do not directly represent the unique features of a twin biometric. As such, before the measurement task, additional processes should be included. This study proposes use of the Mean- Discrete feature based fusion algorithm before the identification task.

4. PROPOSED MEAN-DISCRETE FEATURE-BASED FUSION

Due to the performance of the collective process on the task of identification, Mean-Discrete Algorithm is dubbed as global combination as well. Furthermore, due to its reliance on each attribute for each feature within the dataset, the Mean-Discrete Algorithm also becomes part of the global

characteristic class. Such reliance allows the calculation of Mean-Discrete value for each attribute for each multi-biometric of twin. The application of Mean-Discrete feature vector leads to improved representation of data for the twin's Kurdish handwriting-fingerprint's individuality. Accordingly, the Mean-Discrete algorithm methodologies are presented in this section. Mean-Discrete algorithm is used at the feature level and it entails a blend of twins' multiple features for the concluding decision making. In the task of feature extraction for the multi-biometric of each twin, AUMI is used in producing the columns of eight feature vector, and for the process of Mean-Discrete, eight features are generated from the twin's Kurdish handwriting-fingerprint. For this reason, it is not impossible to keep the initial amount of invariant feature vector columns within the moment function that is utilized within the feature extraction task. Accordingly, the following section provides the elaboration of the process of Mean-Discrete feature-based fusion, and Fig. 3 details the flowcharts of the Mean-Discrete algorithm proposed in this study.

The feature value of Mean-Discrete is computed alongside both biometrics for a twin. This is in line with the class of the individual due to the fact that within a twin set, every individual has distinctive style of writing and shape of fingerprint. Hence, there is individuality of handwriting-fingerprint in twin identification. Using the individual's class, computation is made to the feature value of Mean-Discrete. The application of this method affirms the protection of the characteristic's uniqueness or individuality. In addition, the supervised method demonstrates its aptness for twin's handwriting-fingerprint particularly with respect to individuality. This is because this method maintains the individual features of each twin. In this context, if the two twins have a close or indistinguishable feature vector, then the two classes will be regarded as possessing indistinguishable or nearly indistinguishable Mean-Discrete feature. For this reason, the Mean-Discrete feature will be identical or nearly identical as well.

Moreover, the obtained information and the characteristics of each twin will not be altered by the algorithm proposed. Rather, it denotes the initially extracted multi-biometric feature vector within the Mean-Discrete feature vector of a uni-representation. The process of Mean-Discrete will provide a clear elucidation on the linkages between features, while the characteristics of the features remain the same. For this reason, Mean-Discrete algorithm is appropriate while also fulfilling the individuality of the twin's handwriting-fingerprint in the context of twin identification. Fig. 4 presents the terms as well as the Mean-Discrete process.

The process of Mean-Discrete feature-based fusion entails the labeling of the person's class, and the conversion of the multi-representation features into uni-representation features. In the line of Mean-Discrete, first concatenate twins Kurdish handwriting-fingerprint then the intervals are computed using the minimum (Fe_{min}) and maximum (Fe_{max}) feature vectors (*ifv*)

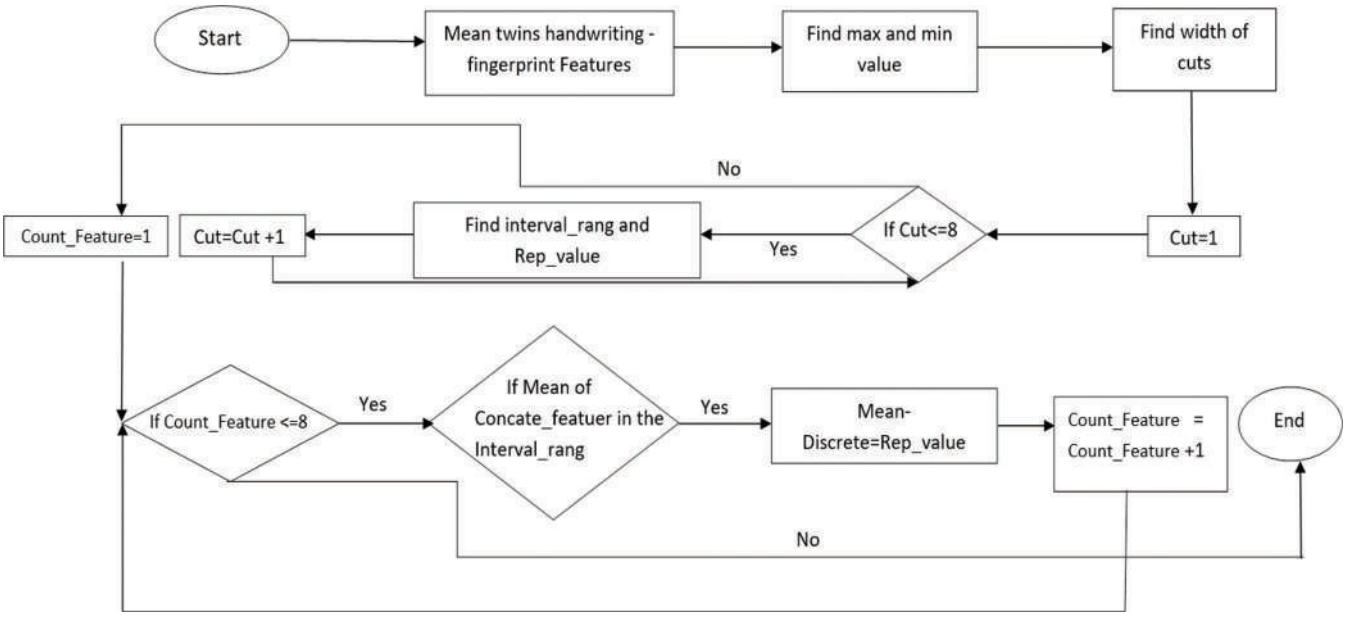

Fig. 3. Flowchart of Proposed Mean-Discrete Algorithm.

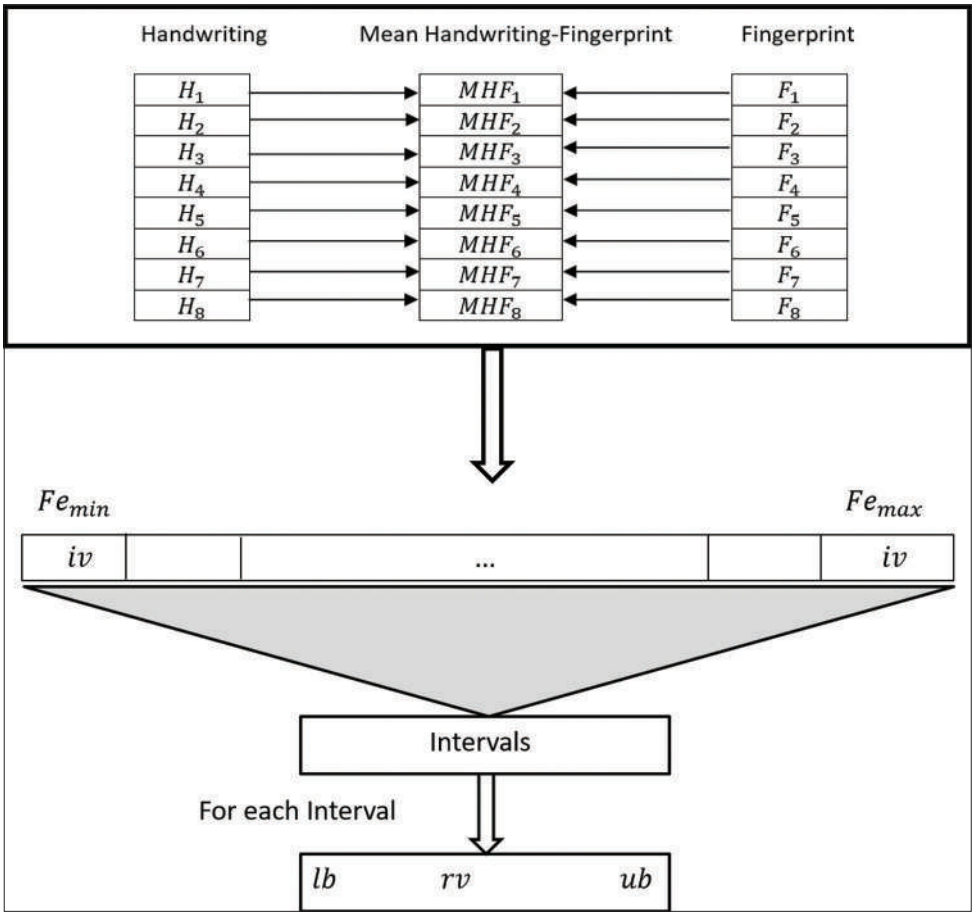

Fig. 4. Mean-discrete (uni-representation) features.

for an individual. The line of Mean-Discrete line entails a line of invariant feature vectors. This line begins from the minimum (Fe_{min}) invariant feature vector value and finishes with the maximum (Fe_{min}) invariant feature vector value for an individual twin. An interval encompasses the average of the line of Mean-Discrete apportioned by the number of columns within the invariant feature vector. The following is the calculation of the width (*wd*) of an interval:

$$wd = (Fe_{max} - Fe_{min}) / f \quad (9)$$

where

Fe_{min}: Minimum value of invariant feature vector for a person in a twin.

Fe_{max}: Maximum value of invariant feature vector for a person in a twin.

f: Number of columns in the invariant features vector.

The width describes the interval's cut points. It also computes the value of representation value. The "*f*" value denotes eight for the number of columns of the feature from AUMI. Meanwhile, the cut point denotes the intervals' divider (iv) within the line of Mean-Discrete. For invariant feature vectors with similar interval, they have the exact value of representation. For each interval, the value of representation (rv) comprises the average of an interval computed using the following formula: $rv = \frac{ub - lb}{2}$. The value of representation value for all intervals (1-8) denotes the invariant feature vector that is in the following range: if MHF $\geq 1b$ and if MHF $\leq ub$. Meanwhile, mean features (*MHF*) for each twin are computed using the invariant feature vectors of the twin's handwriting (H_{ij}) and fingerprint (F_{ij}).

Eight features were created in this study, which represents the number of columns for the number of features of the AUMI applied for the twin's multi-biometric. These features are called the Mean-Discrete feature vector. This vector symbolizes the individuality of the twin's handwriting-

fingerprint to the person. Tables 1 and 2 exemplify the transformation of the twin's multi-biometric feature vector into the Mean-Discrete feature vector.

Tables 1 and 2 exhibit a total of eight columns. These columns signify the eight columns of the invariant feature vectors in the AUMI. The Mean-Discrete process is then performed using these data. Fig. 5 shows the Mean-Discrete process for twin number a1.

Table 3 shows the Mean-Discrete feature vector produced from the Mean-Discrete algorithm process. The Mean-Discrete features vector includes the generalized features of a twin individual. These features clearly represent the general individual features for each individual in a twin.

5. EXPERIMENT AND RESULTS

Mean-Discrete algorithm generates more accurate results of identification task results, and for this reason, it is of value to the context of this study. Within the context of multi-representation analysis, the individuality of the twin's handwriting-fingerprint is this study's focal point. The twin's multi-biometric identification has been improved using the Score Histogram which is based on false Non-Match Rate (FNMR) and False Match Rate (FMR), and the improved aspect is its individuality. An example of the performance of identification with the current accuracy in twin identification task shows the feasibility of Mean-Discrete data in generating better performance. In other words, the prospect of attaining better level of individuality of a twin's Kurdish handwriting-fingerprint with Mean-Discrete feature based fusion data utilization is proven in this work. Comparison was made between this study's outcomes of the uni-representation analysis with the Mean-Discrete feature based fusion data and those from the analysis of multi-representation.

5.1. Matching Performance with Mean-discrete Algorithm

In this study, the matching performance is evaluated using Score Histogram which is based on false Non-Match Rate (FNMR) and False Match Rate (FMR). The number of multiple biometric such as the true and non-true match datasets, taken into consideration for the experimental purpose, is also included in the section.

In this study, the datasets used for the experimental purposes are summarized in Table 4:

5.1.1. Score histogram

Here, the histogram illustrates the comparative probability distribution of score for both matches and non-matches over

TABLE 1: Real data for handwriting and fingerprint for twins

F1	F2	F3	F4	F5	F6	F7	F8	Twin
1.0318	0.1098	1.7241	0.3362	0.0117	83.1055	3.0619	5.7089	Ha1
1.0347	0.0976	1.7239	0.3362	0.0103	93.6710	3.4440	5.7071	Ha1
1.0299	0.1026	1.7241	0.3362	0.0109	88.7336	3.2760	5.7082	Ha1
1.0300	0.1024	1.7241	0.3362	0.0109	88.9304	3.2831	5.7082	Ha1
1.0178	0.1602	1.7237	0.3363	0.0175	56.1404	2.0994	5.7059	Fa1
1.0142	0.1418	1.7242	0.3361	0.0156	63.2681	2.3703	5.7100	Fa1
1.0305	0.0901	1.7238	0.3363	0.0096	101.105	3.733	5.7062	Fa1
1.0178	0.1021	1.7239	0.3362	0.0110	88.8608	3.2916	5.7073	Fa1
1.0315	0.1087	1.7242	0.3362	0.0116	83.9064	3.0919	5.7091	Hb1
1.0325	0.0988	1.7240	0.3362	0.0105	92.4349	3.4045	5.7078	Hb1
1.0311	0.1046	1.7241	0.3362	0.0111	87.1319	3.2127	5.7087	Hb1
1.0322	0.1076	1.7242	0.3362	0.0114	84.8370	3.1241	5.7091	Hb1
1.0564	0.0629	1.7239	0.3363	0.0064	148.405	5.3458	5.7064	Fb1
1.0490	0.0616	1.7240	0.3363	0.0063	150.580	5.4608	5.7070	Fb1
1.0644	0.0611	1.7239	0.3362	0.0061	154.040	5.5053	5.7070	Fb1
1.0305	0.1353	1.7248	0.3359	0.0144	67.4441	2.4819	5.7149	Fb1

TABLE 2: Mean handwriting and fingerprint for Twin a1

F1	F2	F3	F4	F5	F6	F7	F8
1.0248	0.1350	1.7239	0.3362	0.0146	69.623	2.5807	5.7074
1.0244	0.1197	1.7241	0.3362	0.0130	78.4695	2.9071	5.7085
1.0302	0.0963	1.7239	0.3362	0.0102	94.9196	3.5048	5.7072
1.0239	0.1023	1.7240	0.3362	0.0110	88.8956	3.2874	5.7077

the full range of possible score. This histogram is computed using the relative equations in (10, 11).

$$\text{Relative matches} = \frac{\text{Number of tru trail}}{\text{Total number of trails}} \quad (10)$$

$$\text{Relative non\_marches} = \frac{\text{Number of false trial}}{\text{Total number of trials}} \quad (11)$$

Fig. 6 thought 14 shows the significant difference for Mean-Discrete, Min, Max, Produced, Weight-Sum, Sum-Produced, Handwriting, Fingerprint, Sum and Concatenate methods and the following Figs. 6-14 shows the characteristics of the whole methods with matched score distribution after the matching process, respectively. Based on the scores distribution, it can be observed that the match score are lower than [48.5700, 99.7900, 32.7900, 8.5708, 44.1100, 99.7901, 86.9926 , 141.9000, and 103] and non-match score are higher than [0.0013, 0.0090, 0.0000299, 0.0105, 0.0122, 0.0061, 0.0020, 0.0154, and 4.2534], respectively. Thus, if a score is higher than [48.5700, 99.7900, 32.7900, 8.5708, 44.1100, 99.7901, 86.9926, 141.9000, and 103], it is definitely represented as false or non-match score with zero probability of error and if a score is lower than [0.0013, 0.0090, 0.0000299, 0.0105, 0.0122, 0.0061, 0.0020, 0.0154, and 4.2534], it is represented as true match score with zero probability of error. However, if the score value falls between scores [0.0013 , 0.0090, 0.0000299, 0.0105 , 0.0122, 0.0061, 0.0020, 0.0154, and 4.2534] and [48.5700, 99.7900, 32.7900, 8.5708 , 44.1100, 99.7901, 86.9926, 141.9000, and

TABLE 3: Example of mean- discrete feature for twins

a	5.9554	5.9554	5.9554	5.9554	5.9554	53.5161	5.9554	5.9554
	5.9554	5.9554	5.9554	5.9554	5.9554	77.2965	5.9554	5.9554
	5.9554	5.9554	5.9554	5.9554	5.9554	65.4063	5.9554	5.9554
	5.9554	5.9554	5.9554	5.9554	5.9554	65.4063	5.9554	5.9554
b5	6.7749	6.7749	6.7749	6.7749	6.7749	60.9026	6.7749	6.7749
	6.7749	6.7749	6.7749	6.7749	6.7749	74.4346	6.7749	6.7749
	6.7749	6.7749	6.7749	6.7749	6.7749	74.4346	6.7749	6.7749
	6.7749	6.7749	6.7749	6.7749	6.7749	74.4346	6.7749	6.7749
a9	5.4436	5.4436	5.4436	5.4436	5.4436	70.6327	5.4436	5.4436
	5.4436	5.4436	5.4436	5.4436	5.4436	70.6327	5.4436	5.4436
	5.4436	5.4436	5.4436	5.4436	5.4436	81.4976	5.4436	5.4436
	5.4436	5.4436	5.4436	5.4436	5.4436	59.7679	5.4436	5.4436
b9	6.9559	6.9559	6.9559	6.9559	6.9559	76.4268	6.9559	6.9559
	6.9559	6.9559	6.9559	6.9559	6.9559	62.5326	6.9559	6.9559
	6.9559	6.9559	6.9559	6.9559	6.9559	90.3210	6.9559	6.9559
	6.9559	6.9559	6.9559	6.9559	6.9559	76.4268	6.9559	6.9559
a20	16.5356	16.5356	16.5356	16.5356	16.5356	49.5981	16.5356	16.5356
	16.5356	16.5356	16.5356	16.5356	16.5356	49.5981	16.5356	16.5356
	16.5356	16.5356	16.5356	16.5356	16.5356	49.5981	16.5356	16.5356
	16.5356	16.5356	16.5356	16.5356	16.5356	181.8482	16.5356	16.5356
b20	5.4474	5.4474	5.4474	5.4474	5.4474	59.8109	5.4474	5.4474
	5.4474	5.4474	5.4474	5.4474	5.4474	59.8109	5.4474	5.4474
	5.4474	5.4474	5.4474	5.4474	5.4474	70.6836	5.4474	5.4474
	5.4474	5.4474	5.4474	5.4474	5.4474	59.8109	5.4474	5.4474
a24	7.9487	7.9487	7.9487	7.9487	7.9487	103.3018	7.9487	7.9487
	7.9487	7.9487	7.9487	7.9487	7.9487	39.7331	7.9487	7.9487
	7.9487	7.9487	7.9487	7.9487	7.9487	71.517	7.9487	7.9487
	7.9487	7.9487	7.9487	7.9487	7.9487	71.5174	7.9487	7.9487
b24	10.0104	10.0104	10.0104	10.0104	10.0104	130.0586	10.0104	10.0104
	10.0104	10.0104	10.0104	10.0104	10.0104	110.0505	10.0104	10.0104
	10.0104	10.0104	10.0104	10.0104	10.0104	90.0425	10.0104	10.0104
	10.0104	10.0104	10.0104	10.0104	10.0104	70.0345	10.0104	10.0104

TABLE 4: Size and characteristic of the multimodal datasets obtained from Kurdistan Reign used in experimental

Total Individuals	**50 twins (100) individuals**			
Type of matched score	Matching		Non-Match	
Type of modality	Handwriting	Fingerprint	Handwriting	Fingerprint
Total Samples	200	200	200	200
Number of modalities per individual	4	4	4	4

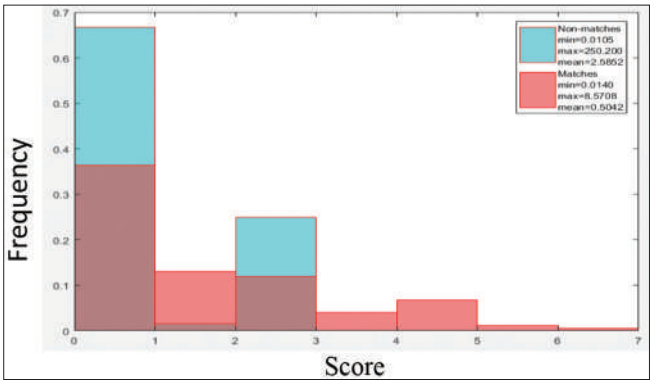

Fig. 8. From histogram for weight-sum matching score where true matches are on range [0.0140 , 8.5708] and non-match score is on range [0.0105, 250.2000].

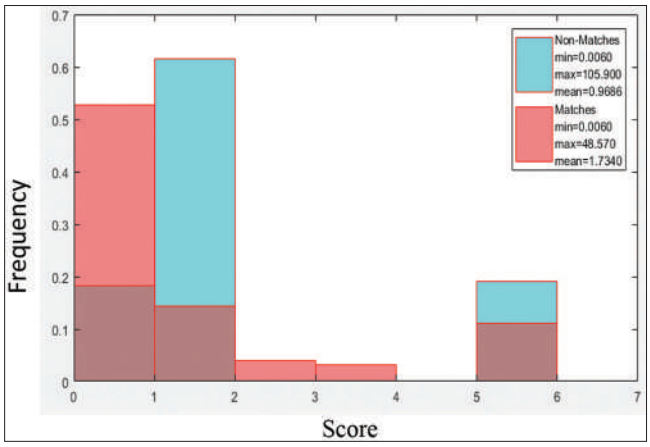

Fig. 5. From histogram for Max matching score where true matches are on range [0.0109, 99.7900] and non-match score is on range [0.0090, 798.9000].

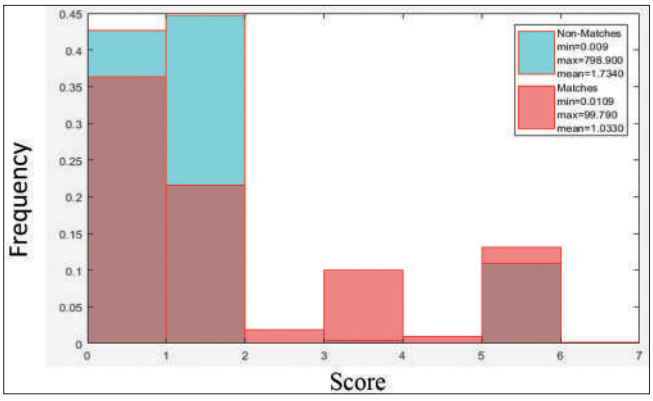

Fig. 6. From histogram for Min matching score where true matches are on range [0.0060, 48.5700] and non-match score is on range [0.0013, 105.9000].

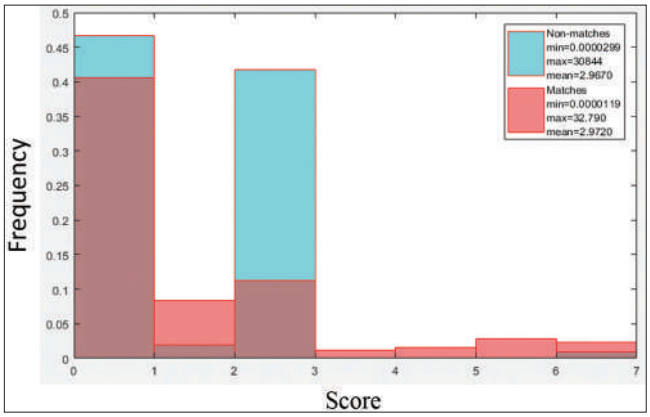

Fig. 7. From histogram for product matching score where true matches are on range [0.0000119, 32.7900] and non-match score is on range [0.0000299, 30844].

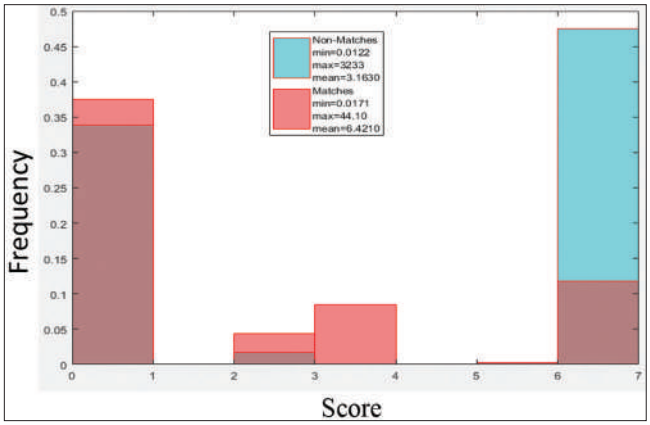

Fig. 9. From histogram for sum-product matching score where true matches are on range [0.0171, 44.1100] and non-match score is on range [0.0122, 31233].

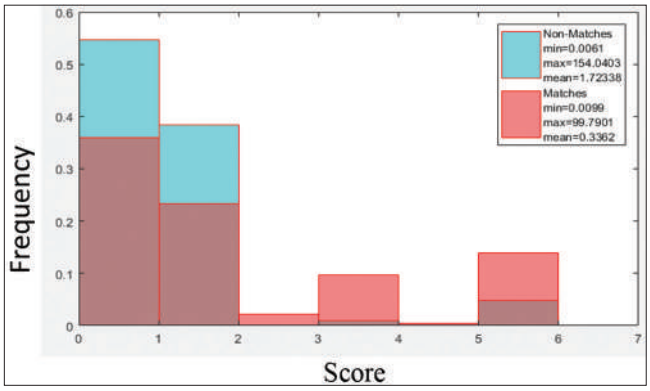

Fig. 10. From histogram for handwriting matching score where true matches are on range [0.0099, 99.7901] and non-match score is on range [0.0061, 154.0403].

103], it is known as undermined score because both true and false match score are in this range value [0.0013, 0.0090, 0.0000299, 0.0105, 0.0122, 0.0061, 0.0020, 0.0154, and 4.2534], [48.5700, 99.7900, 32.7900, 8.5708, 44.1100, 99.7901,

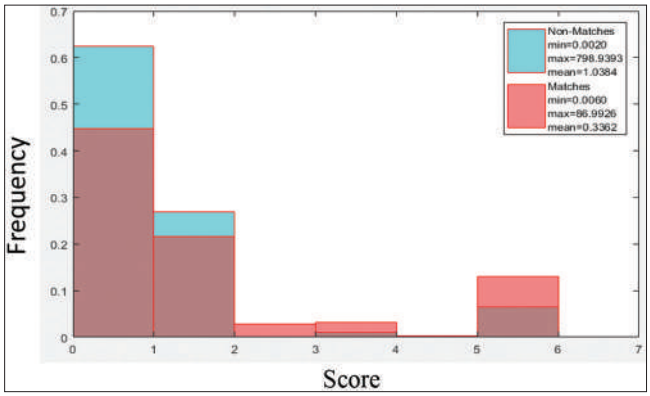

Fig. 11. From histogram for fingerprint matching score where true matches are on range [0.0060, 86.9926] and non-match score is on range [0.0020, 798.9393].

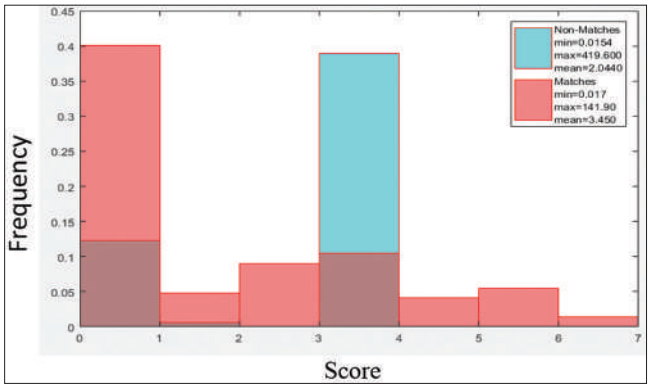

Fig. 12. From histogram for sum matching score where true matches are on range [0.0170, 141.9000] and non-match score is on range [0.0154, 419.6000].

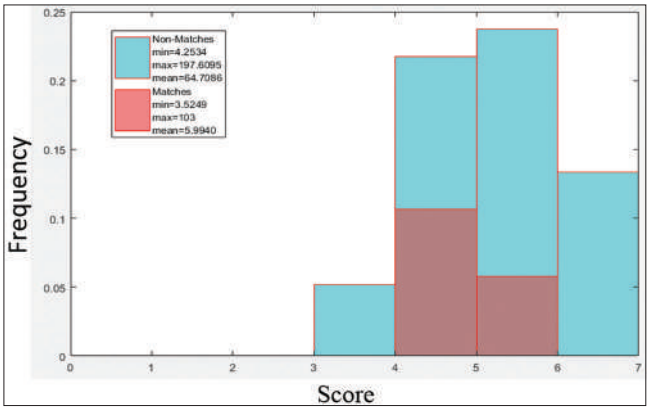

Fig. 13. From histogram for concatenate matching score where true matches are on range [3.5249, 103] and non-match score is on range [4.2534, 197.6095].

86.9926, 141.9000, and 103], respectively . This is where the case of miss-classification or probability of fusion error occurs. Fig. 6 thought 14 shows the histogram of the Min, Max, Produced, Weight-Sum, Sum-Produced, handwriting, fingerprint, Sum, and concatenate, respectively.

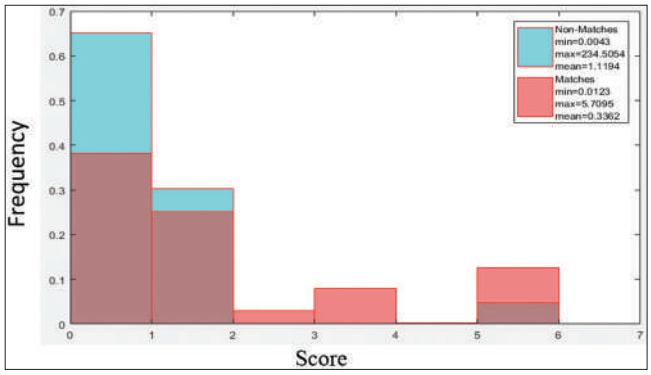

Fig. 14. Score histogram for Mean-Discrete matching score where true matches are on range [0.0123, 5.7095] and non-matches scores are on range [0.0043, 234, 5054].

Fig. 14 shows the histogram of the Mean-Discrete feature matching score. The true Mean-Discrete matching score is lower than 5.7095, while the non-matching Mean-Discrete score is higher than 0.0043. Interestingly, from the figure, it can be seen that they have a very slightly little overlap between the true match and non-match scores [0.0043, 5.7095]. Thus, this technique can minimize the issues of miss-classification and probability of fusion error.

6. CONCLUSION

This study attempted to improve the individuality identical twin's handwriting-fingerprint through the demonstration of Mean-Discrete feature based fusion algorithm. Mean-Discrete method converts the multi-representations of individual features into a uni-representation with the technique of Mean-Discrete algorithm. The data representation signifies an individual's generalized features. The conventional approach and the proposed approach were compared with one another and then, the task of Score Histogram was executed. Using these approaches, the Kurdish handwriting-fingerprints produced by identical twins were identified. Then, the obtained outcomes were scrutinized. With the application of the Mean-Discrete feature, the individual features are represented in a manner that is systematic with representation that is more informative. Hence, better performance is generated with the application of the proposed method particularly with respect to accuracy. The application of the algorithm with the Mean-Discrete process is demonstrated in this study. Then, for biometric identification of a twin, the Mean-Discrete data, un-Mean-Discrete data, and

different fusion algorithms were compared in terms of usage outcomes. In this regard, it appears that using Mean-Discrete data enhance the individuality of a twin's Kurdish handwriting-fingerprint for get better performance with Score Histogram.

REFERENCES

[1] Y. Koda, T. Higuchi and A. K. Jain. "*Advances in Capturing Child Fingerprints: A High Resolution CMOS Image Sensor with SLDR Method*". 2016 International Conference of the Biometrics Special Interest Group IEEE, pp. 1-4, 2016.

[2] S. Karahan, M. Kılınc and H. K. Ekenel. "*How Image Degradations Affect Deep CNN-based Face Recognition*"? IEEE Conference Publications, pp. 1-5, 2016.

[3] S. Easwaramoorthy, F. Sophia and A. Prathik. "*Biometric Authentication Using Finger Nails*". International Conference on Emerging Trends in Engineering, Technology and Science, IEEE Conference Publications, pp. 1-6, 2016.

[4] H, Behravan and K. Faez. "*Introducing a New Multimodal Database from Twins' Biometric Traits*". IEEE Conference Publications, IEEE, pp. 1-6, 2013.

[5] N. Srinivas, G. Aggarwal, P. J. Flynn and R. W. V. Bruegge. "Analysis of facial marks to distinguish between identical twins". *IEEE Transactions on Information Forensics and Security*, vol. 7, pp. 1536-1550, 2012.

[6] C. Kauba, A. UhlWavelab, E. Piciucco, E. Maiorana and P. Campisi. "*Advanced Variants of Feature Level Fusion for Finger Vein Recognition*". IEEE Conference Publications, pp. 1-7, 2016.

[7] N. Nain, B. M. Deepak, D. Kumar, M. Baswal and B. Gautham. "Optimized minutiae-based fingerprint matching". *Lecture Notes in Engineering and Computer Science*, vol. 2170, pp. 682-687, 2008.

[8] W. Y. Leng and S. M. Shamsuddin. "Fingerprint identification using discretization technique". *International Journal of Computer, Electrical, Automation, Control and Information Engineering*, vol. 6, pp. 240-248, 2012.

[9] J. Weber-Lehmann, E. Schilling, G. Gradl, D. C. Richter, J. Wiehler and R. Burkhard. "Finding the needle in the haystack: Differentiating ''identical'' twins in paternity testing and forensics by ultra-deep next generation sequencing". *Forensic Science International: Genetics*, vol. 9, pp. 42-46, 2014.

[10] H. Nejati, L. Zhang, T. Sim E. Martinez-Marroquin and G. Dong. "*Wonder Ears: Identification of Identical Twins from Ear Images*." Proceedings of the 21st International Conference on Pattern Recognition, Nov. 11-15, IEEE Xplorev Press, Tsukuba, Japan, pp. 1201-1204, 2012.

[11] V. Vipin, K. W. Bowyer, P. J. Flynn, D. Huang, L. Chen, M. Hansen, O. Ocegueda, S. K. Shah and I. A. Kakadiaris. "*Twins 3D Face Recognition Challenge*". Proceedings of the International Joint Conference on Biometrics, Oct. 11-13, IEEE Xplore Press, Washington, DC, USA, pp. 1-7, 2011.

[12] J. R. Paone, P. J. Flynn, P. J. Philips, K. W. Bowyer, R. W. V. Bruegge, P. J. Grodher, G. W. Quinn, P. T. Pruitt and J. M. Grant. "Double trouble: Differentiating identical twins by face recognition". *IEEE Transactions on Information Forensics and Security*, vol. 9, pp. 285-295, 2014.

[13] S. N. Srihari, S. H. Cha, H. Arora and S. Lee. "Individuality of handwriting". *Journal of Forensic Sciences*, vol. 47, pp. 1-17, 2002.

[14] B. O. Mohammed and S. M. Shamsuddin. "Improvement in twins handwriting identification with invariants discretization". *EURASIP Journal on Advances in Signal Processing*, vol. 48, pp. 1-19, 2012.

[15] A. S. Al-Waisy, R. Qahwaji, S. Ipson, S. Al-Fahdawi, T. A. M. Nagem. "A multi-biometric iris recognition system based on a deep learning approach". *Pattern Analysis and Applications*, vol. 21, pp. 783-802, 2018.

[16] B. L. Priya, M. P. Rani. "*Authentication of Identical Twins Using Tri Modal Matching*". World Congress on Computing and Communication Technologies, IEEE, 2017.

[17] K. M. Azah, S. M. Shamsuddin and A. Abrahamz. "Improvement of authorship invarianceness for individuality representation in writer identification". *Neural Network World*, vol. 3, pp. 371-387, 2010.

[18] P. Feng P. and M. Kean. "A new set of moment invariants for handwritten numeral recognition". *IEEE International Conference of Image Processing*, vol. 1, pp. 154-158, 1994.

[19] S. Yinan, L. Weijun and W. Yuechao. "*United Moment Invariants for Shape Discrimination*". Proceedings of the IEEE International Conference on Robotics, Intelligent Systems and Signal Processing, Oct. 8-13, IEEE Xplore Press, Changsha, Hunan, China, pp. 88-93, 2003.

[20] M. K. Hu. "Visual pattern recognition by moment invariants". *IEEE Transactions on Information Theory*, vol. 8, pp. 179-187, 1962.

[21] C. C. Chen. "Improved moment invariants for shape discrimination". *Pattern Recognition*, vol. 26, pp. 683-686, 1993.

[22] B. O. Mohammed and S. M. Shamsuddin. "Twins multimodal biometric identification system with aspect united moment invariant". *Journal of Theoretical and Applied Information Technology*, vol. 95, p. 2895, 2017.

[23] B. O. Mohammed and S. M. Shamsuddin. "A multimodal biometric system using global features for identical twins identification". Journal *of Computer Science*, vol. 14, pp. 92-107, 2018.

[24] B. O. Mohammed and S. M. Shamsuddin. "Feature discretization for individuality representation in twins handwritten identification". *Journal of Computer Science*, vol. 7, pp. 1080-1087, 2011.

p-ISSN 2521-4209
e-ISSN 2521-4217

زانکۆی گەشەپێدانی مرۆیی
جامعة التنمية البشرية
UNIVERSITY OF HUMAN DEVELOPMENT

UHD Journal of Science and Technology

A Scientific periodical issued by University of Human Developement

Vol.4 No.(2) December 2020

2020 2720

e.mail:jst@uhd.edu.iq